NASA TN D-231

TECHNICAL NOTE
D-231

A STUDY OF EQUILIBRIUM REAL-GAS EFFECTS IN HYPERSONIC AIR NOZZLES, INCLUDING CHARTS OF THERMODYNAMIC PROPERTIES FOR EQUILIBRIUM AIR

By Wayne D. Erickson and Helen S. Creekmore

Langley Research Center
Langley Field, Va.

NATIONAL AERONAUTICS AND SPACE ADMINISTRATION
WASHINGTON
April 1960

1R

CONTENTS

L
7
7
9

NATIONAL AERONAUTICS AND SPACE ADMINISTRATION

TECHNICAL NOTE D-231

A STUDY OF EQUILIBRIUM REAL-GAS EFFECTS IN HYPERSONIC AIR NOZZLES, INCLUDING CHARTS OF THERMODYNAMIC PROPERTIES FOR EQUILIBRIUM AIR

By Wayne D. Erickson and Helen S. Creekmore

SUMMARY

Charts of thermodynamic properties for equilibrium air are presented with sufficient accuracy to permit the calculation of flow parameters in hypersonic nozzles operating at stagnation temperatures up to 4,950° R and pressures up to 1,000 atm. Flow parameters calculated from these charts are presented for a series of stagnation temperatures between 2,790° R and 4,950° R and pressures between 40 atm and 1,000 atm. By use of these parameters, it is possible to calibrate a nozzle in the conventional way. A method is also presented from which the flow parameters for conditions other than those chosen herein may be calculated. Real-gas effects on the calculation of a hypersonic nozzle contour are shown by an example calculation in which the nozzle contour for Mach number 12 was determined by including real-gas effects, and this contour was compared with one calculated by ideal-gas considerations. Also presented are the approximate limiting Mach numbers at which equilibrium air will just condense for various combinations of stagnation temperatures and pressures.

INTRODUCTION

The operation of air nozzles at high Mach numbers requires that the stagnation air be heated to high temperatures to avoid condensation of its constituents upon expansion. In some cases it is also desirable to operate at high stagnation pressures.

At high temperatures dissociation of the constituents of air occurs, the degree of which is a function of temperature and pressure. As the pressure is decreased at a constant temperature, the degree of dissociation increases; conversely, the greater the pressure the less the degree of dissociation. At pressures approaching 100 atm and temperatures below 5,000° R, the degree of dissociation is negligible; however, the contribution of intermolecular force fields becomes important.

One purpose of this report is to present real-gas flow parameters for air from which a hypersonic nozzle may be calibrated. The Mach number range to be considered is from 10 to that limited by air condensation when the stagnation temperature is in the range from 2,790° R to 4,950° R and for stagnation pressures up to 1,000 atm.

When both intermolecular force effects and dissociation are important, as is the case herein, it is expedient to calculate the flow parameters for equilibrium air with the aid of thermodynamic charts because an analytic equation of state (which would account for both effects) is inconvenient to use. Another purpose of this study, then, is to present the necessary thermodynamic charts with sufficient accuracy to permit the calculation of the desired flow parameters.

Also of interest are the real-gas effects on the calculation of the inviscid nozzle contour for high stagnation temperatures and pressures. As an example, a Mach number 12 nozzle contour is calculated by including the real-gas effects and is compared with the contour calculated for an ideal gas.

Finally, the approximate limiting Mach number for avoiding condensation at various stagnation temperatures and pressures is calculated by including the real-gas effects for air.

For all calculations presented herein it has been assumed that the air was at all times in chemical equilibrium. This is felt to be a good assumption for the conditions chosen. For conditions under which chemical equilibrium is not attained, the method given in reference 1 or a similar approach must be used.

SYMBOLS

A	cross-sectional area, sq ft
a	velocity of sound, ft/sec
a/a_o	velocity of sound, dimensionless (a_o = 1087.4 ft/sec)
H	enthalpy, ft^2/sec^2
H/RT_o	enthalpy, dimensionless
M	Mach number
p	pressure, atm

R	gas constant $\left(\text{for eq. (1), } R = 0.0252098 \frac{\text{atm-ft}^3}{\text{lb-}^\circ\text{R}}\text{; for eqs. (2), (5), and (12), } R = 1716.36 \frac{\text{ft}^2}{\text{sec}^2\text{-}^\circ\text{R}}\right)$
S	entropy, $\text{ft}^2/\text{sec}^2\text{-}^\circ\text{R}$
S/R	entropy, dimensionless
T	temperature, $^\circ$R
T_o	reference temperature, 491.688° R
V	velocity, ft/sec
V_l	limiting velocity, ft/sec
x	distance along nozzle center line
y	distance perpendicular to nozzle center line
Z	compressibility factor, $p/\rho RT$
γ	ratio of specific heats
ρ	density, lb/cu ft

Subscripts:

i	ideal
t,1	stagnation conditions upstream of shock
t,2	stagnation conditions downstream of shock
1	static conditions upstream of shock
2	static conditions downstream of shock

Superscript:

*	conditions at throat (M = 1)

CHARTS OF THERMODYNAMIC PROPERTIES FOR AIR

In order to calculate the flow parameters and the contour of a hypersonic nozzle, it is first necessary to know the thermodynamic properties for air with sufficient accuracy. It is convenient to have the thermodynamic properties in chart form for the calculations considered herein. Since there are no thermodynamic charts for air available with sufficient accuracy in the desired temperature and pressure range, charts were prepared to meet the present requirements. Thermodynamic properties for air in the desired temperature range were presented by Hilsenrath, et al. (ref. 2); however, the pressure range considered was 0.01 atm to 100 atm. The data of reference 2 were calculated by considering both dissociation and intermolecular force effects. Above 100 atm the thermodynamic properties for air were extended by the method discussed in the appendix. Below 0.01 atm and down to the approximate saturated vapor line, the properties of interest were calculated from the ideal gas law. The approximate saturated vapor line was estimated from the vapor-pressure data of references 2 and 3.

The data of reference 2 and the extensions above 100 atm and below 0.01 atm were used to prepare charts of entropy, enthalpy, compressibility factor, and velocity of sound, each plotted against pressure for a series of constant temperatures. These supplementary charts of thermodynamic properties for air are presented in a separate section at the end of the paper and were used as a basis for calculations herein. These charts are included to facilitate additional calculations of particular interest to the reader.

METHOD FOR CALCULATING FLOW PARAMETERS

The flow parameters for Mach numbers between 10 and that limited by condensation have been calculated. The results of these calculations are presented in figures 1 to 18 in the form of correction factors which must be applied to the ideal-gas ratios. The method used for calculating the correction factors is discussed in this section.

Consider the flow of air through a hypersonic nozzle as shown in sketch A.

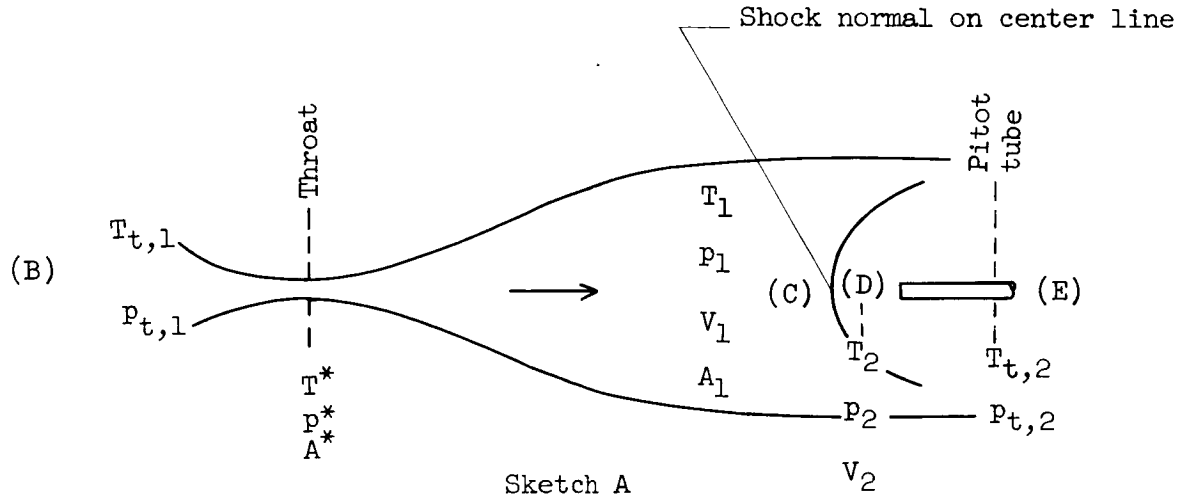

Sketch A

In the region of flow from the stagnation chamber (point B) to the free-stream flow just upstream of the normal shock (point C) the flow is assumed to expand at constant entropy, the value of which is determined from $T_{t,1}$ and $p_{t,1}$. For a gas in equilibrium the state is determined when any two state functions are fixed; for example, T and p or T and S. Therefore, for a given value of $T_{t,1}$ and $p_{t,1}$, any one state variable in the stream determines the state of the gas during the isentropic expansion upstream of the normal shock. Sketch B shows this process on a pressure-entropy diagram by the vertical line BC.

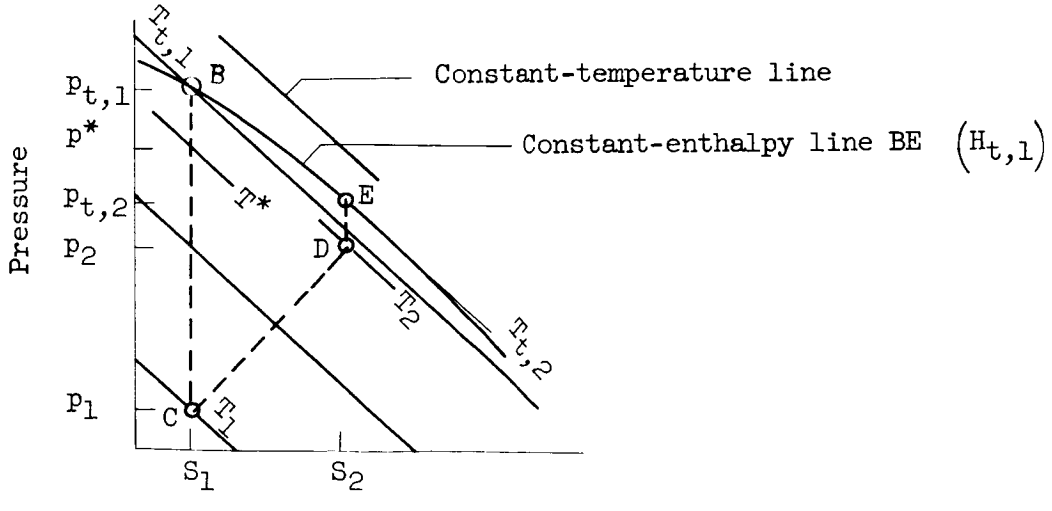

Sketch B

When the velocity of the stream has reached the velocity of sound, the state of the air is given by T^* and p^* which correspond to the conditions at the throat in sketch A. Beyond the throat the expansion continues at constant entropy S_1 until point C is reached.

The air experiences a gain in entropy from S_1 to S_2 in passing through the normal shock. This irreversible process is shown by passing from point C to point D. Point D represents the state of the air just downstream of the normal shock and may be calculated from the Rankine-Hugoniot equations, as shown in the section entitled "Entropy Gain Across Normal Shock."

Sketch A shows a pitot tube just downstream of the normal shock which isentropically decelerates the flow to rest. This process is shown in sketch B by line DE which is located by S_2. Since the enthalpy in the stagnation chamber $H_{t,1}$ is equal to the enthalpy of the air at rest in the pitot tube $H_{t,2}$, the state of the air at point E is determined by the intersection of DE with the constant enthalpy line equal to $H_{t,1}$. Point E is defined by $T_{t,2}$ and $p_{t,2}$.

The state properties shown in sketches A and B are calculated by separating the flow system into three successive processes: (1) the isentropic expansion BC, (2) the entropy gain across the normal shock CD, and (3) the isentropic compression DE.

Isentropic Expansion

The entropy remains constant and equal to the value determined at point B from $T_{t,1}$ and $p_{t,1}$ during the isentropic expansion. Now by arbitrarily choosing a series of temperatures T_1 along line BC (sketch B), it is possible to determine the temperature-pressure relationship for an isentropic expansion starting with $T_{t,1}$ and $p_{t,1}$. These points are chosen in a temperature range so that the desired range of Mach numbers is obtained. (This range of T_1 will become obvious after a few trials.) For each chosen value of T_1, the corresponding value for p_1 may be found. Once T_1 and p_1 are known, the other thermodynamic properties at a point may be determined - namely, density ρ_1, enthalpy H_1, and velocity of sound a_1. These thermodynamic properties may be determined from the supplementary charts. Density ρ_1 is not plotted as such; however, the compressibility factor Z is plotted. If T_1 and p_1 are known, Z may be determined from the charts and p_1 may be determined

from the following relation:

$$\rho = \frac{p}{ZRT} \tag{1}$$

The energy equation for the isentropic expansion when the velocity in the stagnation chamber is negligible is

$$V_1 = \sqrt{2\left(H_{t,1} - H_1\right)} \tag{2}$$

The Mach number $M_1 \equiv \frac{V_1}{a_1}$ corresponding to T_1 and a given $T_{t,1}$ and $p_{t,1}$ is immediately determined when the velocity of sound a_1 is obtained from the supplementary thermodynamic charts.

Entropy Gain Across Normal Shock

The state variables T_1, p_1, ρ_1, H_1, V_1, and a_1 at point C are determined from the isentropic-expansion calculation from the previous section and are used in conjunction with the Rankine-Hugoniot equations to calculate point D. These equations are:

Conservation of mass,

$$\rho_1 V_1 = \rho_2 V_2 \tag{3}$$

conservation of momentum,

$$p_1 + \rho_1 V_1^2 = p_2 + \rho_2 V_2^2 \tag{4}$$

and conservation of energy,

$$H_{t,1} = H_1 + \frac{1}{2} V_1^2 = H_2 + \frac{1}{2} V_2^2 \tag{5}$$

There are four unknowns in equations (3) to (5): namely, ρ_2, V_2, p_2, and H_2. The additional required relationship is the equation of state

for air which is given by the combination of pressure-enthalpy plots, the pressure-compressibility plots, and equation (1).

Point D is calculated by an iterative procedure. First, take a value for ρ_2. (The value for the ideal gas may be used for a first approximation.) Then, calculate a value for V_2 from equation (3). Use these values for ρ_2 and V_2 in equations (4) and (5) to calculate values for p_2 and H_2. These values of p_2 and H_2 are then used with the pressure-enthalpy charts to find a value for T_2. This value of T_2 is used with the value obtained for p_2 to find a value for Z_2 from the compressibility-factor charts; these values, in turn, permit the calculation of a value of ρ_2 from equation (1). The solution is found when the assumed value of ρ_2 is equal to the value calculated by the last step of the procedure. This iterative method usually requires three or less trials.

Isentropic Compression

This isentropic compression is shown in sketch B by the vertical line DE. The value of S_2 is determined from T_2 and p_2. Equation (5) shows that the enthalpy at any point in the flow is equal to $H_{t,1}$ when the velocity is zero. This is the case at point E. Point E is therefore found by the intersection of a vertical line S_2 and $H_{t,1}$ $\left(H_{t,2}\right)$ in sketch B.

The supplementary thermodynamic charts present enthalpy as a function of pressure at constant temperature rather than constant enthalpy as a function of pressure and entropy. This means that point E must also be found by an iterative procedure. The value of S_2 at point D is equal to $S_{t,2}$ at point E. A value for $T_{t,2}$ is assumed from which a value for $p_{t,2}$ may be read from the pressure-entropy charts. These values of $T_{t,2}$ and $p_{t,2}$ are used to find a value for $H_{t,2}$ from the pressure-enthalpy charts. The solution for point E is found when the calculated value for $H_{t,2}$ equals that for $H_{t,1}$. This value also may be found within three trials or less.

Conditions at Nozzle Throat

The state of air in the throat may be calculated by two different methods, both of which depend on the procedure outlined for the isentropic

expansion. In the first method the product $\rho_1 V_1$ is plotted against a series of values for T_1 for a given value of $T_{t,1}$ and $p_{t,1}$. The range of values for T_1 are so chosen that a range of Mach numbers greater and less than 1 are obtained. The value of $\rho_1 V_1$ is a maximum at the throat. This maximum ($\rho^* V^*$) corresponds to a temperature T^*. Since S_1 is fixed, T^* determines p^*. The one-dimensional mass-flow relationship between the throat and test section is

$$\rho^* A^* V^* = \rho_1 A_1 V_1 \tag{6}$$

The method for calculating values of ρ_1 and V_1 as a function of M_1 for various fixed values of $T_{t,1}$ and $p_{t,1}$ has been shown. The ratio of test-section area to throat area is then

$$A_1/A^* = \rho^* V^*/\rho_1 V_1 \tag{7}$$

The second method for determining the throat conditions makes use of the velocity-of-sound data in the throat region. A series of values for T_1 for a given value of $T_{t,1}$ and $p_{t,1}$ are chosen as for the first method. The velocity V_1 is calculated at each chosen T_1. Since a_1 is known for any combination of T_1 and p_1, the Mach number may be calculated as a function of T_1. When M_1 equals 1, the temperature is T^*. The value of p^* is determined in like manner. This permits the calculation of $\rho^* V^*$ and the remaining calculations are the same as for the first method.

FLOW PARAMETER CHARTS

The flow parameters can be determined with the use of correction factors presented in figures 1 to 18, which were obtained in the following manner. The flow parameters which have been calculated for various fixed combinations of $T_{t,1}$ and $p_{t,1}$ are T_1, p_1, ρ_1, M_1, T_2, p_2, ρ_2, $T_{t,2}$, $p_{t,2}$, T^*, p^*, and A_1/A^*. It is convenient to express these parameters as ratios. The combination of ratios chosen were $T_1/T_{t,1}$, $T_{t,2}/T_{t,1}$, $p_1/p_{t,1}$, p_2/p_1, $p_{t,2}/p_{t,1}$, ρ_2/ρ_1, $T^*/T_{t,1}$, $p^*/p_{t,1}$,

and A_1/A^*. These ratios were plotted as a function of M_1 for various combinations of $T_{t,1}$ and $p_{t,1}$. (Only Mach numbers of 10 and greater were calculated.) These plots all had a form similar to that shown in sketch C for $T_1/T_{t,1}$.

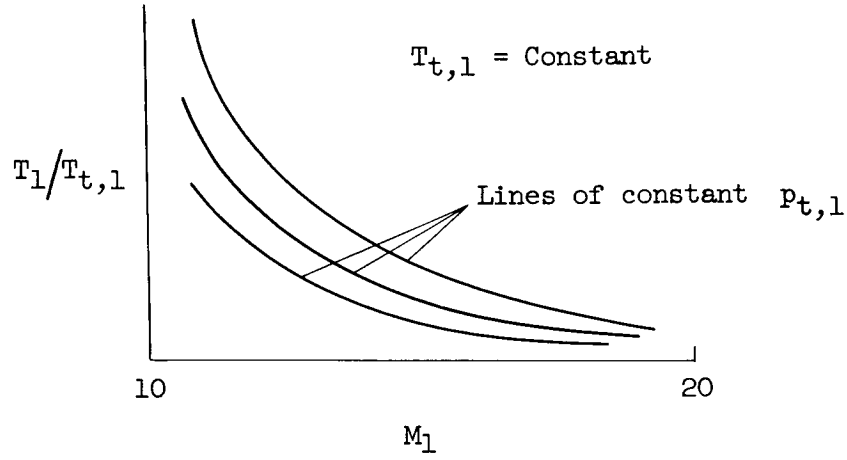

Sketch C

Reference 4 presents tables of these various ratios as a function of Mach number for an ideal gas with a constant value of γ of 1.4. For an ideal gas with a constant γ the relationships between the flow ratios and Mach number are independent of $T_{t,1}$ and $p_{t,1}$. In addition to this tabulation, reference 4 presents a correction factor for each ratio which takes into account the variation of γ with temperature. This correction factor is the quotient of the ratio calculated by considering the γ variation divided by the ratio calculated for constant γ of 1.4. The correction factors presented in reference 4 have a form similar to that shown in sketch D.

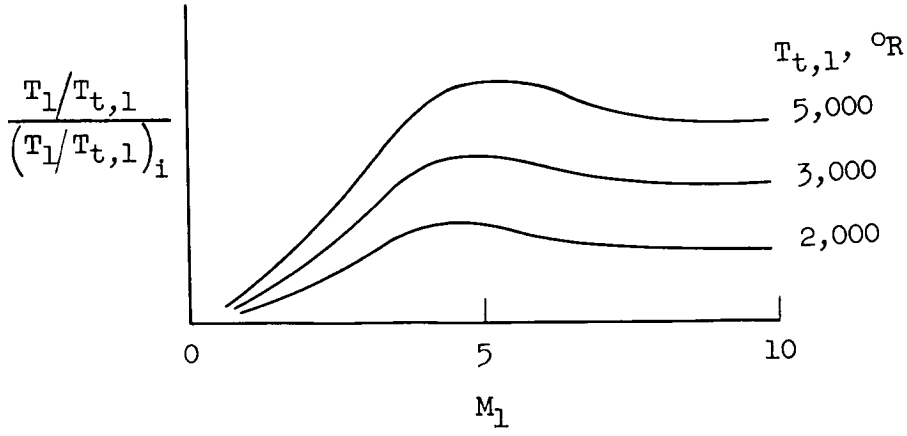

Sketch D

These correction factors are convenient and easy to use; however, they do not consider the effect of $p_{t,1}$ which becomes important for pressures approaching 100 atm and above.

Since the flow parameters calculated herein are a function of $p_{t,1}$ as well as $T_{t,1}$, it would be necessary to have a plot similar to sketch D for each value of $p_{t,1}$. Inspection of the results of reference 4 for correction factors as indicated in sketch D shows the trend that the correction factors are independent of M_1 for $M_1 > 7$. This is true for the other ratios as well as $\frac{T_1/T_{t,1}}{\left(T_1/T_{t,1}\right)_i}$. Now if the effect of $p_{t,1}$ on a correction factor is only to displace the curves vertically and independently of M_1, the correction factors may be presented as a function of $p_{t,1}$ for a series of values of $T_{t,1}$. This was found to be the case. When the ratio of the calculated parameter (for example, $T_1/T_{t,1}$) was divided by the ratio for a perfect gas with γ constant at 1.4, the quotient was found to be independent of Mach number for $M_1 \geqq 10$. The only exception to this is the correction factor for ρ_2/ρ_1 and $T_{t,2}/T_{t,1}$ above $T_{t,1} \geqq 3{,}510^\circ$ R. The correction factors for these two ratios above $3{,}510^\circ$ R are plotted as a function of M_1 for a series of values of $p_{t,1}$ at constant values of $T_{t,1}$.

The correction factors for the various flow parameters presented in figures 1 to 18 are for Mach numbers greater than 10. The symbols indicate the calculated points. The use of these charts is best shown by an example. Consider a case where $T_{t,1} = 3{,}510^\circ$ R, $p_{t,1} = 400$ atm, and the measured pitot total pressure is 0.145 atm. The ratio $p_{t,2}/p_{t,1}$ is $0.145/400$ or 3.62×10^{-4}. From figure 4 the value for $\frac{p_{t,2}/p_{t,1}}{\left(p_{t,2}/p_{t,1}\right)_i}$ is 0.852 for $T_{t,1} = 3{,}510^\circ$ R and $p_{t,1} = 400$ atm. The hypothetical value for $\left(p_{t,2}/p_{t,1}\right)_i$ is then $\frac{3.62 \times 10^{-4}}{0.852}$ or 4.25×10^{-4}. The value for M_1 corresponding to this value for $p_{t,2}/p_{t,1}$ may be calculated or obtained from reference 4. For this case, $M_1 = 15.1$. The other flow parameters are calculated in a similar way.

Figure 19 shows the approximate combinations of $T_{t,1}$ and $p_{t,1}$ at which condensation of equilibrium air can begin in a hypersonic nozzle for various test-section Mach numbers. These plots were obtained by calculating the point on the pressure-entropy charts where the isentropic-expansion line first intersects the approximate saturated vapor line.

INVISCID-FLOW NOZZLE CALCULATIONS

The calculation of an inviscid-flow nozzle contour is dependent on the equation of state for air in the same manner as the flow parameters previously determined. It is, therefore, desirable to calculate the inviscid contour by use of the thermodynamic charts for air. When the operating conditions are such that the air deviates a great deal from the ideal gas, it is expected that there will be a considerable difference between the calculated real-gas and ideal-gas contours based on figure 18. Since the interdependency of temperature, pressure, and Mach number determines the deviation from ideal gas, it is difficult to define under what conditions the inviscid nozzle contour should be calculated by using real-gas properties. The effect of real-gas properties is shown by four examples.

The two equations which relate the state of the air to its velocity in the inviscid nozzle calculation for an ideal gas are

$$(V_l/V)^2 = 1 + \left(\frac{2}{\gamma - 1}\right)\frac{1}{M^2} \tag{8}$$

and

$$\rho_1/\rho_{t,1} = \left[1 - (V/V_l)^2\right]^{1/(\gamma-1)} \tag{9}$$

If γ is equal to 1.4, equation (8) reduces to

$$(V_l/V)^2 = 1 + 5(1/M^2) \tag{10}$$

and equation (9) reduces to

$$\rho_1/\rho_{t,1} = \left[1 - (V/V_l)^2\right]^{5/2} \tag{11}$$

The stagnation conditions for the four examples considered are as follows:

$$T_{t,1} = 2{,}790^\circ \text{ R}; \quad p_{t,1} = 300 \text{ atm}$$

$$T_{t,1} = 3{,}960^\circ \text{ R}; \quad p_{t,1} = 100 \text{ atm}$$

$$T_{t,1} = 3{,}960^\circ \text{ R}; \quad p_{t,1} = 1{,}000 \text{ atm}$$

$$T_{t,1} = 4{,}770^\circ \text{ R}; \quad p_{t,1} = 100 \text{ atm}$$

The inviscid nozzle calculation for a real gas requires the real-gas relationship between V/V_l and M^2 and the real-gas relationship between $\rho_1/\rho_{t,1}$ and V/V_l. The values for M^2 and $\rho_1/\rho_{t,1}$ were determined by the methods presented previously. The value for V/V_l was calculated as follows. The limiting velocity V_l is the hypothetical velocity obtained when a gas is expanded isentropically to the point where all the total enthalpy has been converted to kinetic energy. This point also corresponds to zero temperature. For the charts presented herein, the enthalpy is zero at zero temperature. The limiting velocity from equation (2) is, therefore,

$$V_l = \sqrt{2H_{t,1}} \tag{12}$$

and the value for the limiting velocity ratio at any point along an isentropic expansion is

$$V/V_l = \sqrt{1 - \left(H_1/H_{t,1}\right)} \tag{13}$$

The values for $\left(\frac{V_l}{V}\right)^2$ were calculated for air by using real-gas properties at several values of $1/M^2$ for each of the four examples. The results of this calculation are shown along with the ideal relationship (eq. (10)) in figure 20. This figure shows the effect of $T_{t,1}$ and $p_{t,1}$ on the departure from the ideal-gas calculation of equation (10). In general, the greatest deviation is in the throat region (near $1/M^2 = 1$).

The two cases calculated for $p_{t,l} = 100$ atm - namely, $T_{t,l} = 3,960^\circ$ R and $T_{t,l} = 4,770^\circ$ R - show that the higher the stagnation temperature for a given stagnation pressure, the greater the departure from the ideal calculation. On the other hand, comparing the results for the two cases at $T_{t,l} = 3,960^\circ$ R - namely, $p_{t,l} = 100$ atm and $p_{t,l} = 1,000$ atm - shows that the higher the stagnation pressure at a given stagnation temperature, the less the departure from ideality (eq. (10)).

These general statements are true in the restricted temperature and pressure ranges considered herein but are likely to show the opposite effect at temperatures near 500° R. In other words, the larger the stagnation pressure for a given low stagnation temperature, the greater the departure from the ideal-gas calculations.

The calculation for $T_{t,l} = 2,790^\circ$ R and $p_{t,l} = 300$ atm is also shown in figure 20. The curve for this condition falls between the curve for $T_{t,l} = 3,960^\circ$ R and $p_{t,l} = 100$ atm and the curve for $T_{t,l} = 3,960^\circ$ R and $p_{t,l} = 1,000$ atm. This shows the interdependency of both $T_{t,l}$ and $p_{t,l}$ and the necessity for knowing both $T_{t,l}$ and $p_{t,l}$ before the magnitude of the deviation from ideality can be determined.

The relationship between $\rho_l/\rho_{t,l}$ and $1 - (V/V_l)^2$ is shown in figure 21. The relative positions of these curves are the same as for the relationship between $(V_l/V)^2$ and $1/M^2$ (fig. 20). In other words, the condition given by $T_{t,l} = 4,770^\circ$ R and $p_{t,l} = 100$ atm shows the greatest deviation from ideality, and so forth. The important difference between the two relationships is that the deviations from ideality for the curves of $(V_l/V)^2$ against $1/M^2$ are greatest in the region of $M = 1$ in the nozzle and tend to become very small as M_l becomes large (fig. 20); whereas, the deviations for the curves of $\rho_l/\rho_{t,l}$ against $1 - (V/V_l)^2$ are small in the throat region and increase with continual expansion to a point at which the percent deviation becomes constant (fig. 21). Therefore, the deviation from ideality caused by the combination of these two effects cannot be determined without calculating the inviscid contour for both cases.

In order to show the combined effect of the deviations, a contour for a Mach number 12 axisymmetric nozzle with $T_{t,l} = 2,790^\circ$ R and $p_{t,l} = 300$ atm was calculated and compared with the calculated ideal

contour. These conditions were chosen because they were representative of the operating conditions for a nozzle under construction at the Langley Research Center. Equations (10) and (11) were used for the ideal calculation. The relationships between $(V_l/V)^2$ and $1/M^2$ and between $\rho_1/\rho_{t,1}$ and $1 - (V/V_l)^2$ for the real-gas case were determined by successive approximations to the curves shown in figures 20 and 21 for $T_{t,1} = 2{,}790^\circ$ R and $p_{t,1} = 300$ atm. The curve for the first relationship was divided into four segments and each segment was found to be represented by an equation of the form,

$$(V_l/V)^2 = K_1 + K_2(1/M^2) + K_3(K_4 \pm 1/M^2)^m \tag{14}$$

where K_1, K_2, K_3, K_4, and m are constants. (Note that when $K_1 = 1$, $K_2 = 5$, and $K_3 = K_4 = m = 0$, eq. (14) reduces to eq. (10), the ideal relationship.)

The curve for $\rho_1/\rho_{t,1}$ as a function of $1 - (V/V_l)^2$ was divided into three segments with each segment giving the general form,

$$\rho_1/\rho_{t,1} = \left\{K_5 + K_6 \log\left[1 - (V/V_l)^2\right]\right\}\left[1 - (V/V_l)^2\right]^n + K_7 \tag{15}$$

where K_5, K_6, K_7, and n are constants. (Note that when $K_5 = 1$, $n = 5/2$, and $K_6 = K_7 = 0$, eq. (15) reduces to eq. (11), the ideal relationship.)

The constants determined for equations (14) and (15) are presented in the following tables:

Constants for equation (14)

Limits	K_1	K_2	K_3	K_4	m
$1.0 \geqq 1/M^2 > 0.5$	1.0	4.960	0.320	0	0.892
$0.5 \geqq 1/M^2 \geqq 0.25$	.9611	5.414	-.2665	-.25	2.02
$0.25 > 1/M^2 \geqq 0.09$	.9611	5.414	5.28	.25	3.65
$0.09 > 1/M^2 > 0$	1.0	4.960	16.25	0	3.14

Constants for equation (15)

Limits	K_5	K_6	K_7	n
$1.0 \geqq \left[1 - \left(V/V_l\right)^2\right] \geqq 0.45$	1.0	0	0.0013	2.625
$0.45 > \left[1 - \left(V/V_l\right)^2\right] \geqq 0.24$	.943	.0903	0	2.5
$0.24 > \left[1 - \left(V/V_l\right)^2\right] > 0$	.868	-.0312	0	2.5

Ferri (ref. 5, p. 264) presents the general characteristics equations which are independent of an equation of state. These equations were used with equations (14) and (15) for the real-gas contour calculation. Both the ideal-gas and real-gas contours were calculated by assuming a radial flow region and a center-line Mach number distribution as presented in reference 6. These calculations were carried out on an IBM 704 electronic data processing machine. The Mach number at the final Mach lines for both ideal-gas and real-gas cases was 12.0 and the flow angle at the inflection point in both cases was 12°.

The results of these calculations are shown in figure 22. The radial distance from the nozzle center line, y/y^* at a given x/y^*, for the real-gas contour is always less than the ideal contour upstream of the inflection point and continues to be so until a point beyond which the two contours cross. Beyond this point the real-gas contour gives a value for y/y^* which is larger than the corresponding point for the ideal case. This change in the direction of the deviation from the ideal calculation along the nozzle is due to the combined effects discussed previously. The degree to which the inviscid contour will vary from the ideal calculation at any given point can, in general, be determined only by carrying out the complete calculation for the inviscid nozzle contour. The deviation in the test section, however, may be determined directly from figure 18.

It is interesting to compare the area ratios for the real-gas and ideal-contours. Since y/y^* at the throat for both cases is unity, the area ratio is given by $(y/y^*)^2$ at the test section. The values for y/y^* at the test section for the real-gas and ideal-gas cases are 37.5 and 35.8, respectively. The quotient of the real-gas area ratio and the ideal-gas area ratio $\dfrac{\left(A_1/A^*\right)}{\left(A_1/A^*\right)_i}$ is, therefore, $(37.5/35.8)^2$ or 1.10. This value is that which would be obtained from figure 18 and is a check for the end points of this calculation.

CONCLUDING REMARKS

Correction factors for the flow-parameter ratios for air as a real gas in chemical equilibrium of Mach numbers 10 and greater have been calculated and show a pressure dependency in addition to the temperature effect. For example, the correction for the ratio of static free-stream temperature to stagnation temperature at 3,510° R is 13 percent when operating at 40 atm but is 18 percent at 1,000 atm. Correction factors for the various flow parameters are presented in chart form for stagnation temperatures from 2,790° R to 4,950° R and pressures from 40 atm to 1,000 atm. The highest Mach number for a given set of stagnation conditions for which calculations were made was that limited by condensation. The method by which these correction factors were calculated is included and may be used with the supplementary charts of thermodynamic properties for additional calculations as desired.

A method for calculating an inviscid hypersonic nozzle contour for air as a real gas in chemical equilibrium has been presented. As an example, a Mach number 12 nozzle contour operating at a stagnation pressure of 300 atm and temperature of 2,790° R was calculated for air as a real gas and compared with the ideal calculated nozzle. The two calculated contours are distinctly different. The real-gas contour gives cross-sectional areas which are less than the ideal-gas contour in the throat region but larger than ideal beyond the inflection point. The maximum deviation occurs in the test section where the real-gas contour is 10 percent greater than the ideal contour.

Langley Research Center,
National Aeronautics and Space Administration,
Langley Field, Va., November 24, 1959.

APPENDIX

EXTENSION OF CHARTS OF THERMODYNAMIC PROPERTIES FOR AIR

The data of Hilsenrath, et al. (ref. 2) for entropy, enthalpy, compressibility factor, and velocity of sound were used in the pressure range from 0.01 atm to 100 atm to prepare the supplementary thermodynamic charts. In reference 7 are calculated the thermodynamic properties for air for pressures near the saturated vapor line to pressures considerably above 100 atm; however, dissociation is not considered. Since there is negligible dissociation for $T \leqq 4{,}950^\circ$ R and $p \geqq 100$ atm, it appears that the thermodynamic properties of reference 2 could be extended simply by adjusting the data of reference 7 at 100 atm for a given temperature to match the data of reference 2 at 100 atm at the same temperature. Then this adjusted data of reference 7 could be used as an extension of reference 2 above 100 atm. The data of reference 7 were not used in this report, however, partly because of a discrepancy in the virial coefficients in the equation

$$Z = 1 + \alpha\rho + \beta\rho^2 \tag{A1}$$

which is used to calculate the thermodynamic properties for air. The coefficients α and β are functions only of temperature. The values for α and β used in reference 2 are presented only up to $2{,}700^\circ$ R. At this temperature, the value of α in reference 7 is 6 percent greater than that in reference 2 and the value of β is 32 percent greater. Another reason for not using the data of reference 7 was that density and temperature are used as independent variables; this would be inconvenient for constructing the present charts.

The pressure virial coefficients B and C for nitrogen are tabulated in reference 2 for temperatures up to and beyond $4{,}950^\circ$ R for the equation of state:

$$Z = 1 + Bp + Cp^2 \tag{A2}$$

where B and C are functions only of temperature.

The virial coefficients in equation (A2) for nitrogen may be used to calculate the coefficients for air when the empirical principle of corresponding states is applied. This principle states that a universal equation of state exists for all substances when the state variables are expressed as reduced quantities. (See ref. 8 for a detailed discussion of this principle.)

The reduced quantities p_r, ρ_r, and T_r are defined as

$$\left.\begin{aligned} p_r &= \frac{p}{p_c} \\ \rho_r &= \frac{\rho}{\rho_c} \\ T_r &= \frac{T}{T_c} \end{aligned}\right\} \qquad (A3)$$

where p_c, ρ_c, and T_c are the pressure, density, and temperature at the critical point. This principle suggests that the value of Z calculated from equation (A2) will be the same for air as for nitrogen when both T_r and p_r are the same for air and nitrogen provided that Z_c, the compressibility factor at the critical point, is the same for the two gases. The values of Z at the critical point for nitrogen, oxygen, argon, and carbon dioxide from reference 9 along with the composition of air as given in reference 2 are as follows:

	Z_c	Percentage of air
N_2 . . .	0.291	78.09
O_2 . . .	0.290	20.95
A . . .	0.290	0.93
CO_2 . . .	0.275	0.03

These values indicate that Z_c for air should be very close to Z_c for nitrogen. The value of Z_c of 0.275 for CO_2 has very little effect on the value for air because it is present in such a small quantity. In addition to this, nitrogen and oxygen which make up more than 99 percent of the air are very similar in size and structure. This tends to make the principle of corresponding states more applicable.

The coefficients B and C of equation (A2) are tabulated for nitrogen for a series of temperatures in reference 2. The temperature of air which corresponds to the tabulated temperature for nitrogen of reference 2 for the same reduced temperature is obtained by the following procedure. Let the temperature of air be T_A and of nitrogen T_N. From equation (A3),

$$\left.\begin{aligned} T_{r,A} &= \frac{T_A}{T_{c,A}} \\ T_{r,N} &= \frac{T_N}{T_{c,N}} \end{aligned}\right\} \tag{A4}$$

Since $T_{r,A} = T_{r,N}$ at the same reduced temperature,

$$T_A = T_N\left(\frac{T_{c,A}}{T_{c,N}}\right) \tag{A5}$$

In other words, the temperature of air corresponding to nitrogen for the same reduced temperature is obtained by multiplying the tabulated nitrogen temperature by the ratio of the critical temperatures for air and nitrogen. Reference 10 gives T_c for air as equal to 238.34° R and reference 2 gives T_c for nitrogen as 227.04° R. The tabulated nitrogen temperatures were therefore multiplied by the ratio $238.34/227.04$ to find the corresponding air temperature.

Since the pressure as well as the temperature is required, in general, to determine the state of a gas, the reduced pressure for air must also be set equal to that for nitrogen. This was done in a manner similar to that for the temperature:

$$\left.\begin{aligned} p_{r,A} &= \frac{p_A}{p_{c,A}} \\ p_{r,N} &= \frac{p_N}{p_{c,N}} \end{aligned}\right\} \tag{A6}$$

Since $p_{r,A} = p_{r,N}$ at the same reduced pressure,

$$p_N = p_A\left(\frac{p_{c,N}}{p_{c,A}}\right) \tag{A7}$$

It also follows from equation (A7) that

$$p_N^2 = p_A^2\left(\frac{p_{c,N}}{p_{c,A}}\right)^2 \tag{A8}$$

The virial equation of state for air as determined from B_N and C_N for nitrogen at a given nitrogen temperature is obtained from combining equations (A2), (A7), and (A8) to get

$$Z_A = 1 + B_N\left(\frac{p_{c,N}}{p_{c,A}}\right)p_A + C_N\left(\frac{p_{c,N}}{p_{c,A}}\right)^2 p_A^2 \qquad \text{(A9)}$$

and remembering from equation (A5) that $T_A = \left(\frac{238.34}{227.04}\right)T_N$. Nitrogen temperature T_N is the temperature at which B_N and C_N are tabulated in reference 2.

Reference 10 gives p_c for air as 37.25 atm and reference 2 gives p_c for nitrogen as 33.49 atm. It follows that

$$\left.\begin{aligned} B_A &= \frac{33.49}{37.25} B_N \\ C_A &= \frac{(33.49)^2}{(37.25)^2} C_N \end{aligned}\right\} \qquad \text{(A10)}$$

The values of B_A and C_A calculated from equation (A10) were plotted against the temperature T_A as determined from equation (A5) to determine B and C for air at the desired temperature which corresponds to the intervals of 90° R of reference 2.

The values of B and C for air as determined from equation (A10) were checked by comparing the values of $Z_A - 1$ as calculated by equation (A9) at several temperatures and 100 atm with the tabulated values of $Z_A - 1$ from reference 2. The two results differ by less than 1.5 percent for $T \leq 4{,}500^\circ$ R. The difference is somewhat larger for $T > 4{,}500^\circ$ R and approaches no more than 4.5 percent at $4{,}950^\circ$ R. From these calculations it is felt that the entropy, enthalpy, compressibility-factor, and velocity-of-sound data for air may be extended with reasonable certainty above 100 atm by using the modified nitrogen data and the foregoing method.

The enthalpy for $100 \leq p \leq 1{,}000$ atm was calculated in the following manner. It can be shown that

$$\left(\frac{\partial H}{\partial p}\right)_T = -\frac{RT^2}{p}\left(\frac{\partial Z}{\partial T}\right)_p \tag{A11}$$

Differentiating equation (A2) at constant pressure gives

$$\left(\frac{\partial Z}{\partial T}\right)_p = p\left(\frac{\partial B}{\partial T}\right)_p + p^2\left(\frac{\partial C}{\partial T}\right)_p \tag{A12}$$

Combining equations (A11) and (A12) and remembering that the coefficients B and C are functions only of temperature yields

$$\left(\frac{\partial H}{\partial p}\right)_T = -RT^2\left[\left(\frac{dB}{dT}\right) + p\left(\frac{dC}{dT}\right)\right] \tag{A13}$$

Multiplying through by dp and integrating from p = 100 atm to p at constant temperature T yields

$$H_p - H_{p=100} = -RT^2\left[(p - 100)\left(\frac{dB}{dT}\right) + \frac{1}{2}\left(p^2 - 10{,}000\right)\left(\frac{dC}{dT}\right)\right] \tag{A14}$$

Transposing and dividing through by RT_o gives the enthalpy at a given temperature T and pressure p:

$$\frac{H}{RT_o} = \left(\frac{H}{RT_o}\right)_{p=100} - \frac{T^2}{T_o}\left[(p - 100)\left(\frac{dB}{dT}\right) + \frac{1}{2}\left(p^2 - 10{,}000\right)\left(\frac{dC}{dT}\right)\right] \tag{A15}$$

The values for dB/dT and dC/dT were determined graphically from the plots of B and C against temperature. The enthalpy charts were extended above 100 atm at the various temperatures by using equation (A15), the values of dB/dT and dC/dT, and the values of $(H/RT_o)_{p=100}$ from reference 2.

From the well-known expression,

$$T\,dS + v\,dp = dH \tag{A16}$$

(where v is specific volume, lb/cu ft) it can be shown in like manner that the entropy at a given temperature and pressure above 100 atm is given by

$$\frac{S}{R} = \left(\frac{S}{R}\right)_{p=100} + T\left[\left(-\frac{dB}{dT}\right)(p - 100) + \frac{1}{2}\left(-\frac{dC}{dT}\right)\left(p^2 - 10{,}000\right)\right]$$

$$- \left[\log_e\left(\frac{p}{100}\right) + B(p - 100) + \frac{1}{2}\,C\left(p^2 - 10{,}000\right)\right] \qquad \text{(A17)}$$

Equation (A17) was used with the values of $(S/R)_{p=100}$ from reference 2 and the calculated values of B and C as a function of temperature to extend the entropy charts above 100 atm.

The velocity of sound was calculated for pressures above 100 atm in much the same way as the enthalpy and entropy. From the three relations,

$$a^2 = \gamma\left(\frac{\partial p}{\partial \rho}\right)_T \qquad \text{(A18)}$$

$$\left(\frac{\partial c_p}{\partial p}\right)_T = -T\left(\frac{\partial^2 v}{\partial T^2}\right)_p \qquad \text{(A19)}$$

and

$$c_p - c_v = T\left(\frac{\partial v}{\partial T}\right)_p\left(\frac{\partial p}{\partial T}\right)_v \qquad \text{(A20)}$$

(where c_p is specific heat at constant pressure, c_v is specific heat at constant volume, and the subscripts T, p, and v are temperature, pressure, and volume, respectively) it can be shown that

$$\frac{a}{a_o} = \frac{1 + Bp + Cp^2}{a_o}\left[\frac{RT\, f_2}{\left(f_2 - f_1\right)\left(1 - Cp^2\right)}\right]^{1/2} \qquad \text{(A21)}$$

where

$$f_1 = 1 + (B + TB')p + (C + TC')p^2$$

$$f_2 = \left(Cp^2 - 1\right)\left\{\left(\frac{c_p}{R}\right)_{p=100} - T\left[(2B' + TB")(p - 100)\right.\right.$$

$$\left.\left. + \left(C' + \frac{1}{2}\,TC"\right)\left(p^2 - 10{,}000\right)\right]\right\}$$

and

$$B' = \frac{dB}{dT}$$

$$B'' = \frac{d^2B}{dT^2}$$

$$C' = \frac{dC}{dT}$$

$$C'' = \frac{d^2C}{dT^2}$$

These calculated values for velocity of sound are tabulated at the end of the supplementary thermodynamic charts.

Below 0.01 atm the ideal gas law was used. The compressibility factor is, of course, 1 or very nearly so in this range. The velocity of sound at pressures below 0.01 atm is a function only of temperature; therefore, the velocity of sound at a given temperature for $p < 0.01$ atm was assumed to be equal to the velocity of sound at the given temperature and 0.01 atm.

The approximate saturated vapor line for air (neglecting carbon dioxide and water vapor) was estimated from the vapor-pressure data of references 2 and 3. Because of the limits of the pressures and temperatures studied herein, the highest temperature at which condensation can occur during an isentropic expansion is about 90° R. Since the triple point for oxygen, 97.9° R, and the triple point for nitrogen, 113.7° R, are both above 90° R, the condensed phase, assuming proper conditions, will be a solid. If the condensed phase is a solid solution of oxygen and nitrogen, the pressure at which condensation of equilibrium air can occur at a given temperature is the vapor pressure of the solid solution. On the other hand, if no solid solution is formed, the pressure at which condensation can occur at a given temperature is the vapor pressure of the pure component which has the greatest ratio of vapor mole fraction divided by vapor pressure. For most conditions this happens to be oxygen. The condensation pressure at a given temperature is greater for the case in which a solid solution is formed than for the case in which no solid solution is formed.

The vapor-pressure line for air may be found approximately for either case from the vapor-pressure data of pure oxygen and pure nitrogen. It is possible, however, in the actual operation of a hypersonic nozzle that the air will become supersaturated. If supersaturation does occur,

the air can in fact condense at a pressure less than that determined by either of the two cases indicated previously. Because of these uncertainties and the fact that only an approximate operational limit is desired, the saturated vapor line was estimated by assuming that the condensed phase will be a solid solution of oxygen and nitrogen. The saturated vapor line estimated in this way is conservative in that it predicts the highest pressure at which an isentropic expansion will encounter condensation.

REFERENCES

1. Bray, K. N. C.: Departure From Dissociation Equilibrium in a Hypersonic Nozzle. A.R.C. 19,983 (British), Mar. 17, 1958.

2. Hilsenrath, Joseph, Beckett, Charles W., et al.: Tables of Thermal Properties of Gases. NBS Cir. 564, U.S. Dept. Commerce, 1955.

3. Aoyama, S., and Kanda, E.: Vapor Tensions of Solid Oxygen and Nitrogen. Tohoku Univ. Sci. and Tech Reps., vol. 24, May 1935, pp. 107-115.

4. Ames Research Staff: Equations, Tables, and Charts for Compressible Flow. NACA Rep. 1135, 1953. (Supersedes NACA TN 1428.)

5. Ferri, Antonio: Elements of Aerodynamics of Supersonic Flows. The MacMillan Co., 1949.

6. Beckwith, Ivan E., Ridyard, Herbert W., and Cromer, Nancy: The Aerodynamic Design of High Mach Number Nozzles Utilizing Axisymmetric Flow With Application to a Nozzle of Square Test Section. NACA TN 2711, 1952.

7. Hall, N. A., and Ibele, W. E.: Thermodynamic Properties of Air, Nitrogen and Oxygen as Imperfect Gases. Tech Paper No. 85, Eng. Exp. Station, Univ. of Minnesota, Dec. 1951.

8. Reid, Robert C., and Sherwood, Thomas K.: The Properties of Gases and Liquids. McGraw-Hill Book Co., Inc., 1958.

9. Hougen, Olaf A., Watson, Kenneth M., and Ragatz, Roland A.: Chemical Process Principles. Part I - Material and Energy Balances. Second ed., John Wiley & Sons, Inc., c.1954.

10. Williams, V. C.: The Thermodynamic Properties of Air at Low Temperatures. Trans. Am. Inst. Chem. Eng., vol. 39, no. 1, Feb. 25, 1943, pp. 93-111.

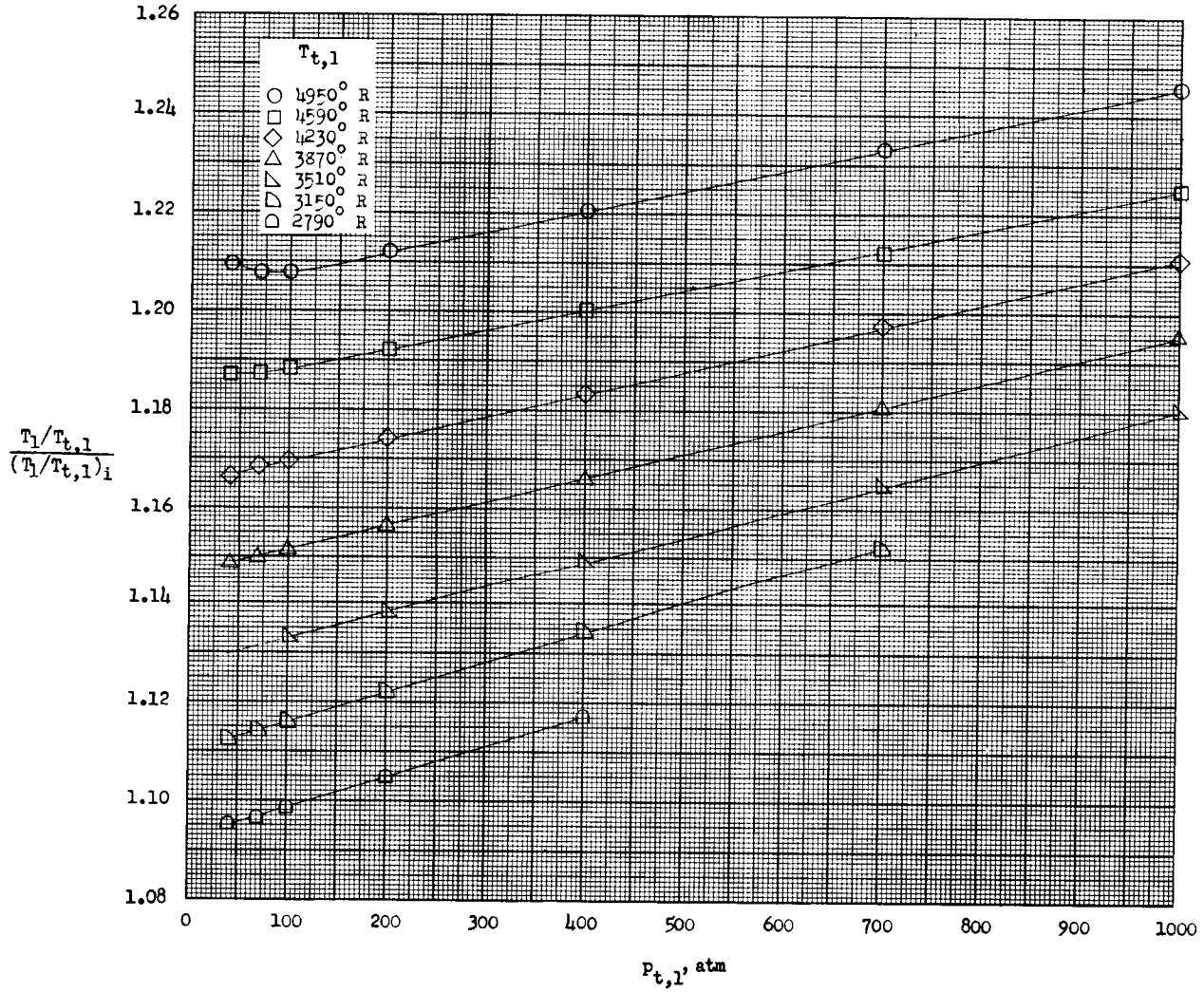

Figure 1.- Correction factor for $T_1/T_{t,1}$ as a function of stagnation pressure for various stagnation temperatures where M_1 is greater than 10.

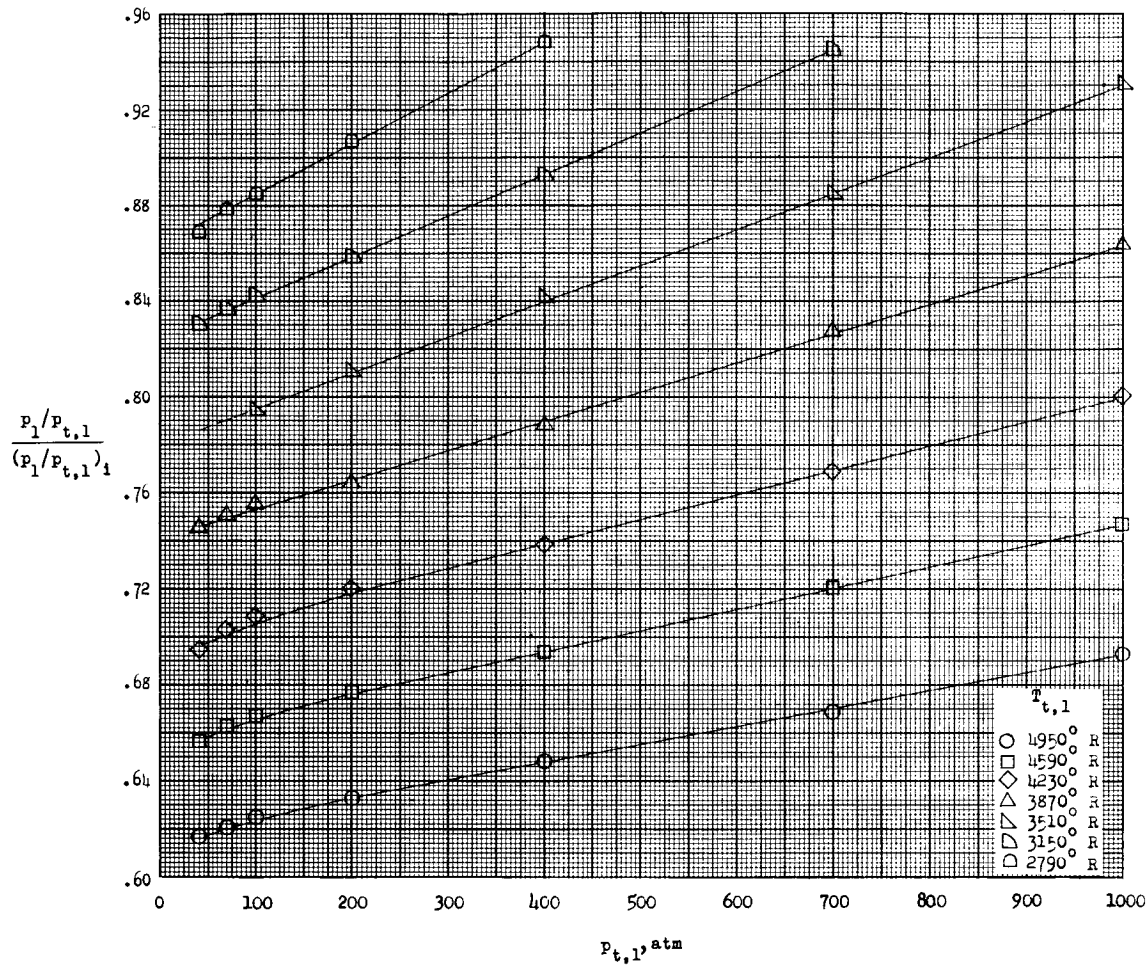

Figure 2.- Correction factor for $p_1/p_{t,1}$ as a function of stagnation pressure for various stagnation temperatures where M_1 is greater than 10.

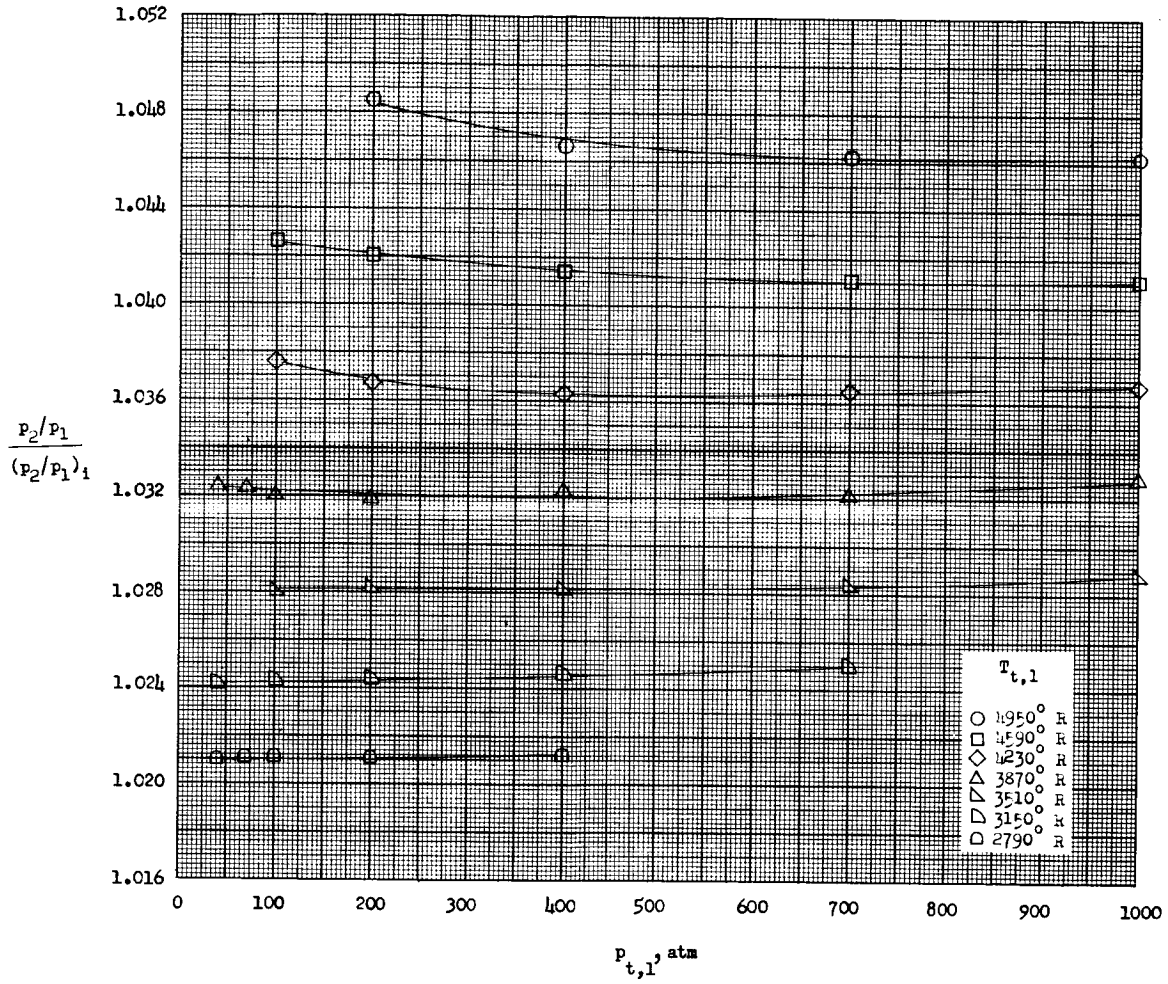

Figure 3.- Correction factor for p_2/p_1 as a function of stagnation pressure for various stagnation temperatures where M_1 is greater than 10.

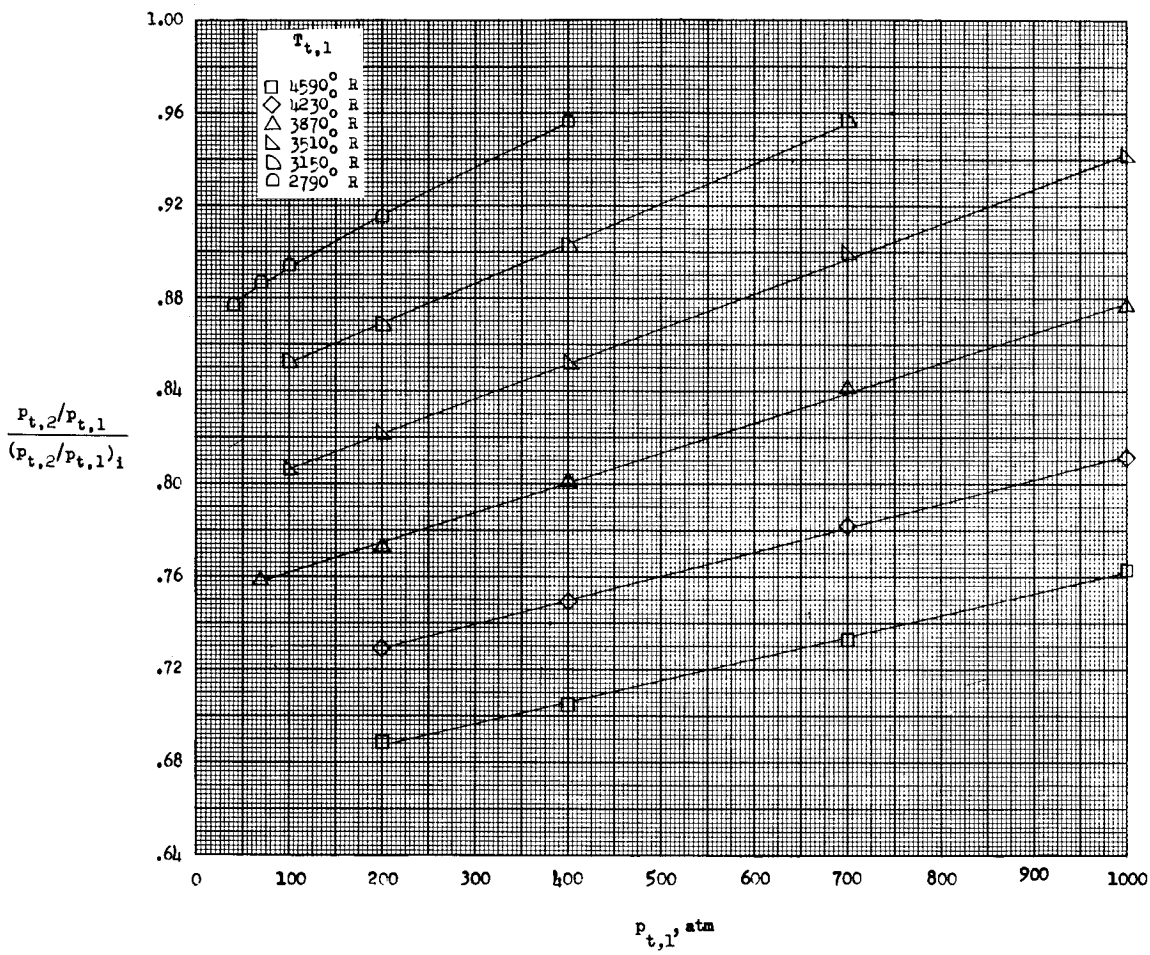

Figure 4.- Correction factor for $p_{t,2}/p_{t,1}$ as a function of stagnation pressure for various stagnation temperatures where M_1 is greater than 10.

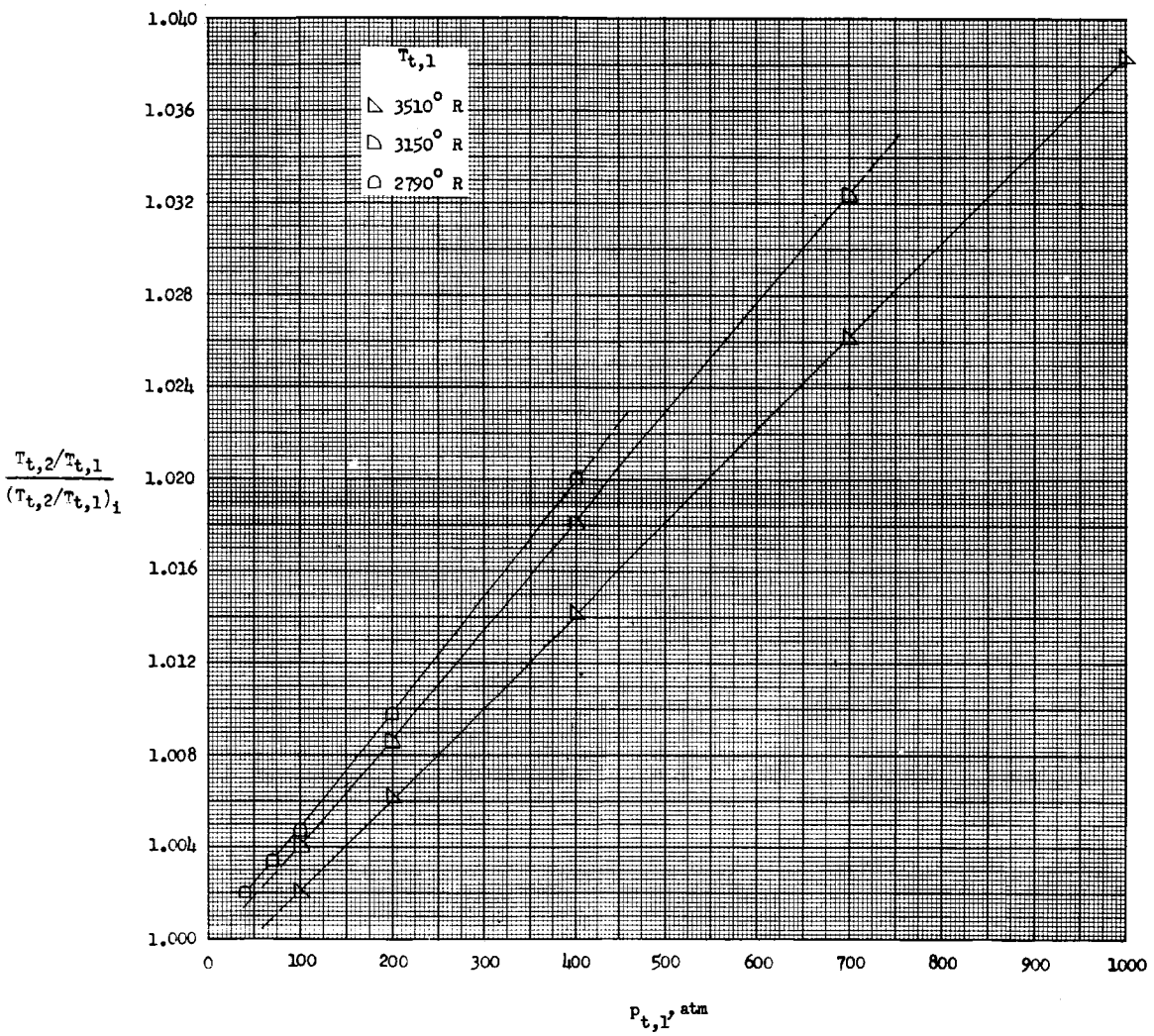

Figure 5.- Correction factor for $T_{t,2}/T_{t,1}$ as a function of stagnation pressure for stagnation temperatures of 2,790° R, 3,150° R, and 3,510° R where M_1 is greater than 10.

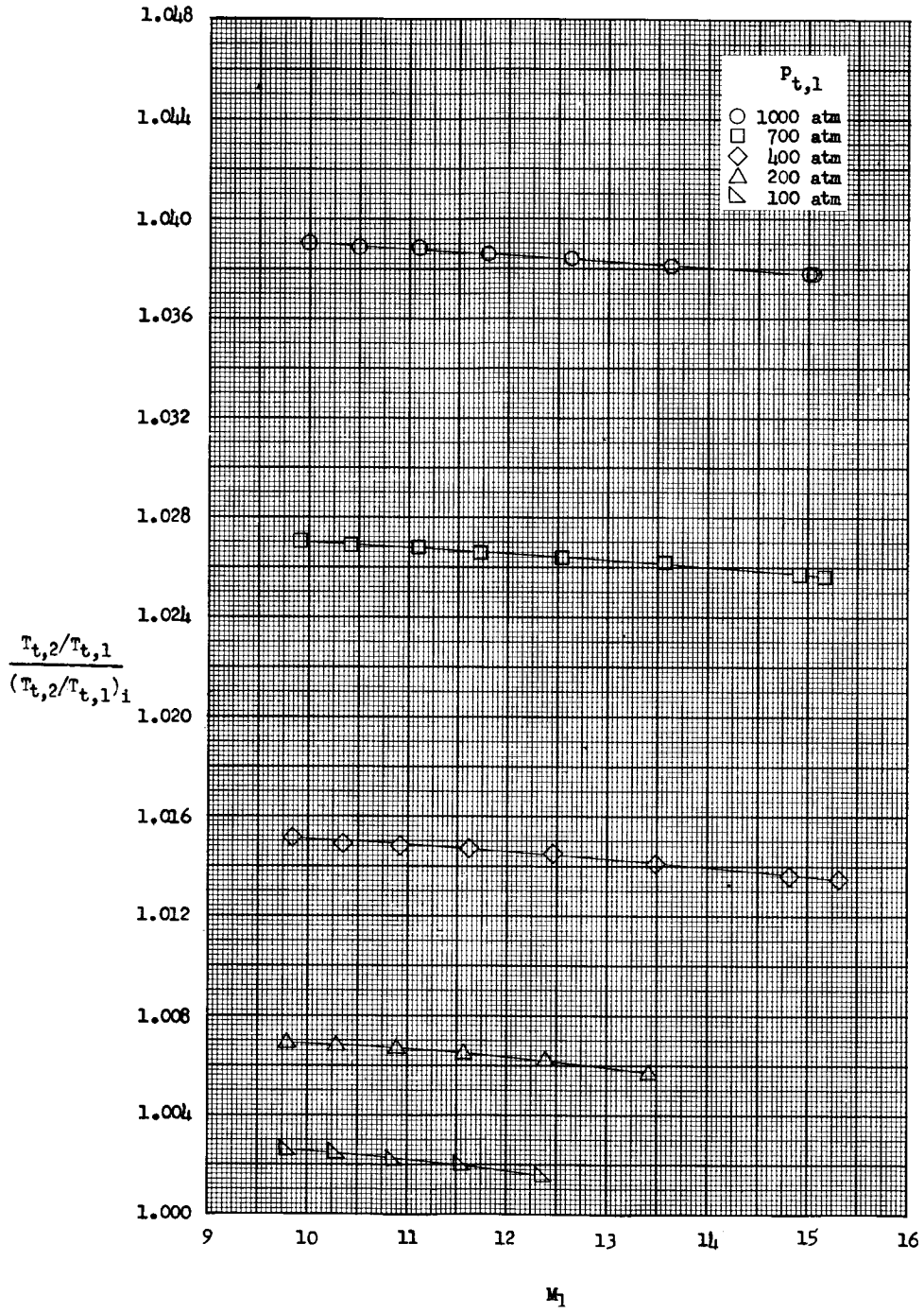

Figure 6.- Correction factor for $T_{t,2}/T_{t,1}$ as a function of M_1 for various stagnation pressures at $T_{t,1} = 3,510^{\circ}$ R.

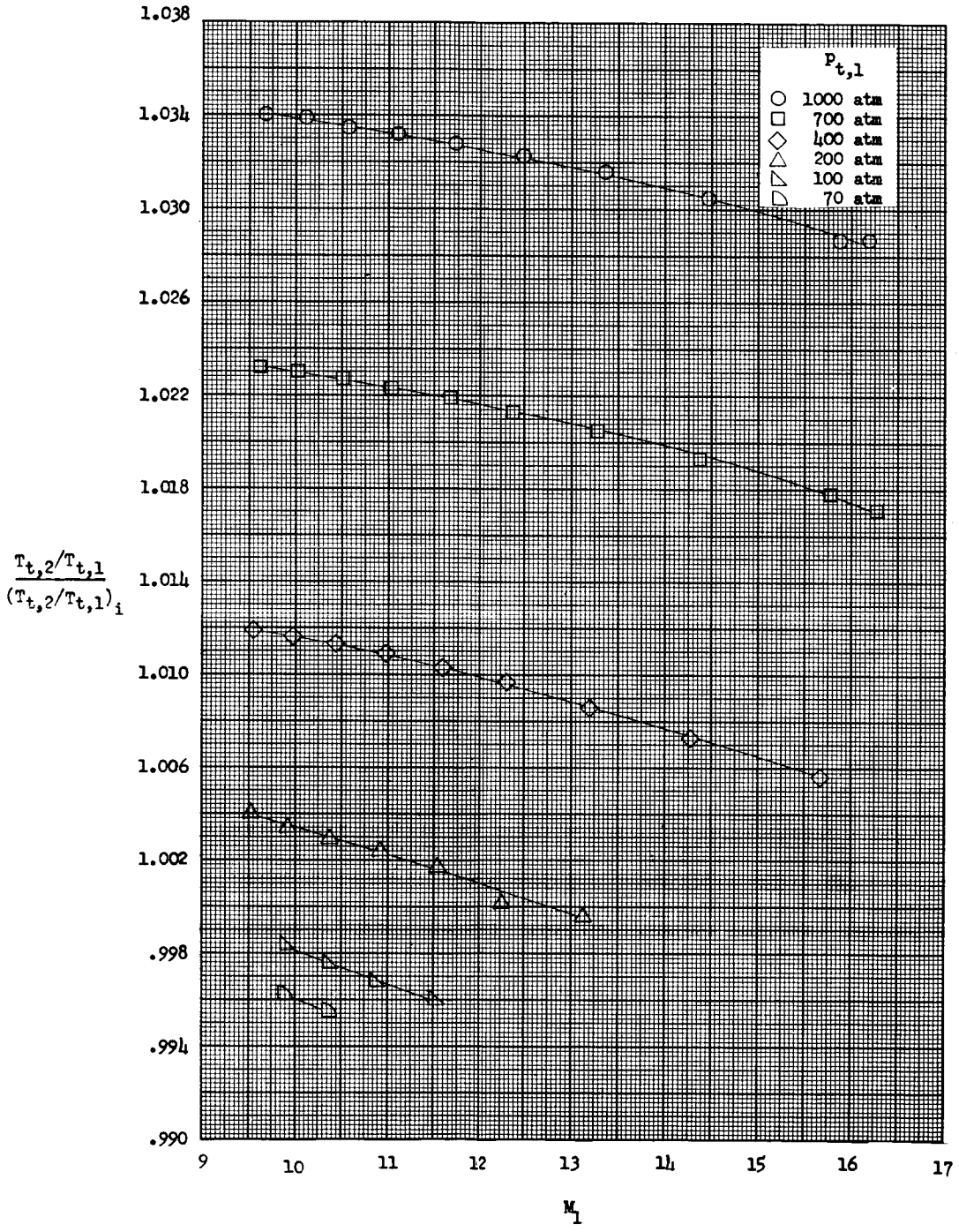

Figure 7.- Correction factor for $T_{t,2}/T_{t,1}$ as a function of M_1 for various stagnation pressures at $T_{t,1} = 3,870^\circ$ R.

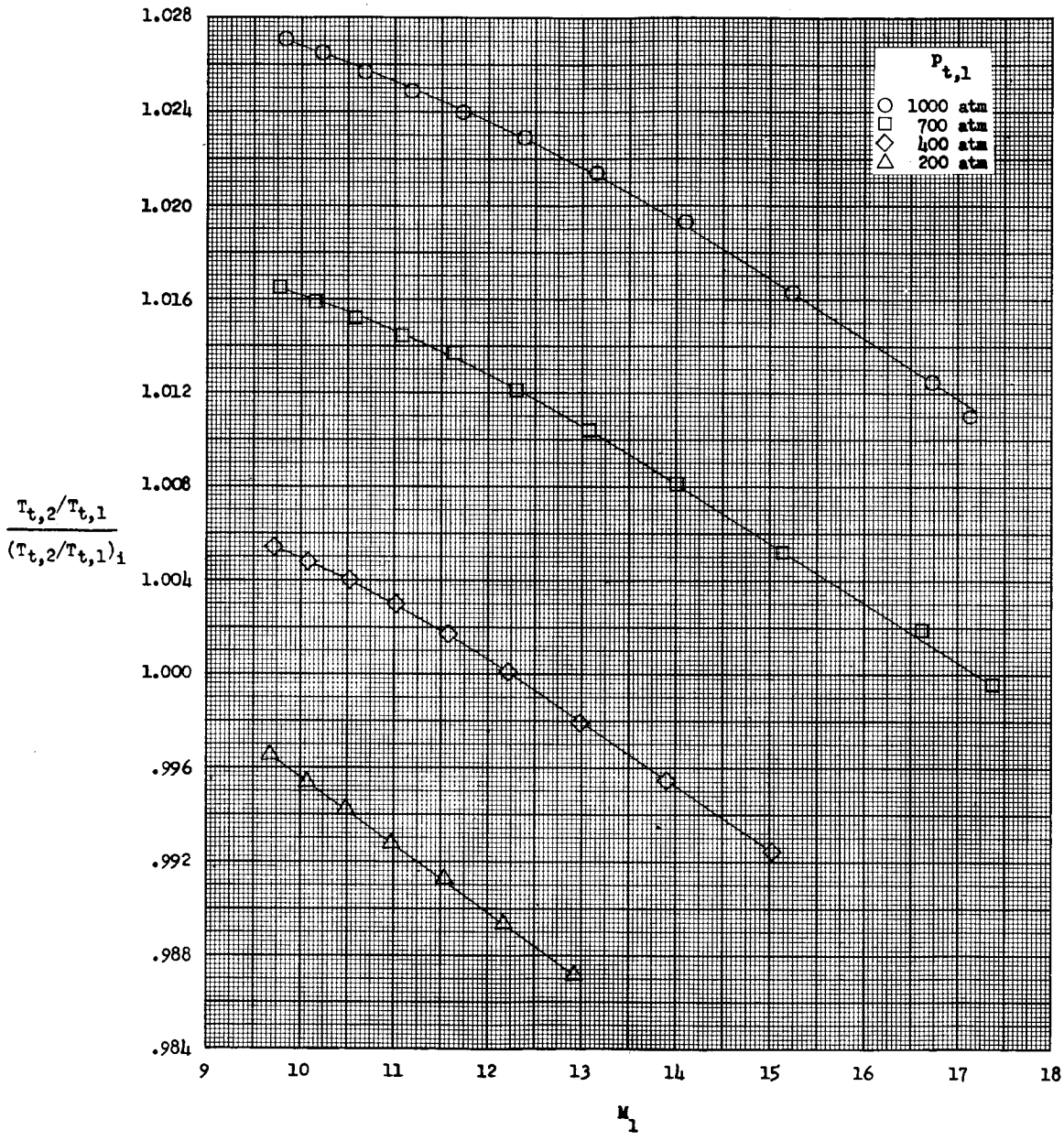

Figure 8.- Correction factor for $T_{t,2}/T_{t,1}$ as a function of M_1 for various stagnation pressures at $T_{t,1} = 4,230^\circ$ R.

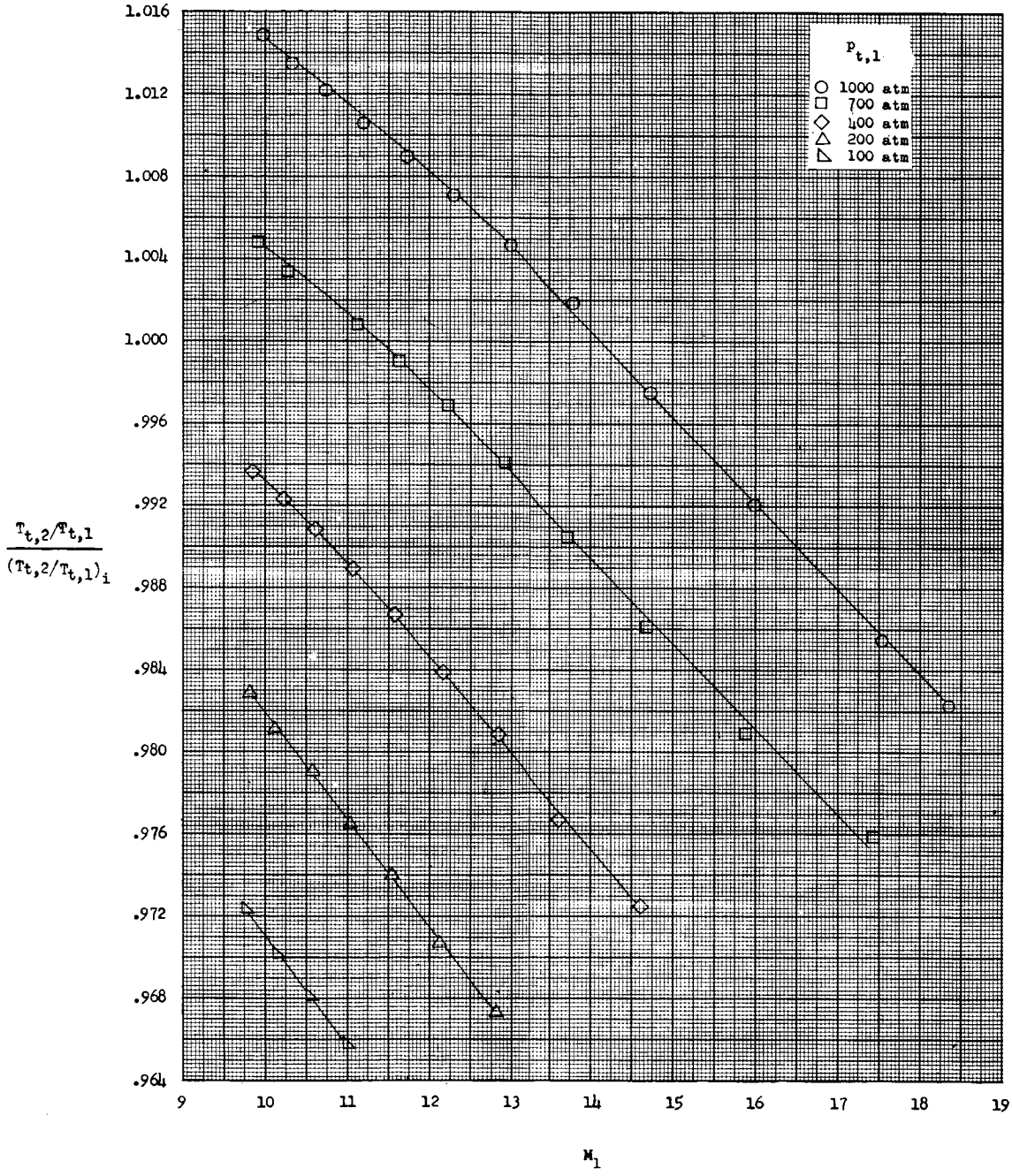

Figure 9.- Correction factor for $T_{t,2}/T_{t,1}$ as a function of M_1 for various stagnation pressures at $T_{t,1} = 4,590^\circ$ R.

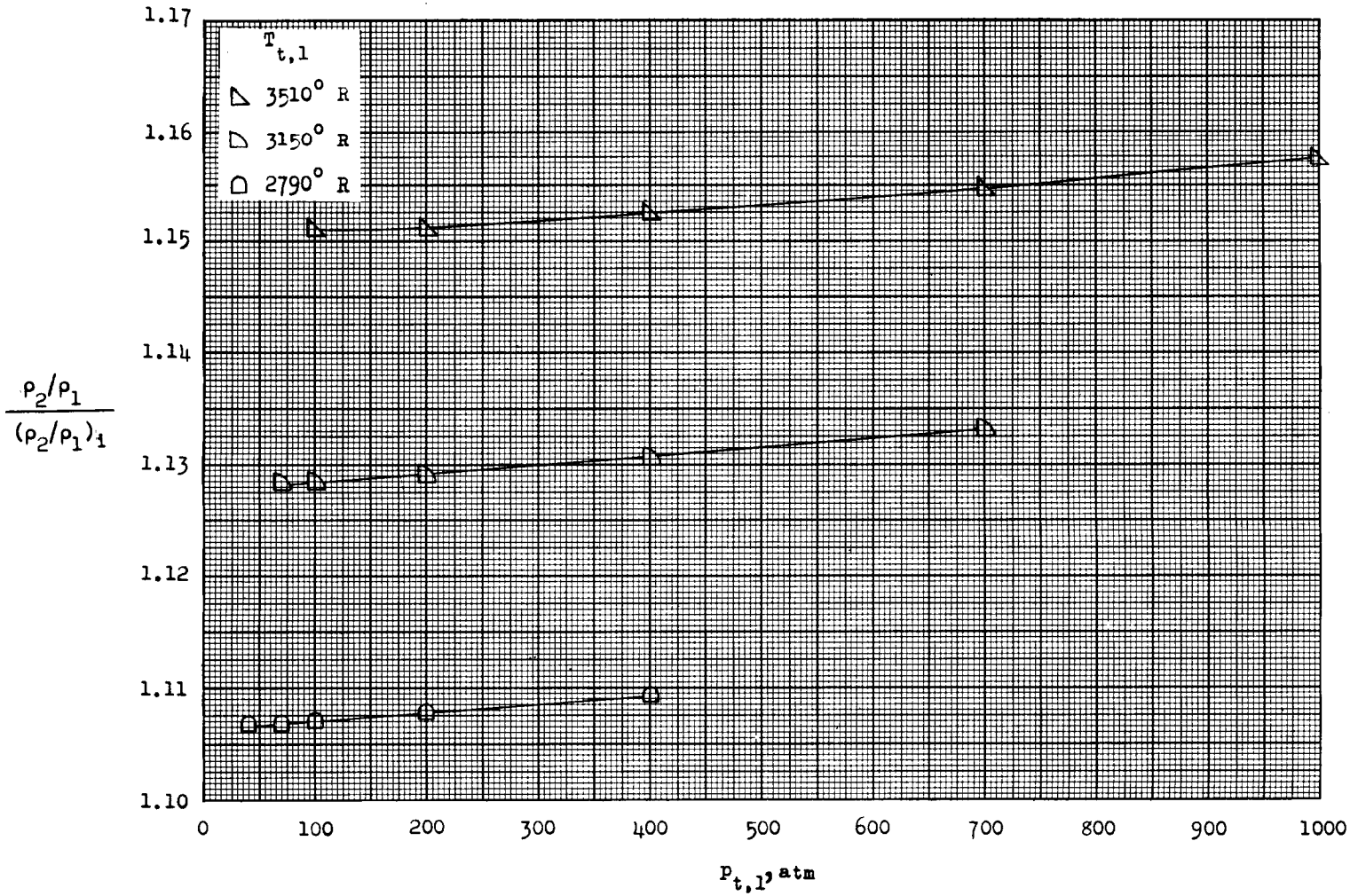

Figure 10.- Correction factor for ρ_2/ρ_1 as a function of stagnation pressure for stagnation temperatures of 2,790° R, 3,150° R, and 3,510° R where M_1 is greater than 10.

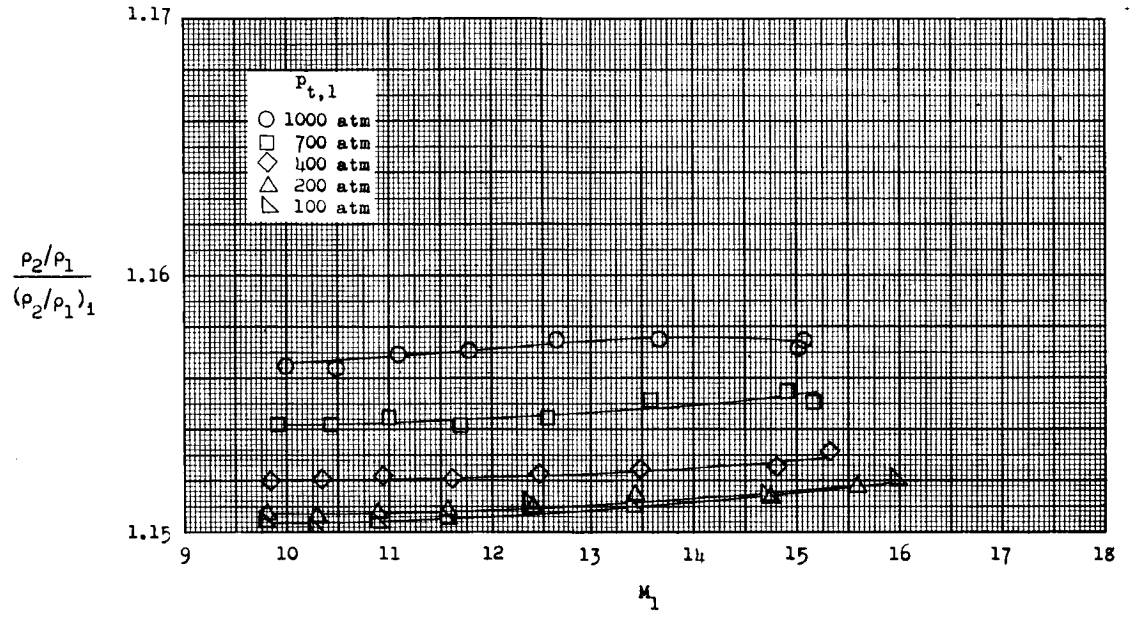

Figure 11.- Correction factor for ρ_2/ρ_1 as a function of M_1 for various stagnation pressures at $T_{t,1} = 3,510^\circ$ R.

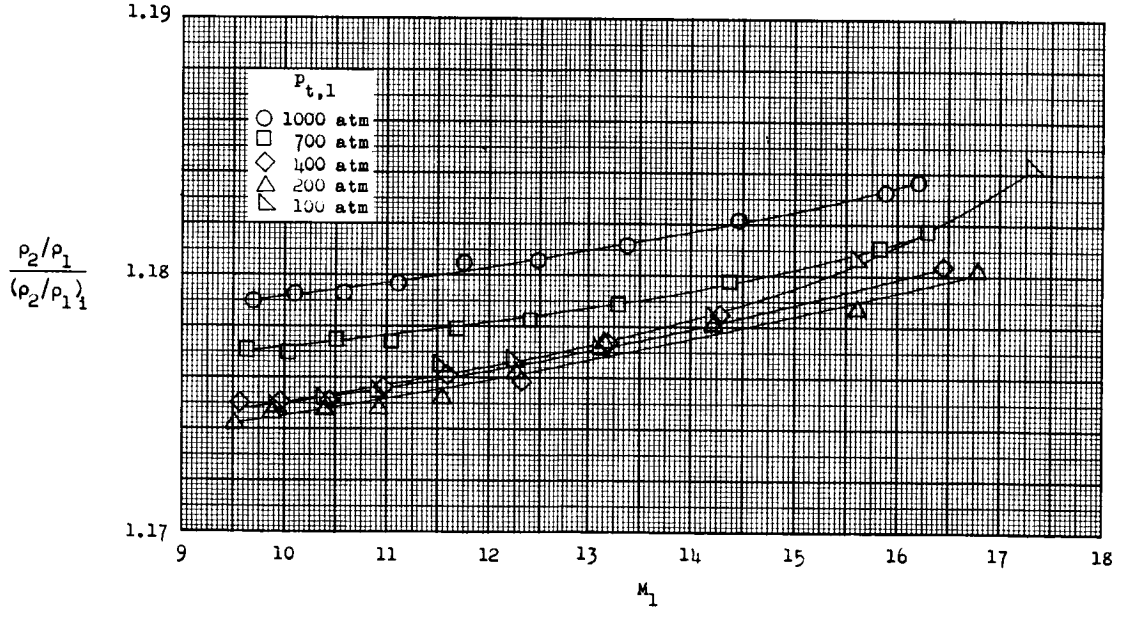

Figure 12.- Correction factor for ρ_2/ρ_1 as a function of M_1 for various stagnation pressures at $T_{t,1} = 3,870^\circ$ R.

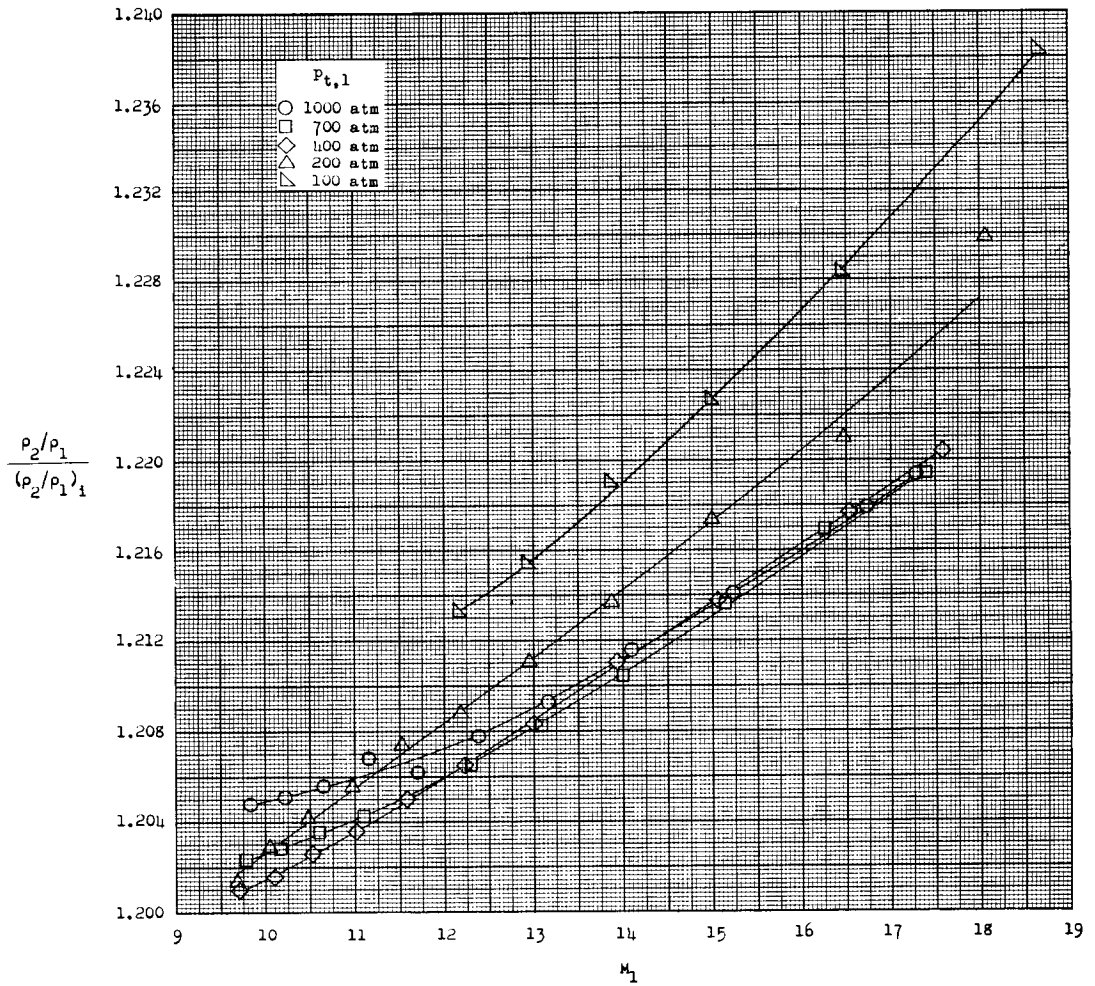

Figure 13.- Correction factor for ρ_2/ρ_1 as a function of M_1 for various stagnation pressures at $T_{t,1} = 4,230^{\circ}$ R.

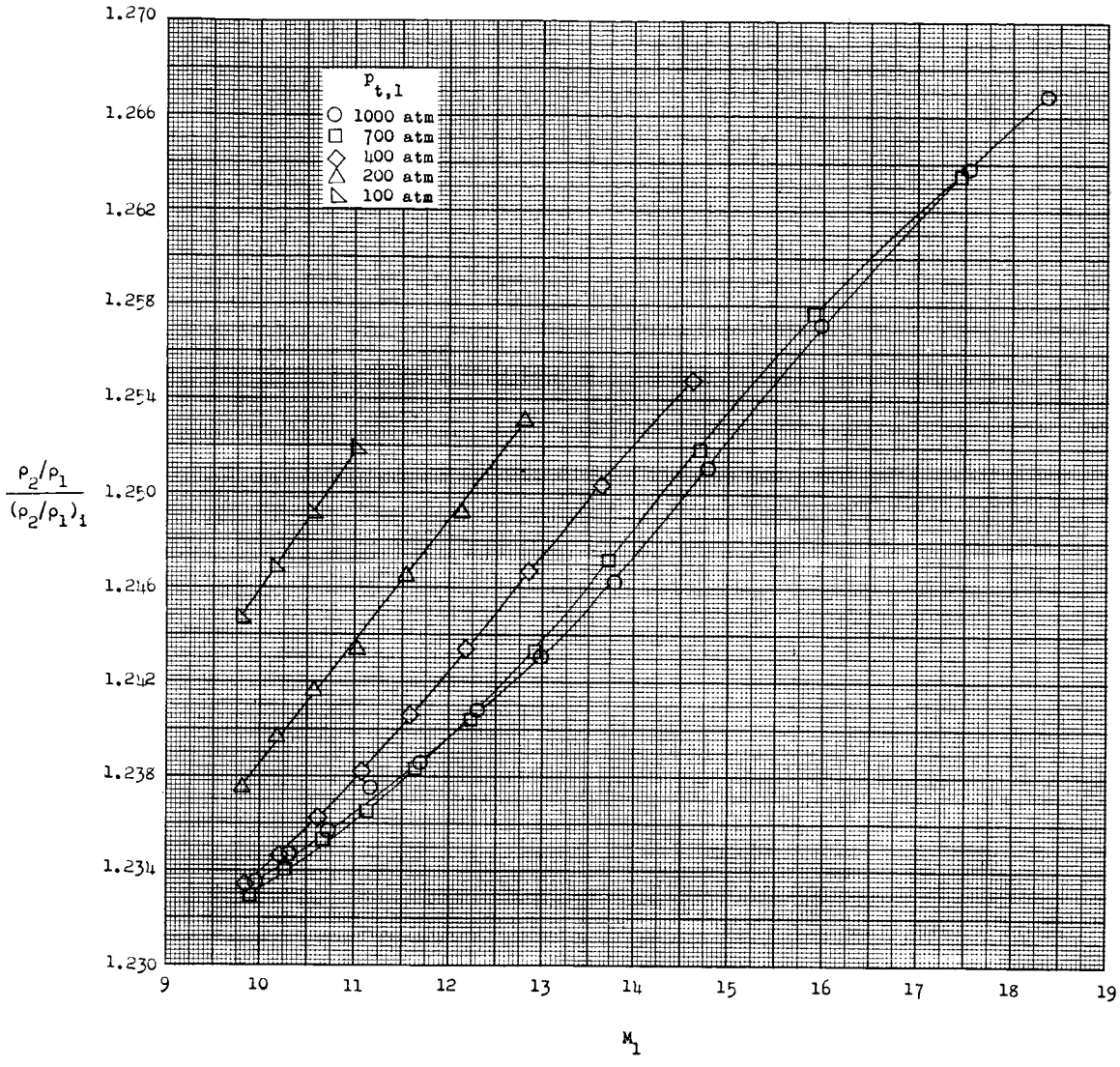

Figure 14.- Correction factor for ρ_2/ρ_1 as a function of M_1 for various stagnation pressures at $T_{t,1} = 4,590^\circ$ R.

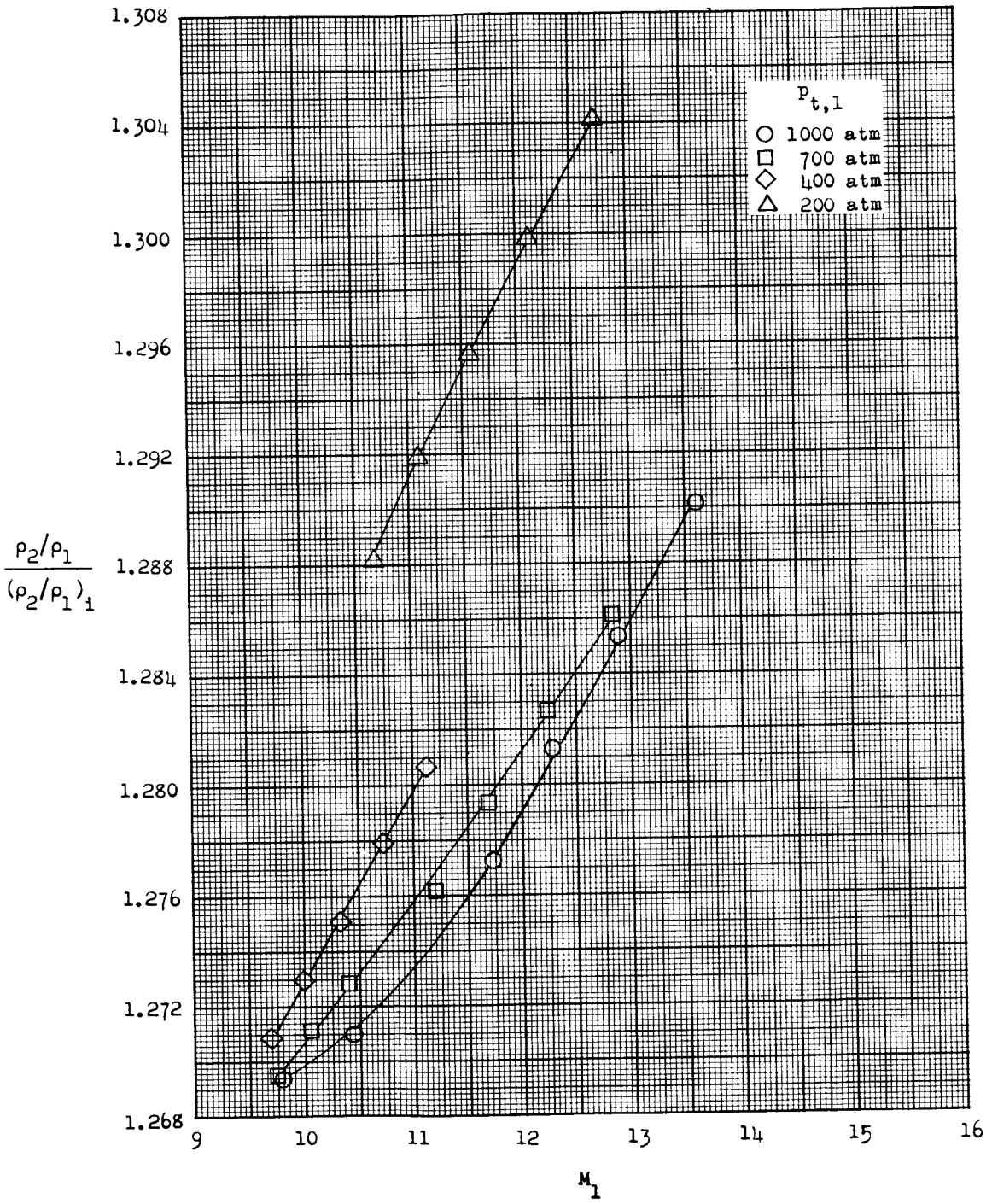

Figure 15.- Correction factor for ρ_2/ρ_1 as a function of M_1 for various stagnation pressures at $T_{t,1} = 4,950^\circ$ R.

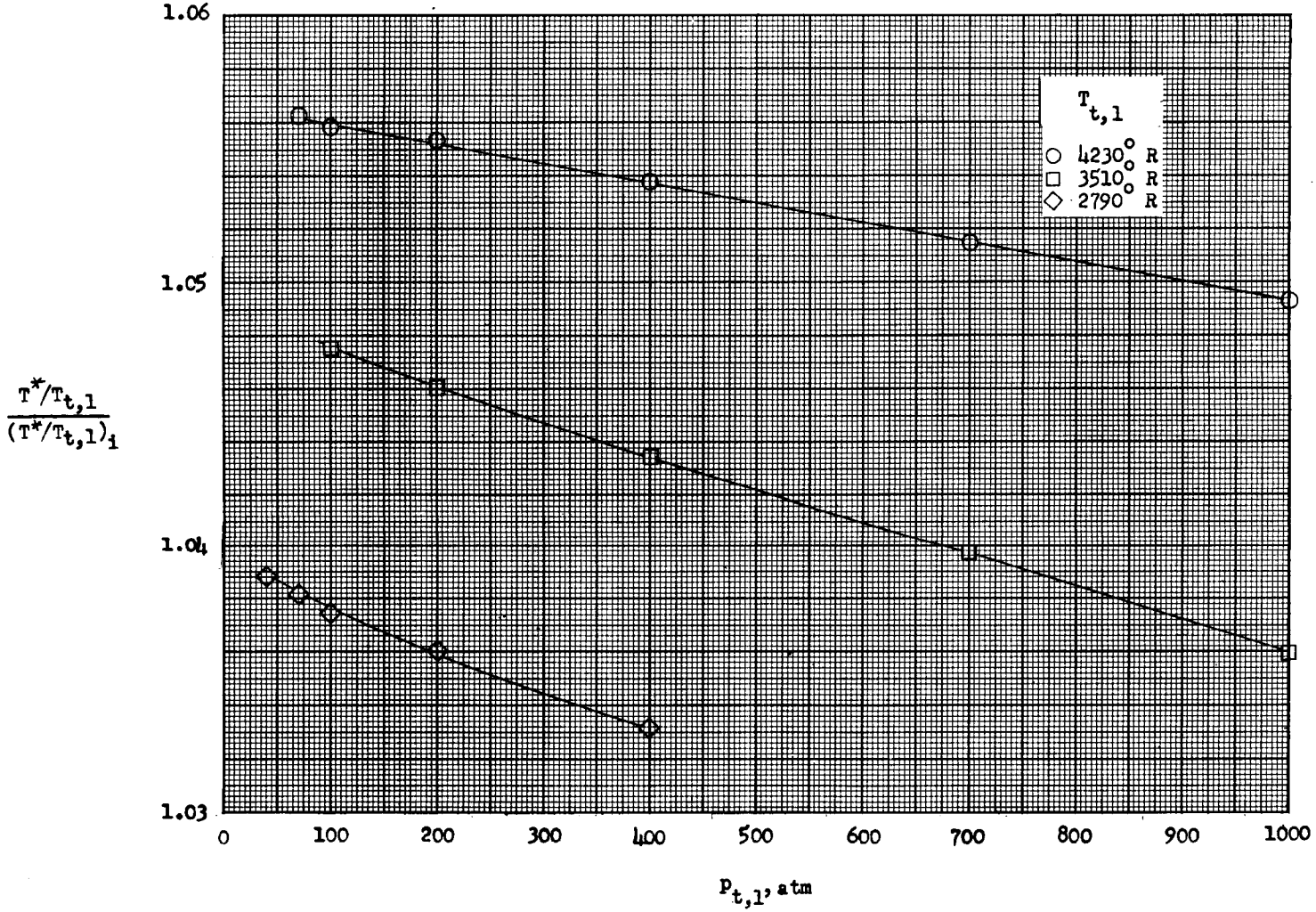

Figure 16.- Correction factor for $T^*/T_{t,1}$ as a function of stagnation pressure for various stagnation temperatures.

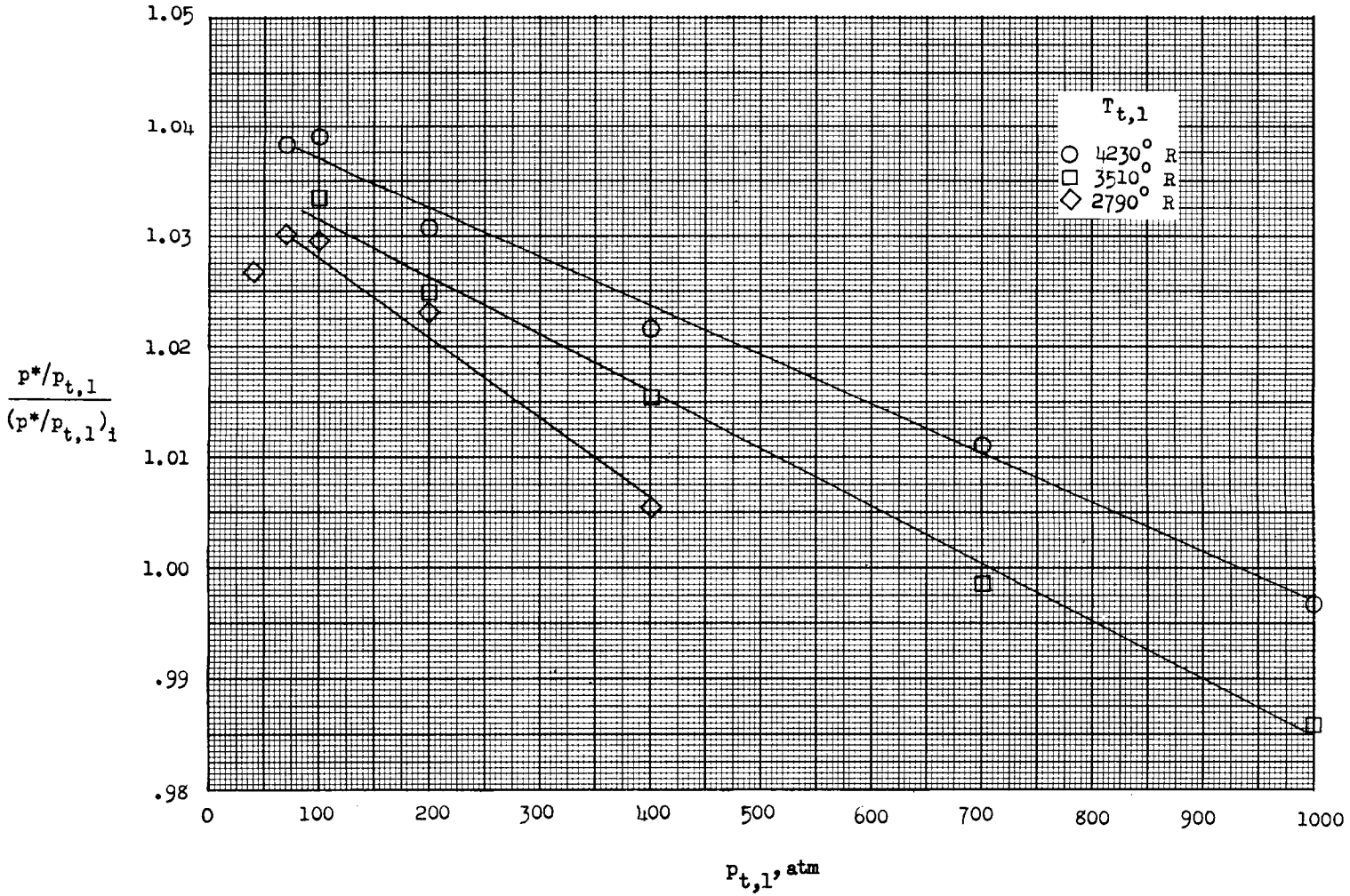

Figure 17.- Correction factor for $p^*/p_{t,1}$ as a function of stagnation pressure for various stagnation temperatures.

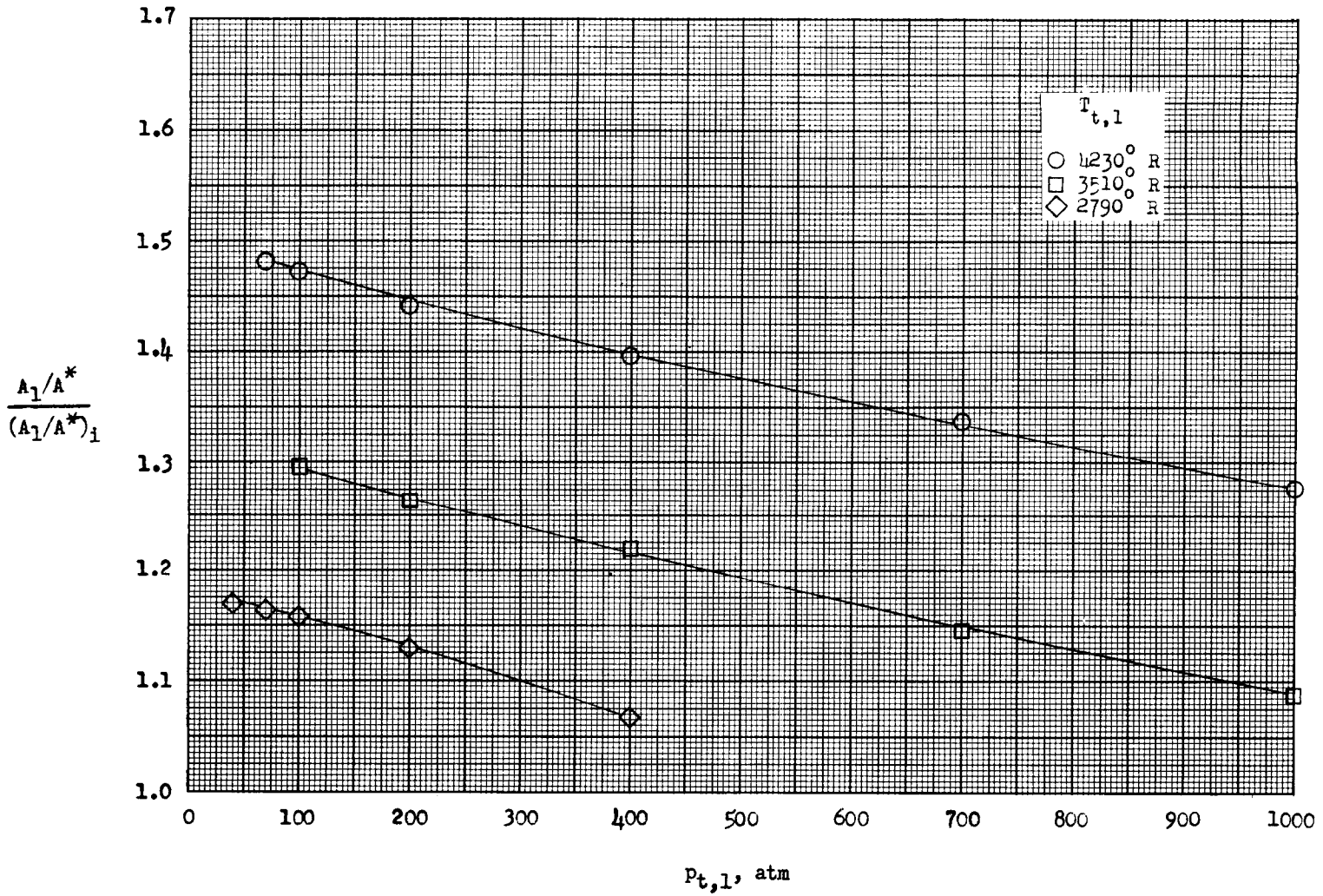

Figure 18.- Correction factor for A_1/A^* as a function of stagnation pressure for various stagnation temperatures where M_1 is greater than 10.

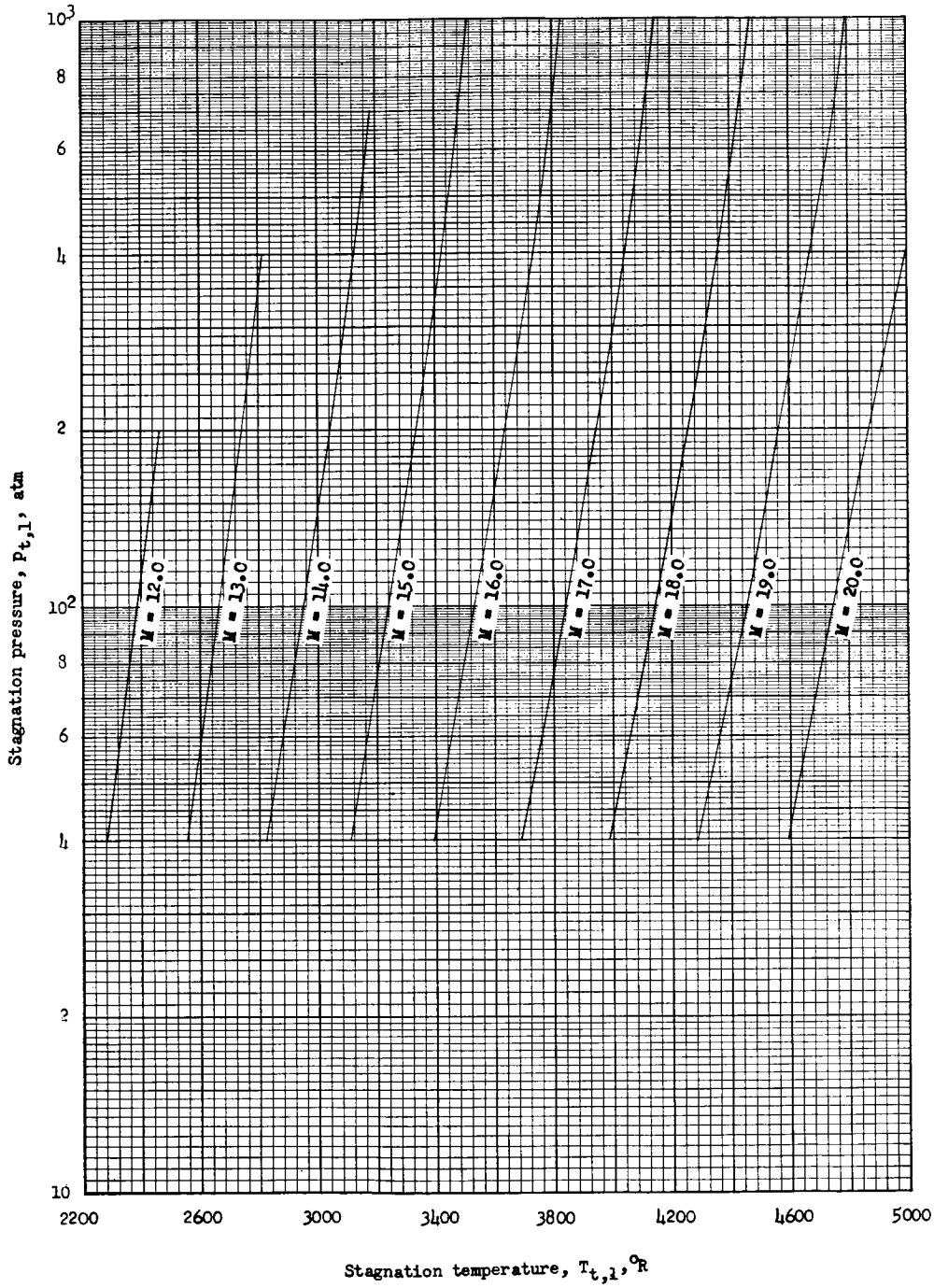

Figure 19.- Approximate combinations of stagnation pressure and temperature at which condensation for equilibrium conditions will just begin at various free-stream Mach numbers M_1.

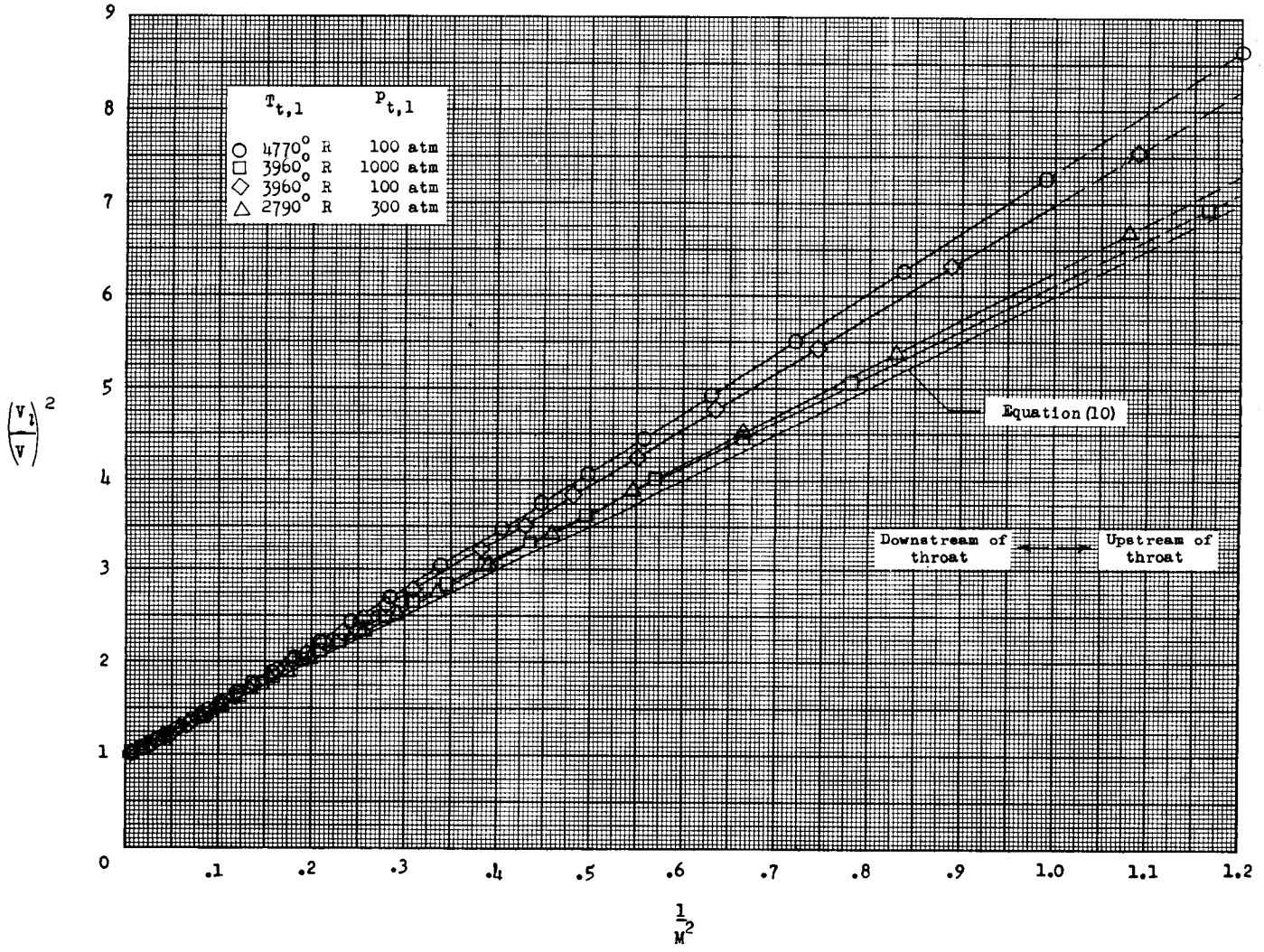

Figure 20.- Effect of $T_{t,1}$ and $p_{t,1}$ on the relationship between $\left(\frac{V_l}{V}\right)^2$ and $\frac{1}{M^2}$.

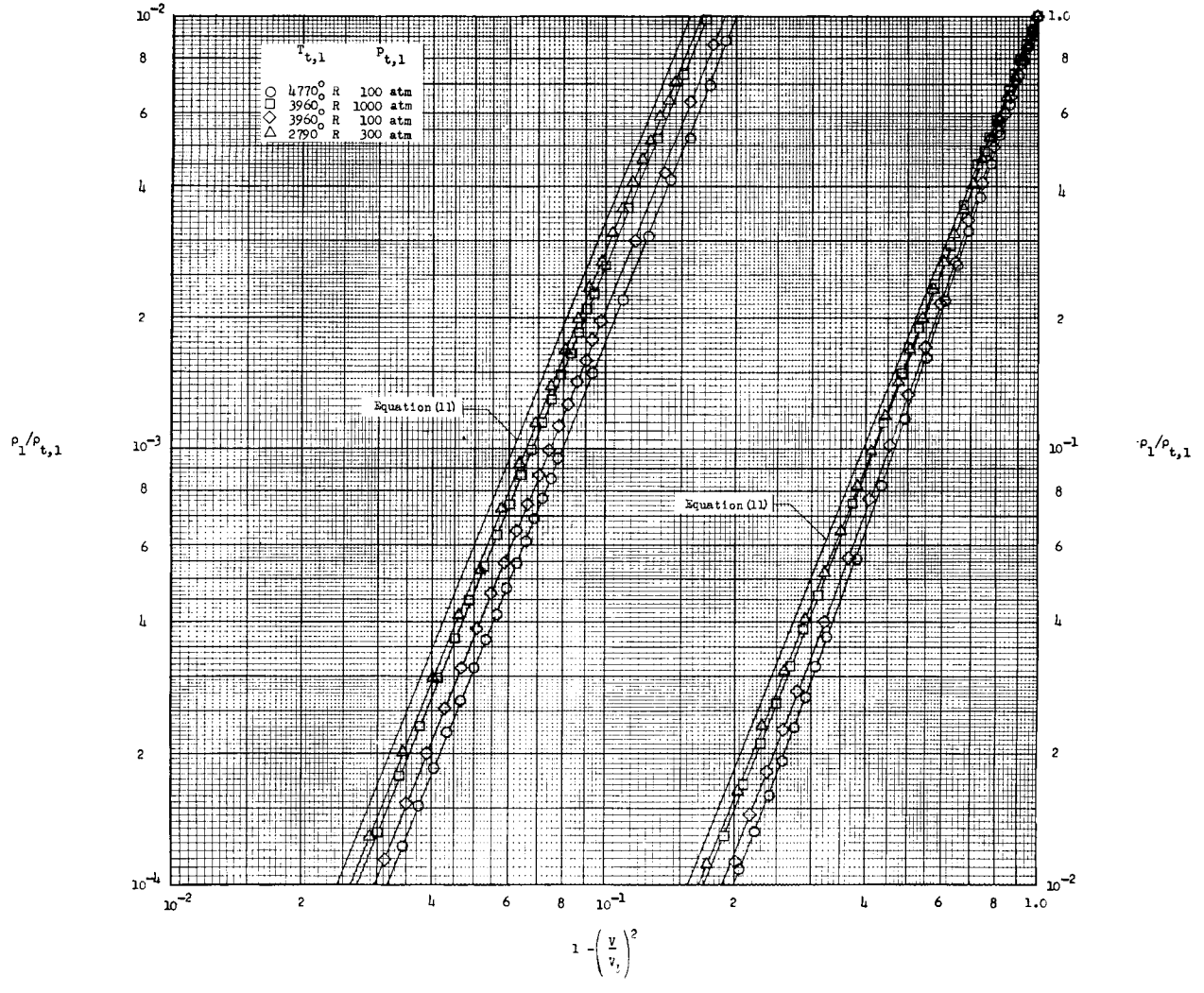

Figure 21.- Effect of $T_{t,1}$ and $p_{t,1}$ on the relationship between $\rho_l/\rho_{t,1}$ and $1-\left(\frac{V}{V_l}\right)^2$.

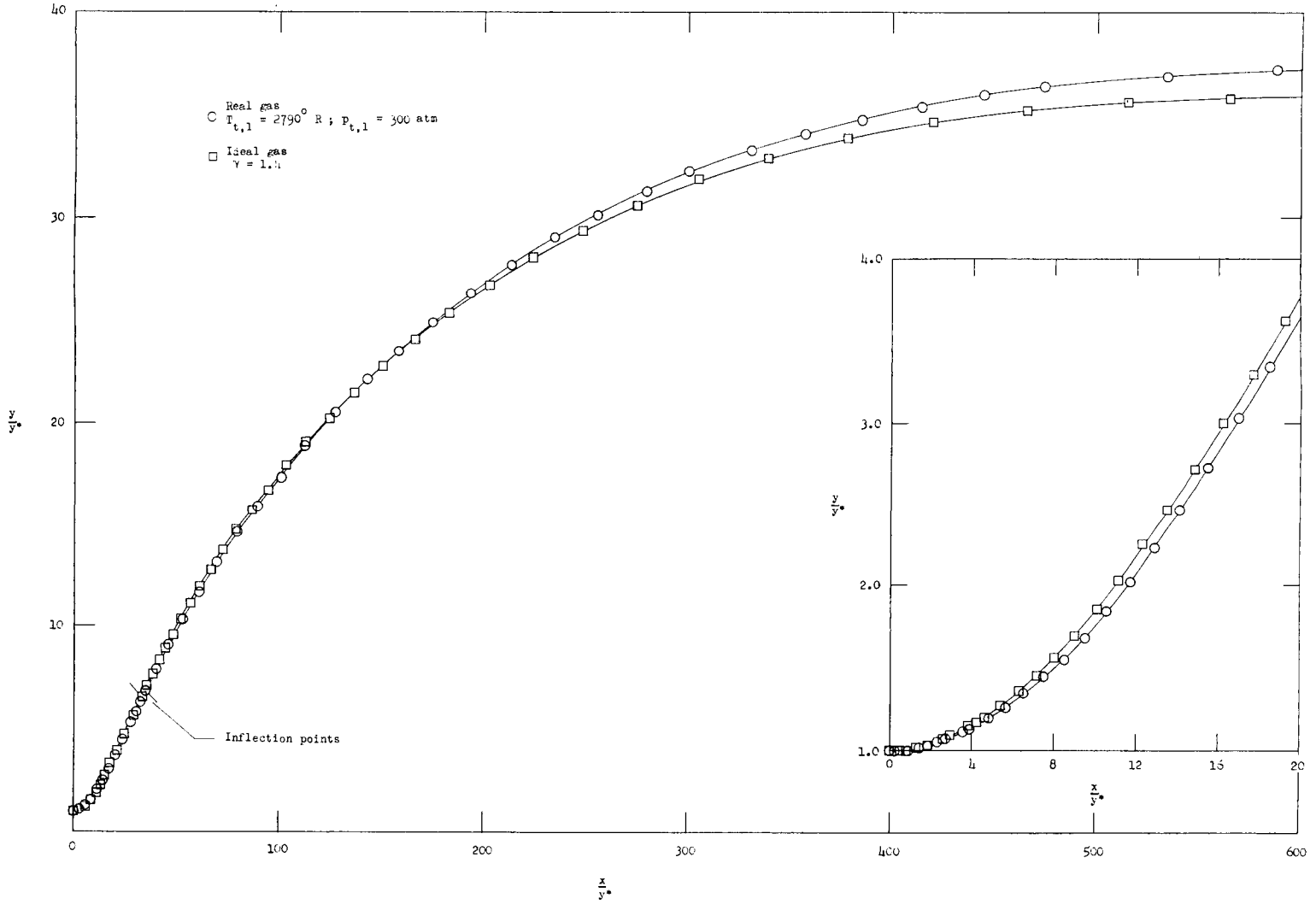

Figure 22.- Comparison of calculated M = 12 axisymmetric nozzle contours considering real-gas effects for $T_{t,1}$ = 2,790° R and $p_{t,1}$ = 300 atm and ideal gas with γ = 1.4.

SUPPLEMENTARY CHARTS OF THERMODYNAMIC PROPERTIES FOR AIR

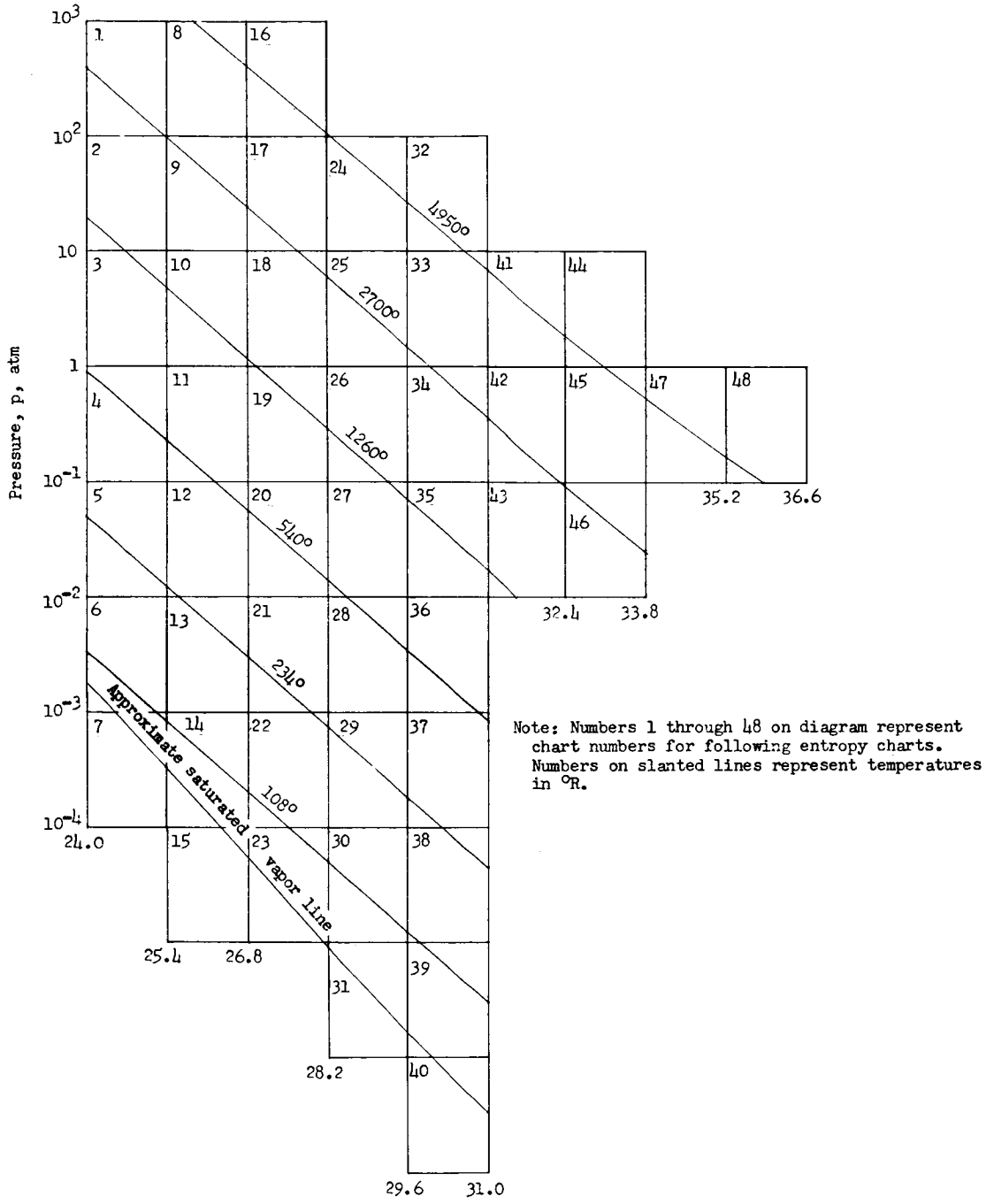

Note: Numbers 1 through 48 on diagram represent chart numbers for following entropy charts. Numbers on slanted lines represent temperatures in °R.

Key to entropy charts

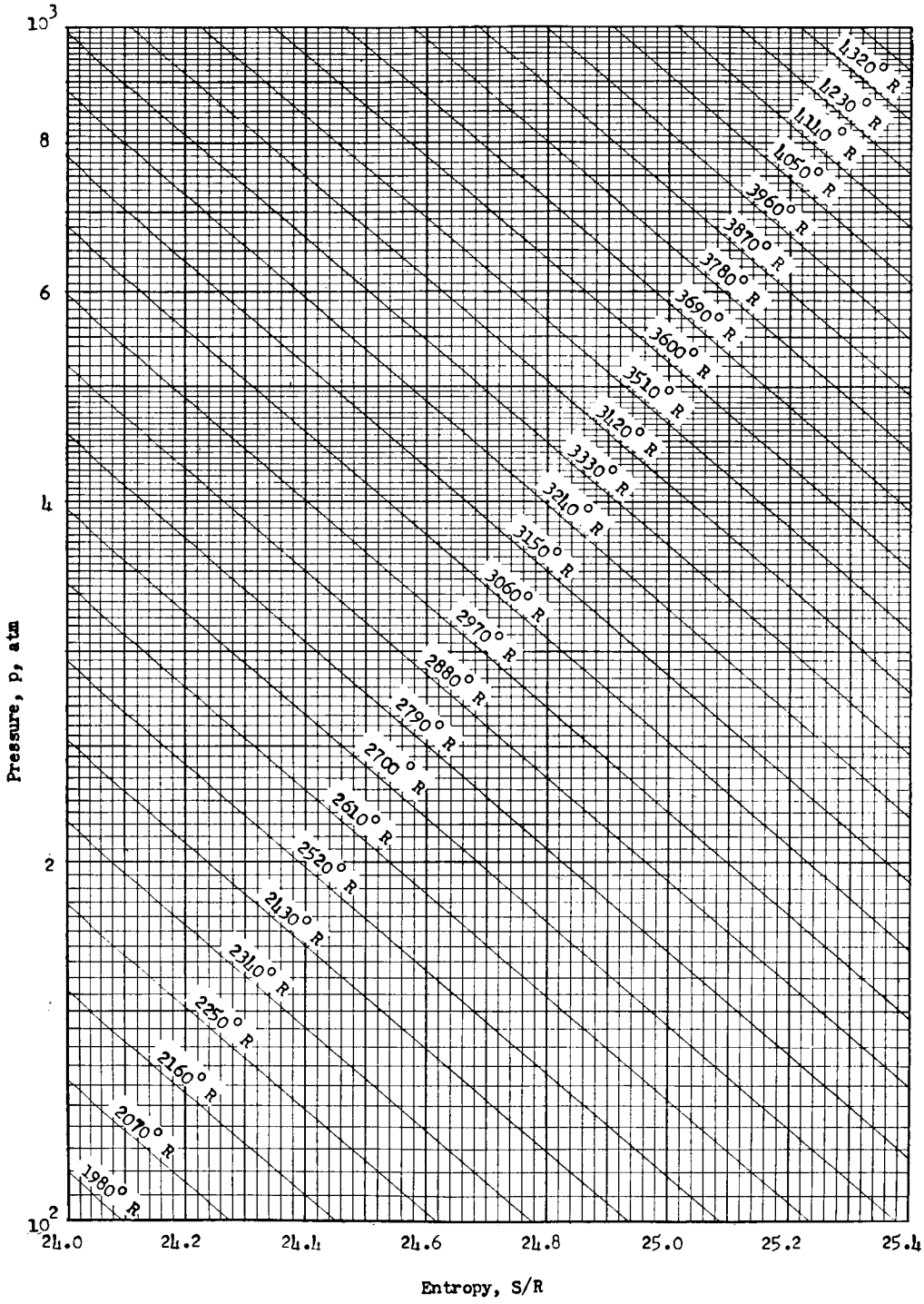

Entropy chart 1

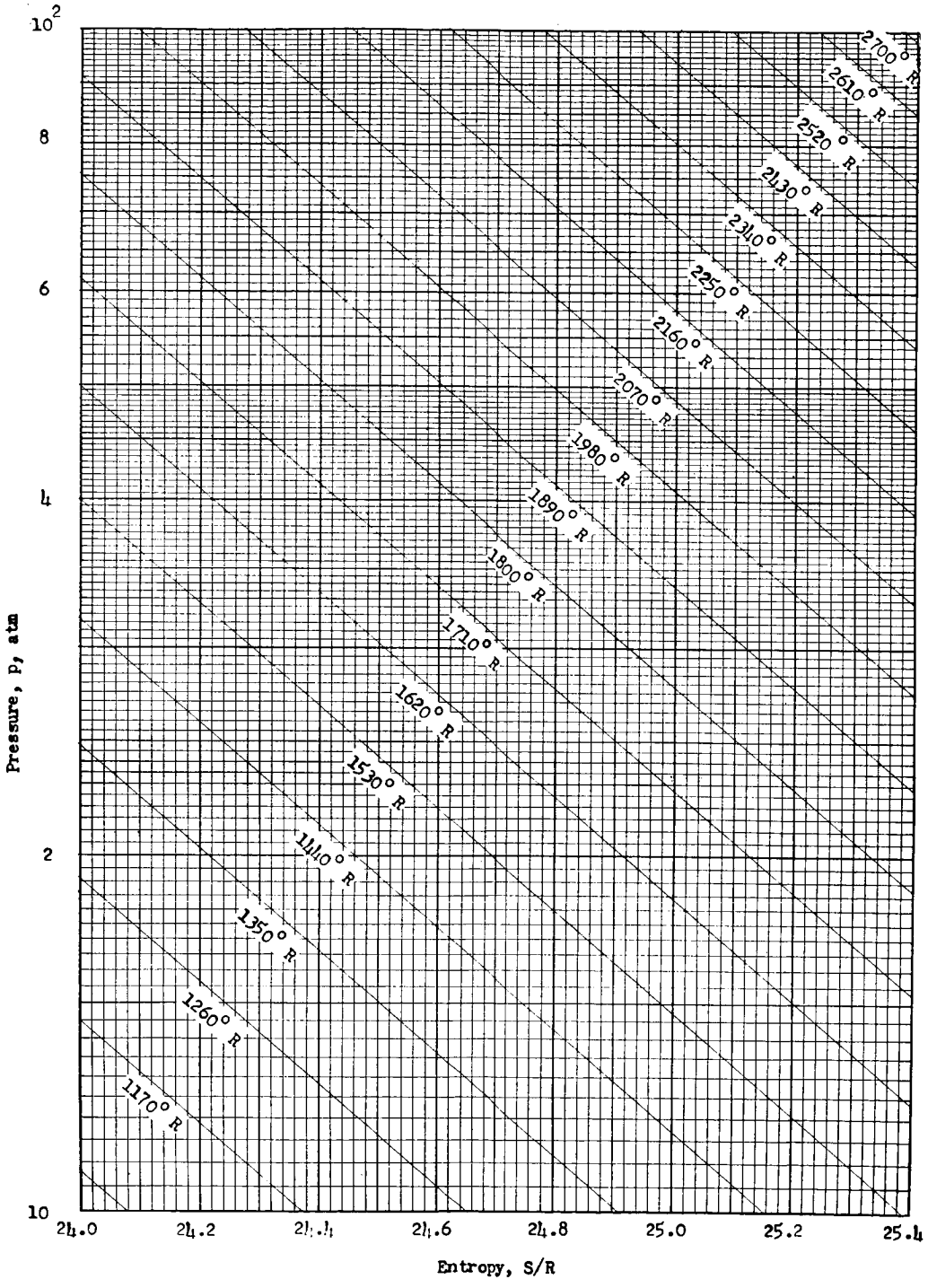

Entropy chart 2

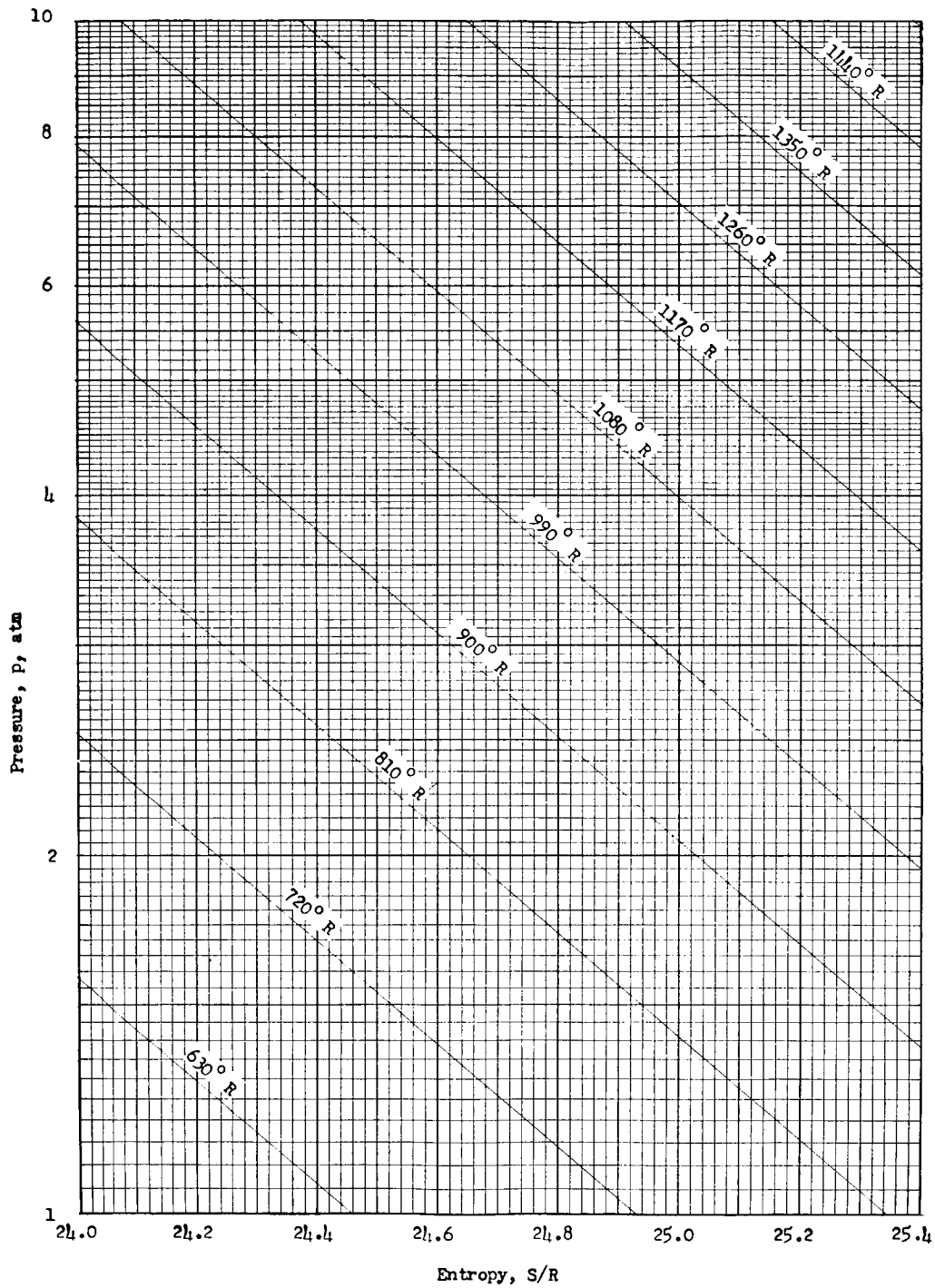

Entropy chart 3

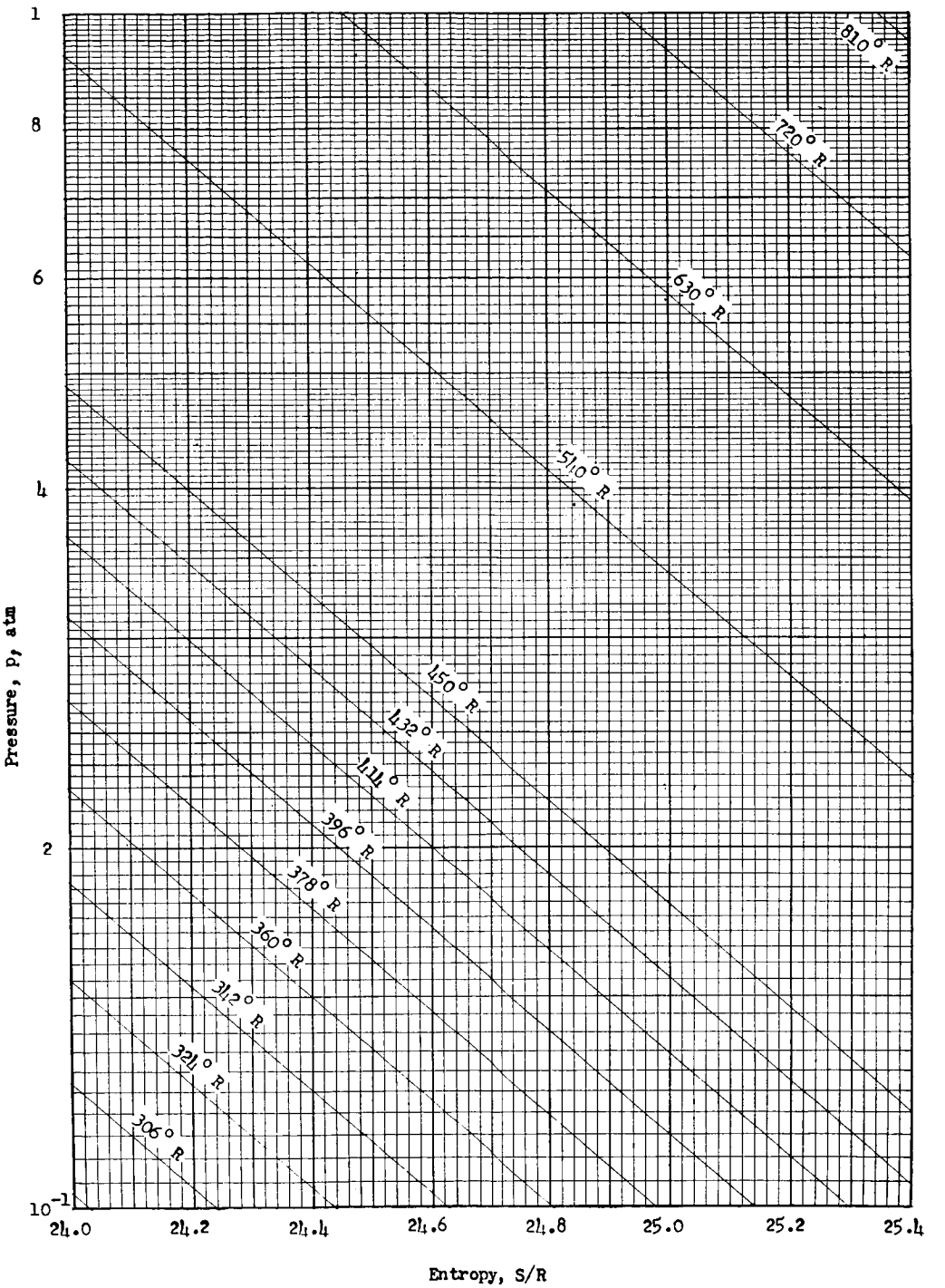

Entropy chart 4

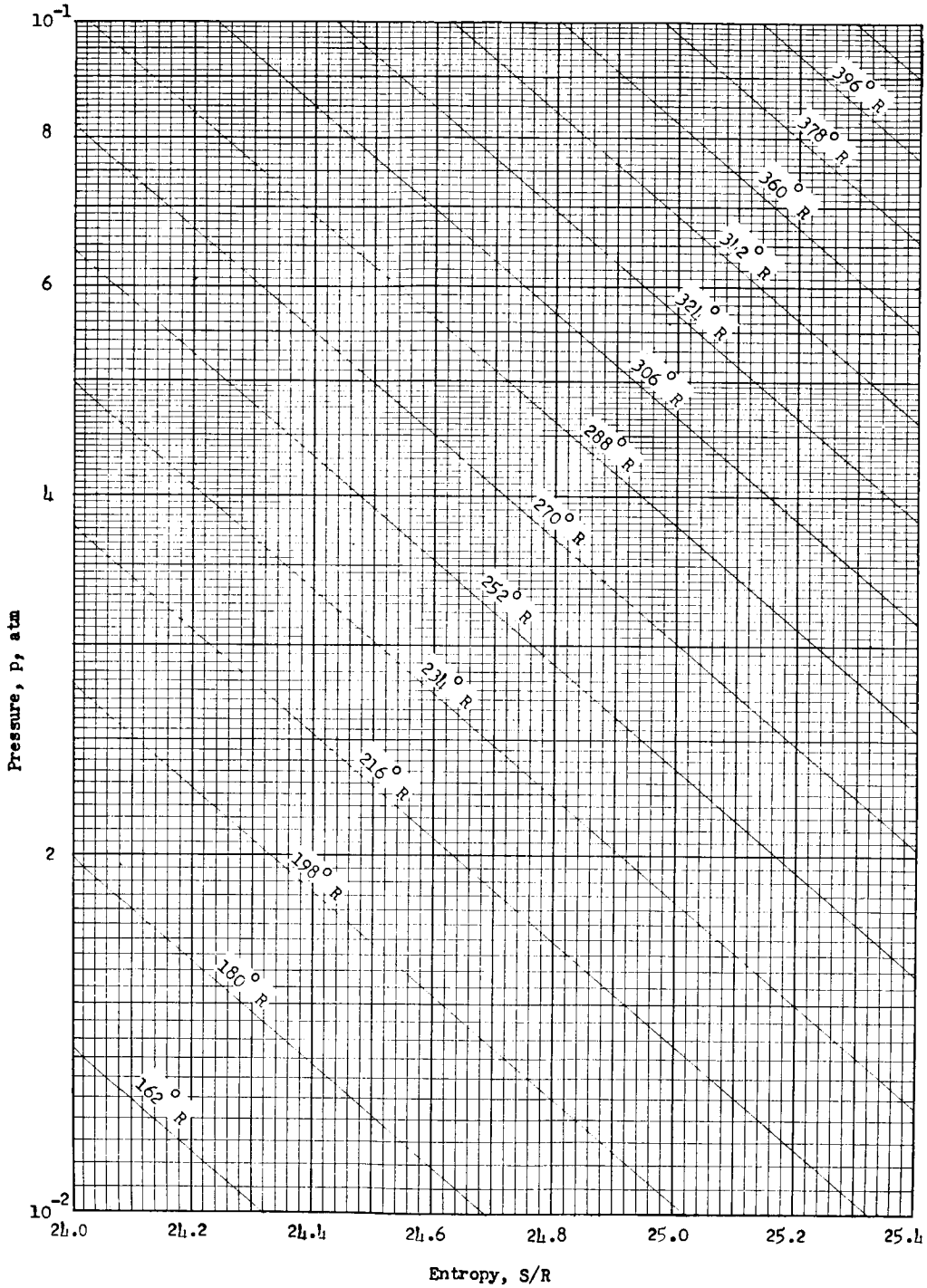

Entropy chart 5

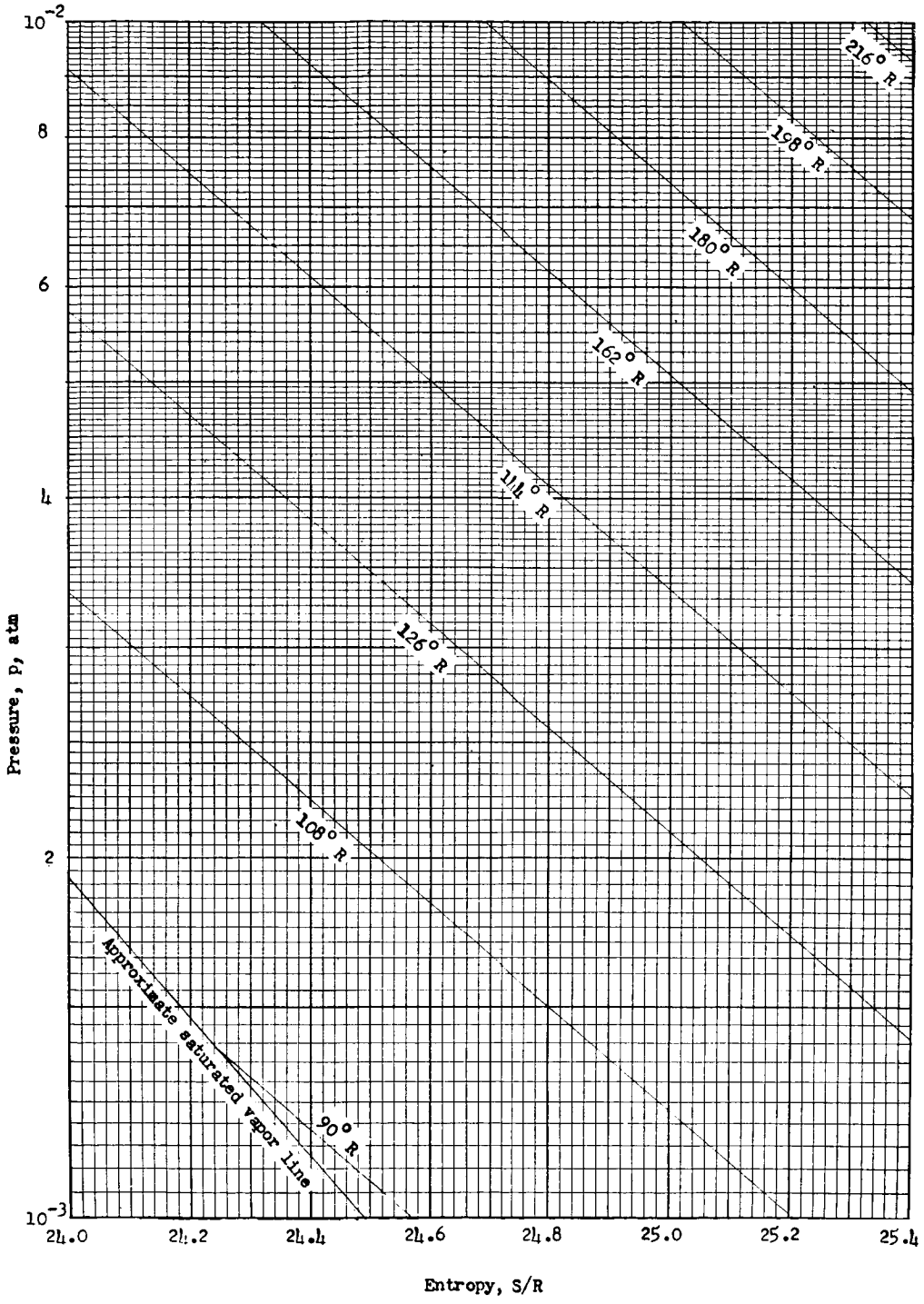

Entropy chart 6

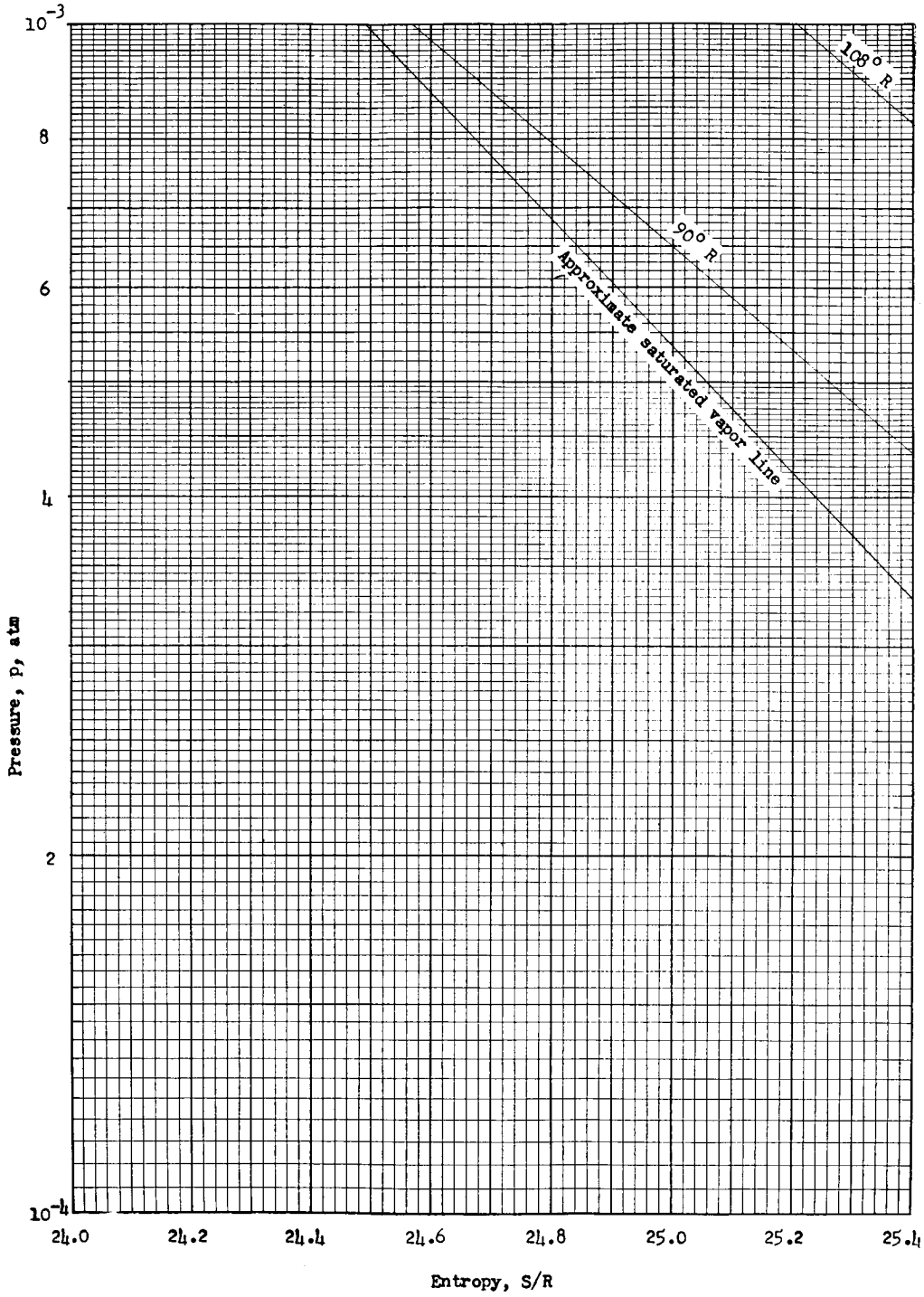

Entropy chart 7

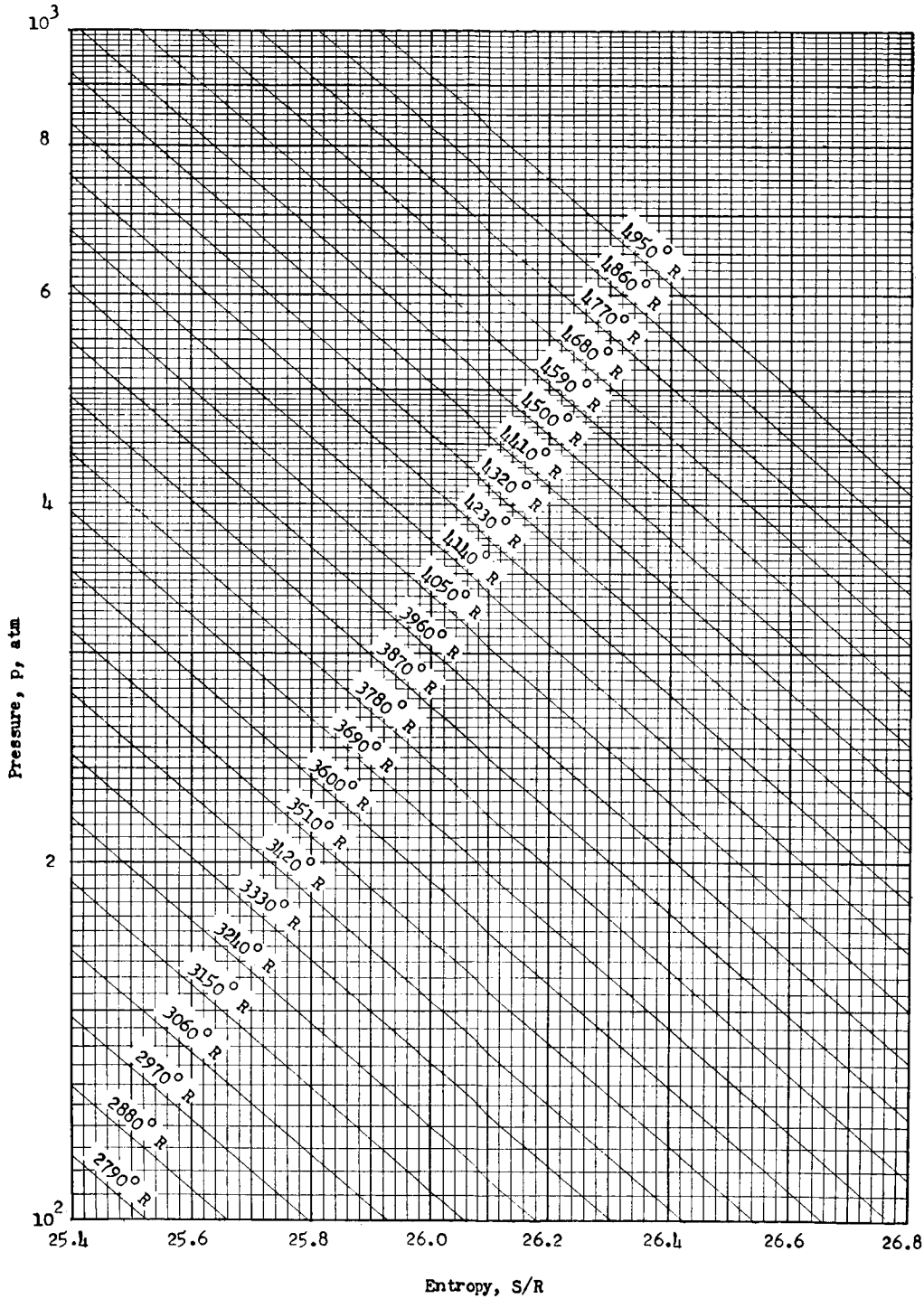

Entropy chart 8

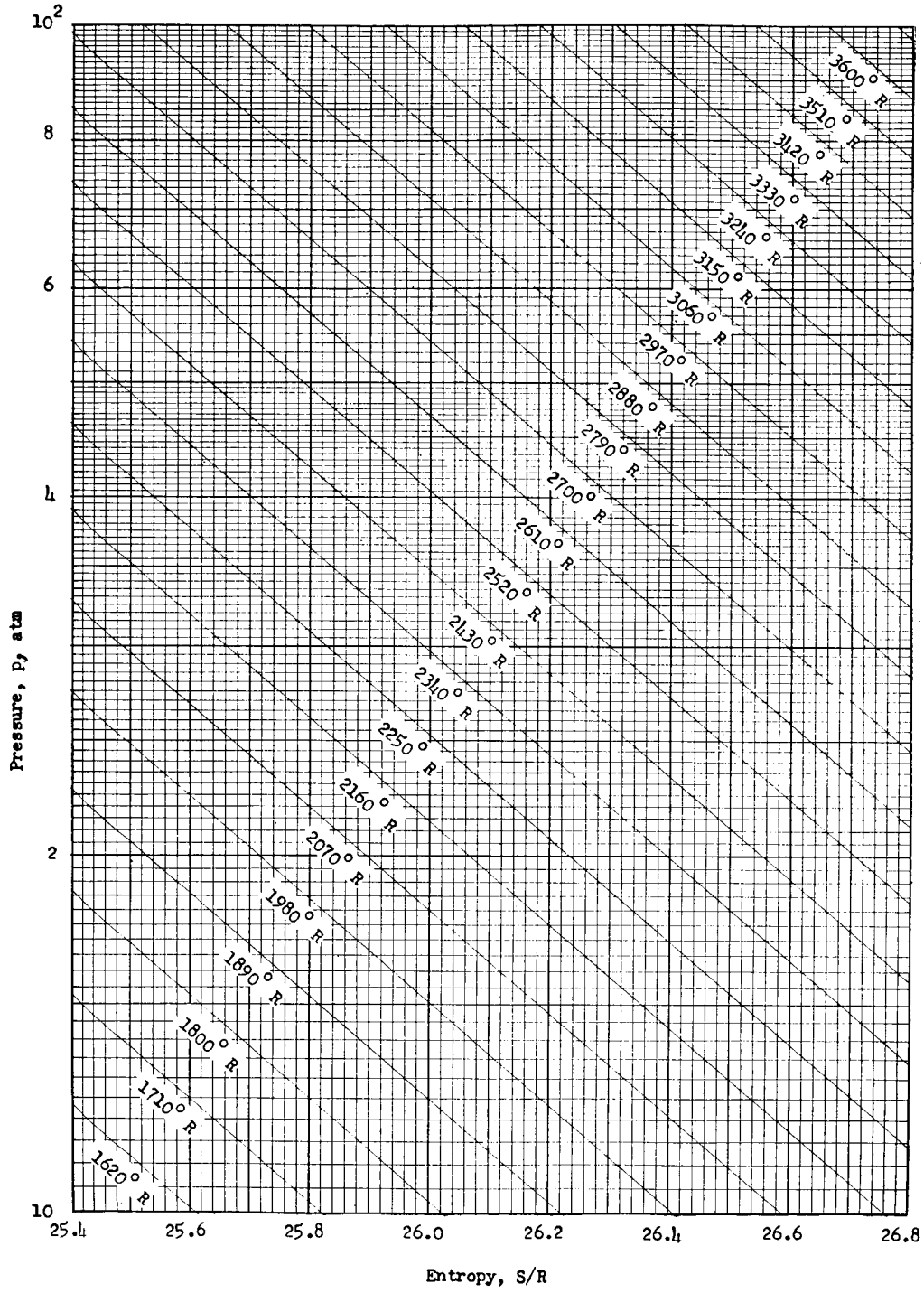

Entropy chart 9

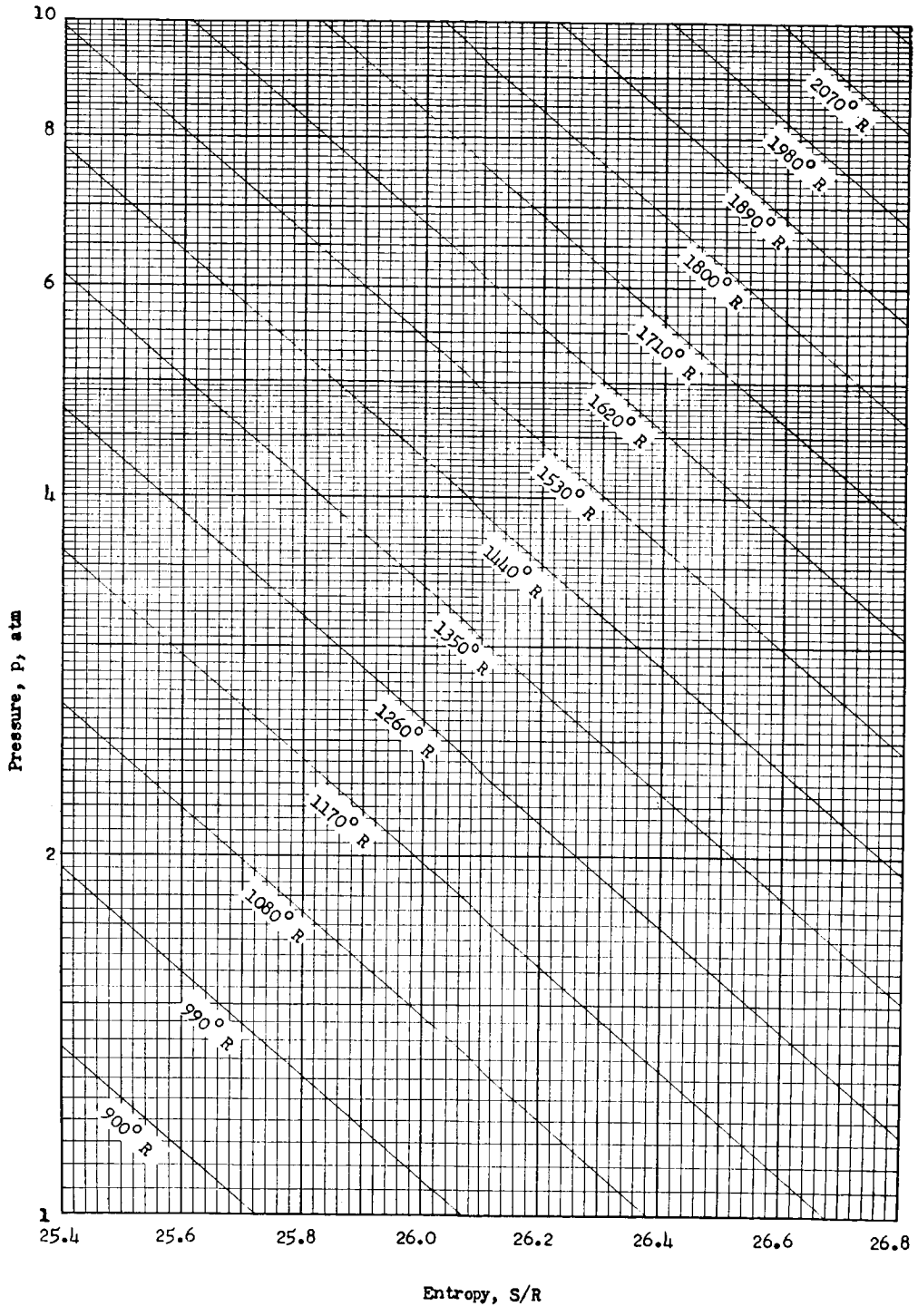

Entropy chart 10

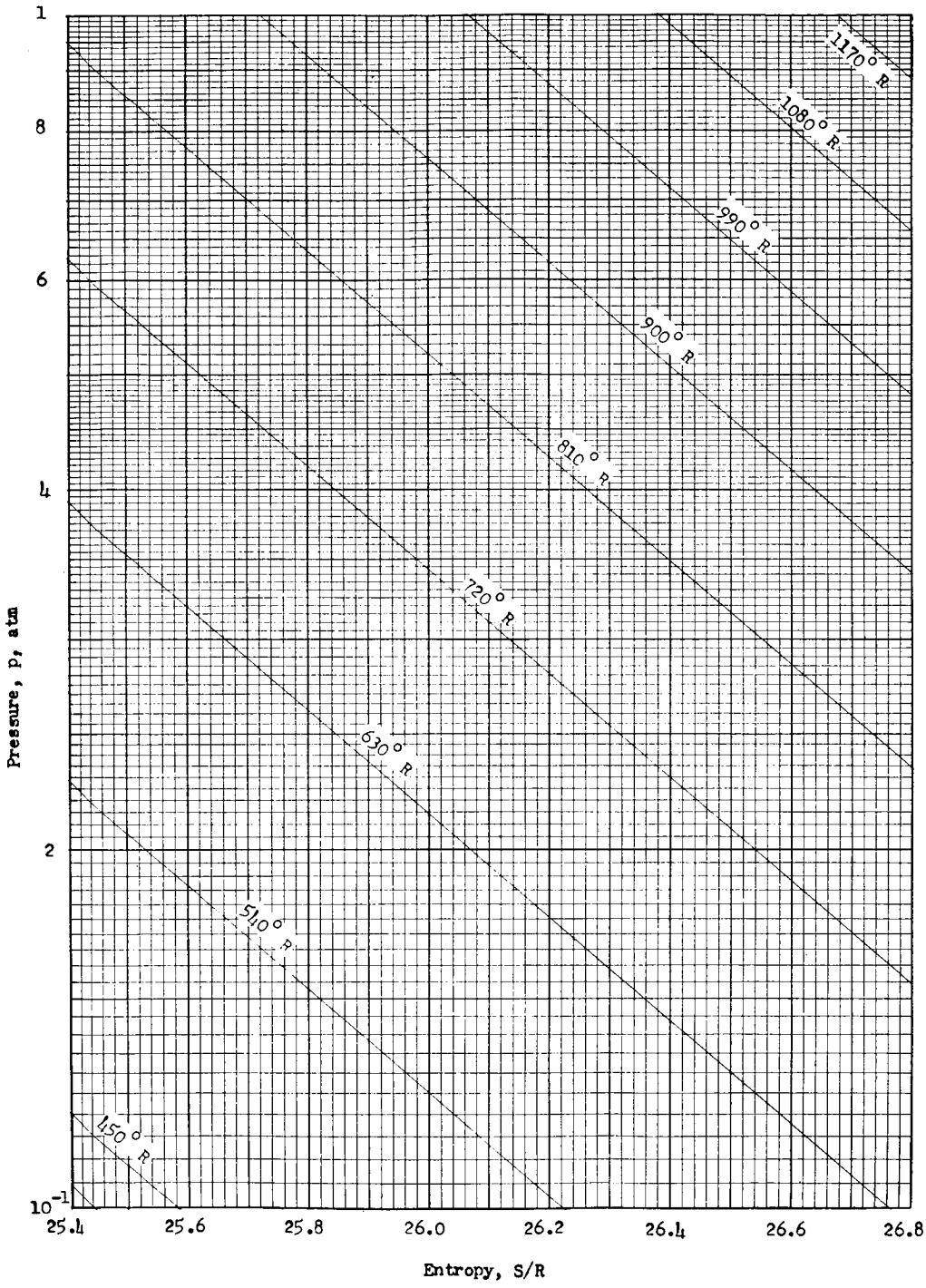

Entropy chart 11

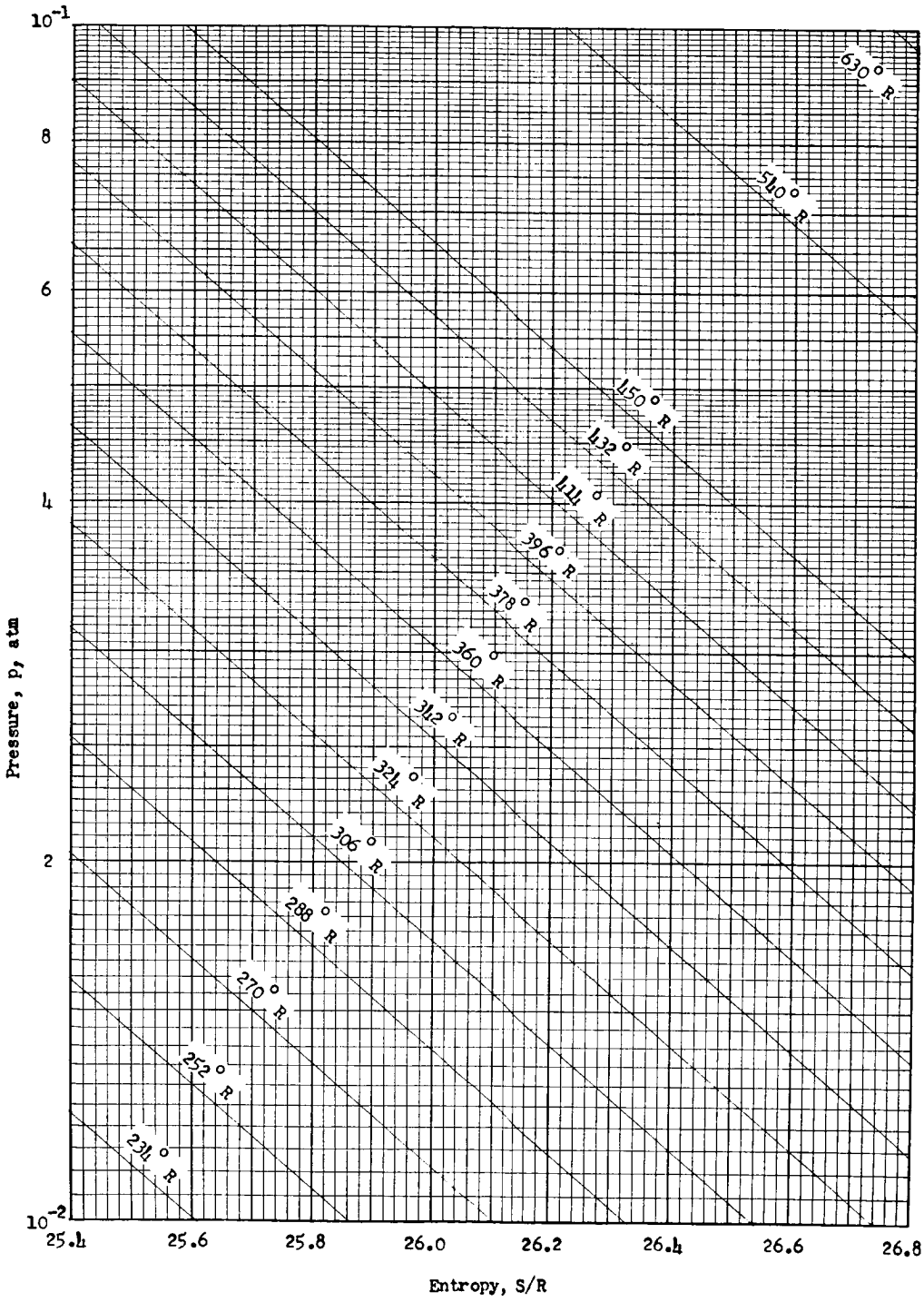

Entropy chart 12

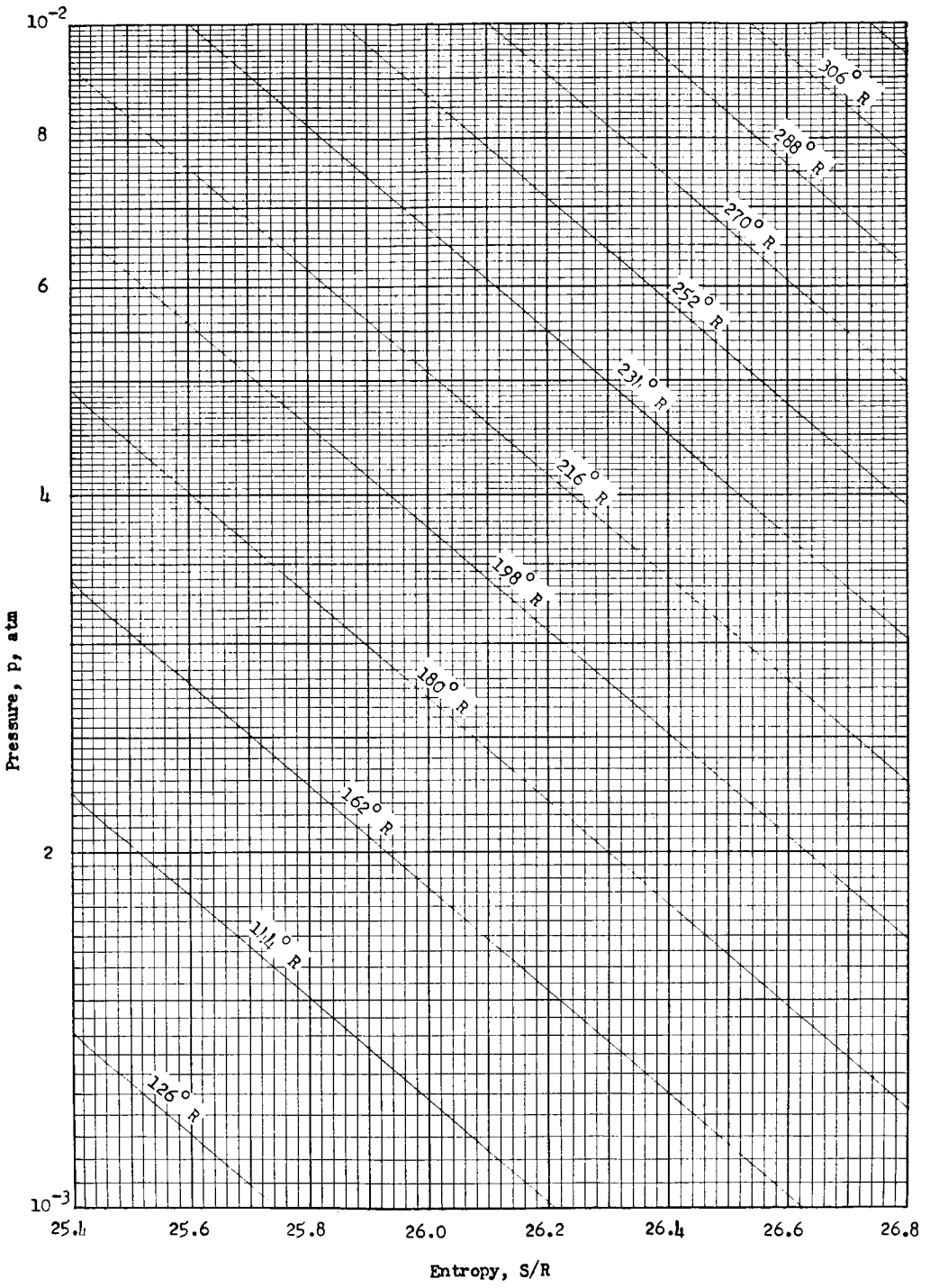

Entropy chart 13

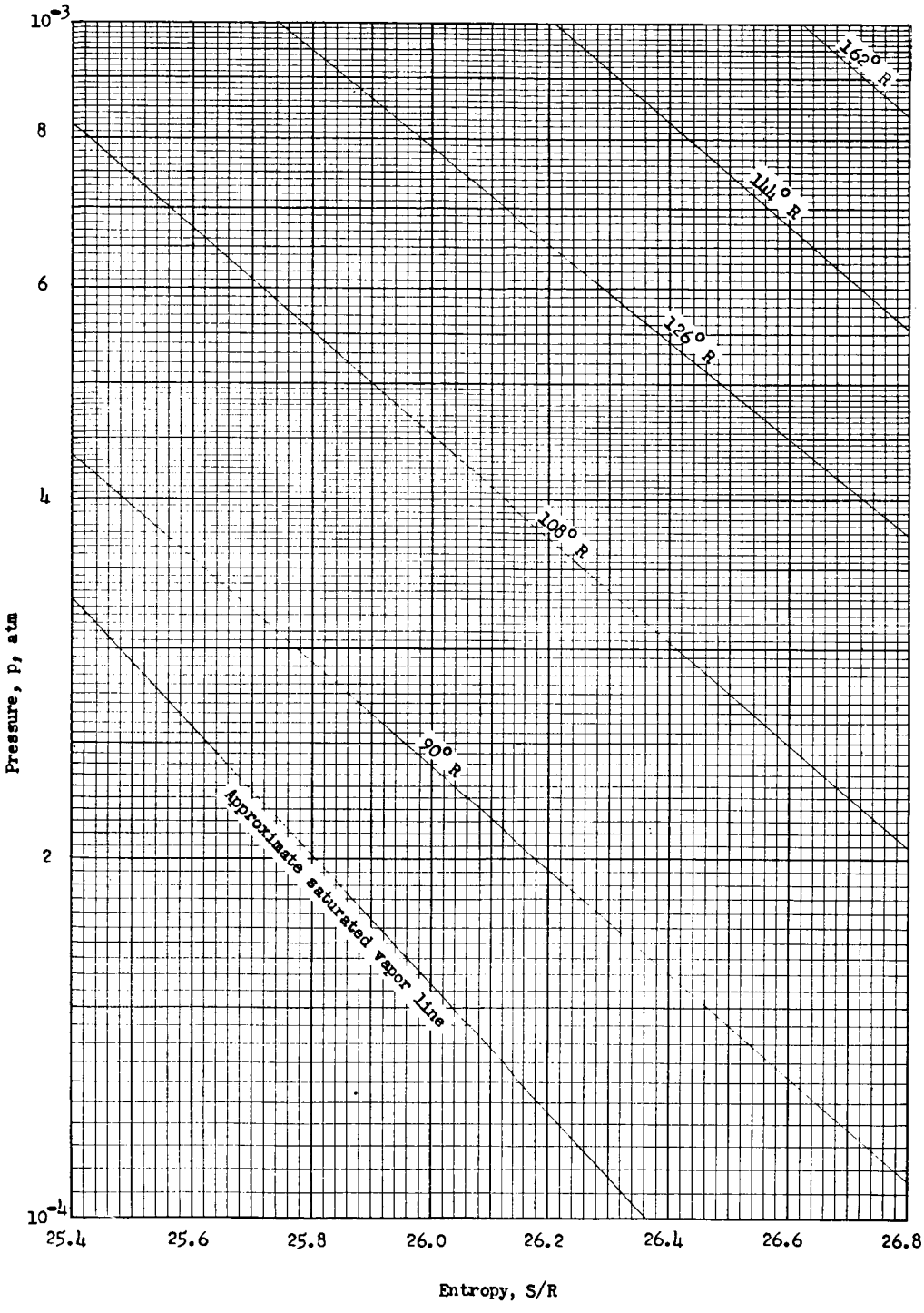

Entropy chart 14

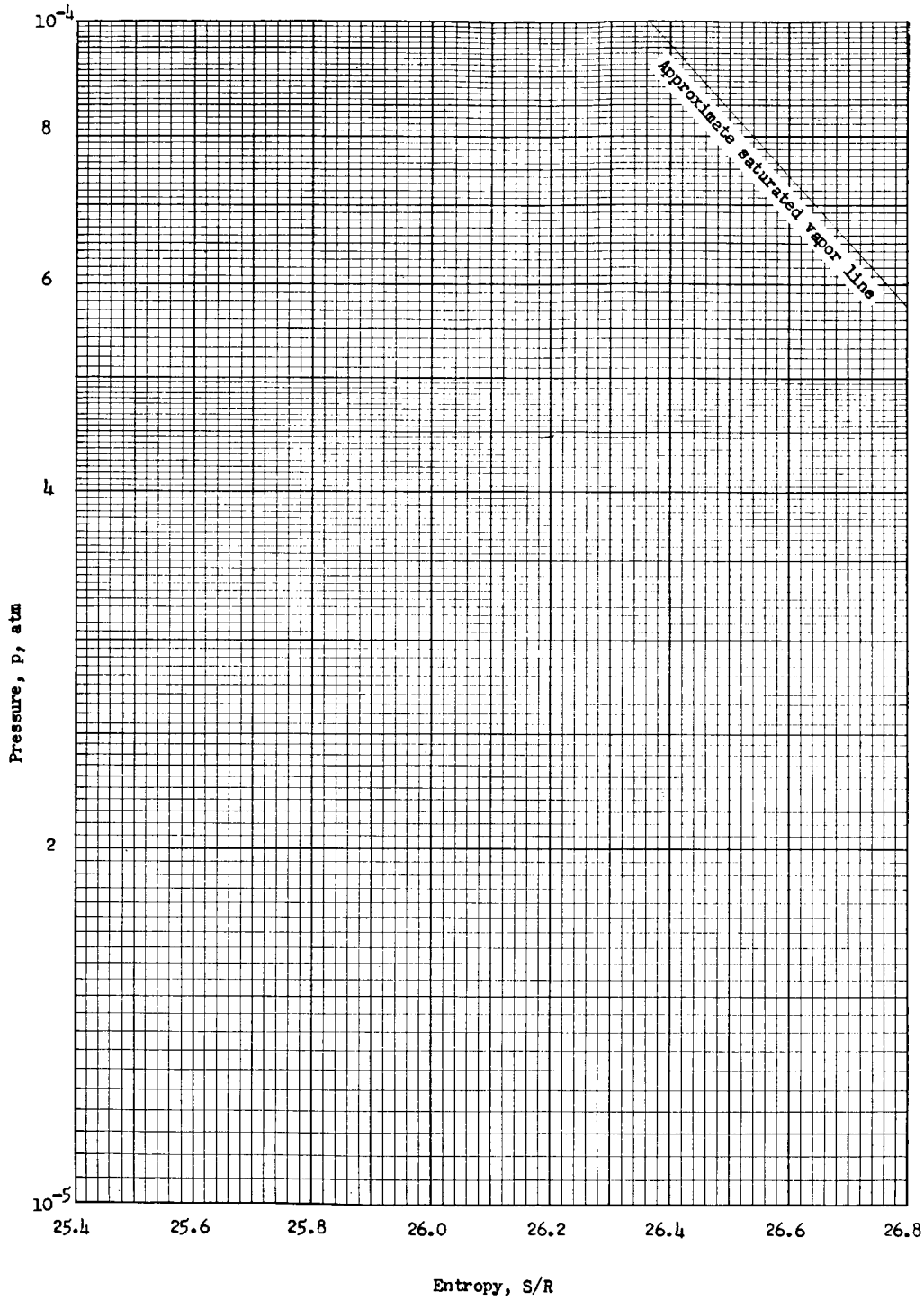

Entropy chart 15

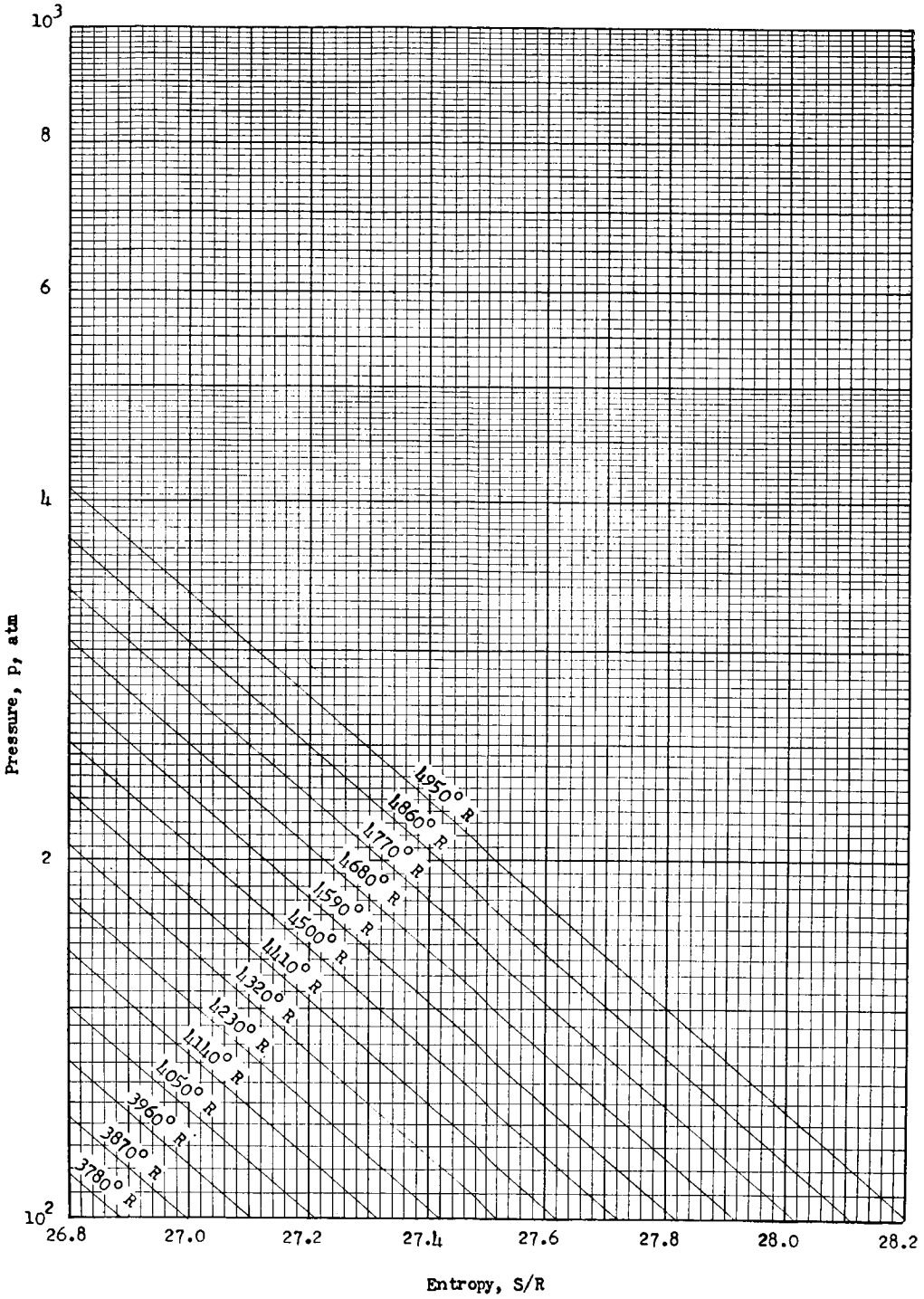

Entropy chart 16

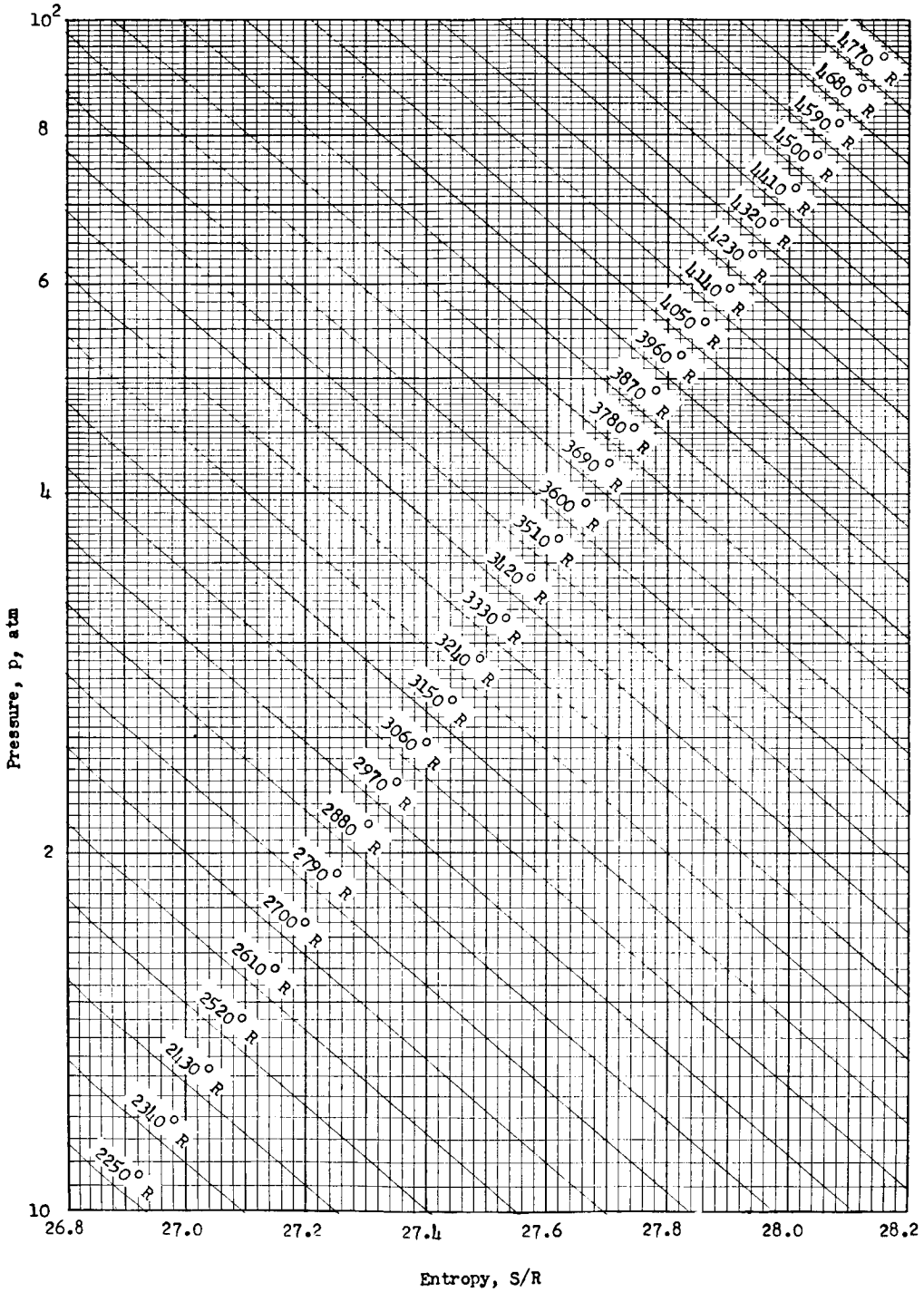

Entropy chart 17

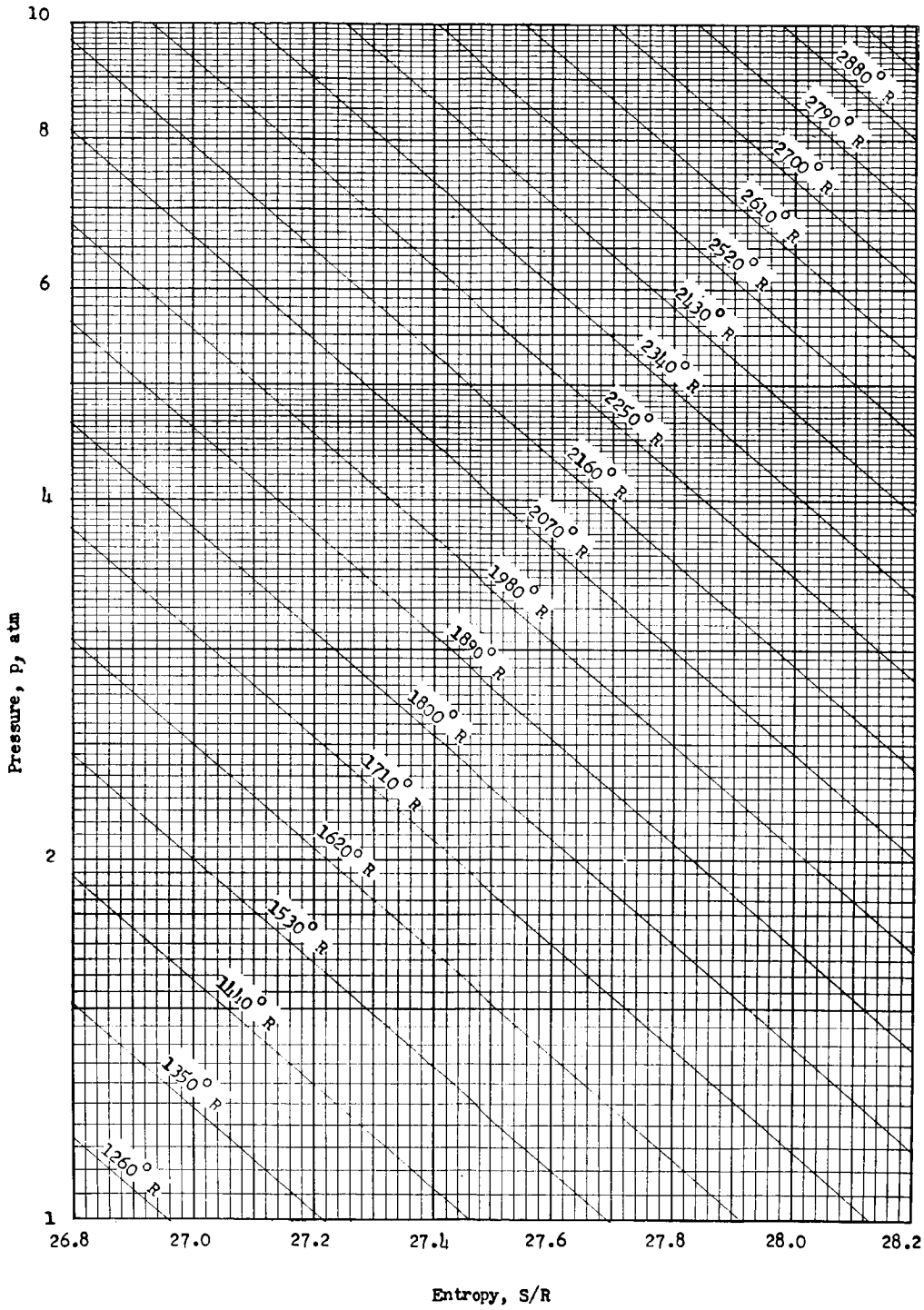

Entropy chart 18

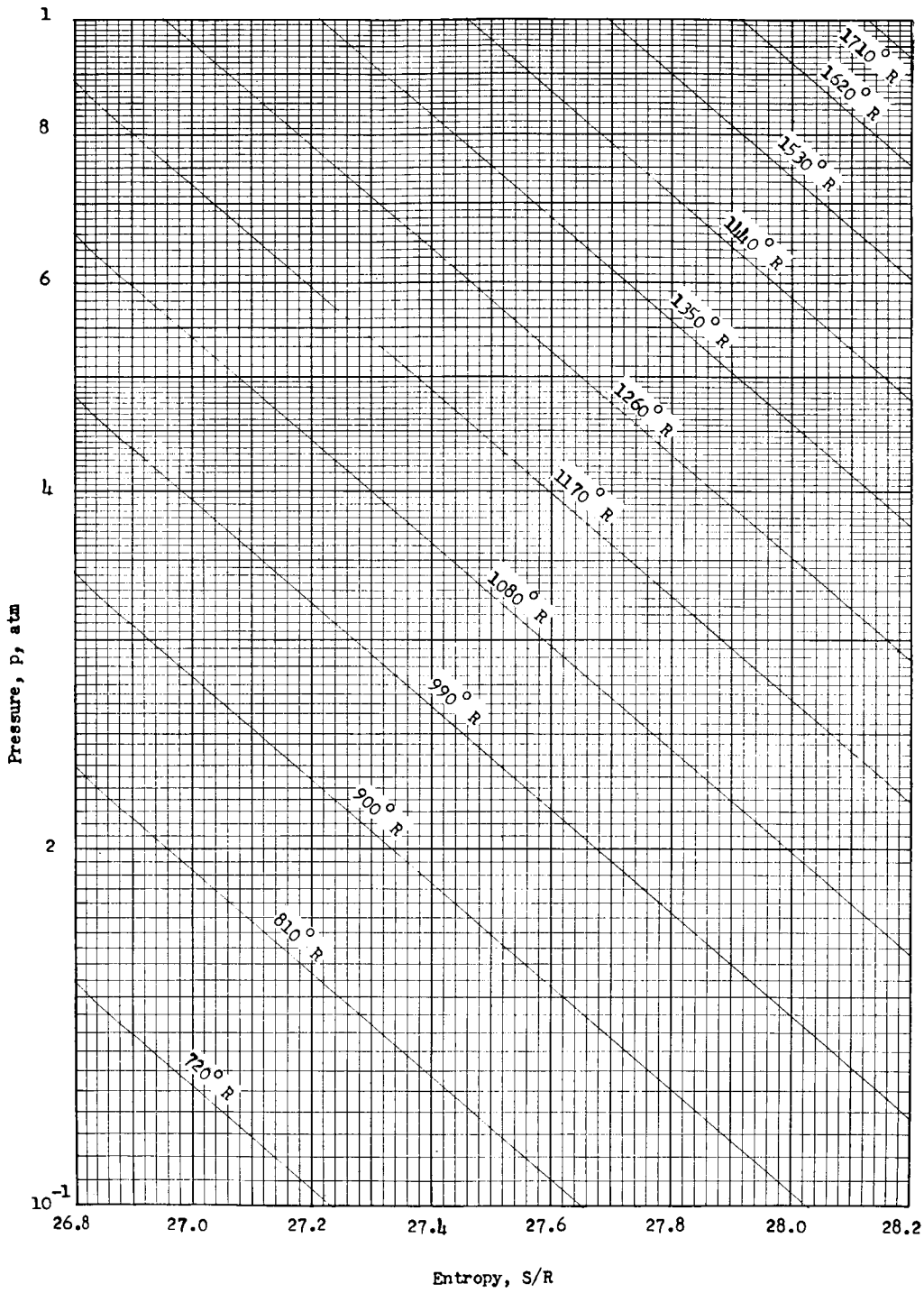

Entropy chart 19

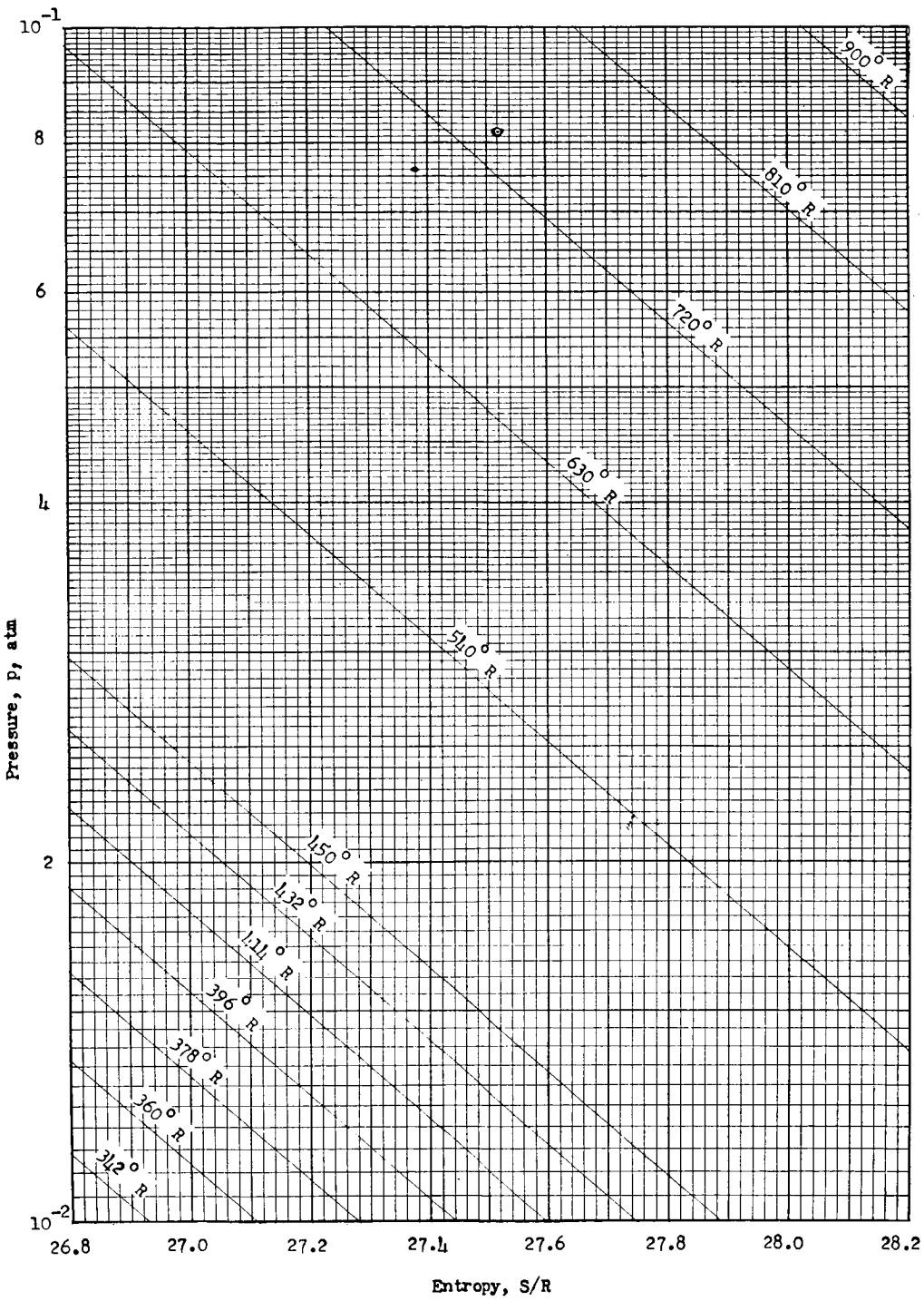

Entropy chart 20

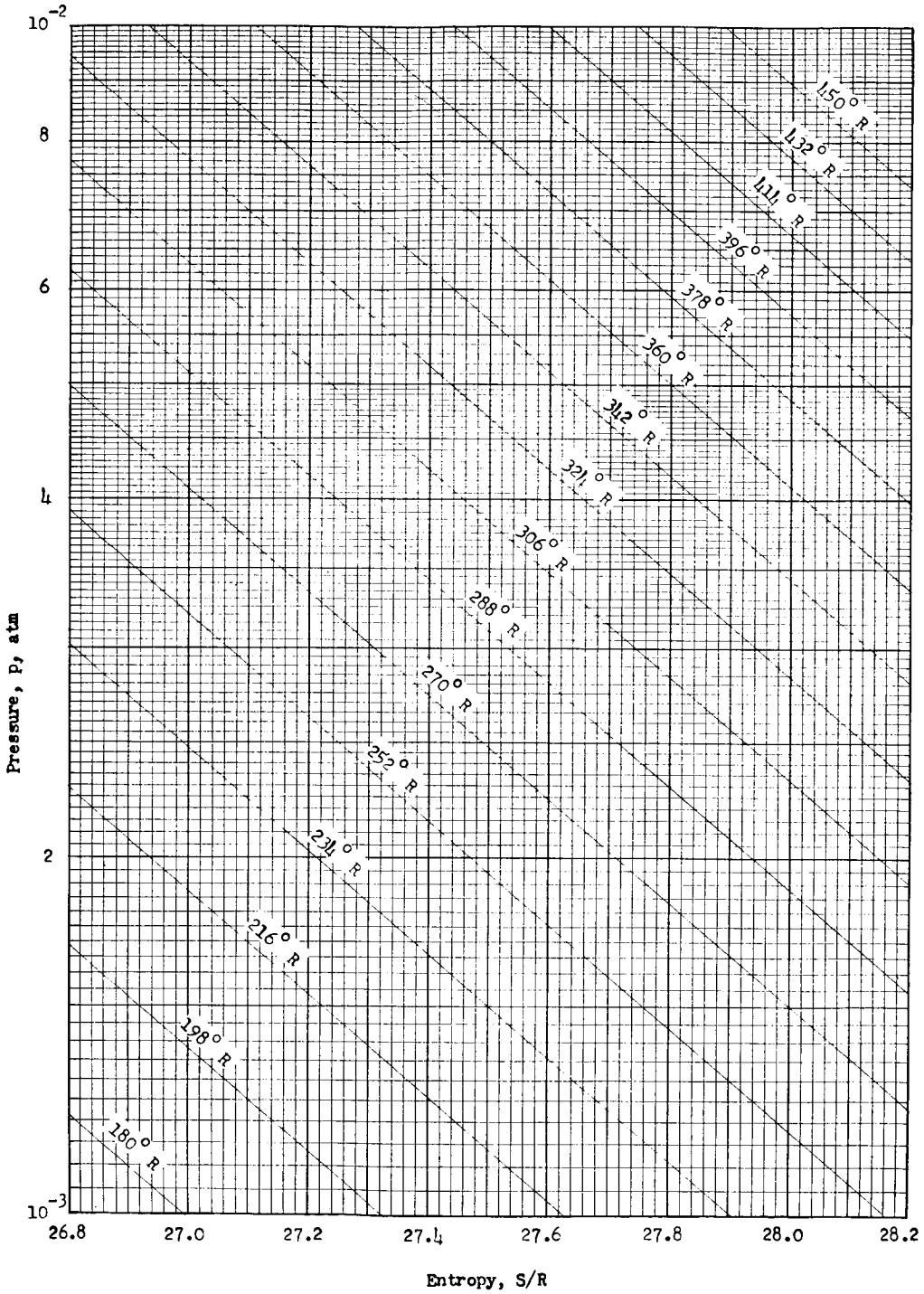

Entropy chart 21

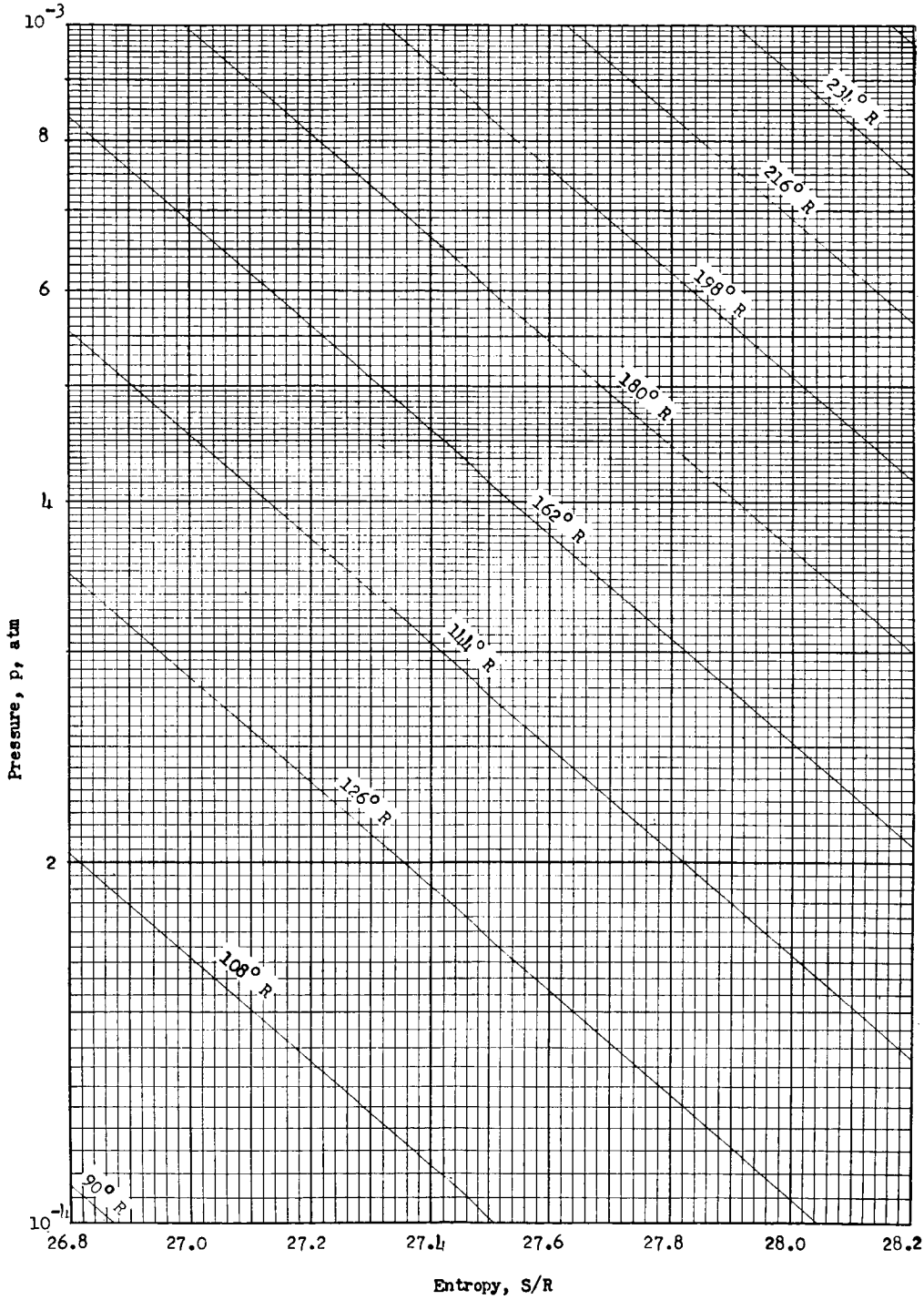

Entropy chart 22

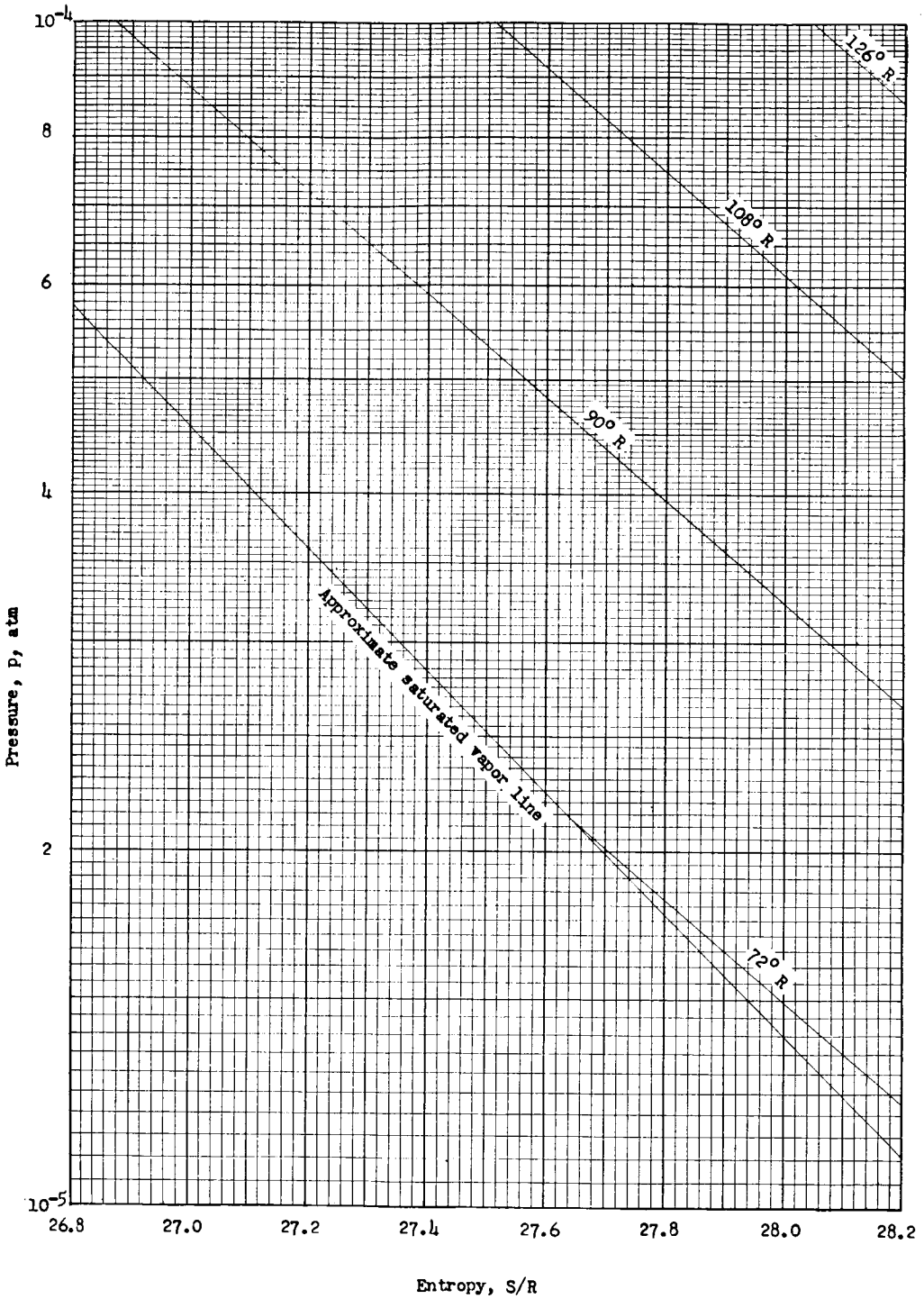

Entropy chart 23

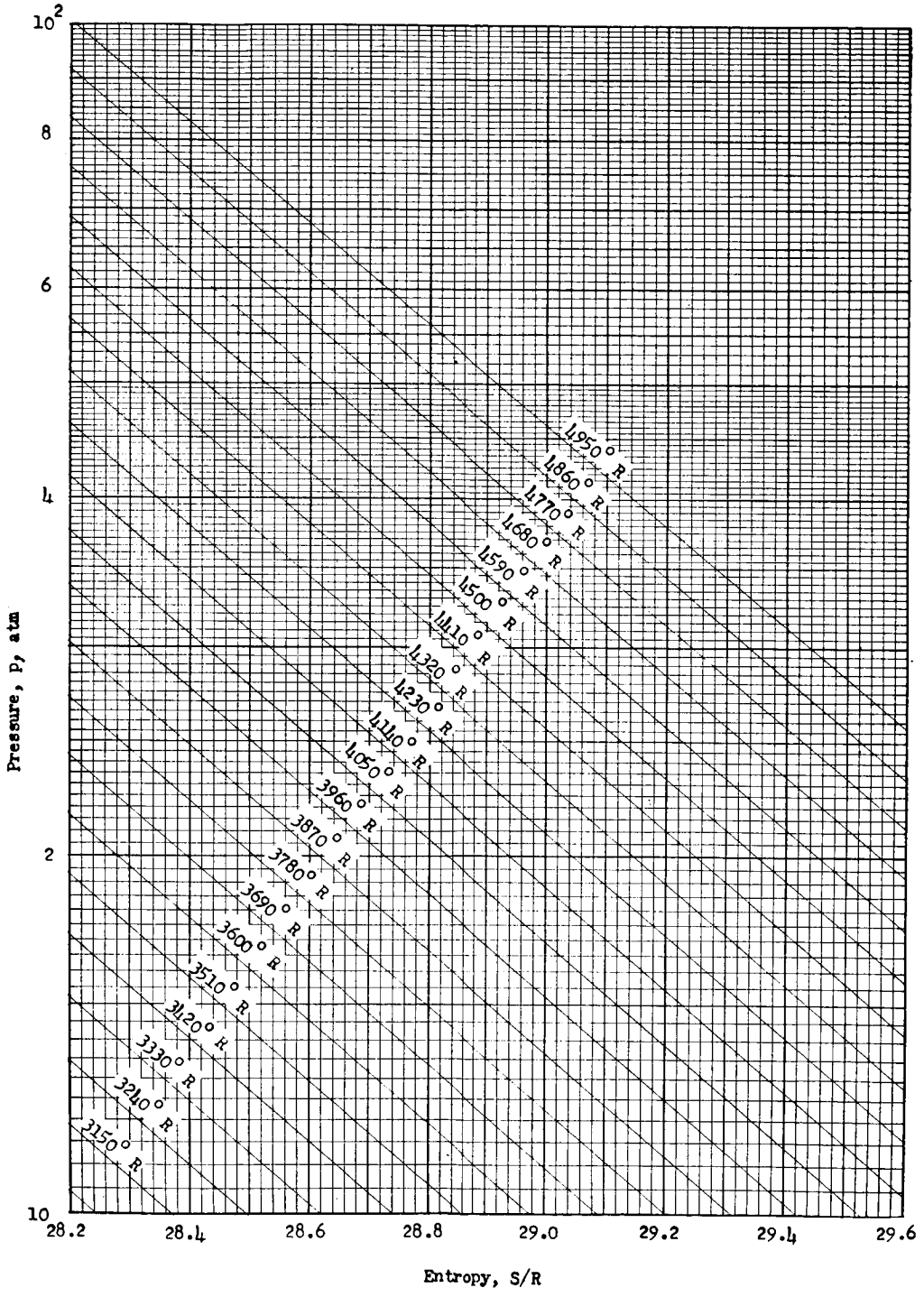

Entropy chart 24

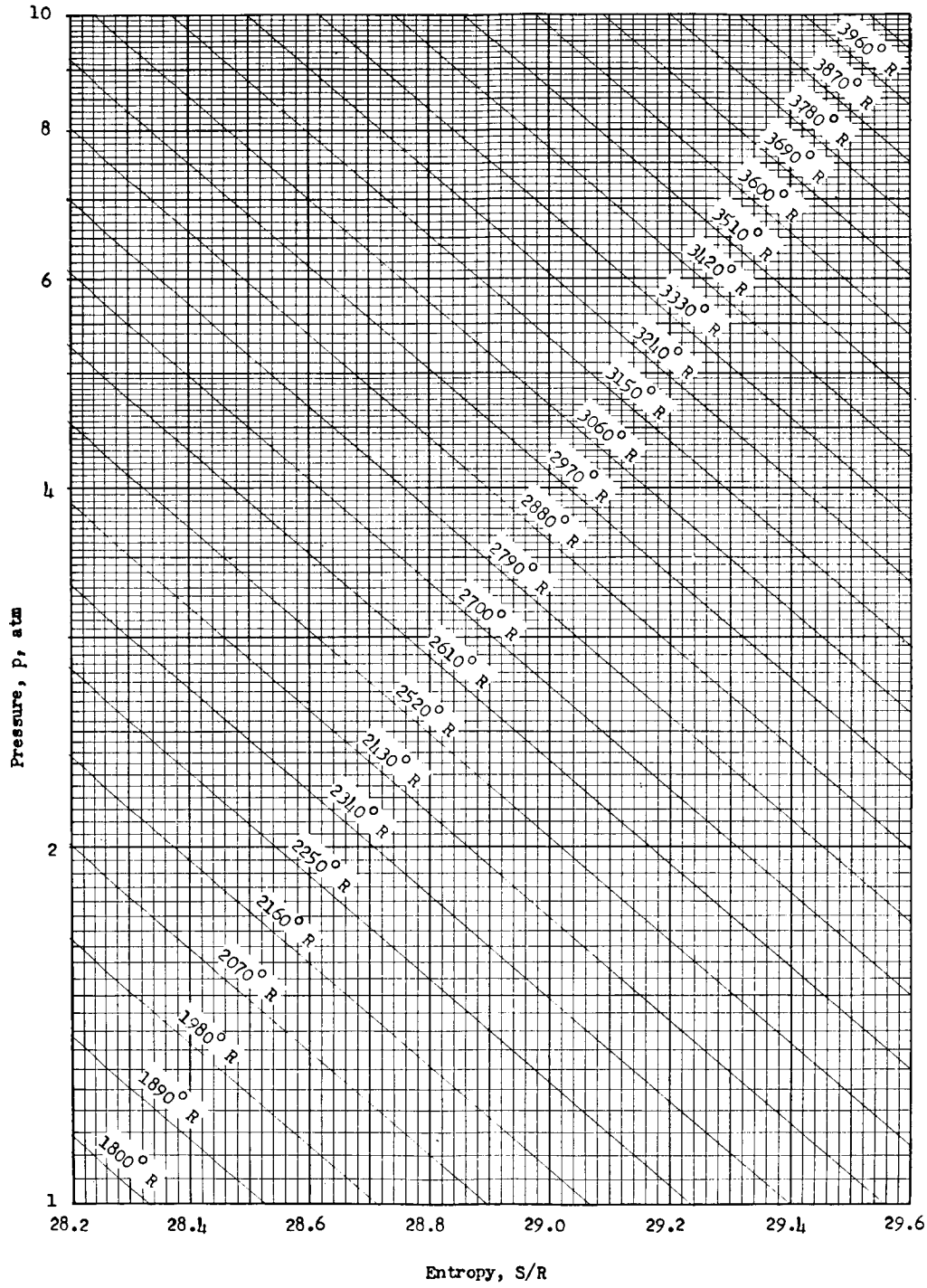

Entropy chart 25

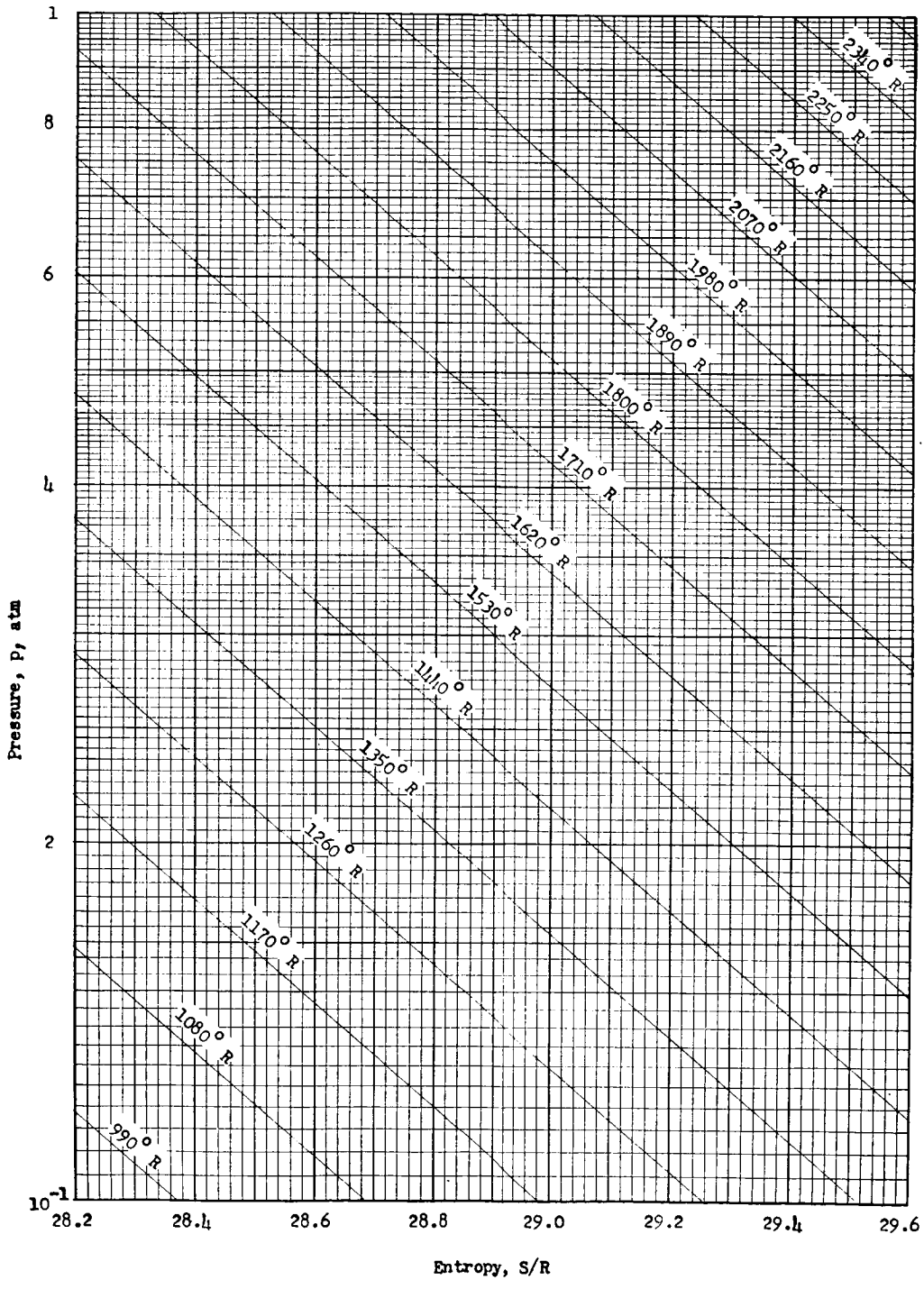

Entropy chart 26

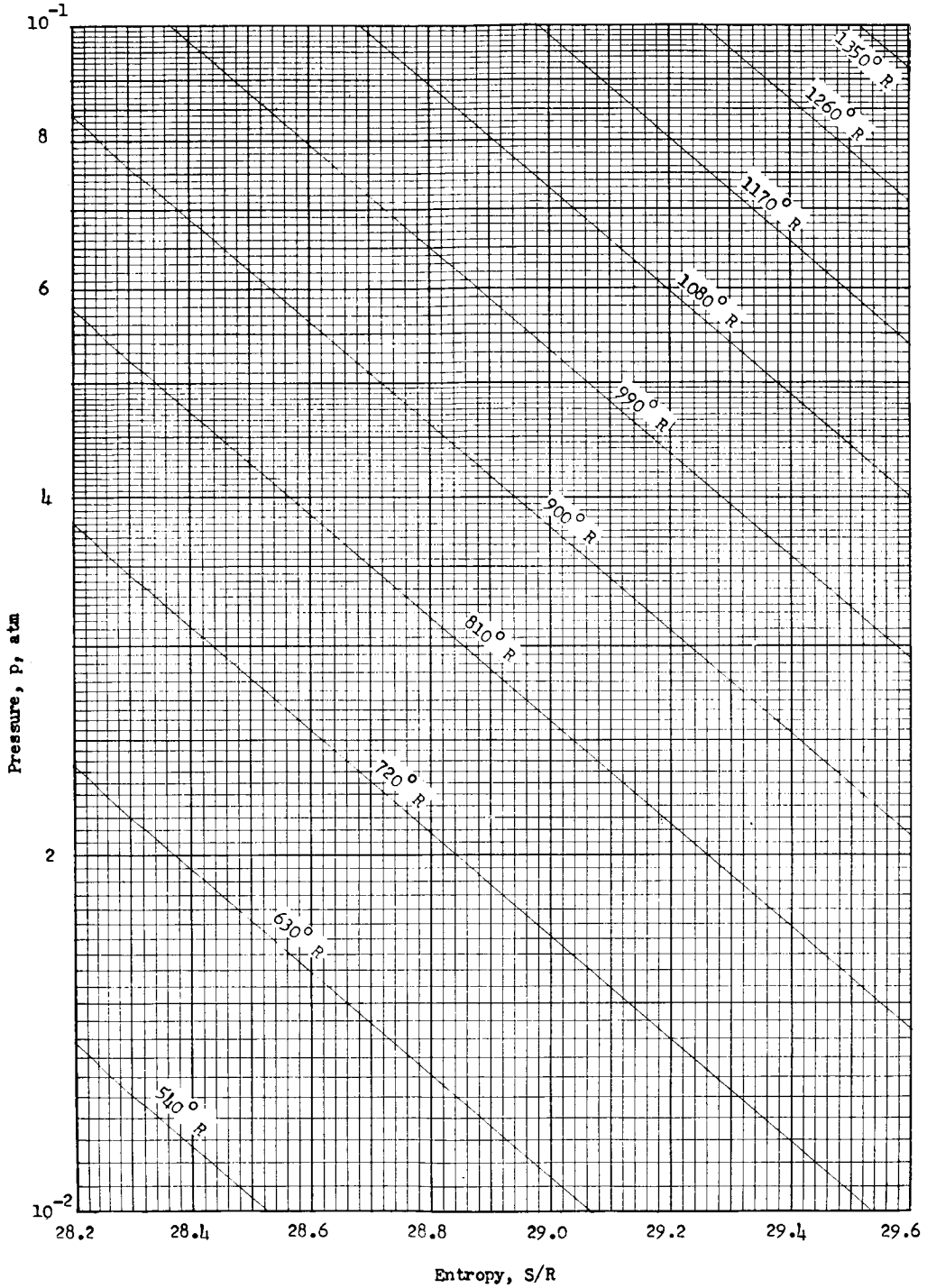

Entropy chart 27

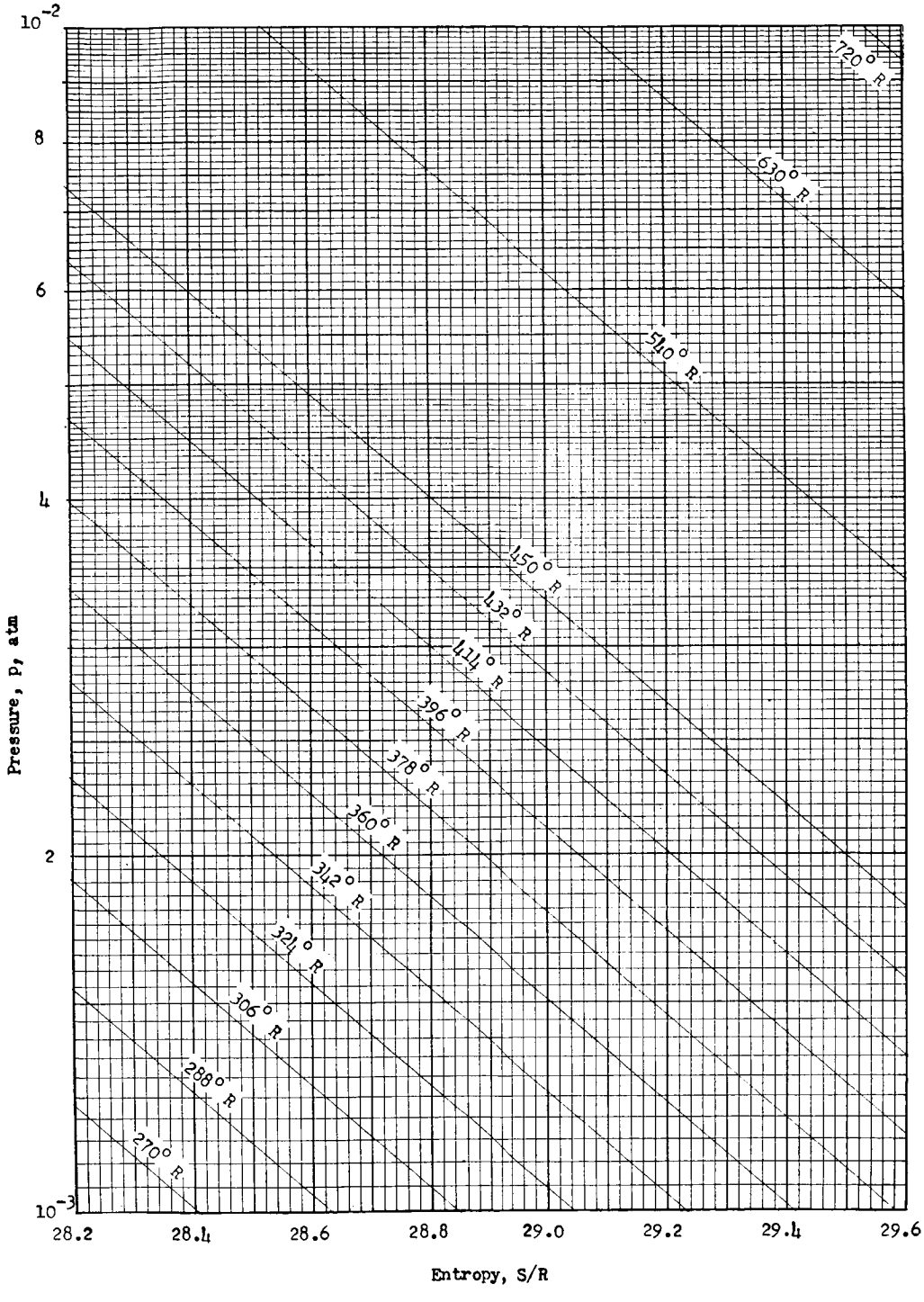

Entropy chart 28

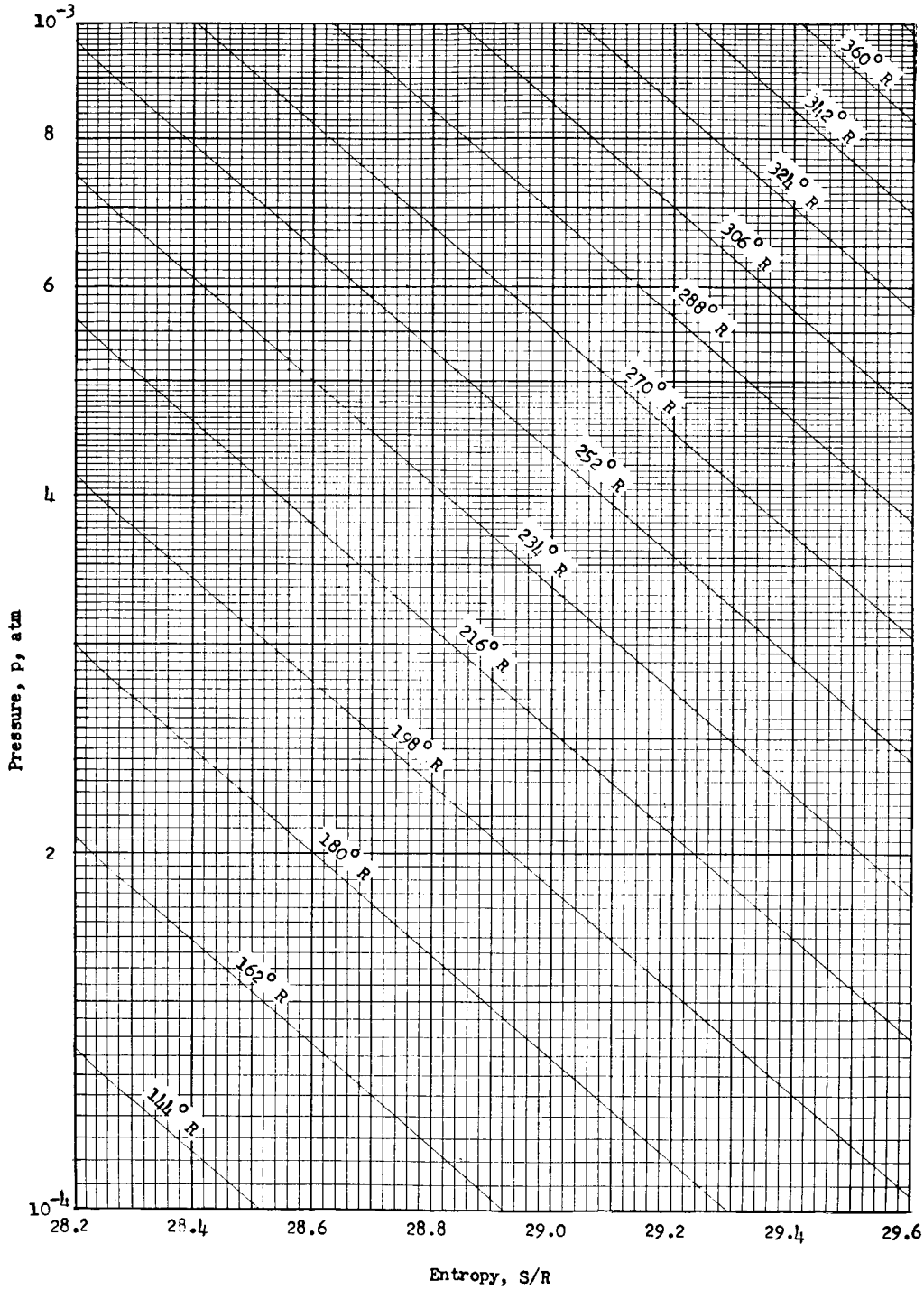

Entropy chart 29

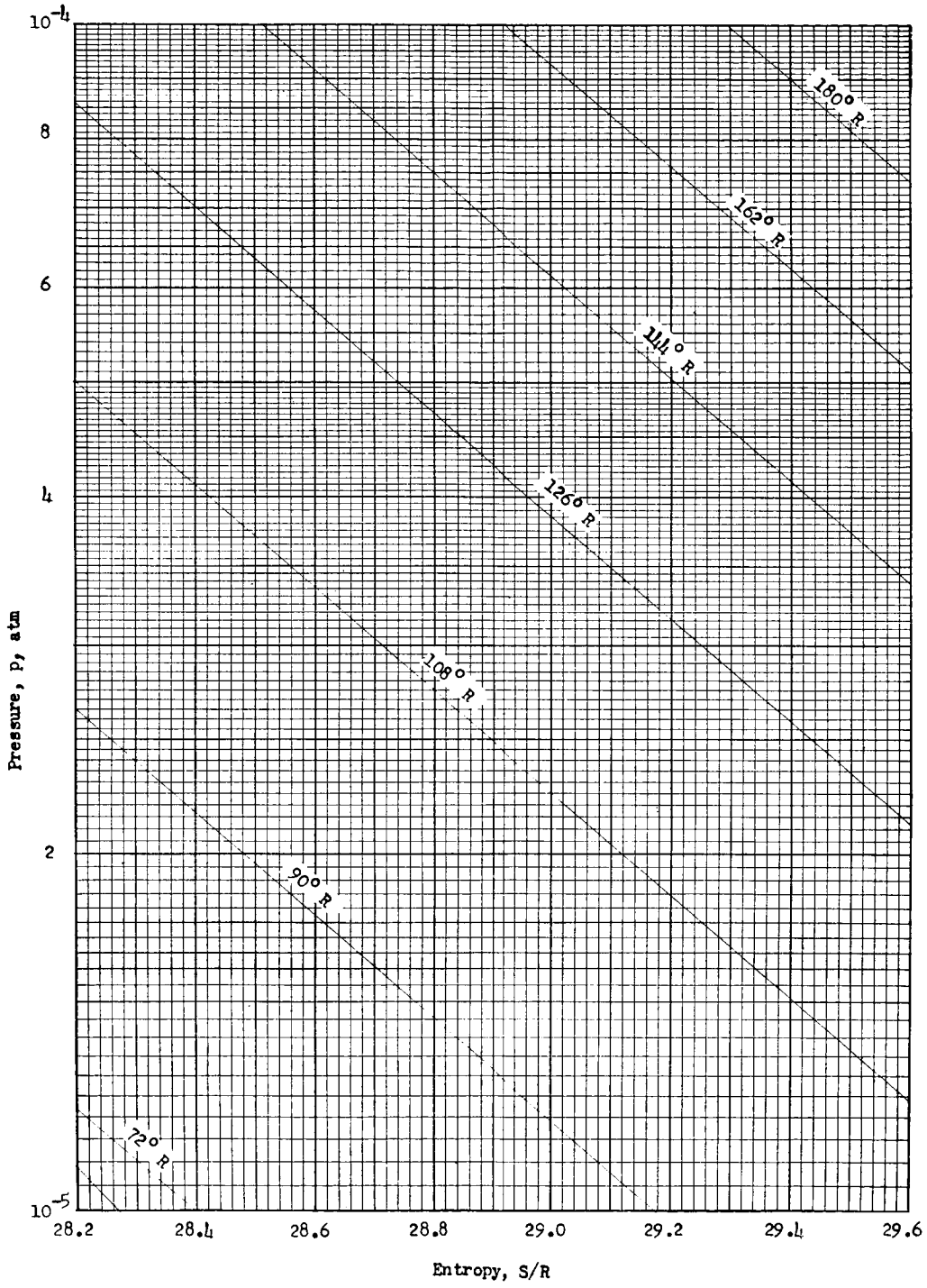

Entropy chart 30

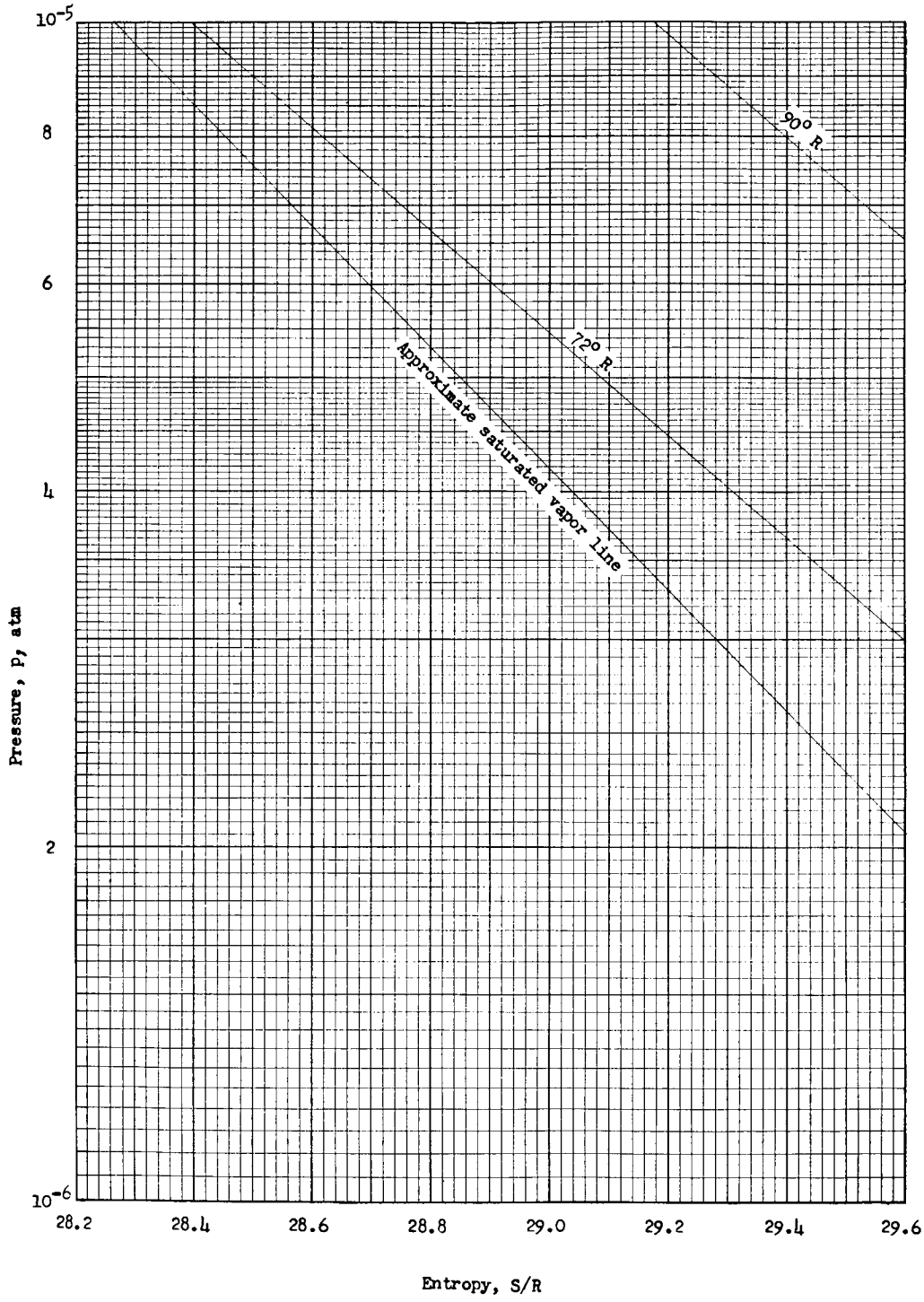

Entropy chart 31

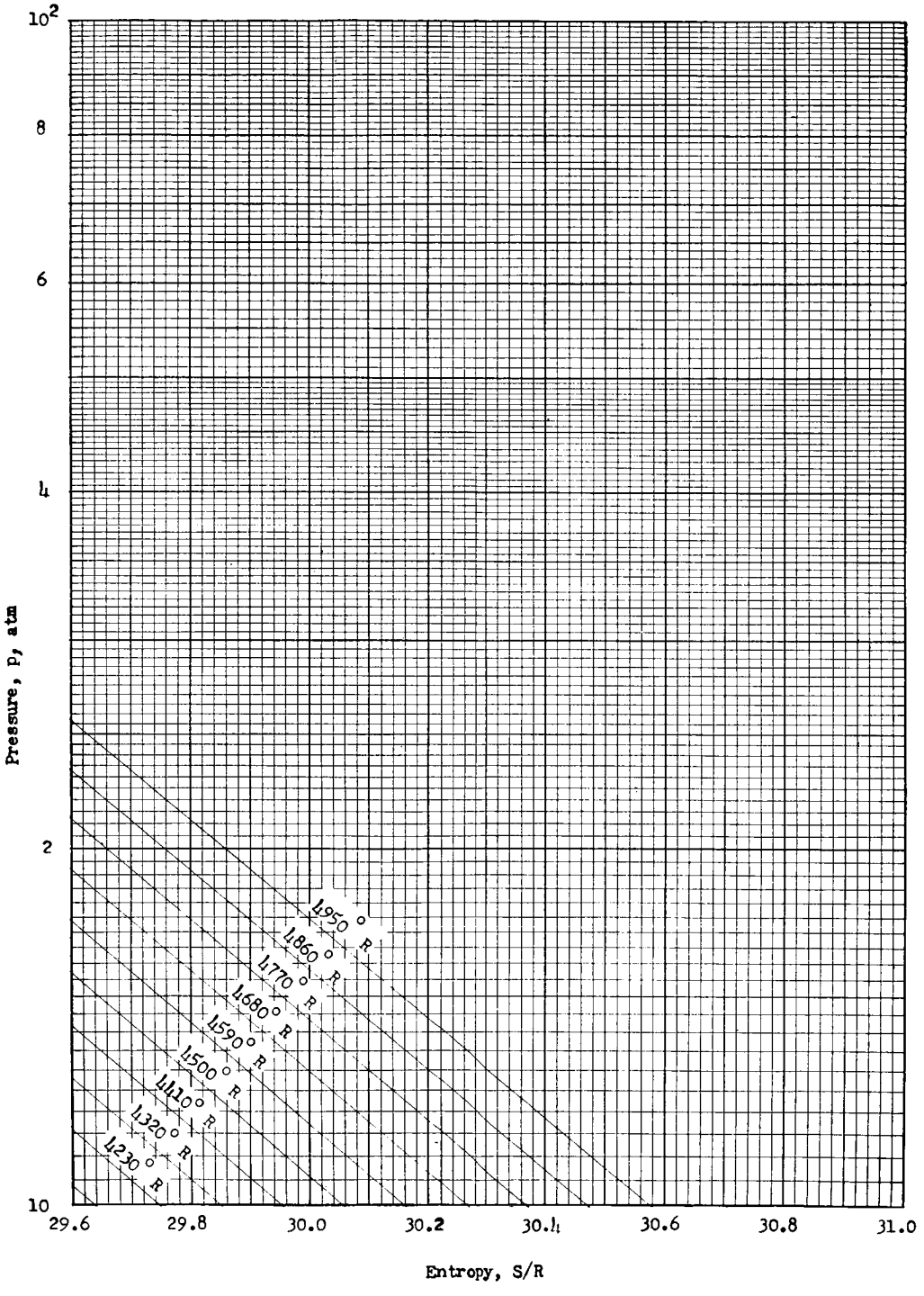

Entropy chart 32

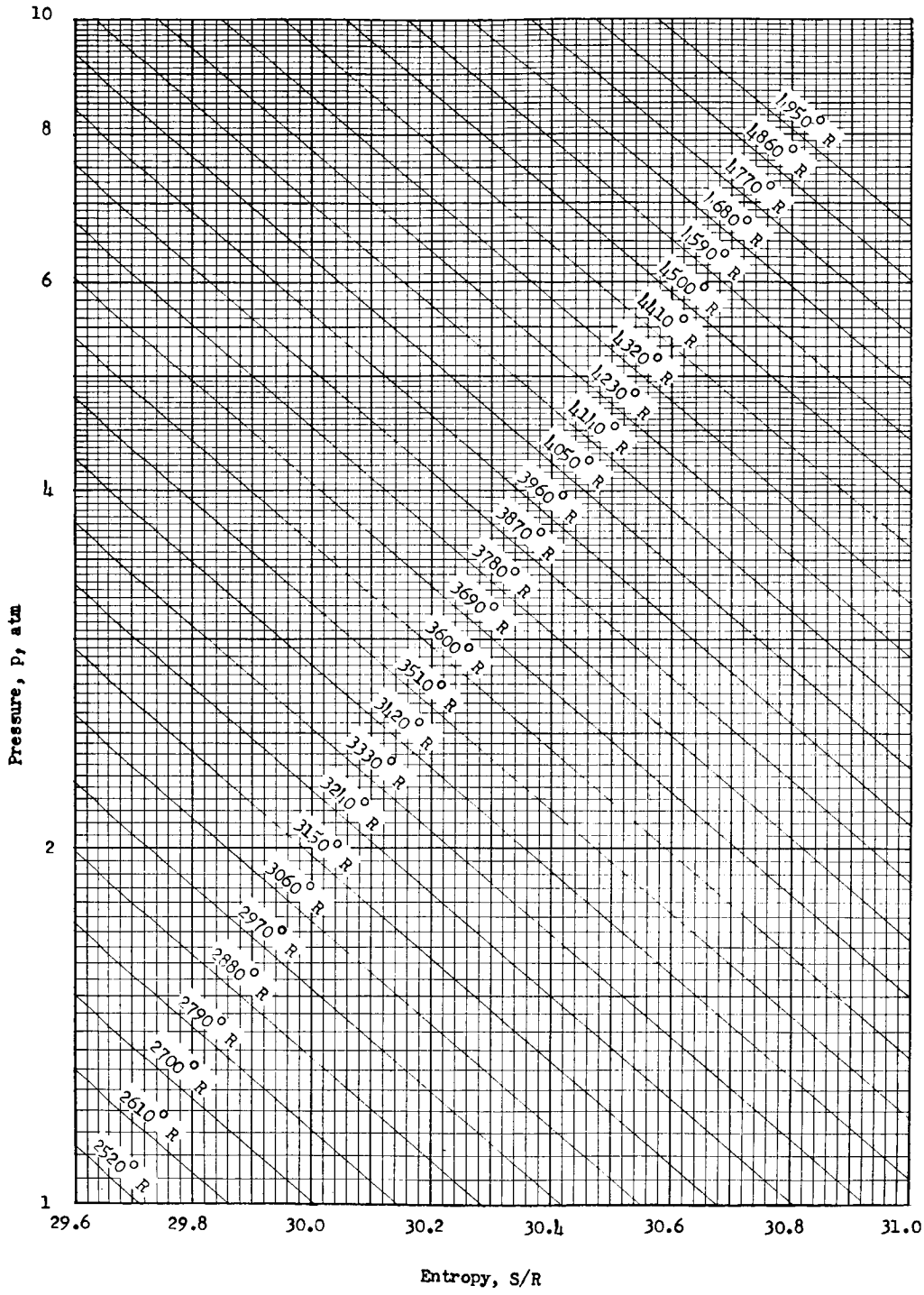

Entropy chart 33

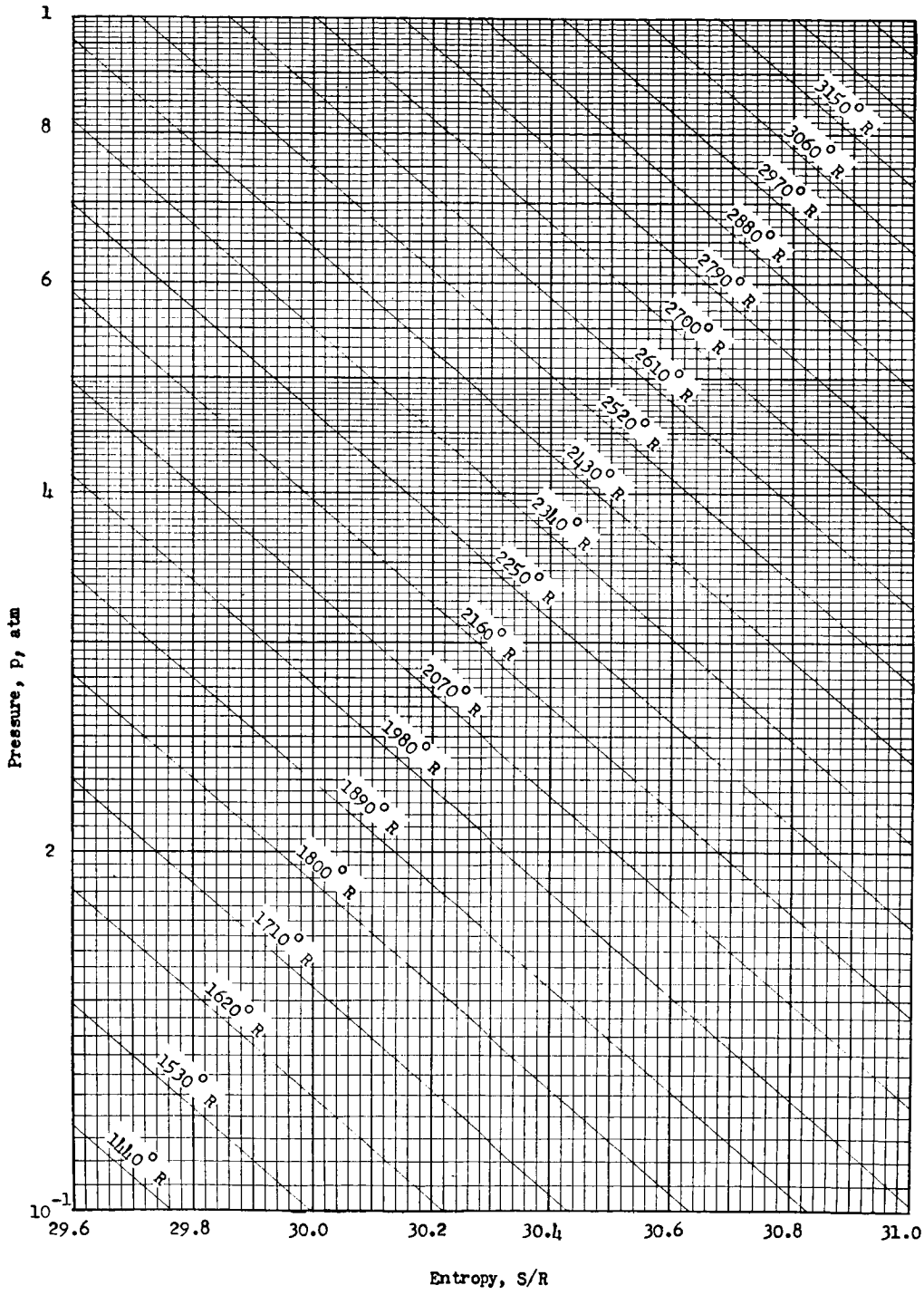

Entropy chart 34

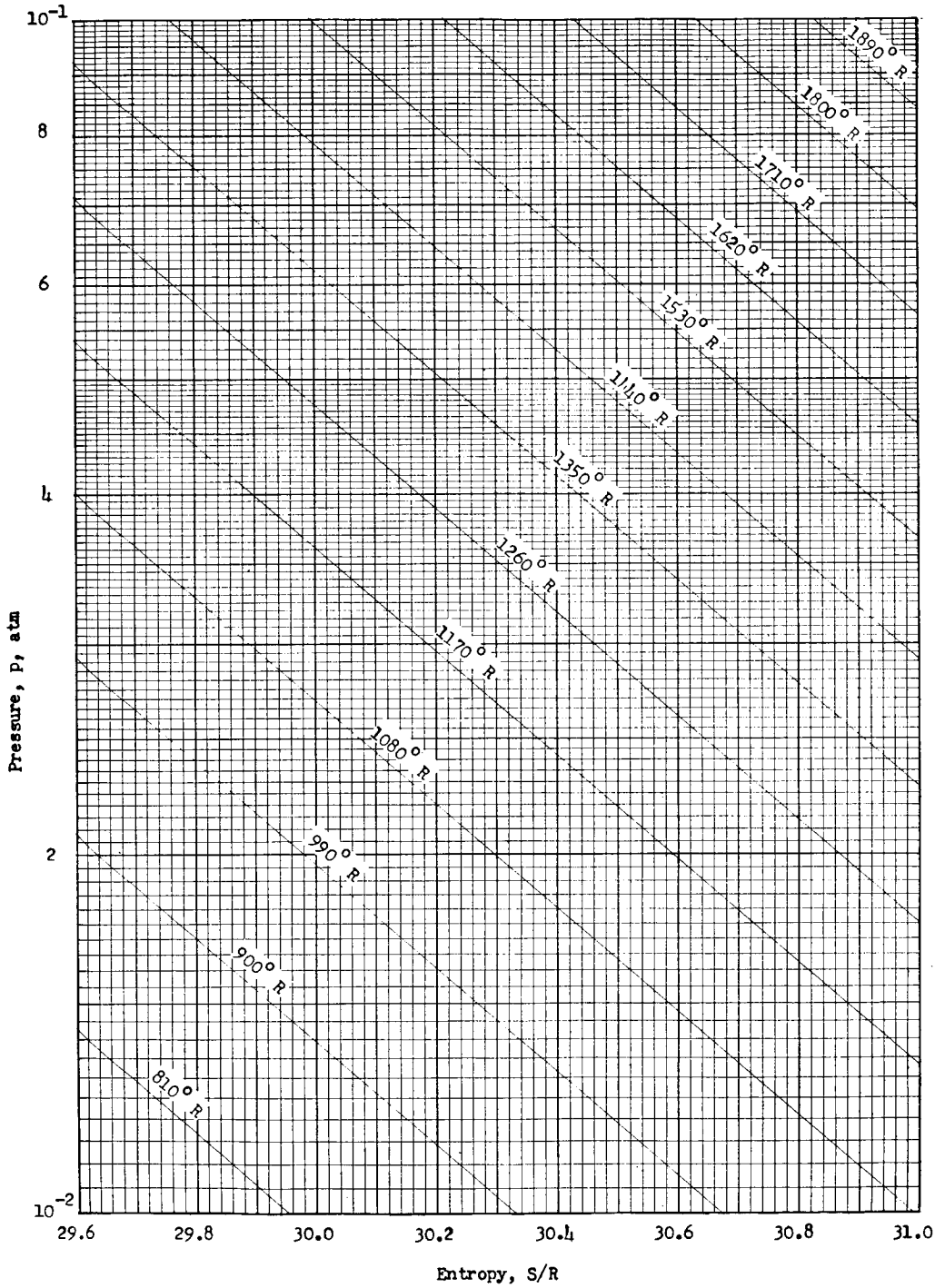

Entropy chart 35

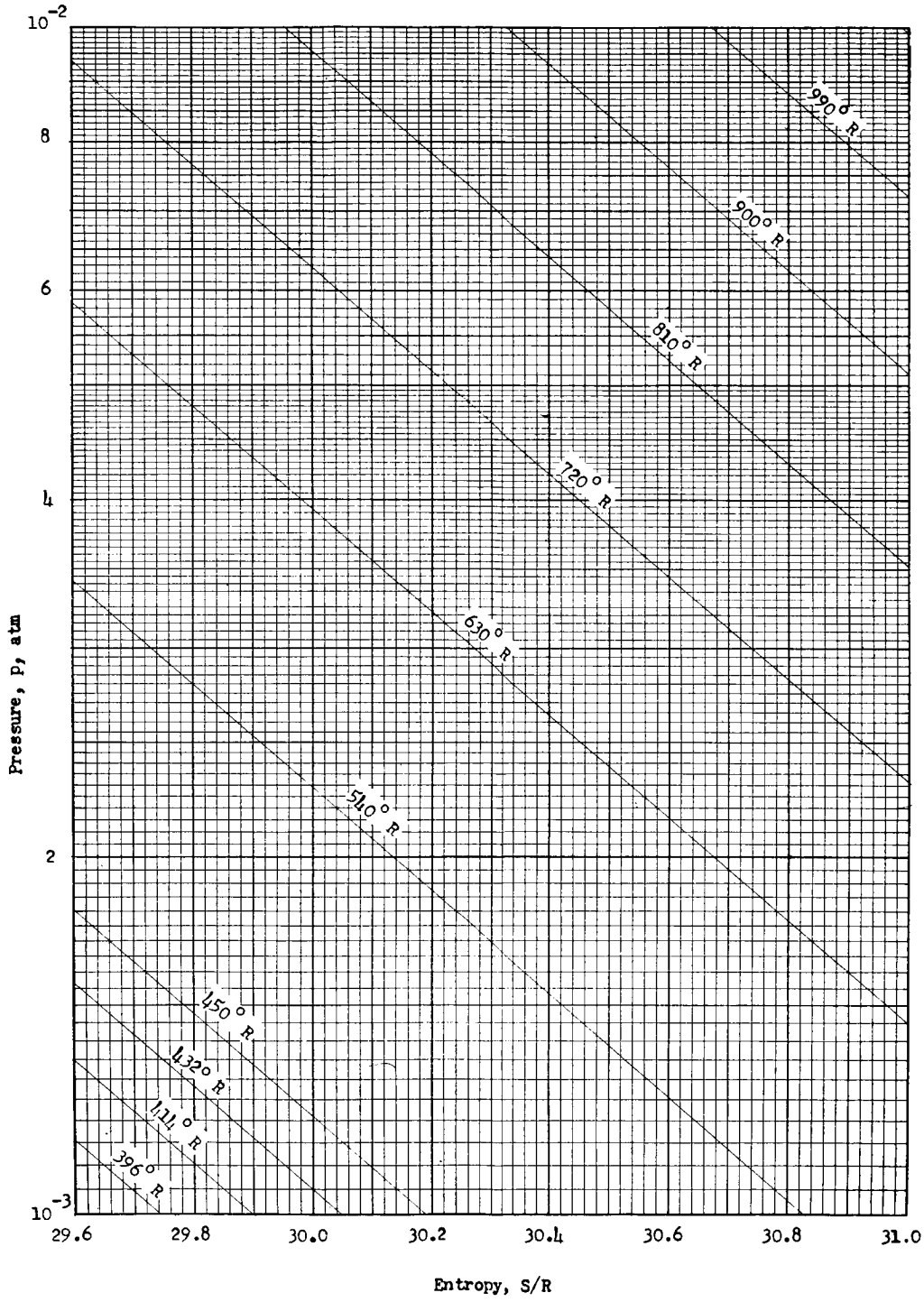

Entropy chart 36

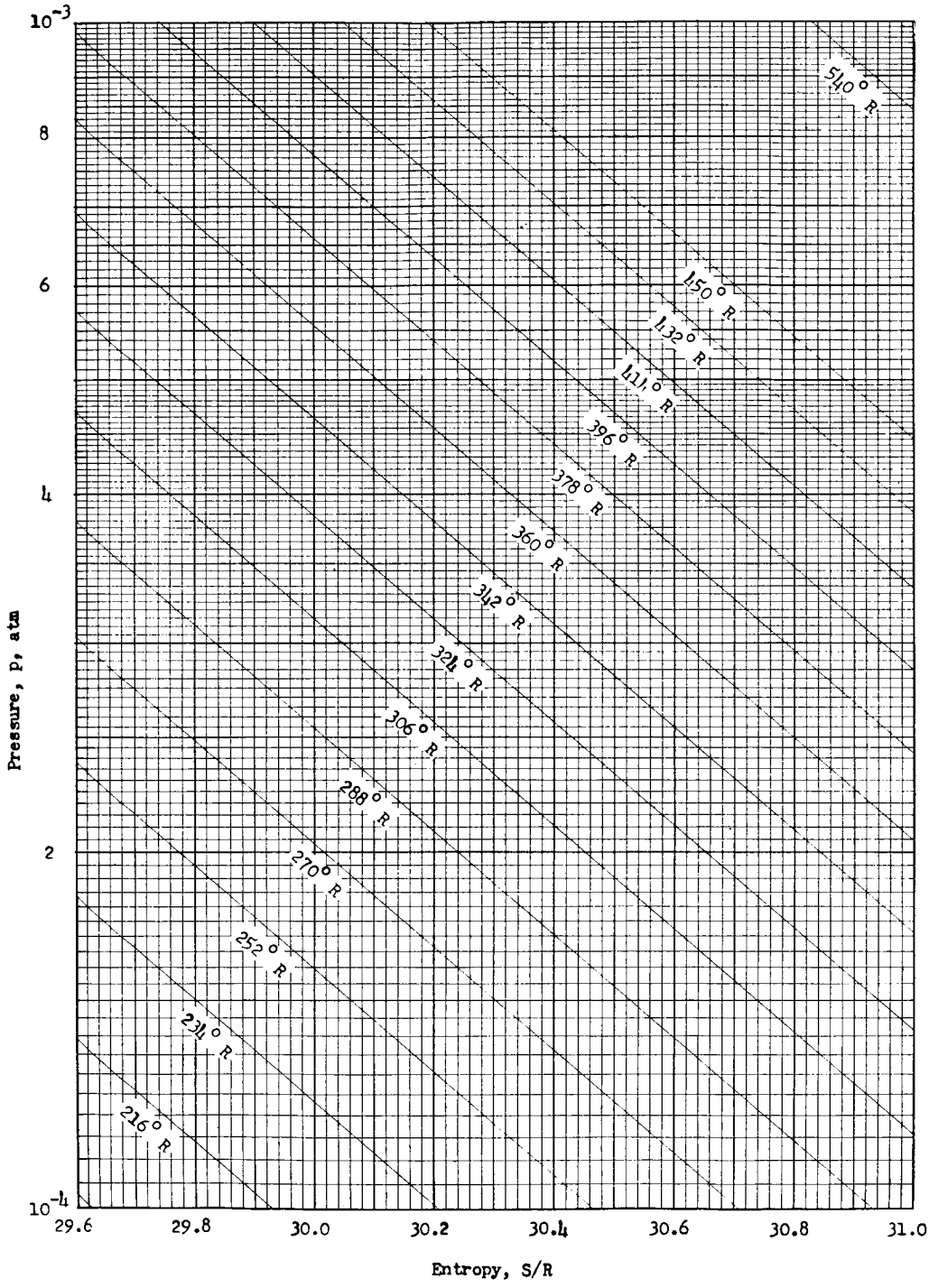

Entropy chart 37

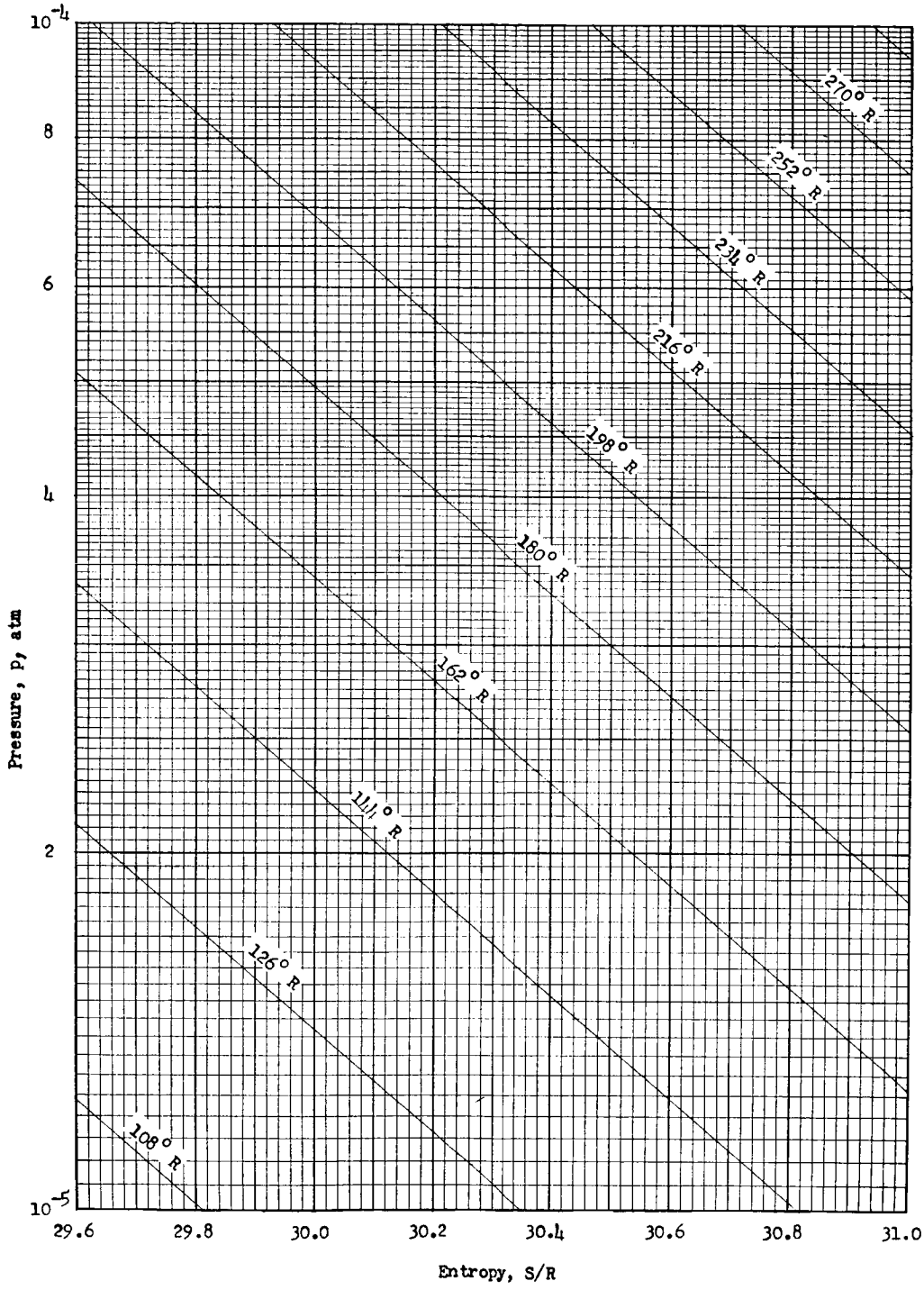

Entropy chart 38

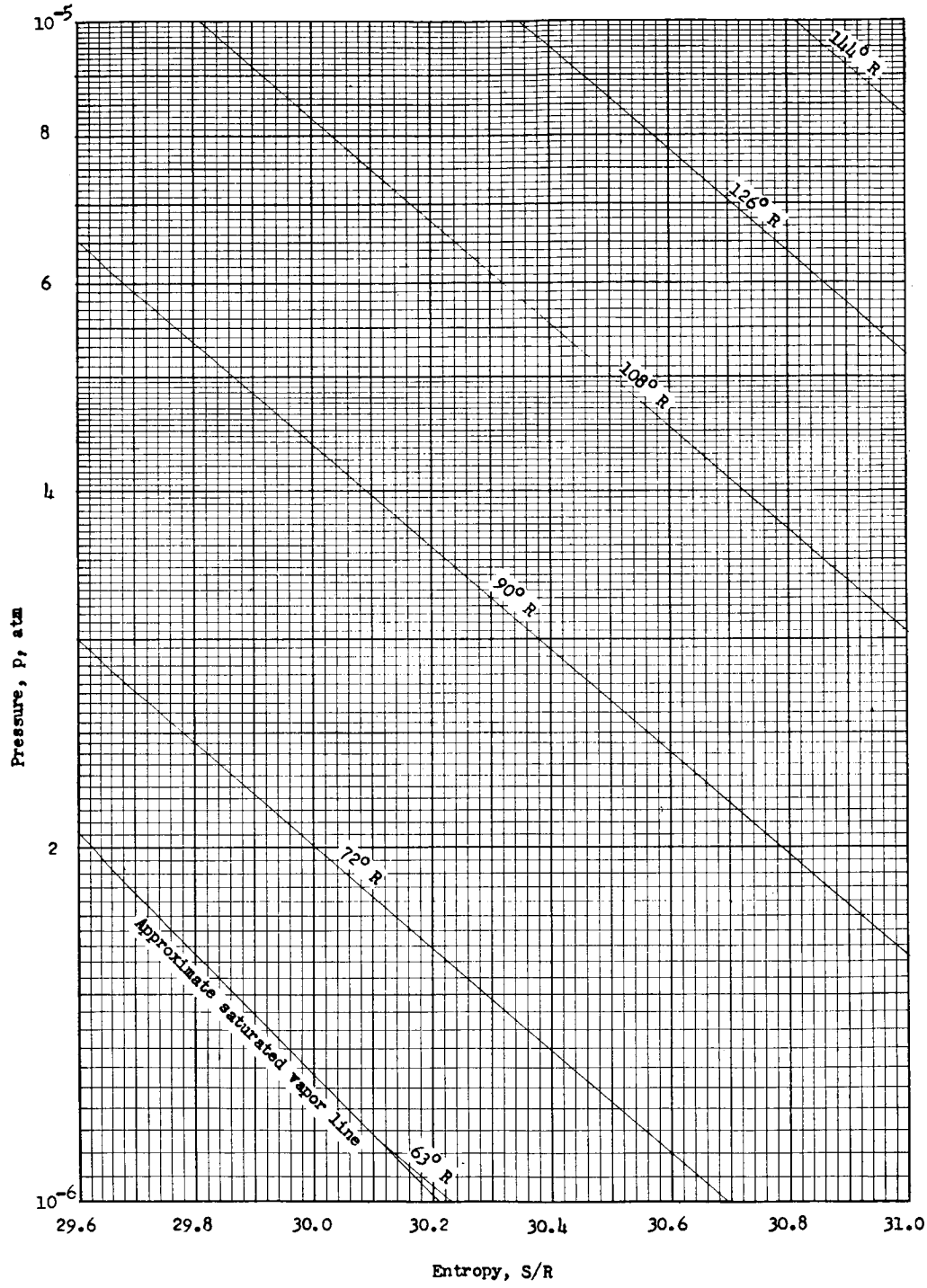

Entropy chart 39

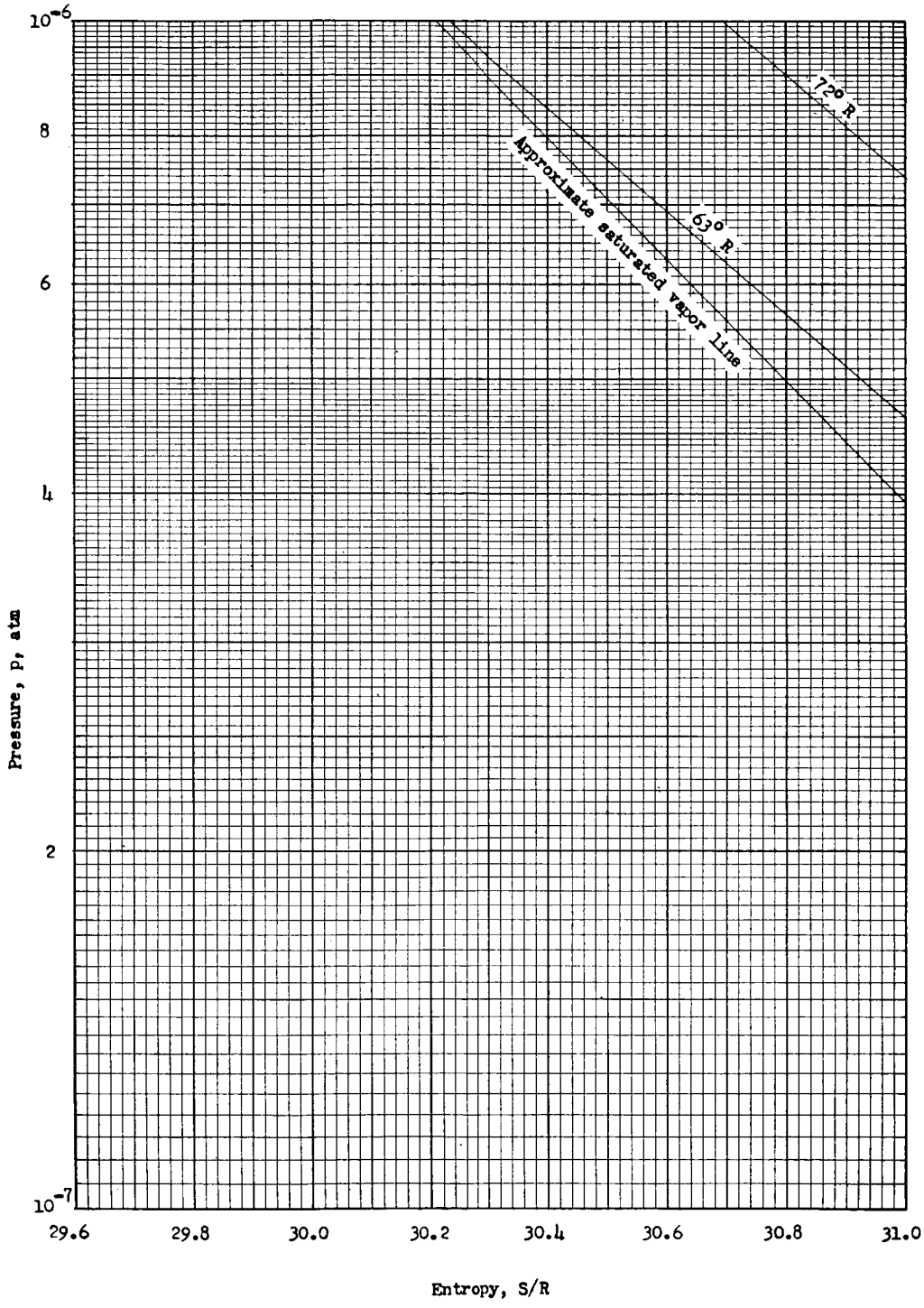

Entropy chart 40

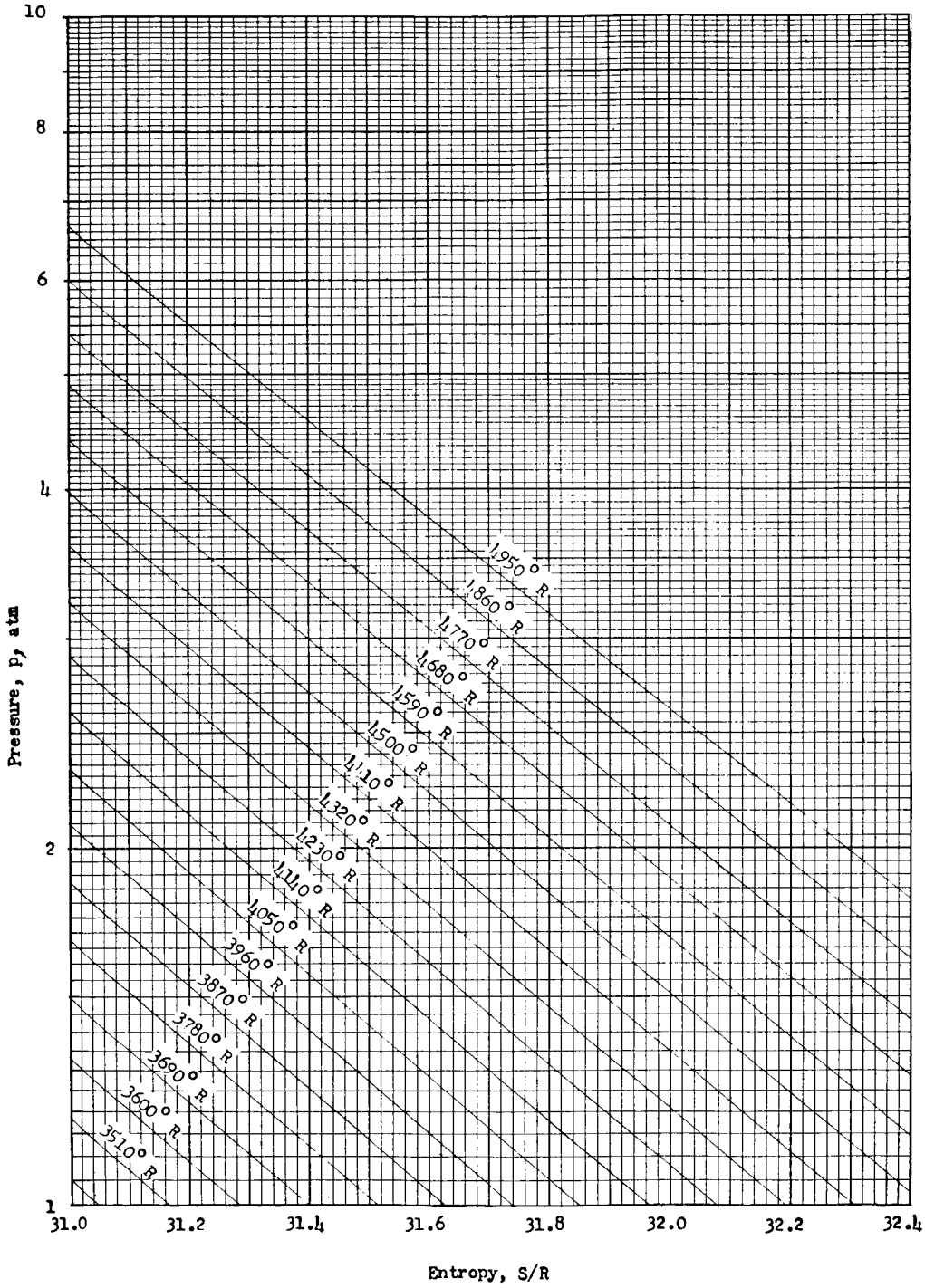

Entropy chart 41

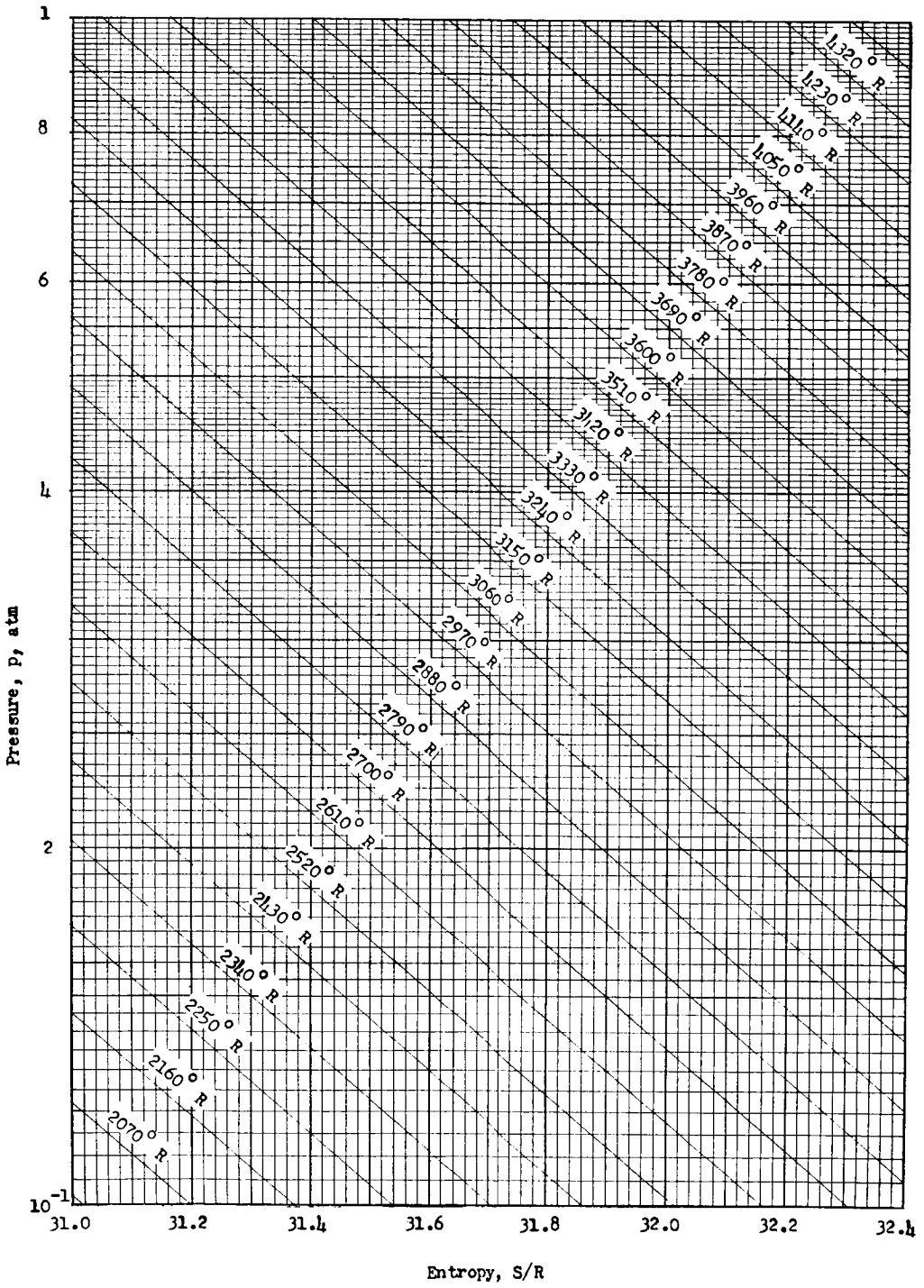

Entropy chart 42

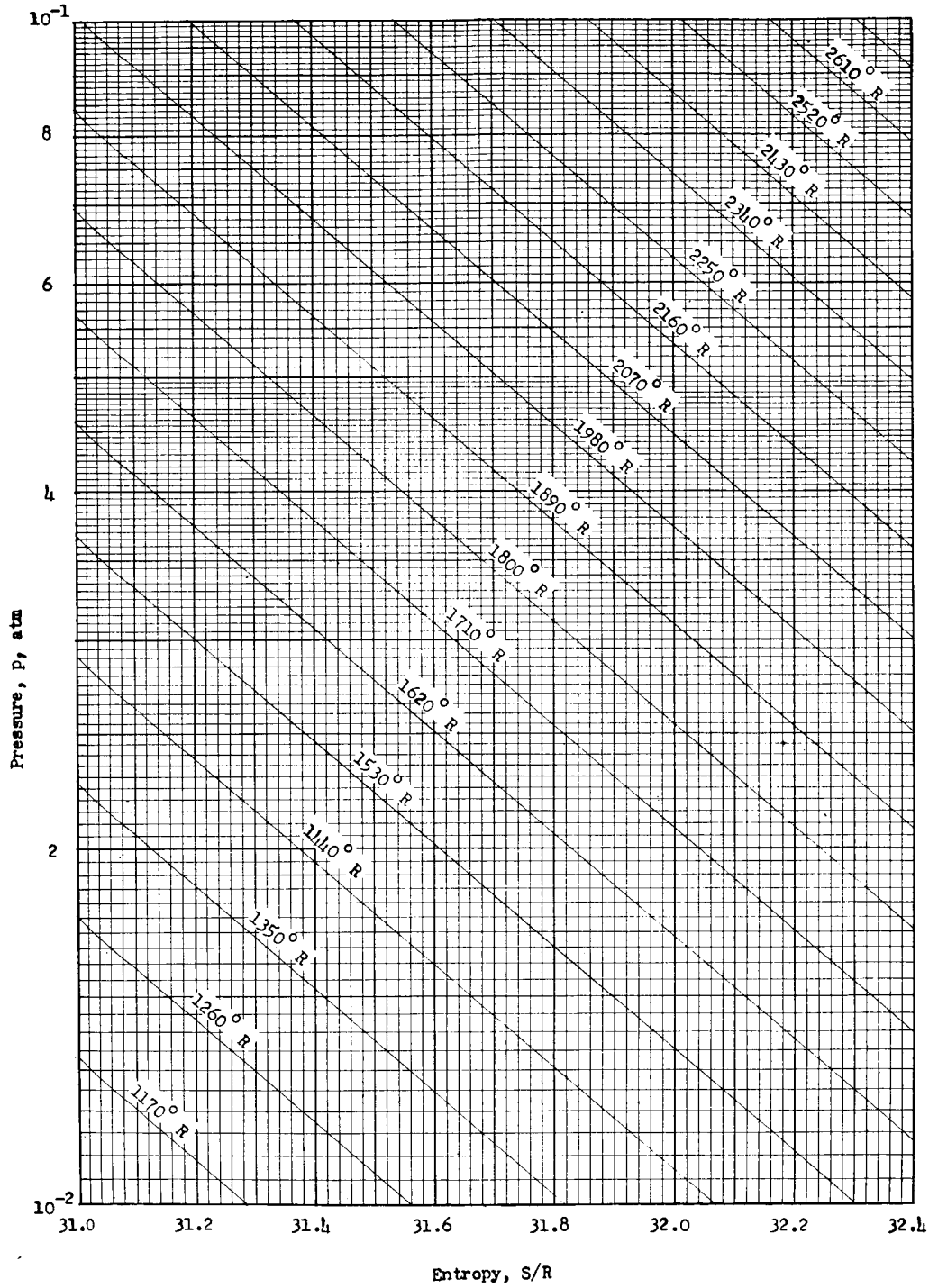

Entropy chart 43

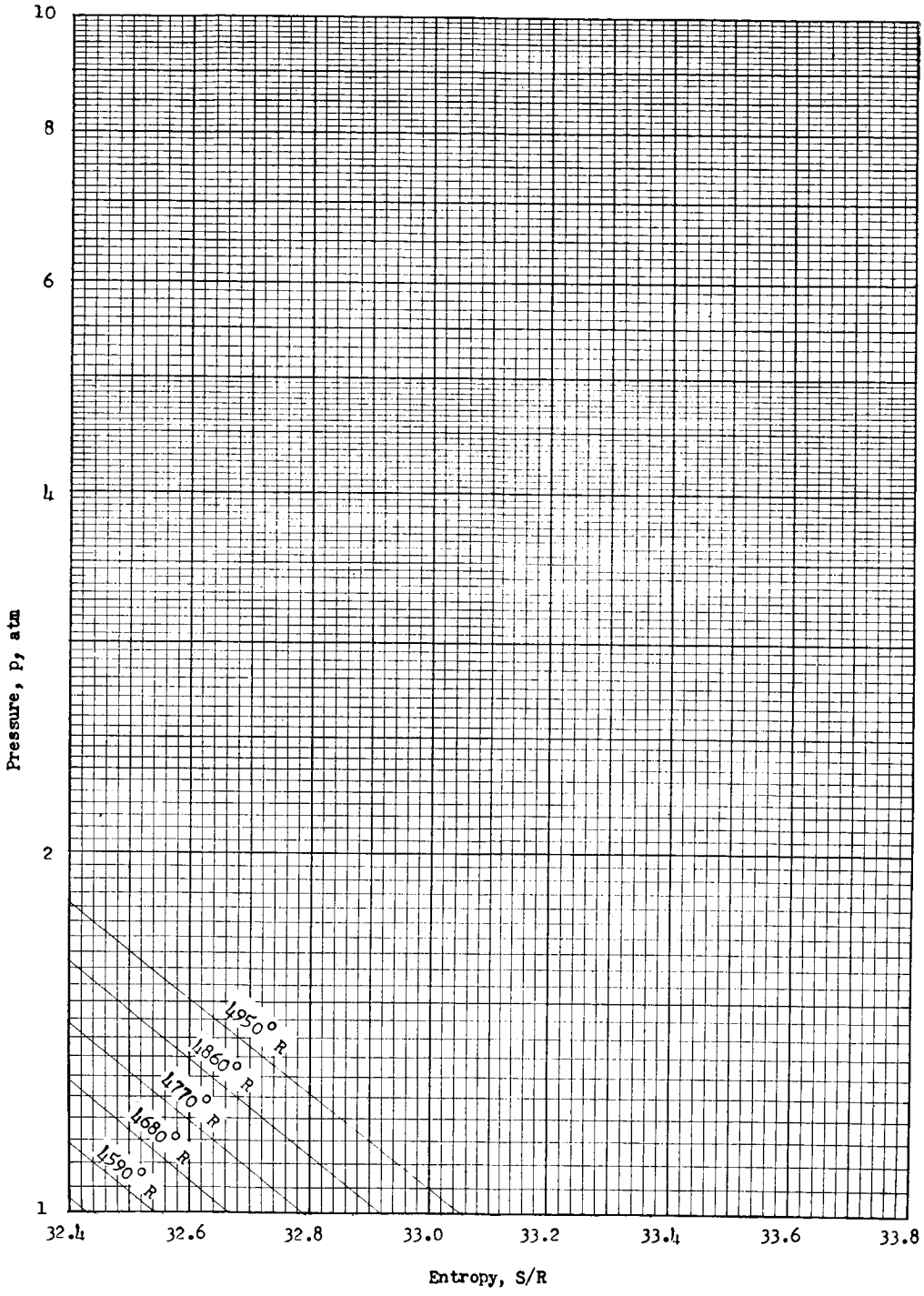

Entropy chart 44

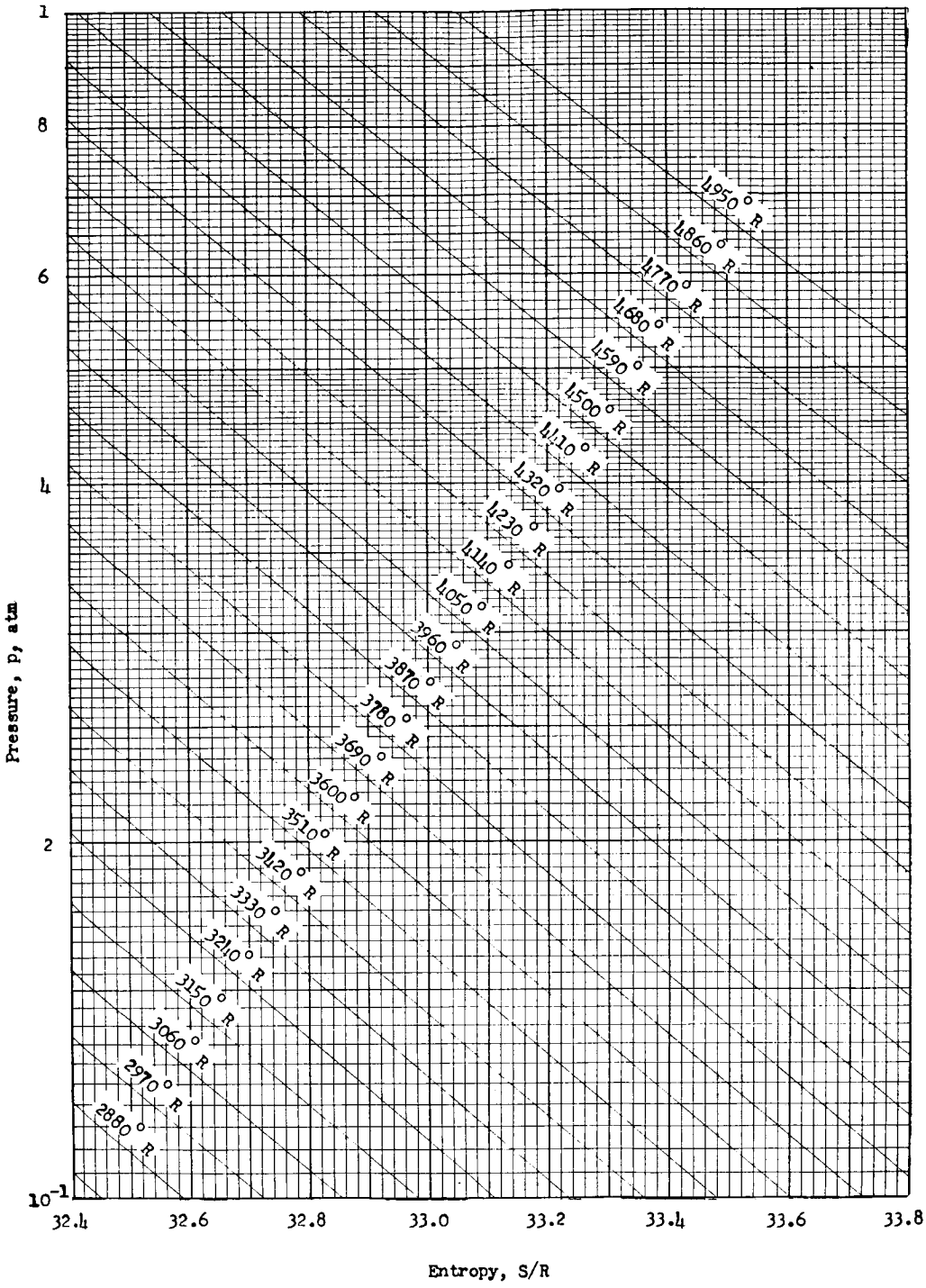

Entropy chart 45

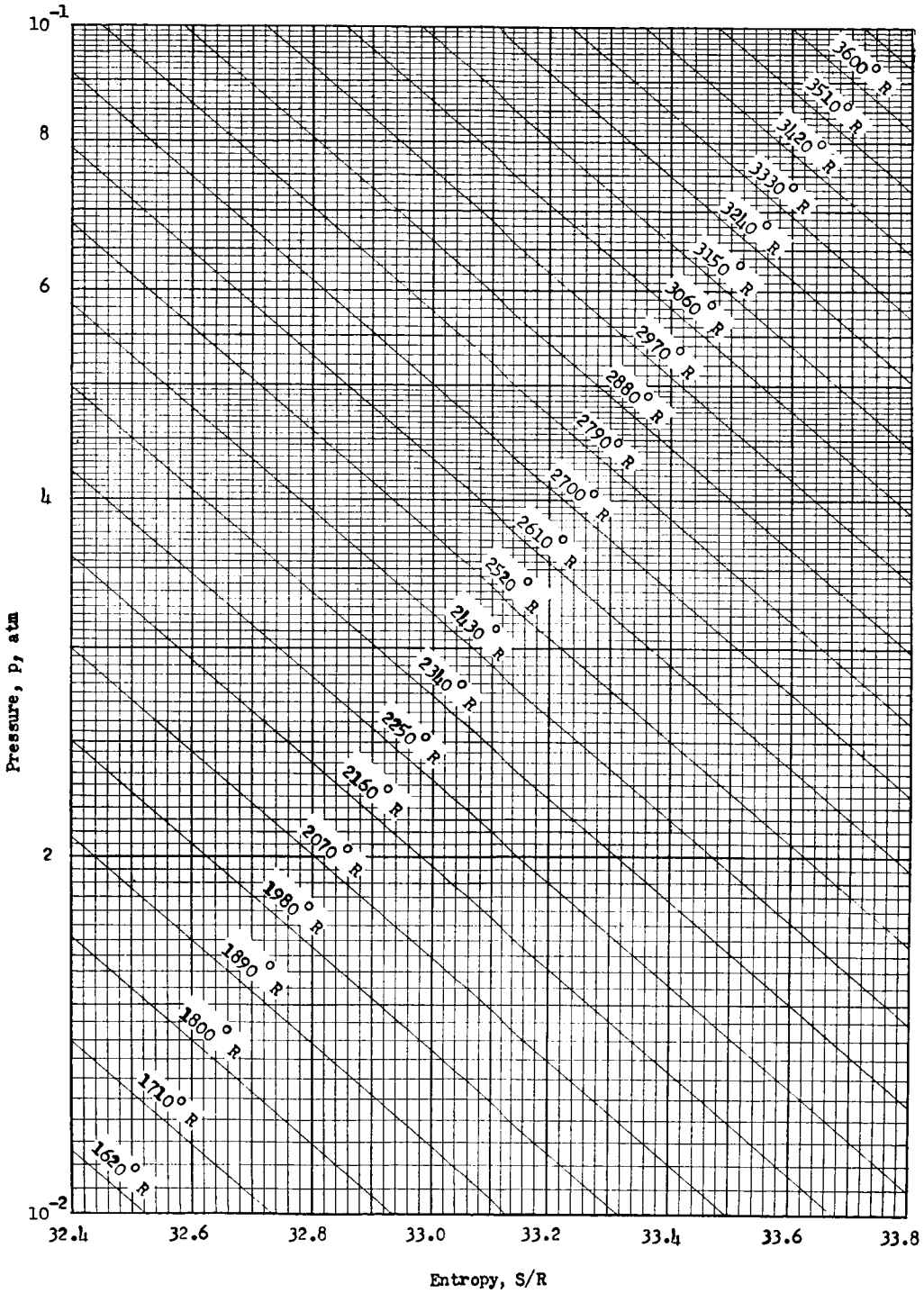

Entropy chart 46

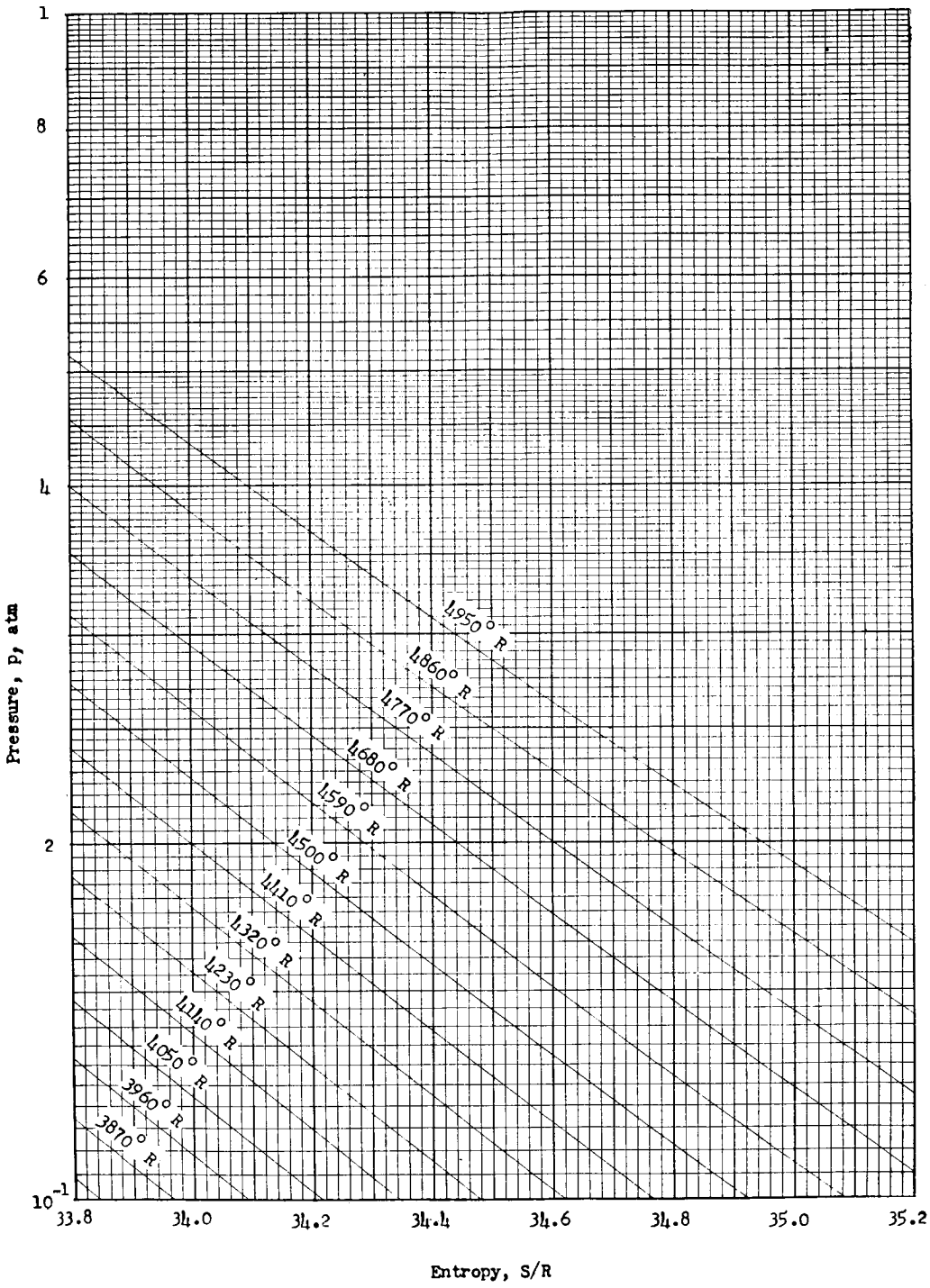

Entropy chart 47

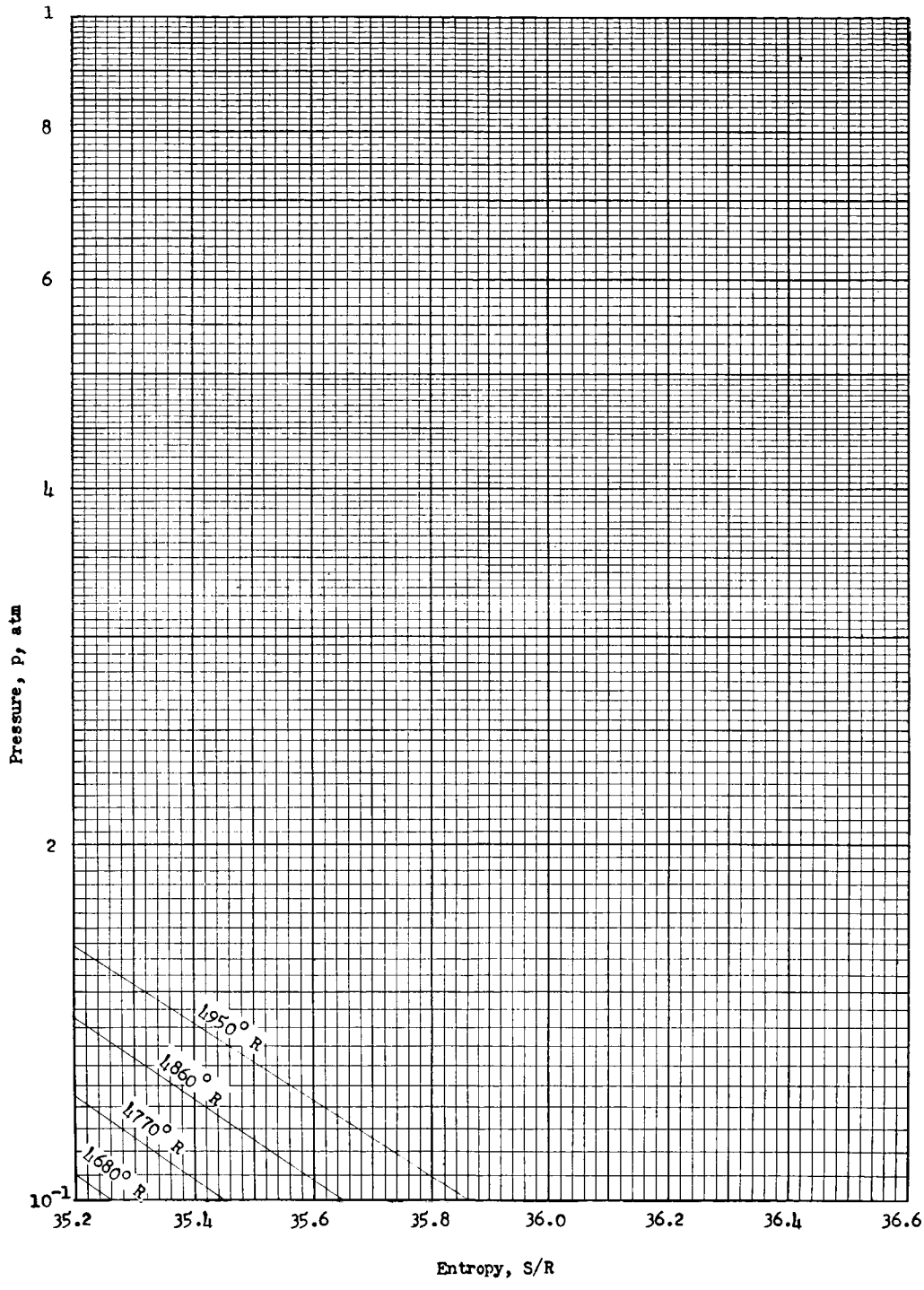

Entropy chart 48

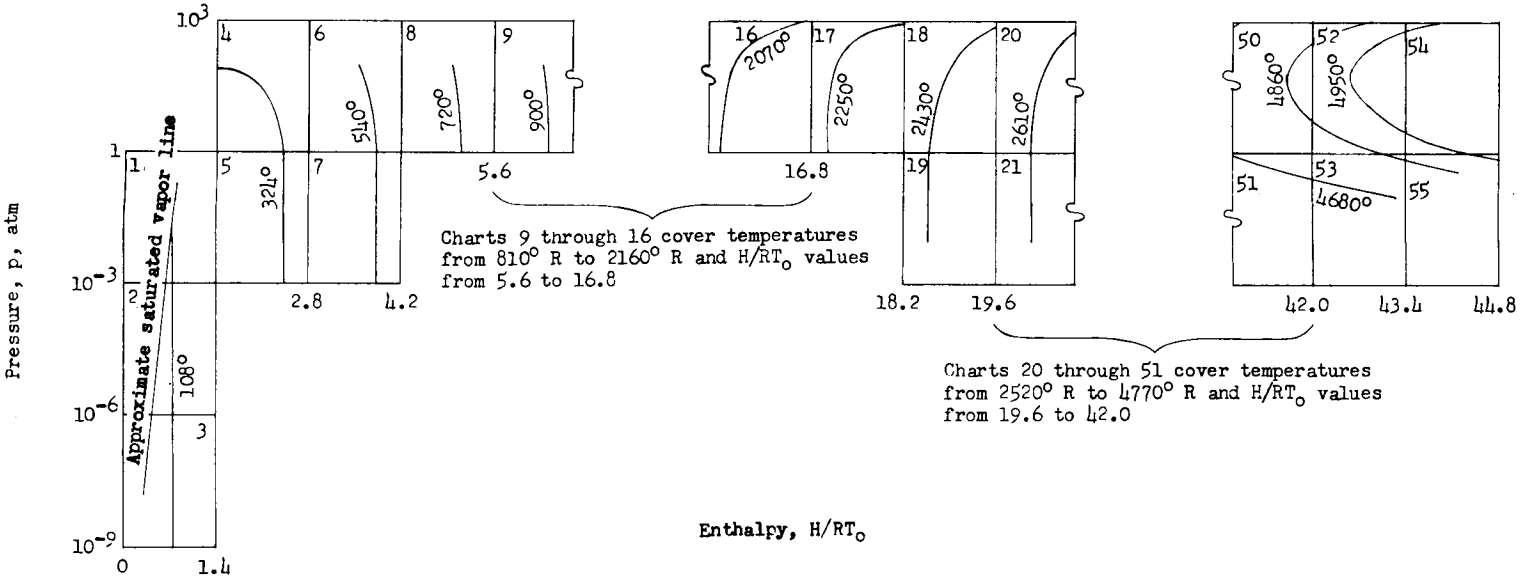

Key to enthalpy charts

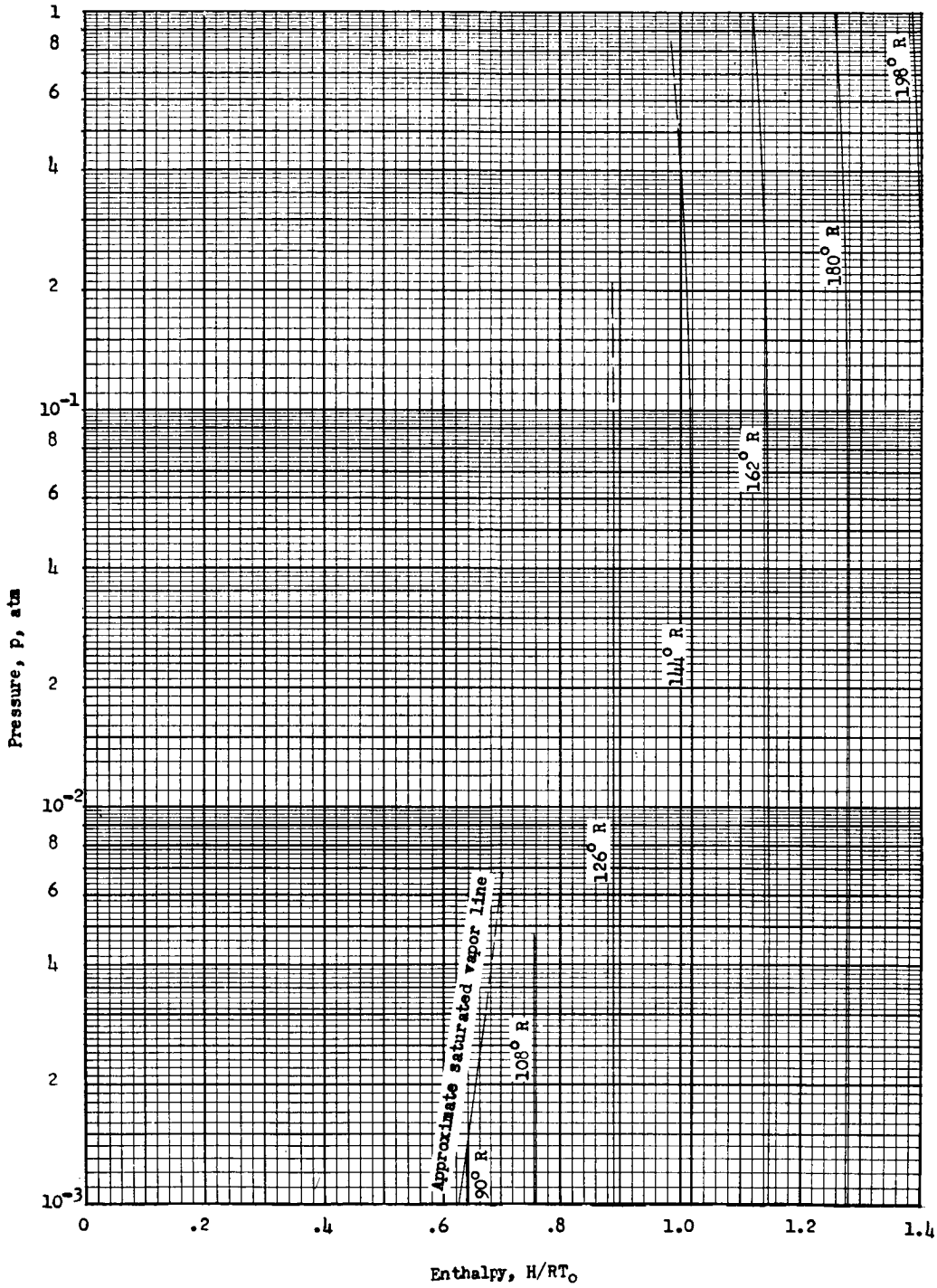

Enthalpy chart 1

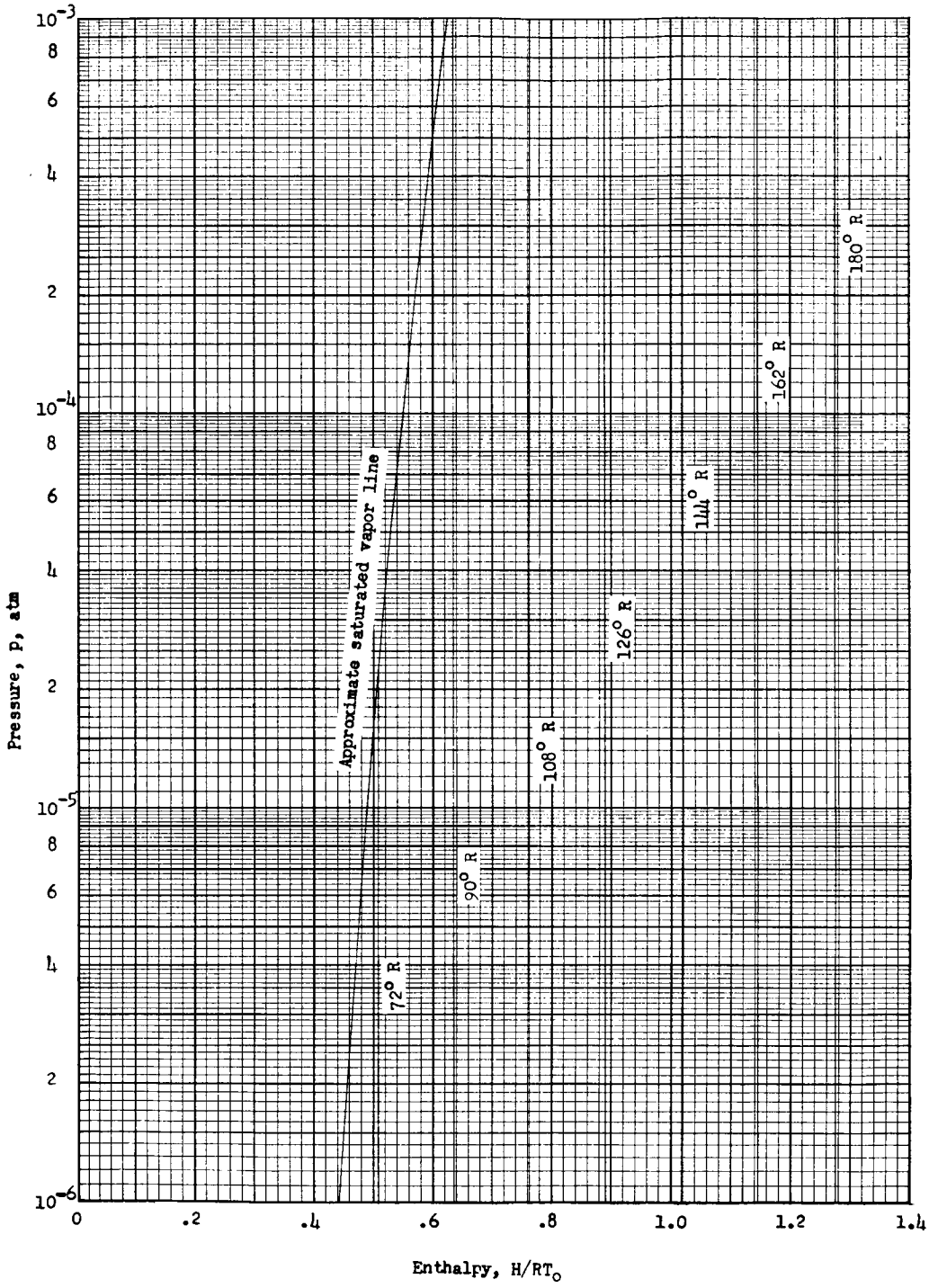

Enthalpy chart 2

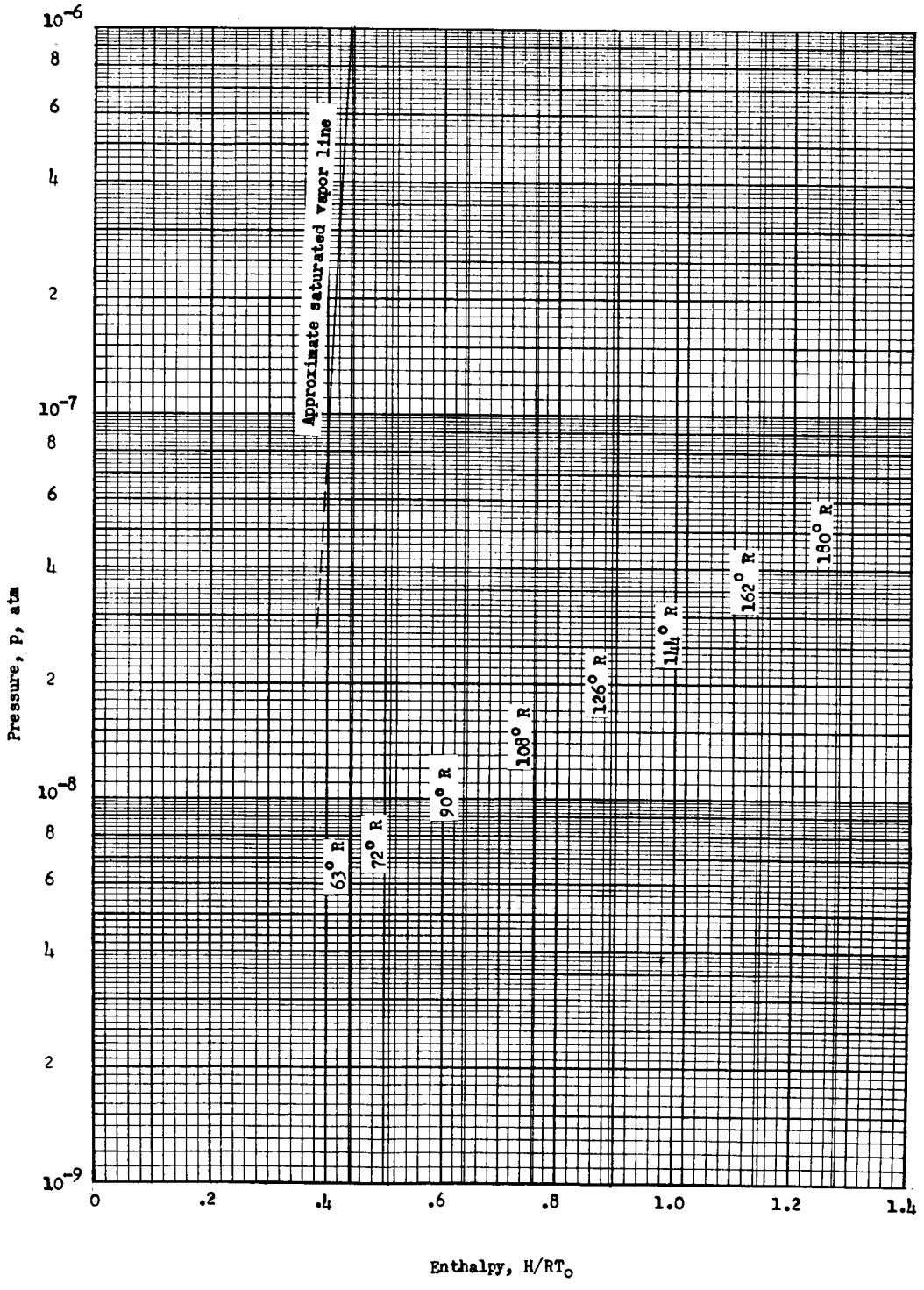

Enthalpy chart 3

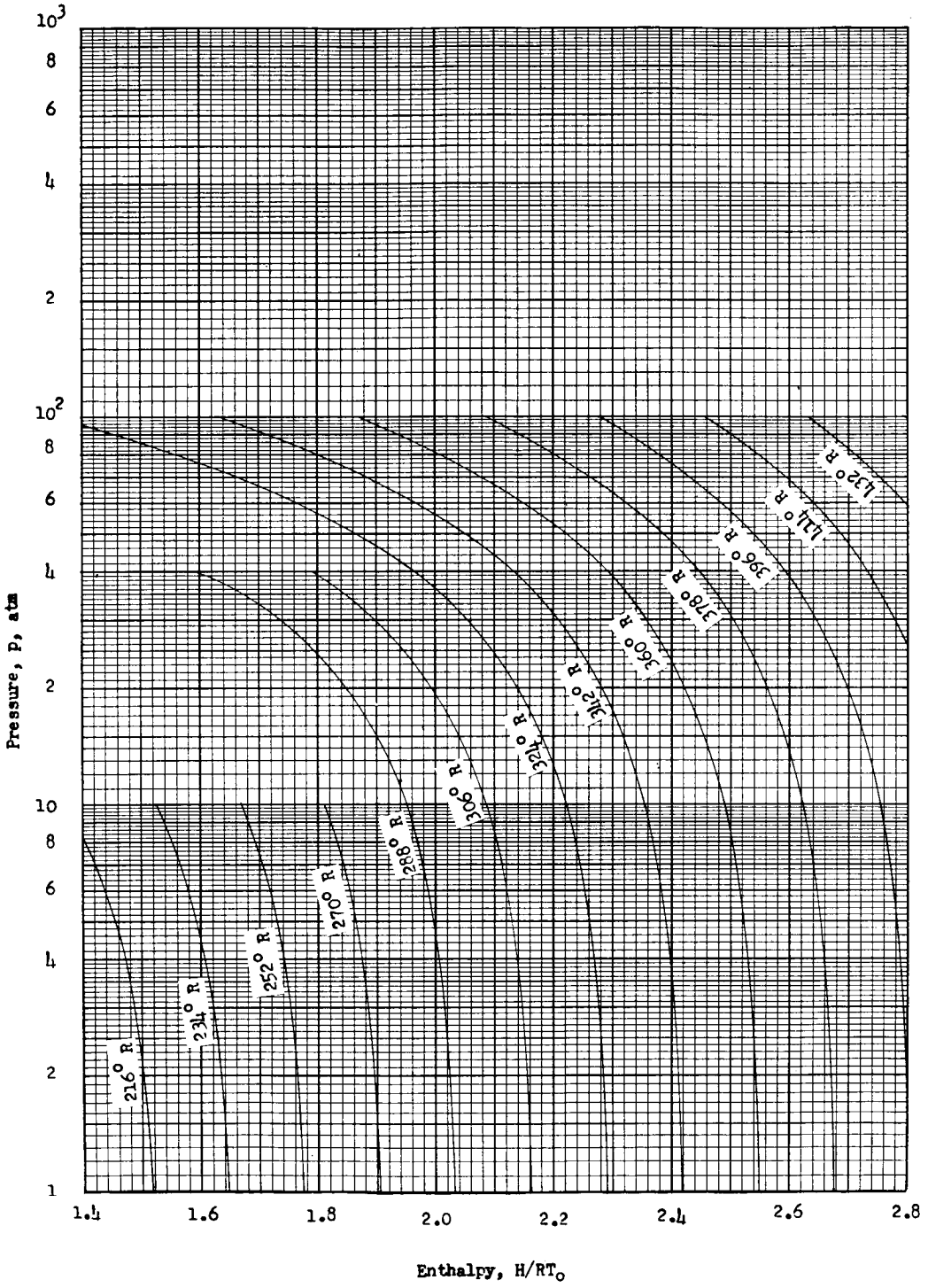

Enthalpy chart 4

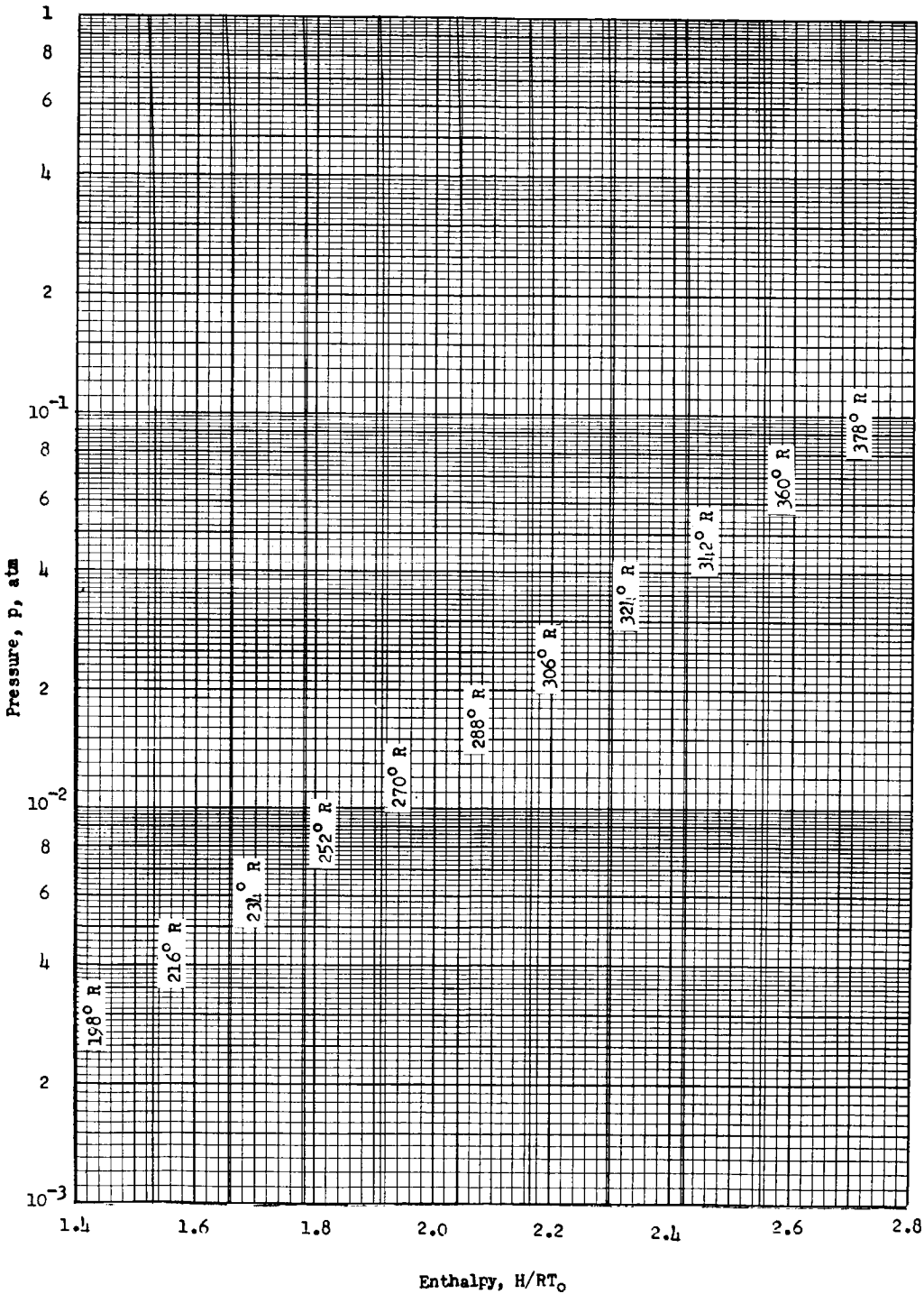

Enthalpy chart 5

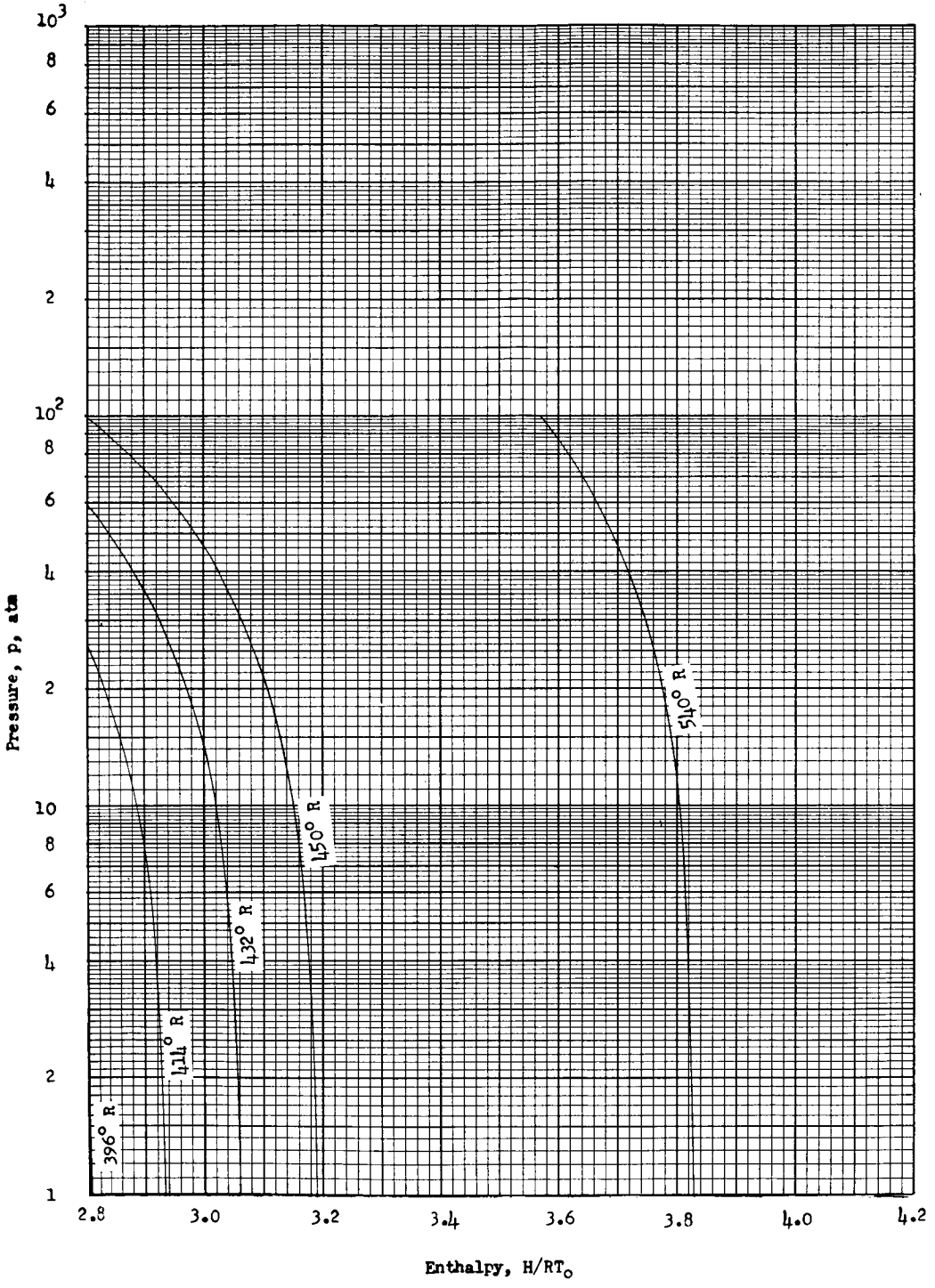

Enthalpy chart 6

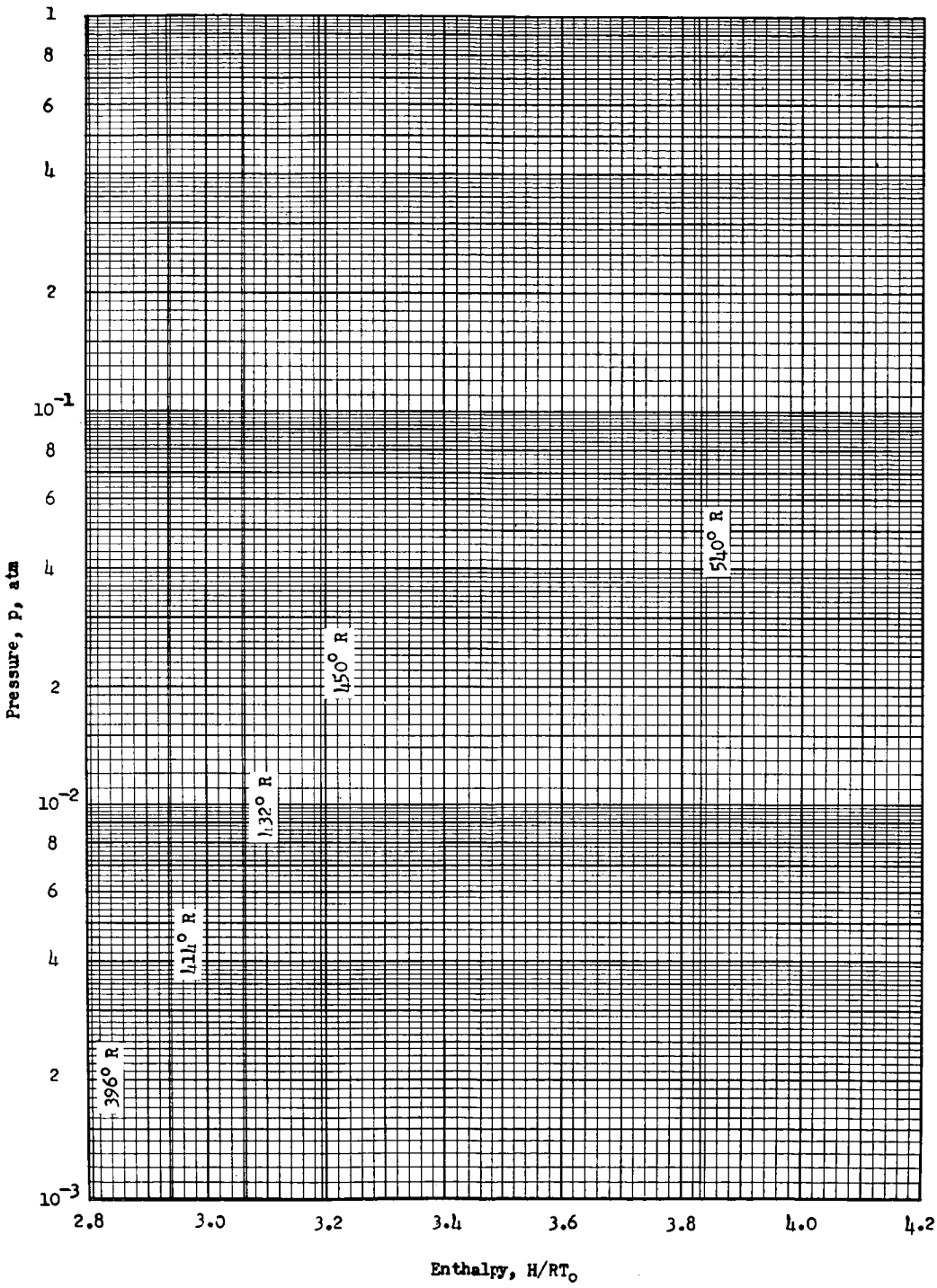

Enthalpy chart 7

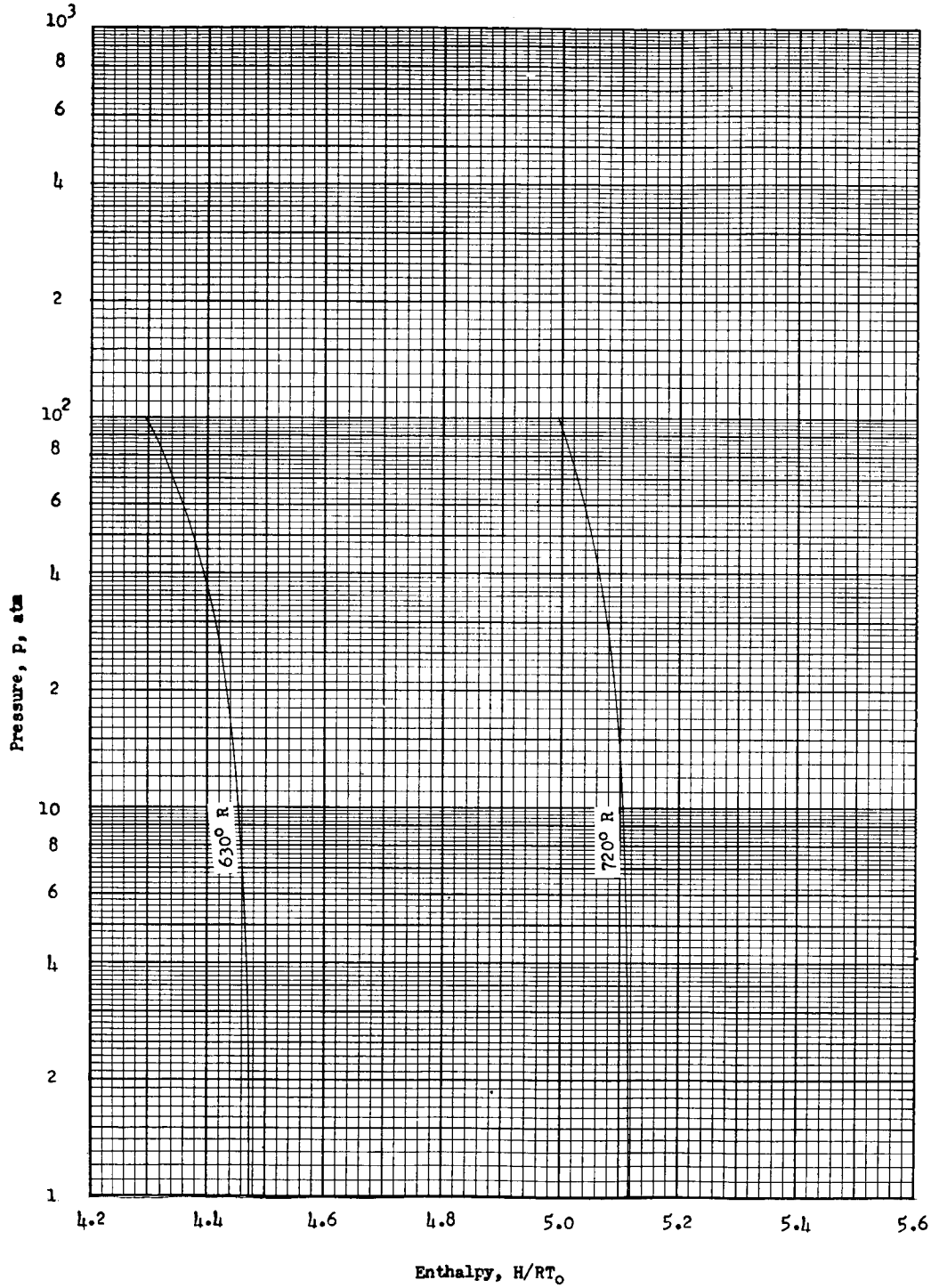

Enthalpy chart 8

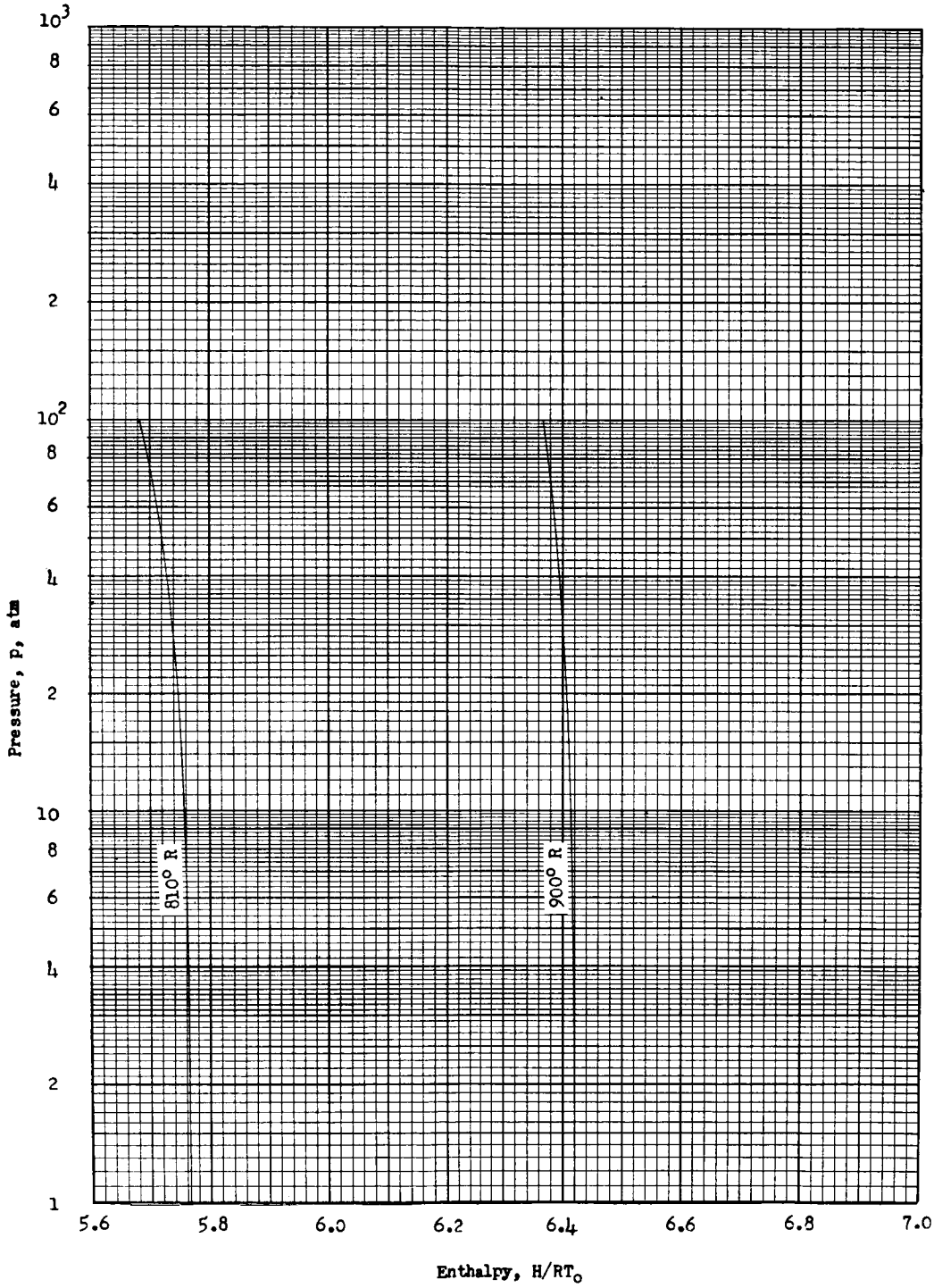

Enthalpy chart 9

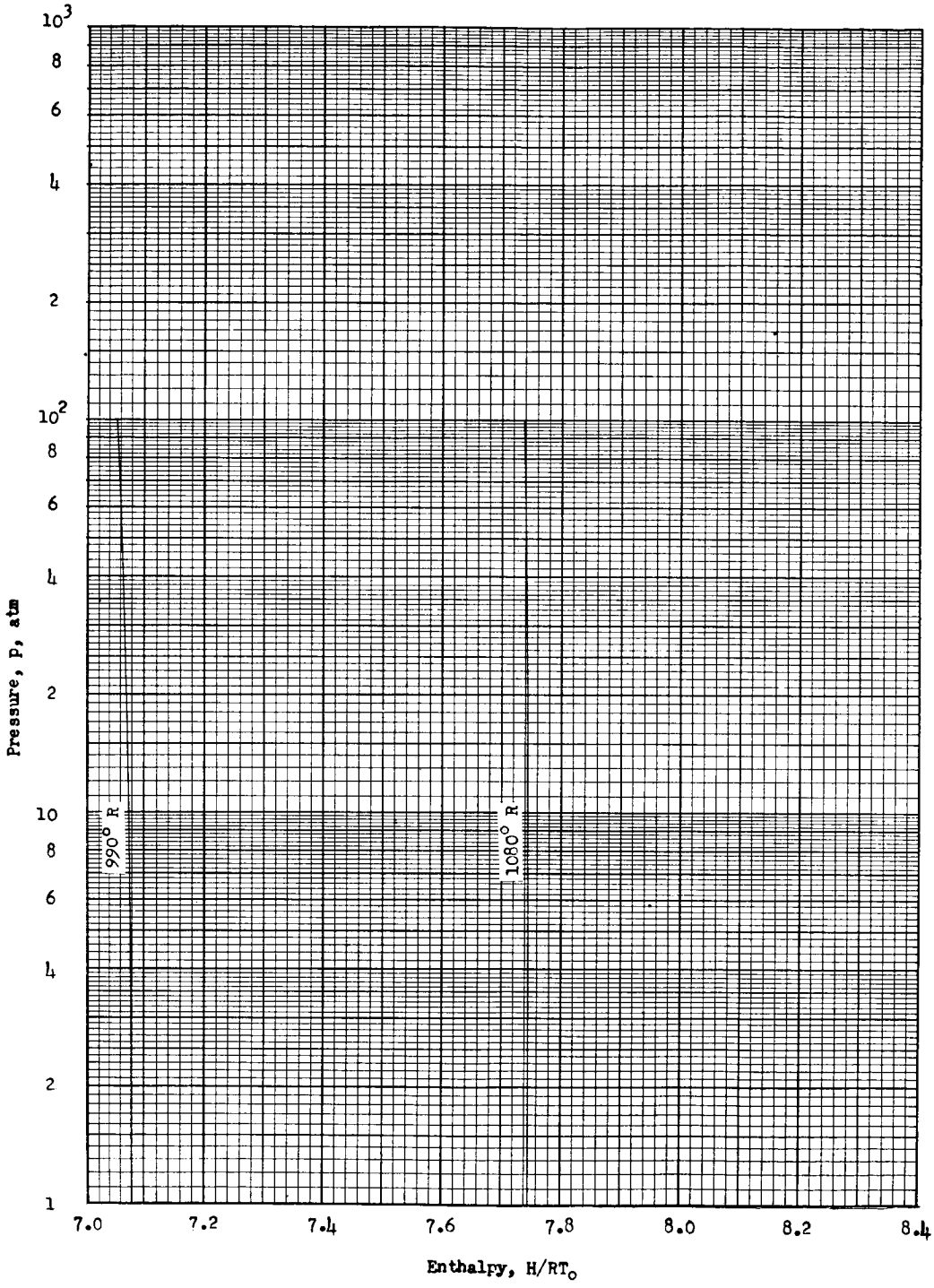

Enthalpy chart 10

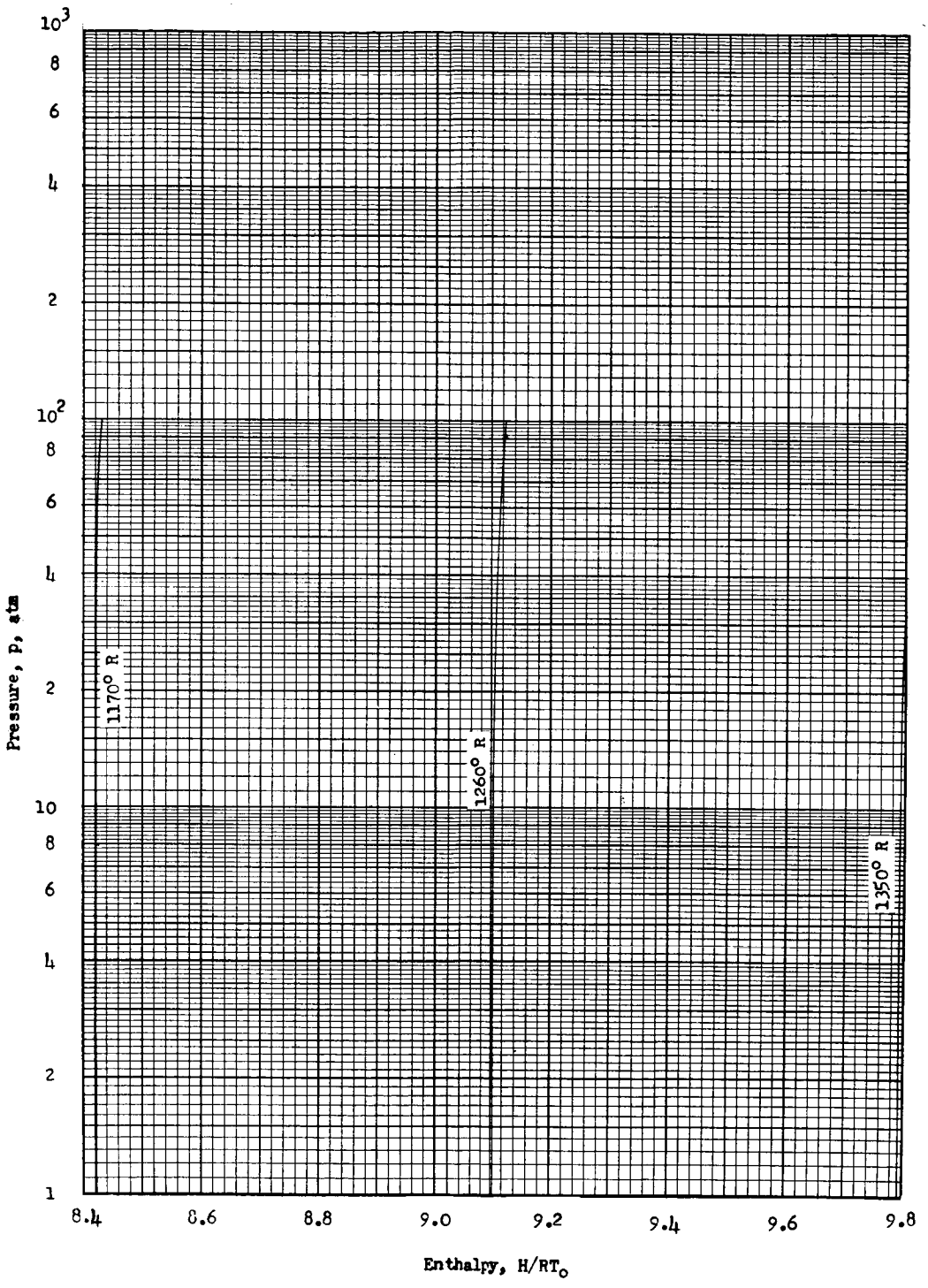

Enthalpy chart 11

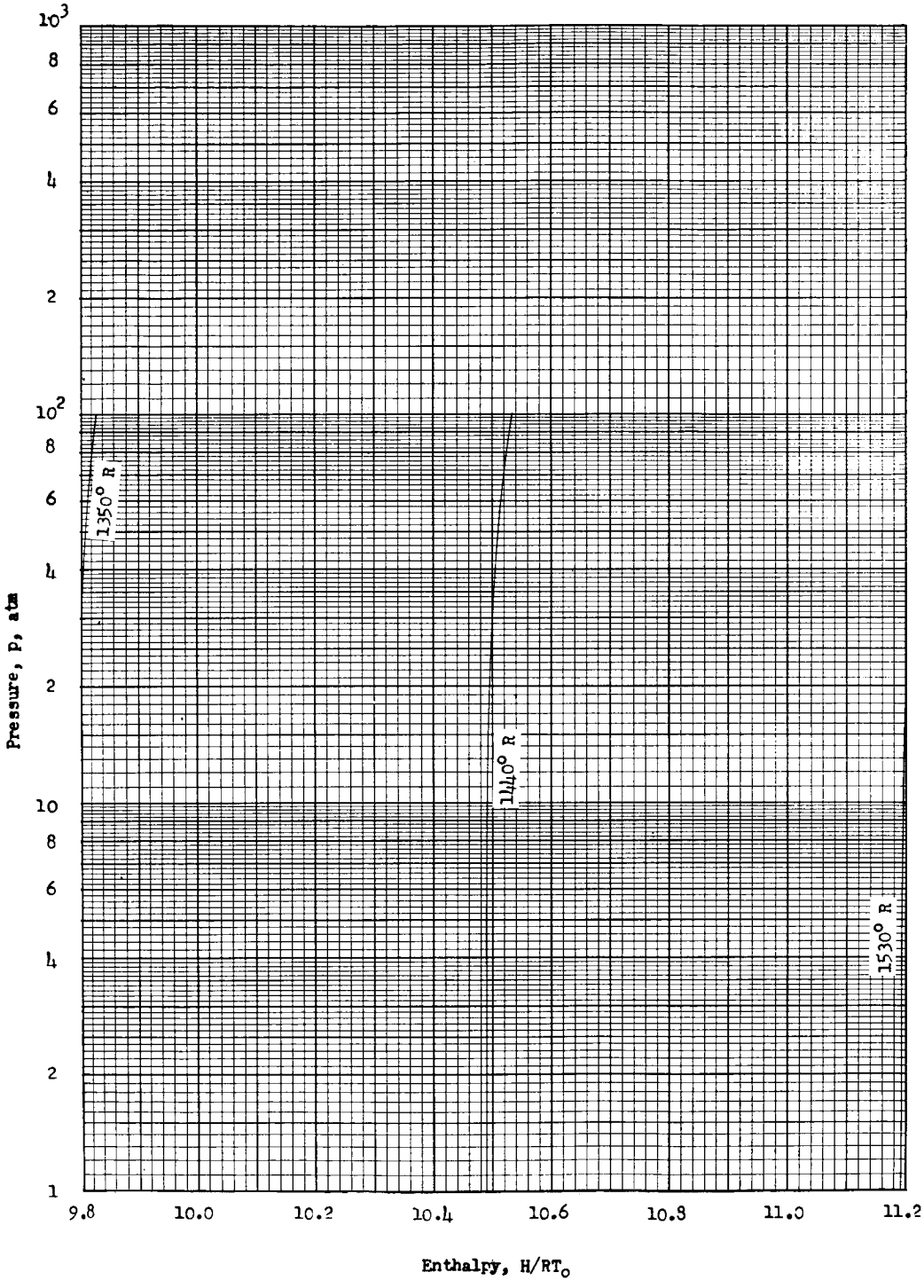

Enthalpy chart 12

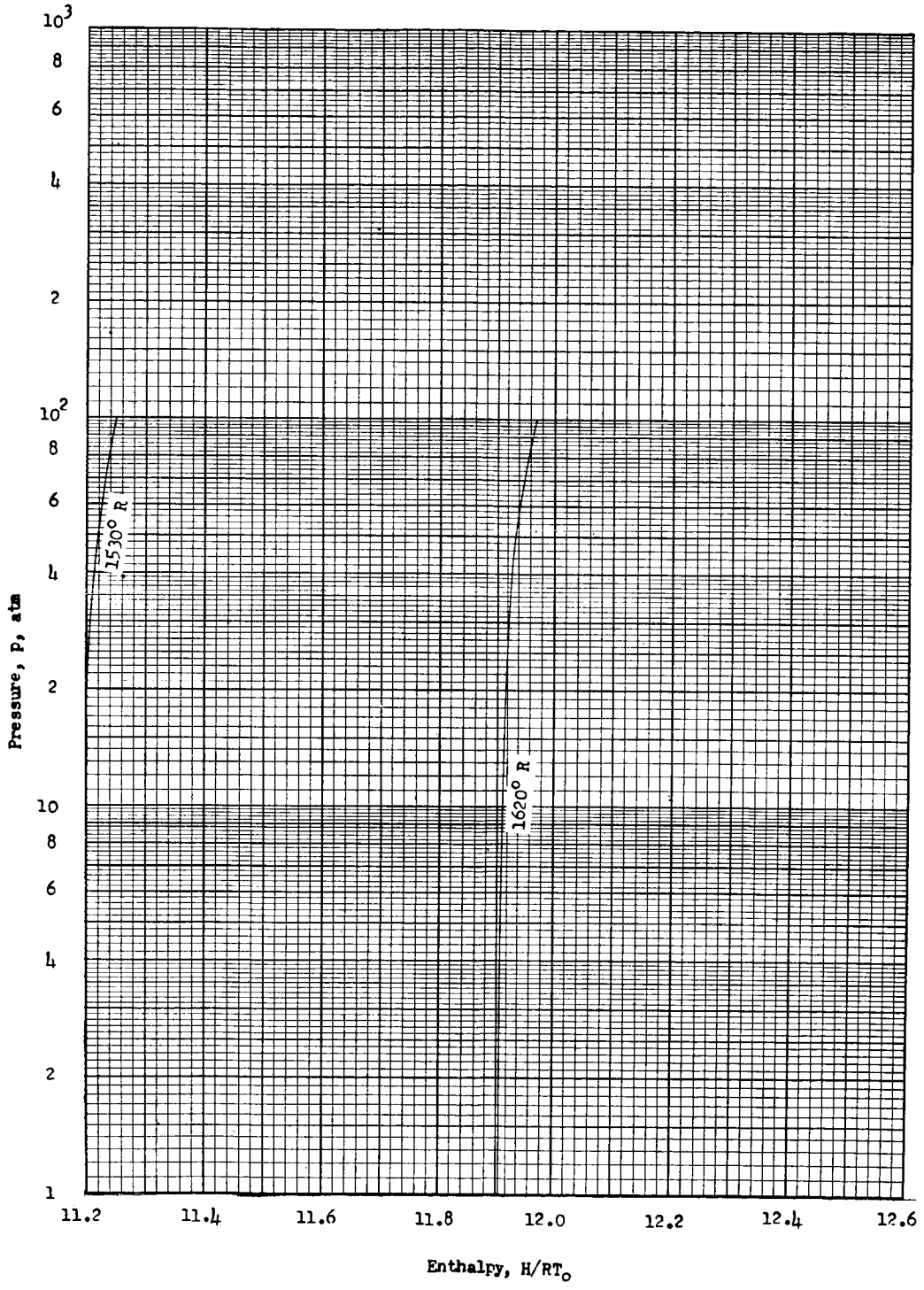

Enthalpy chart 13

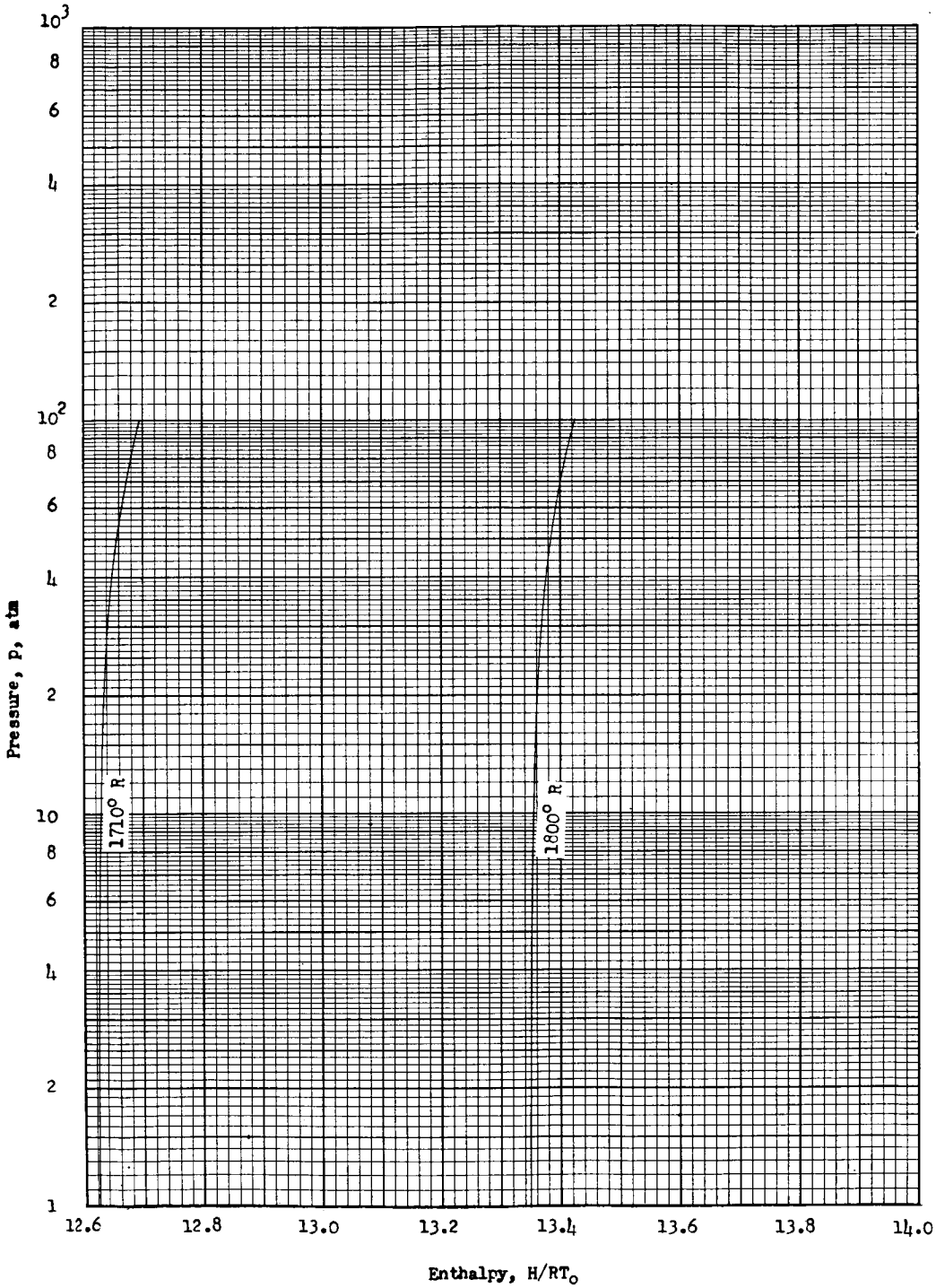

Enthalpy chart 14

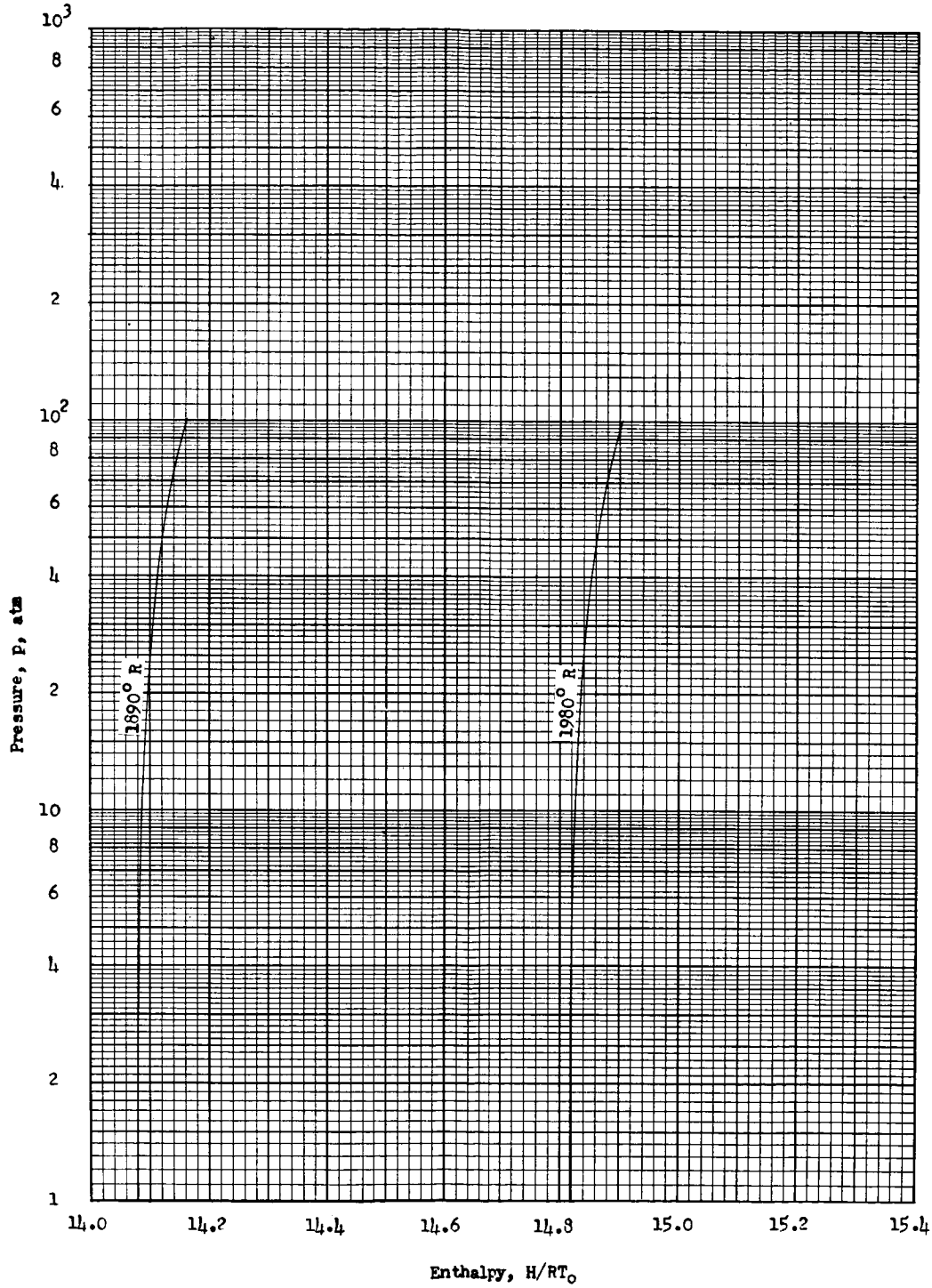

Enthalpy chart 15

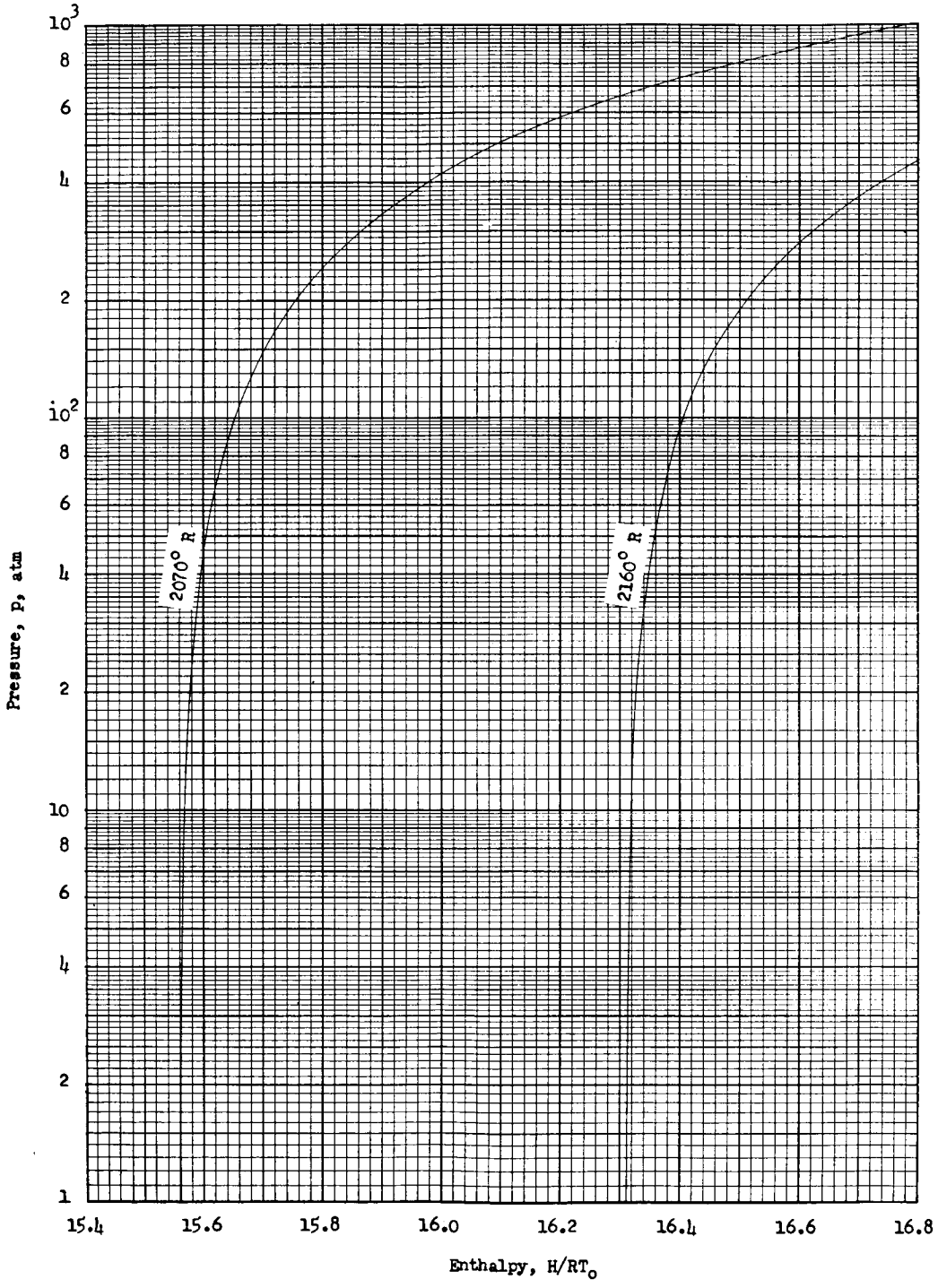

Enthalpy chart 16

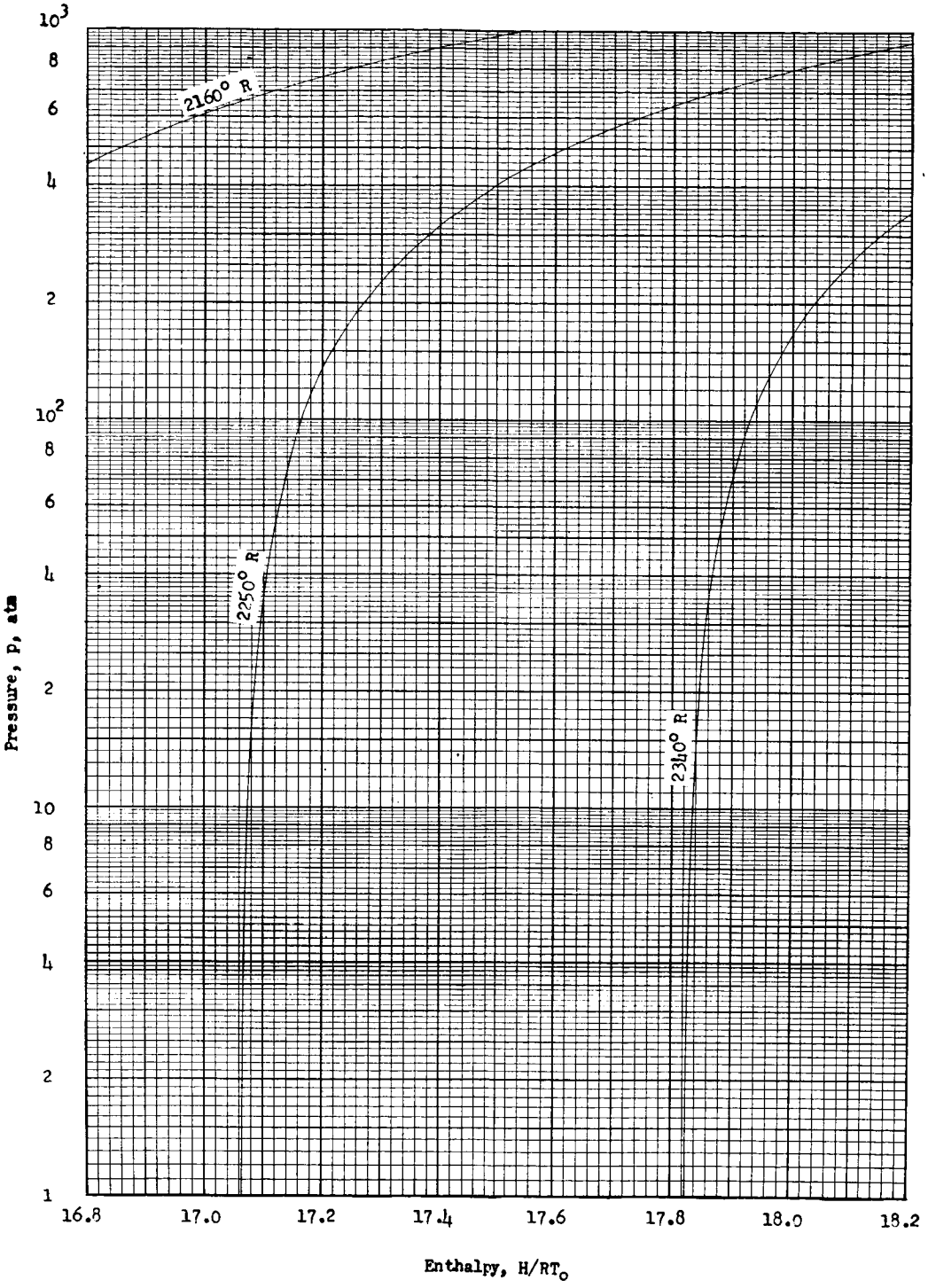

Enthalpy chart 17

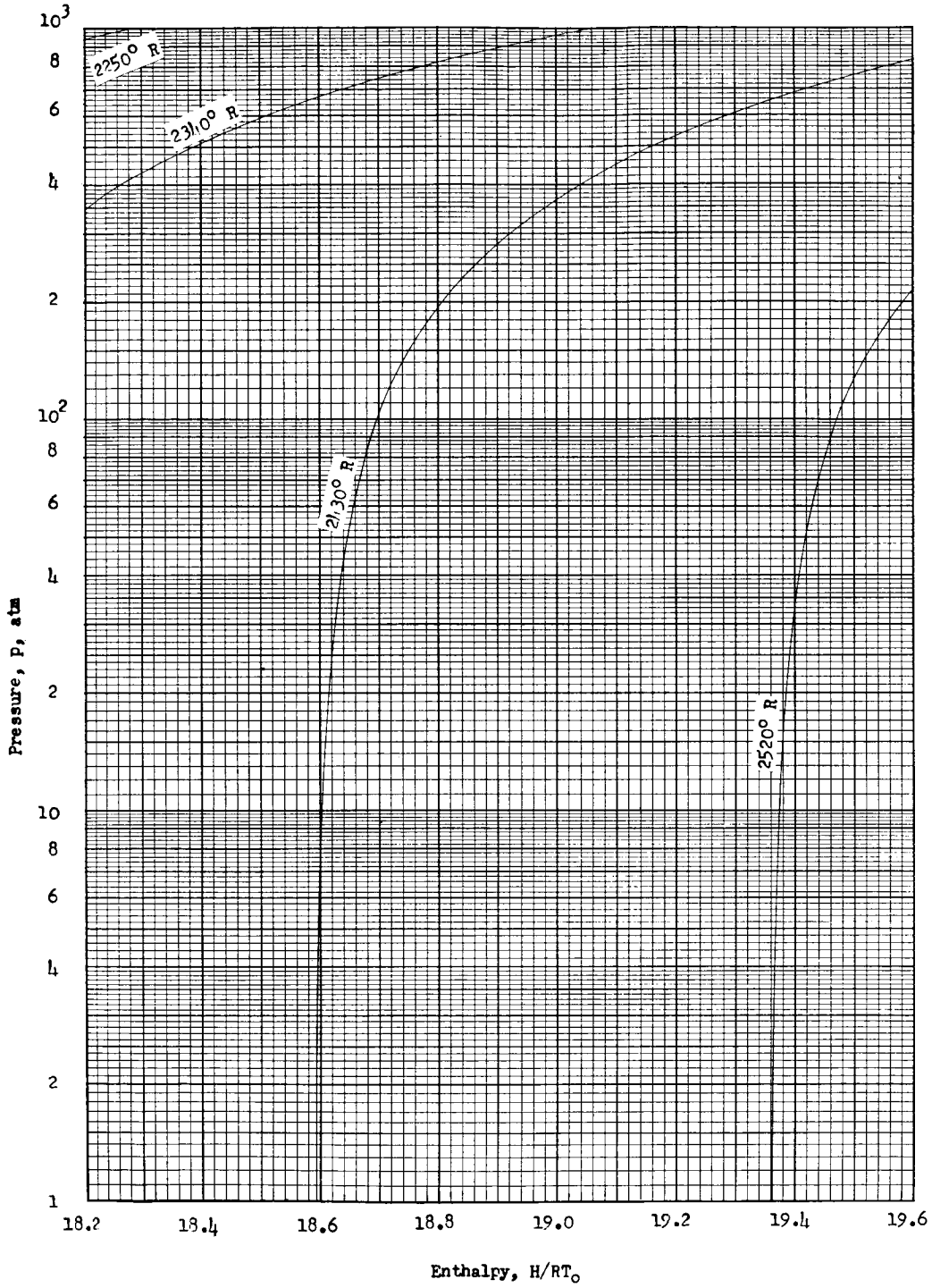

Enthalpy chart 18

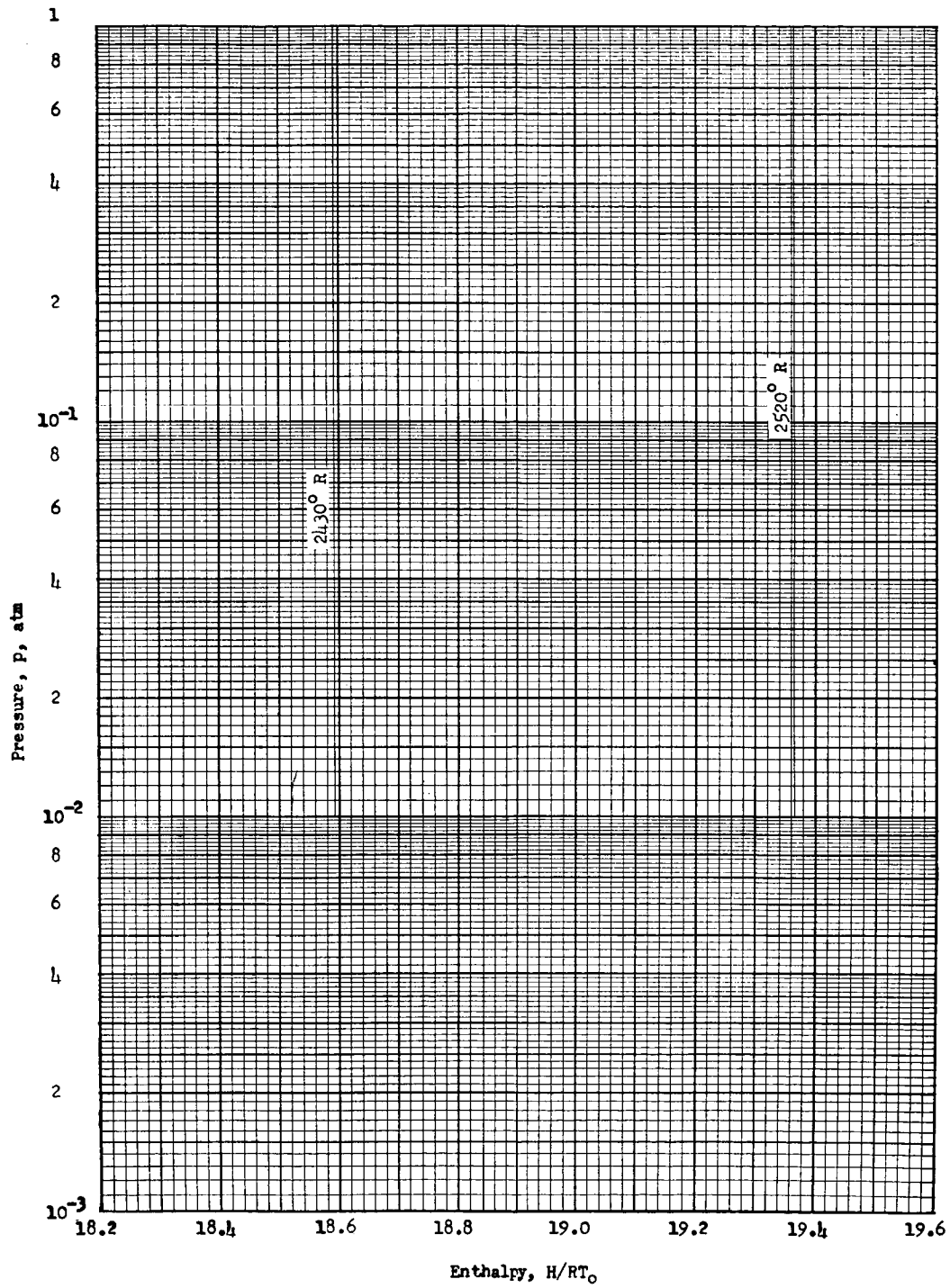

Enthalpy chart 19

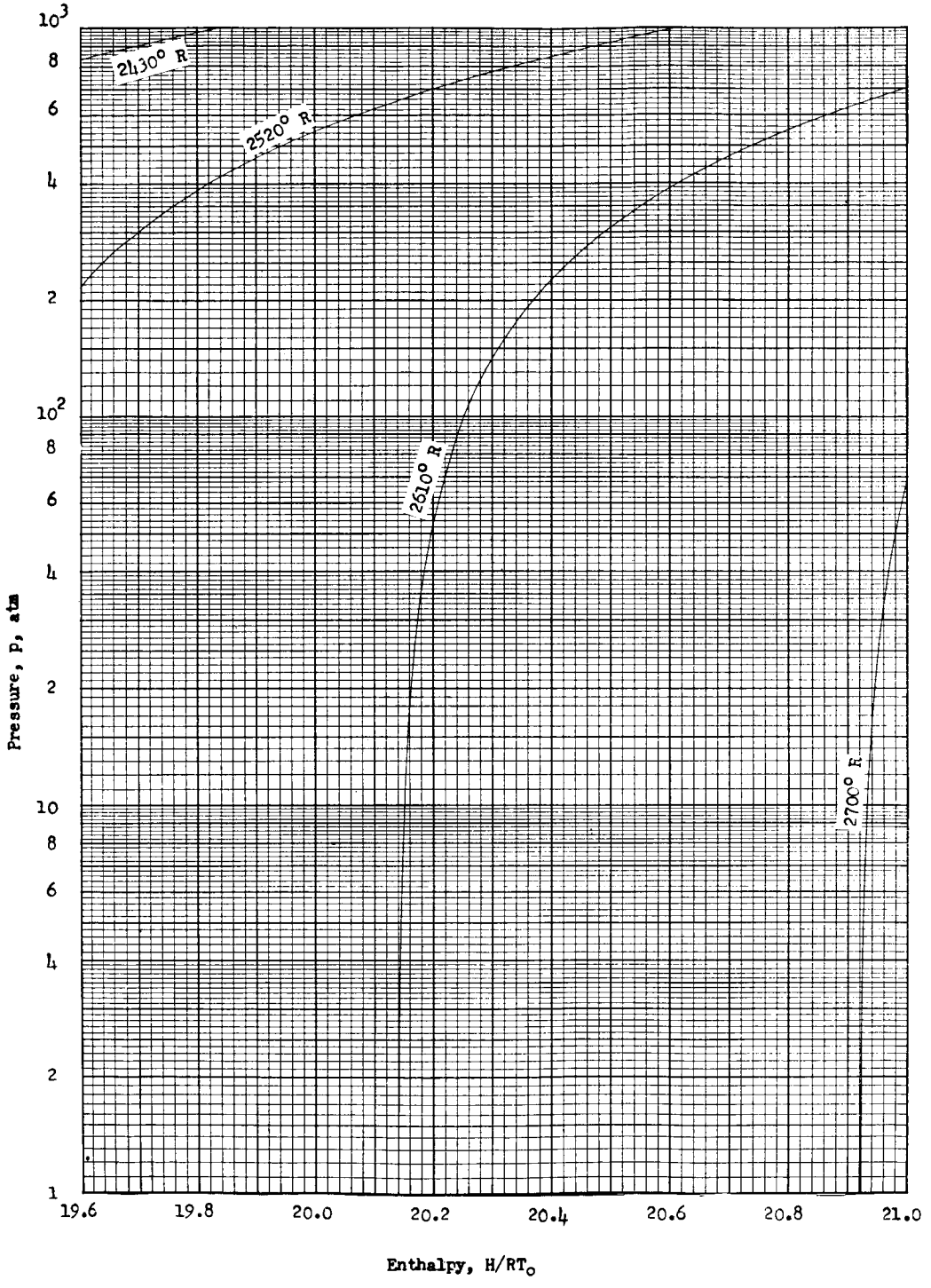

Enthalpy chart 20

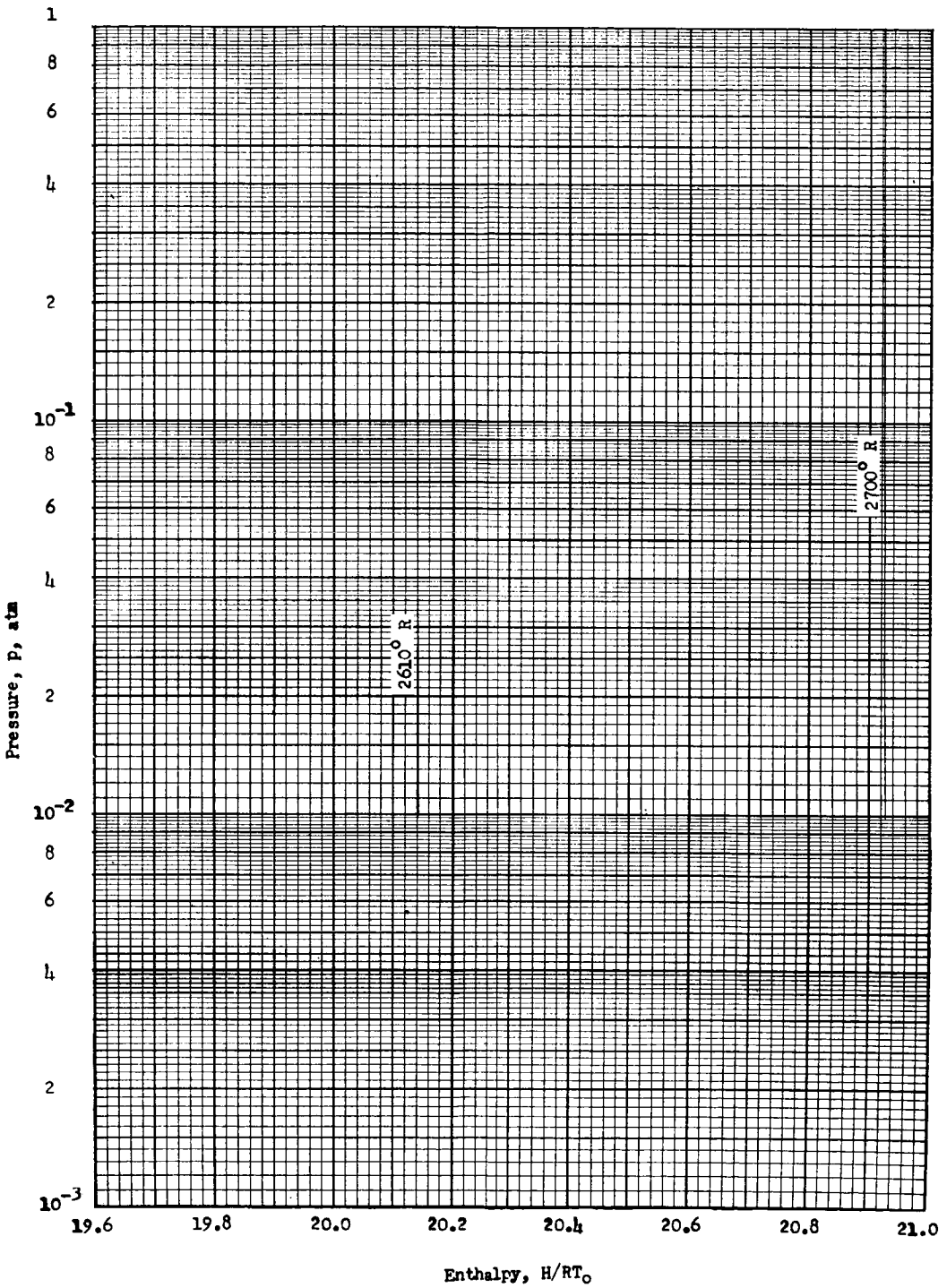

Enthalpy chart 21

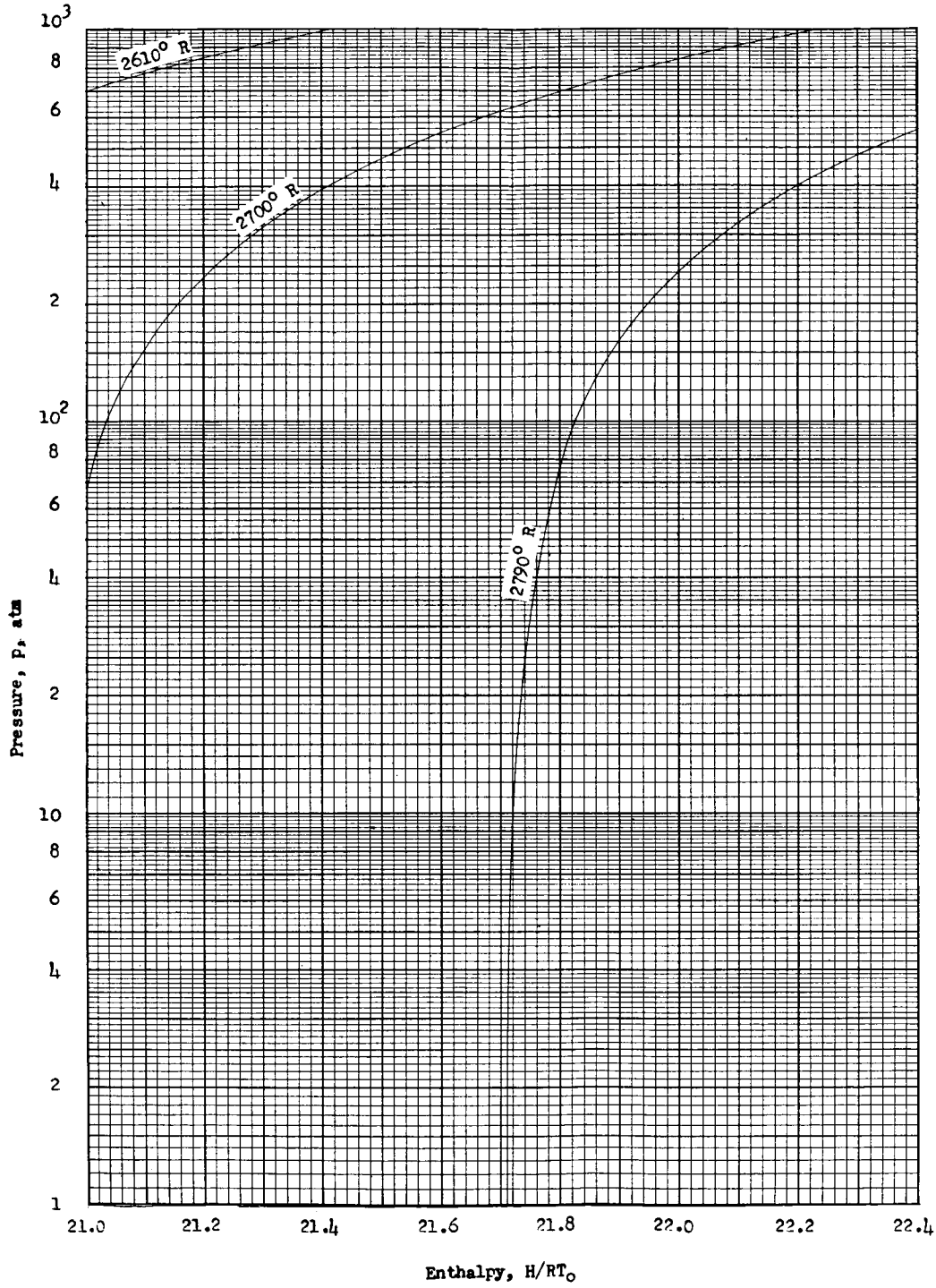

Enthalpy chart 22

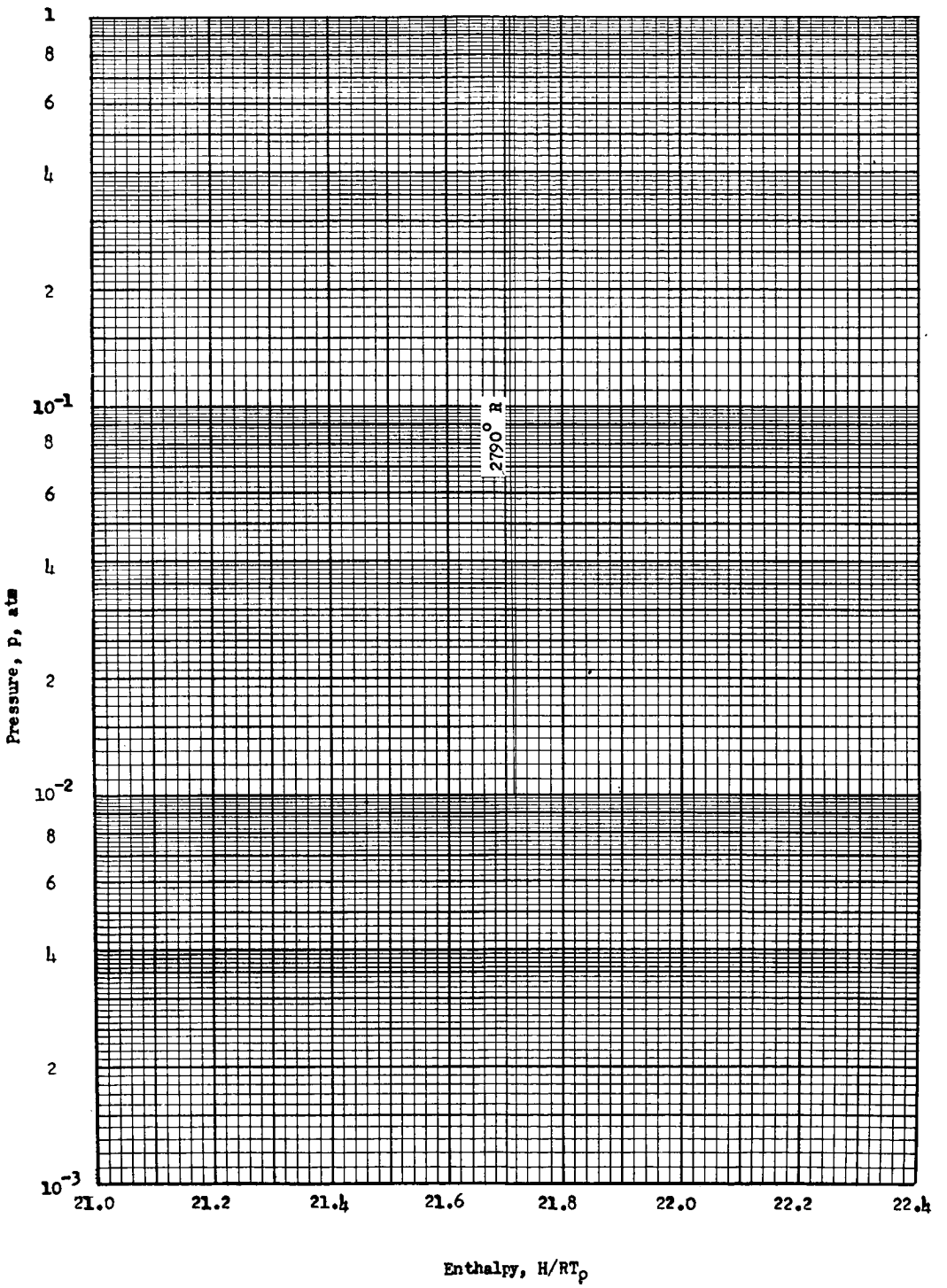

Enthalpy chart 23

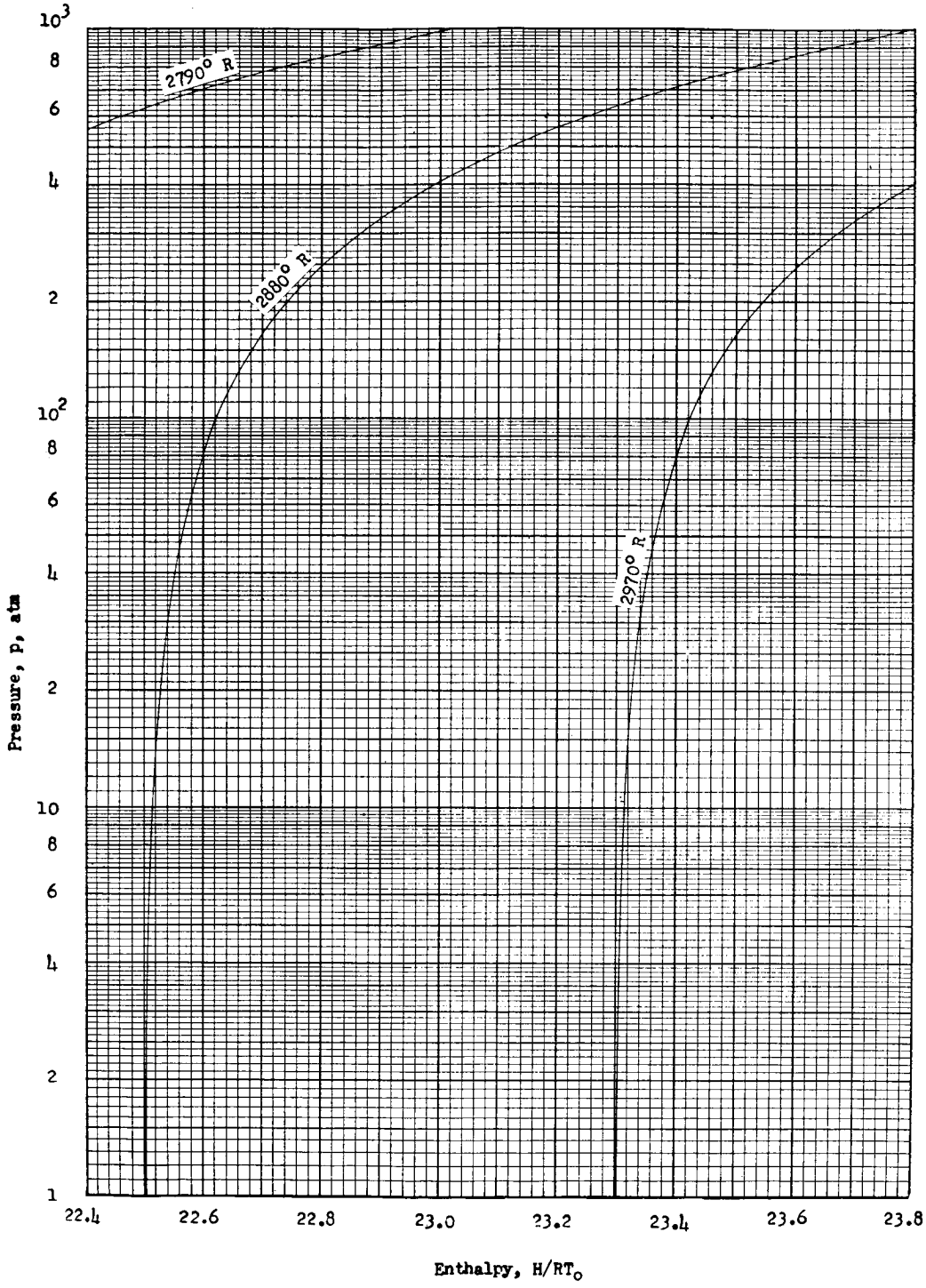

Enthalpy chart 24

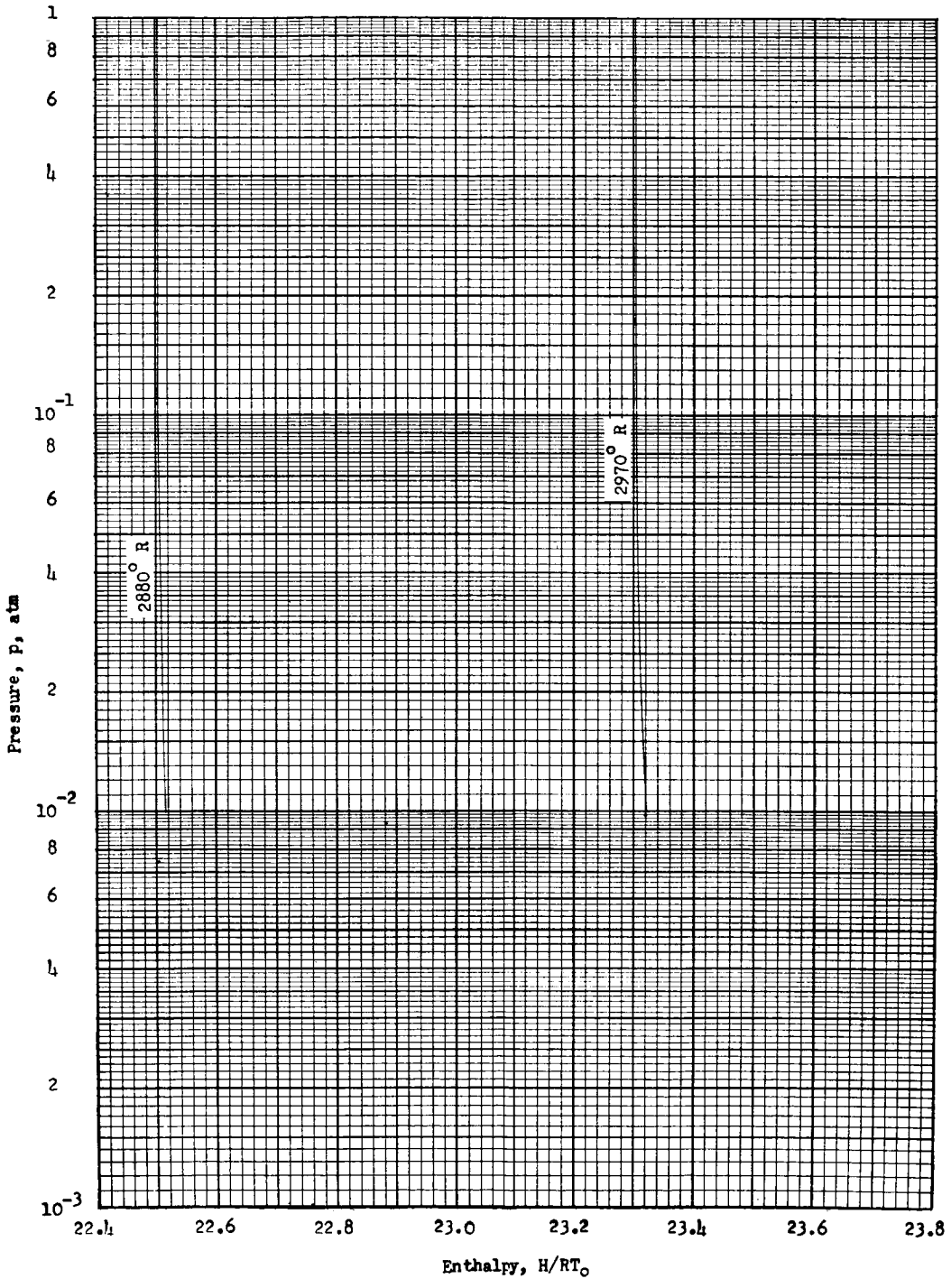

Enthalpy chart 25

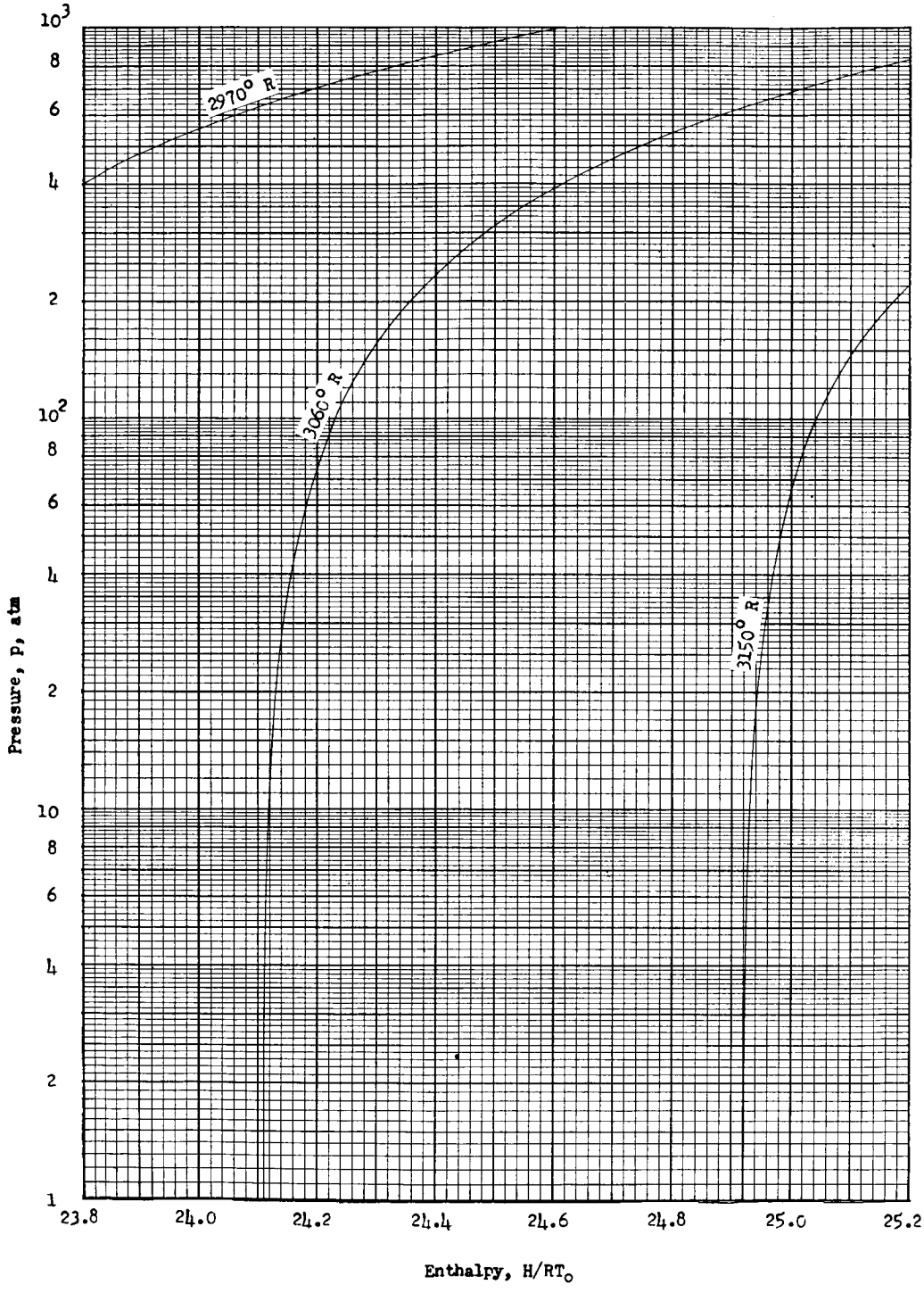

Enthalpy chart 26

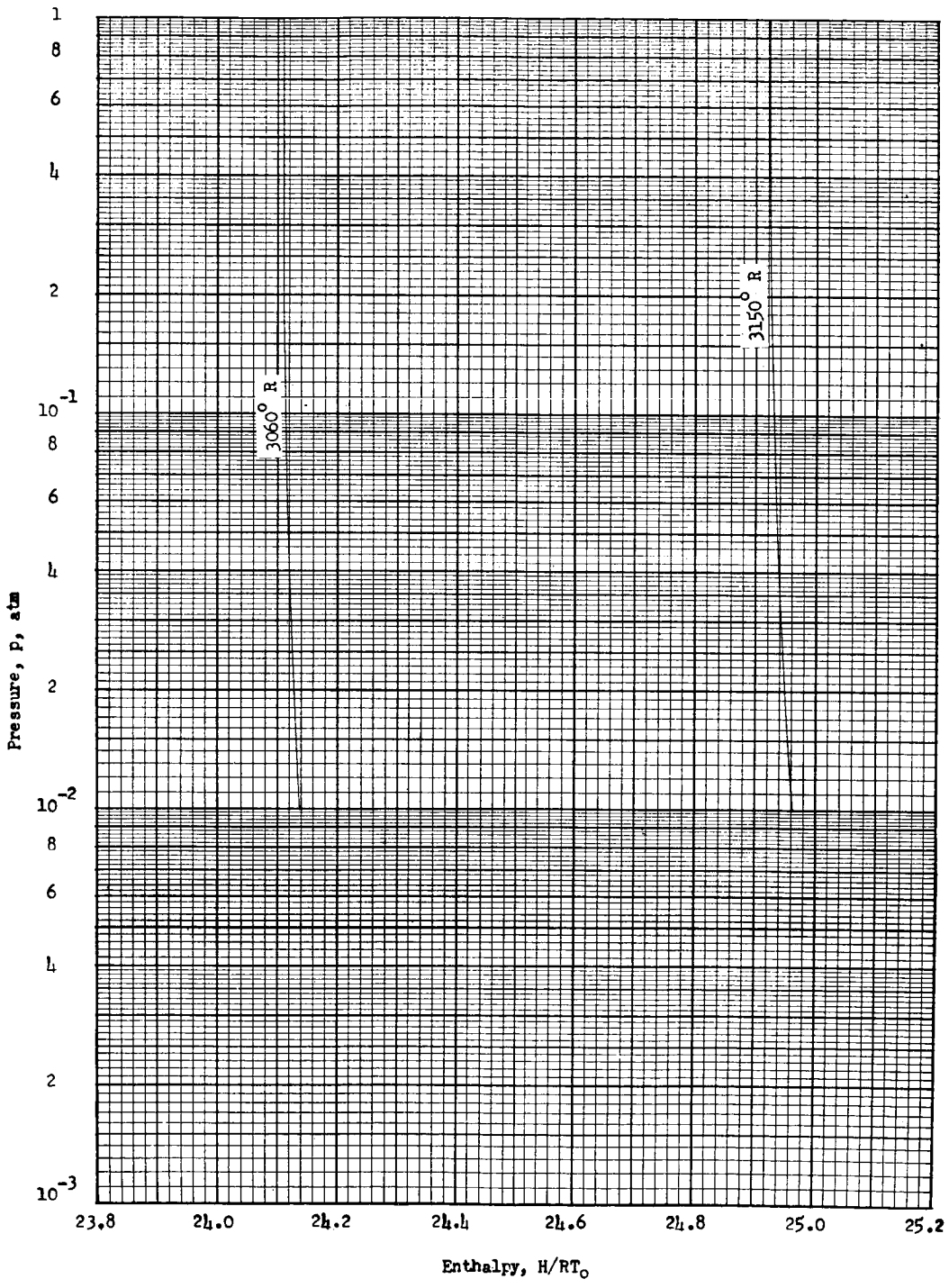

Enthalpy chart 27

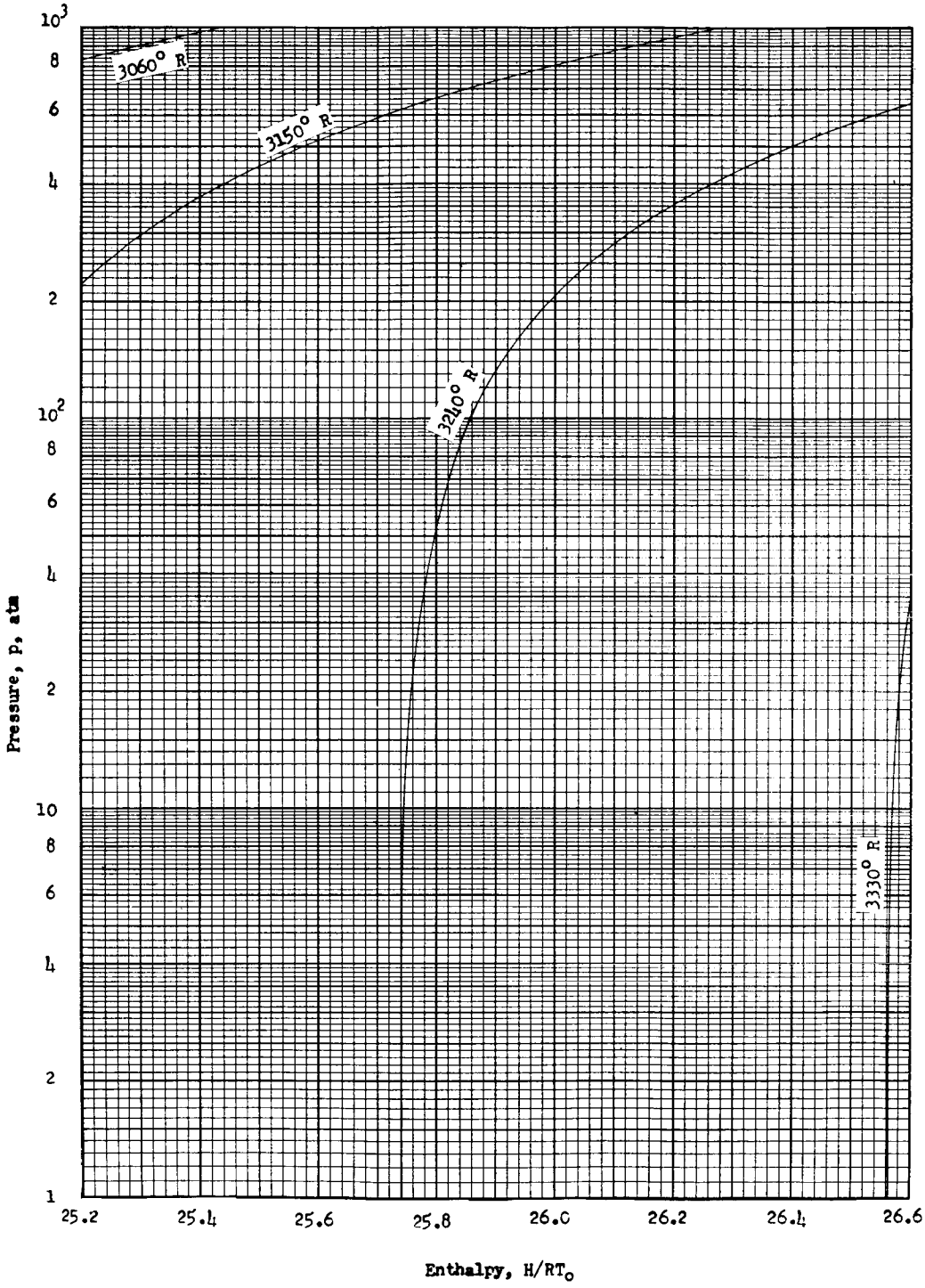

Enthalpy chart 28

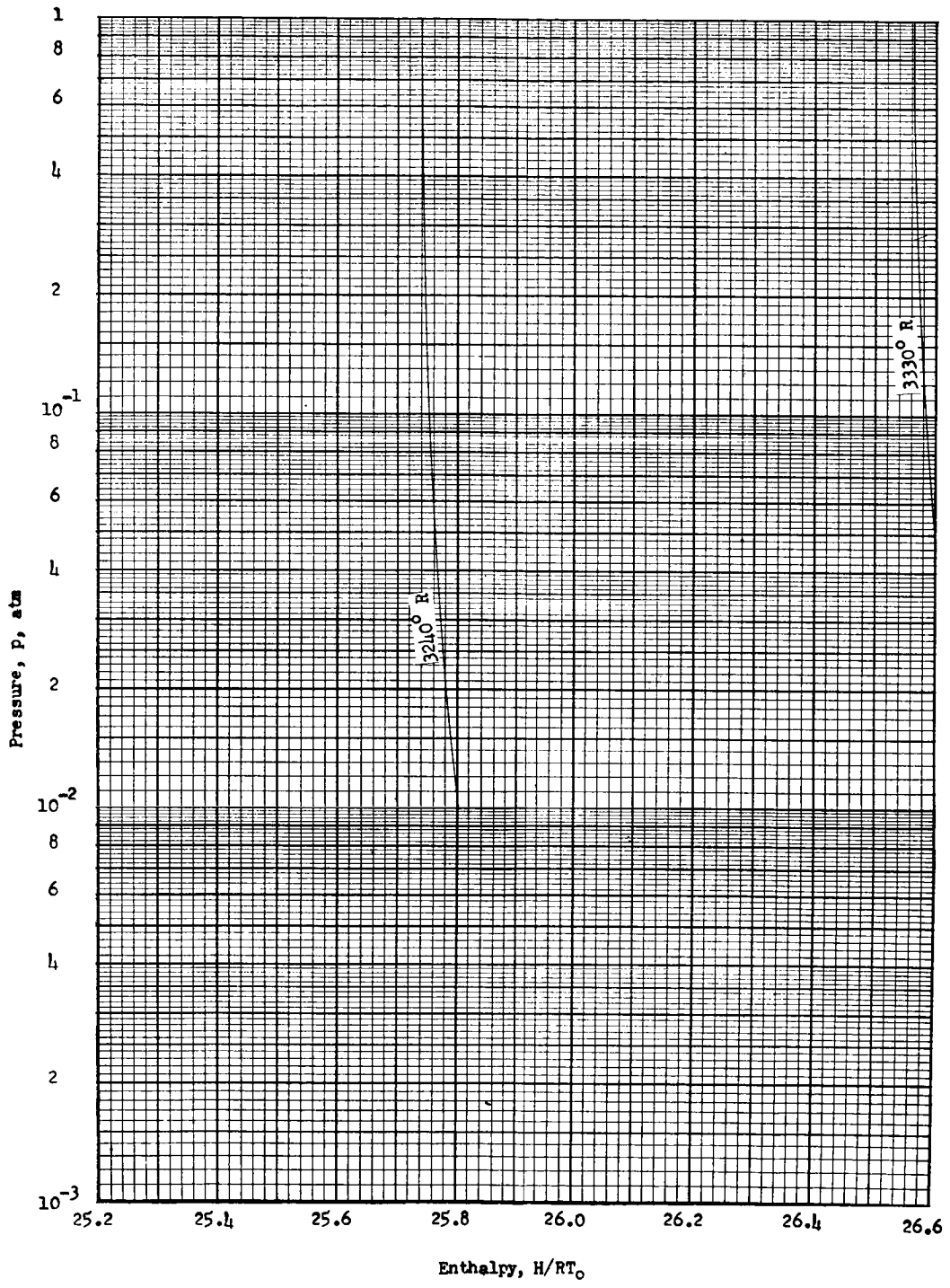

Enthalpy chart 29

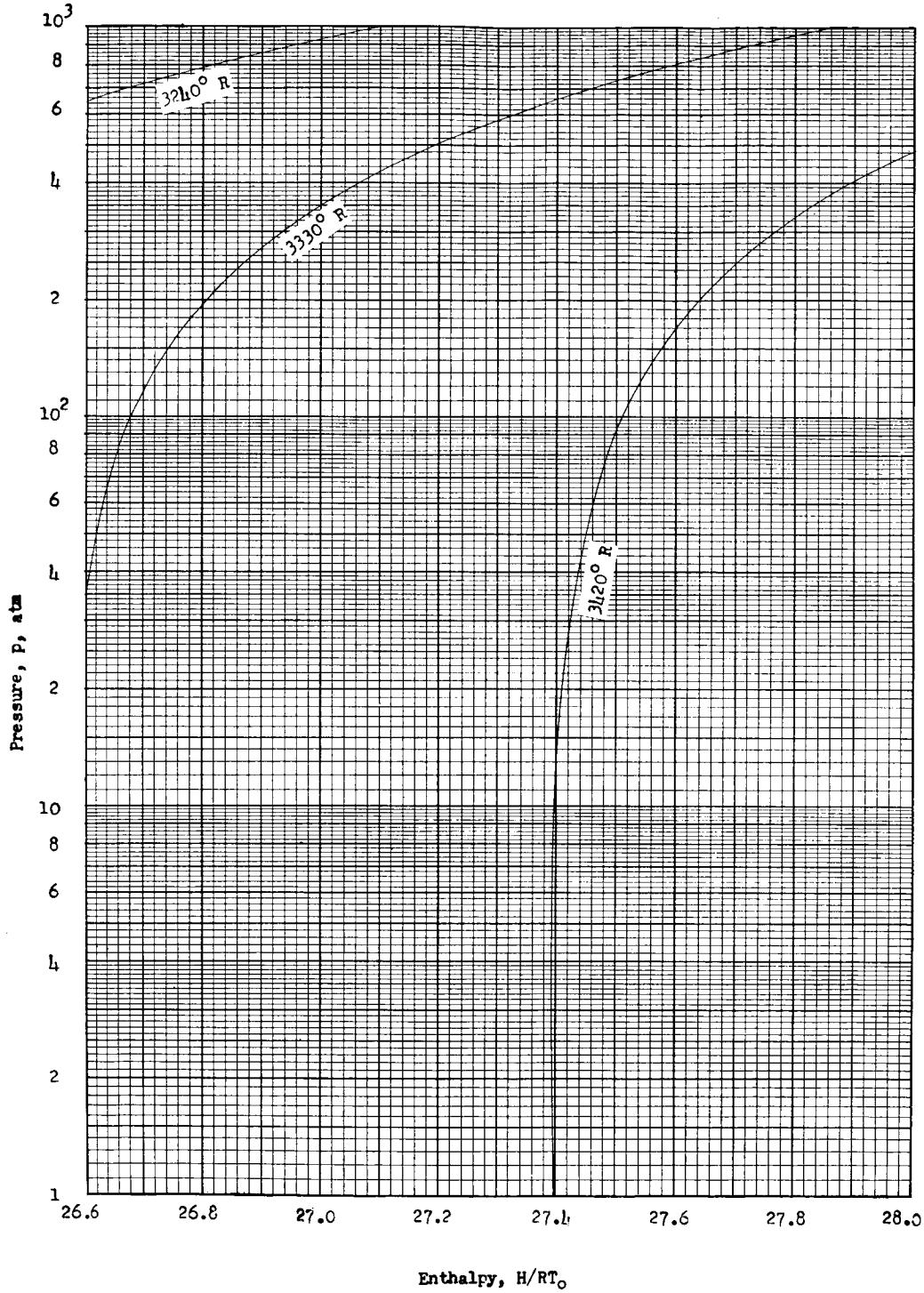

Enthalpy chart 30

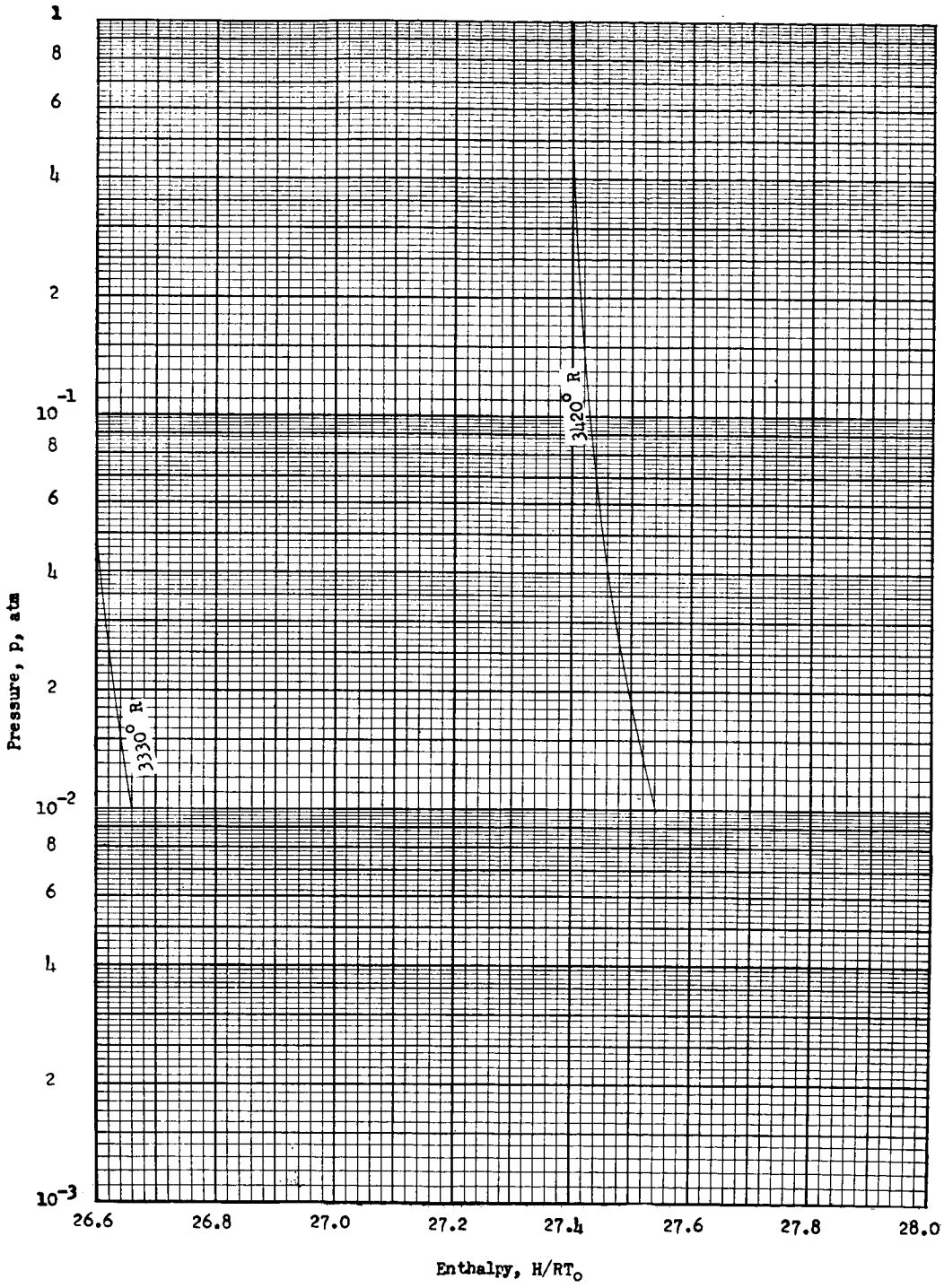

Enthalpy chart 31

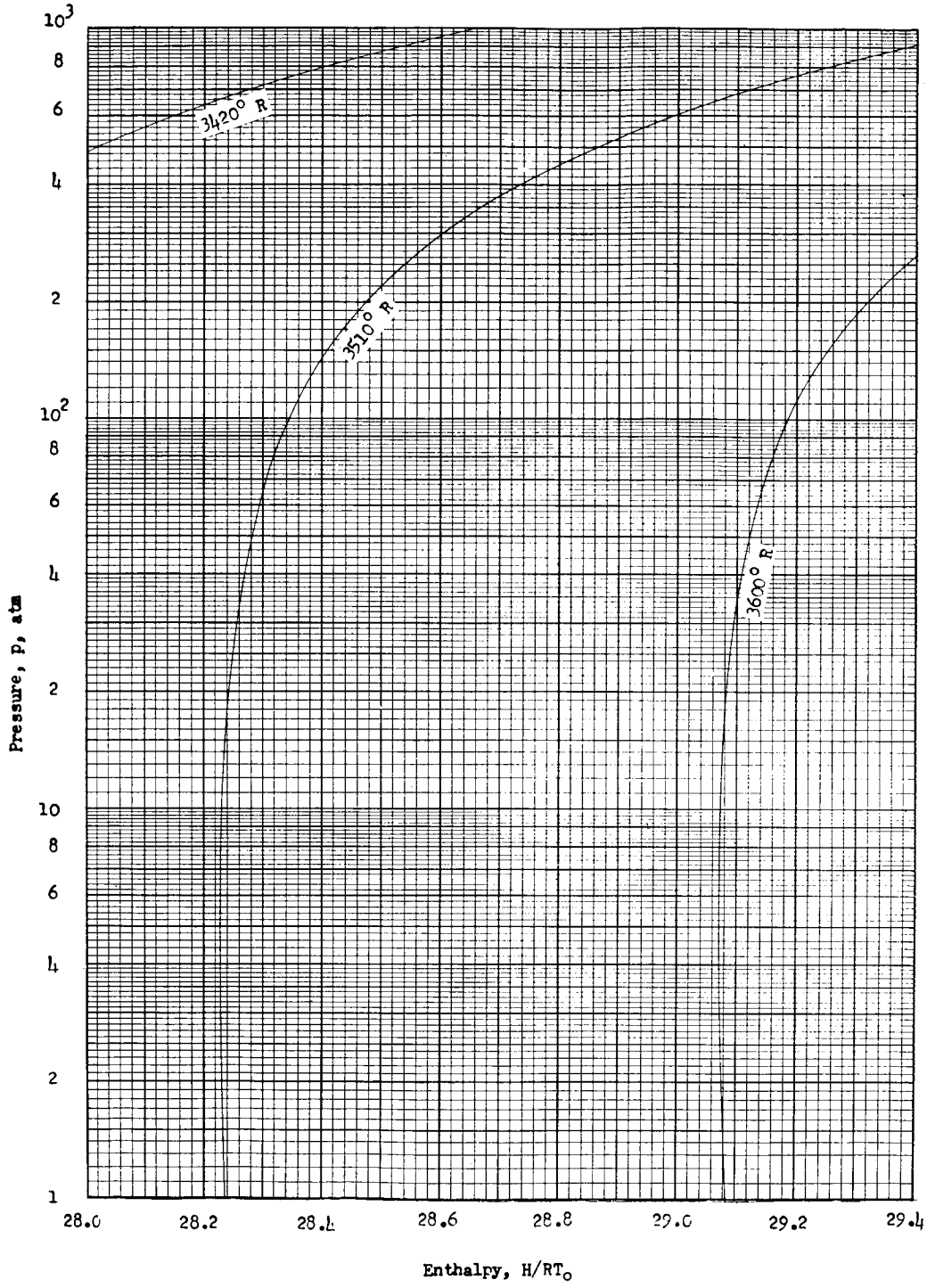

Enthalpy chart 32

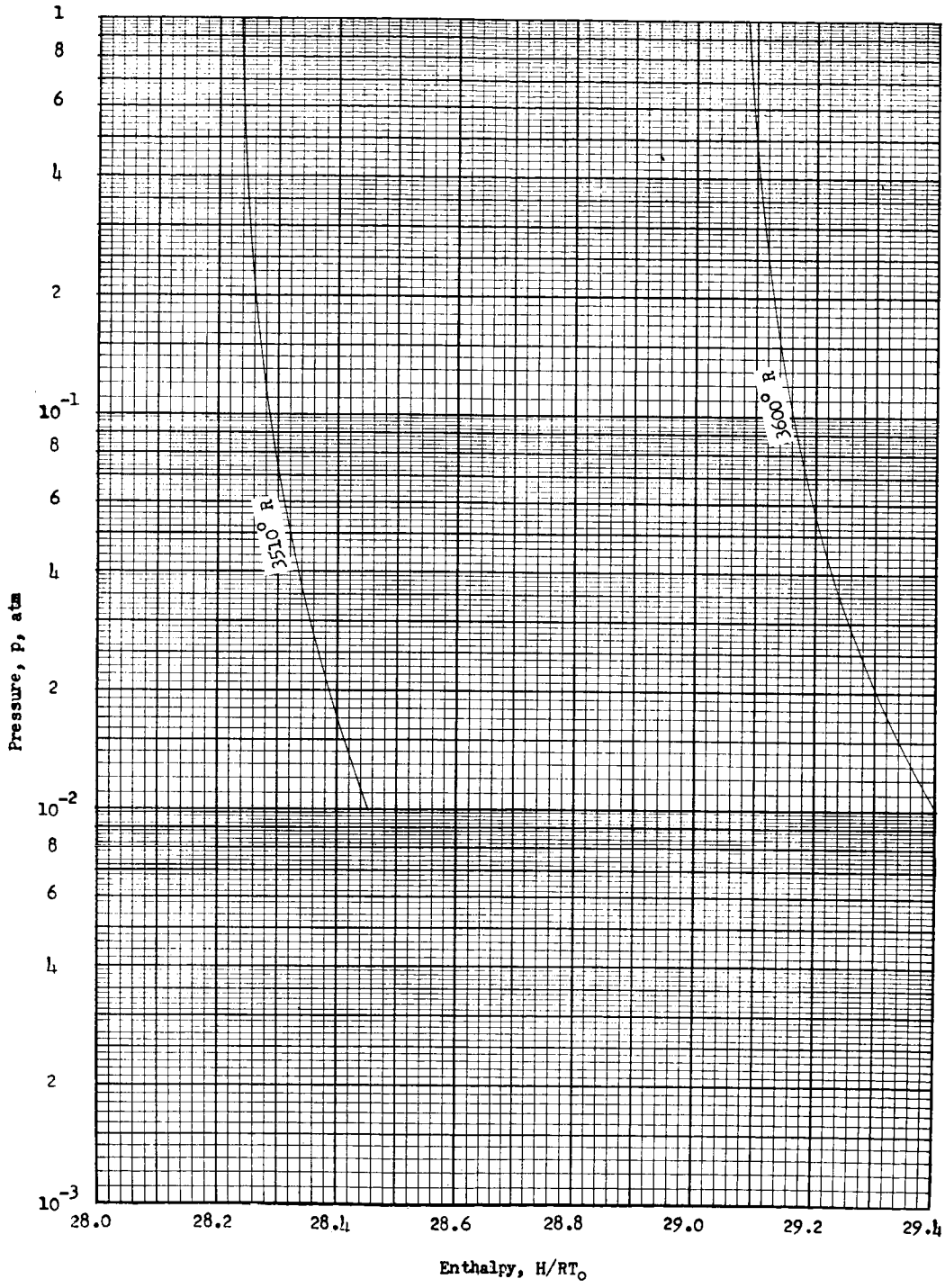

Enthalpy chart 33

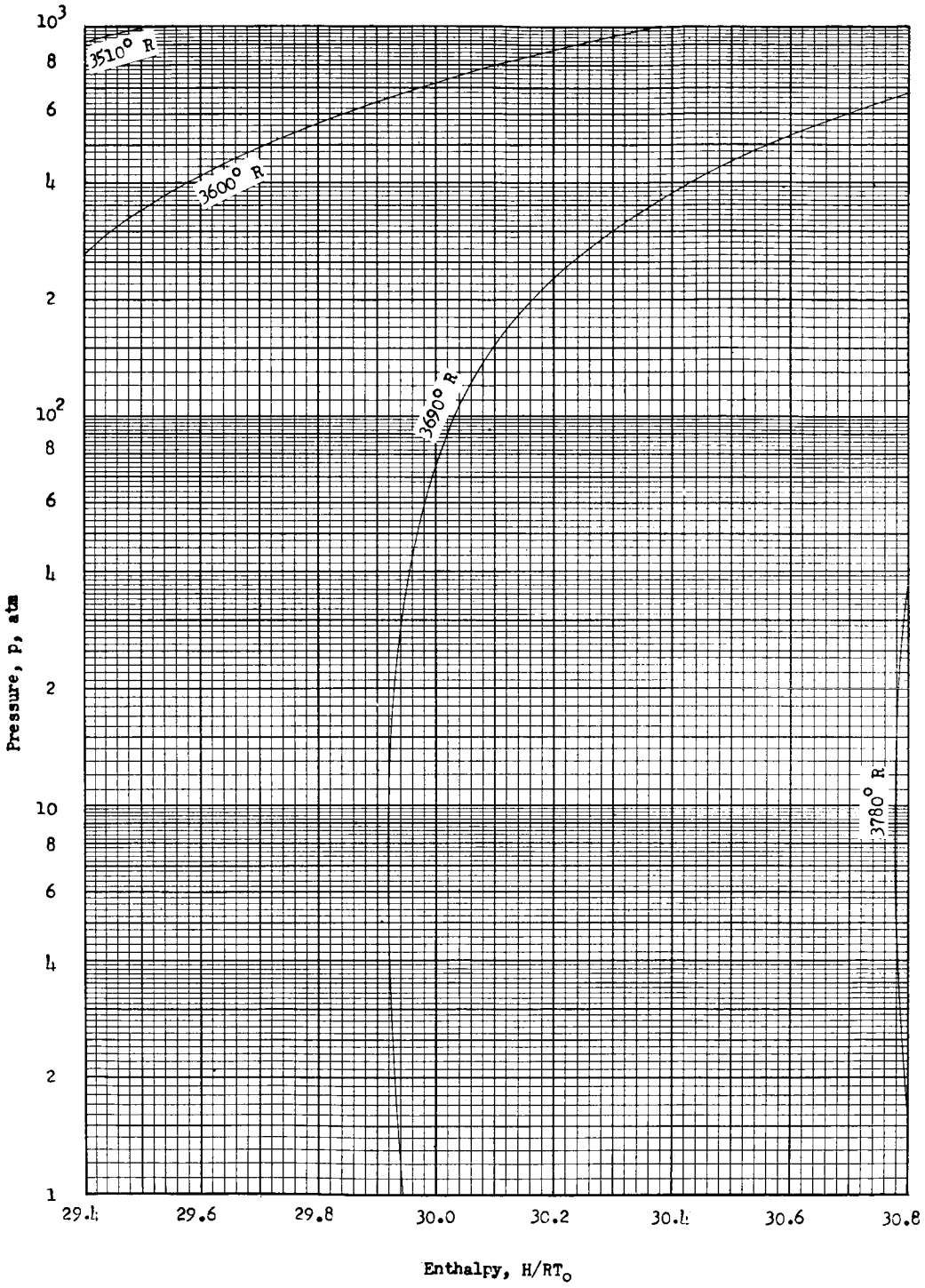

Enthalpy chart 34

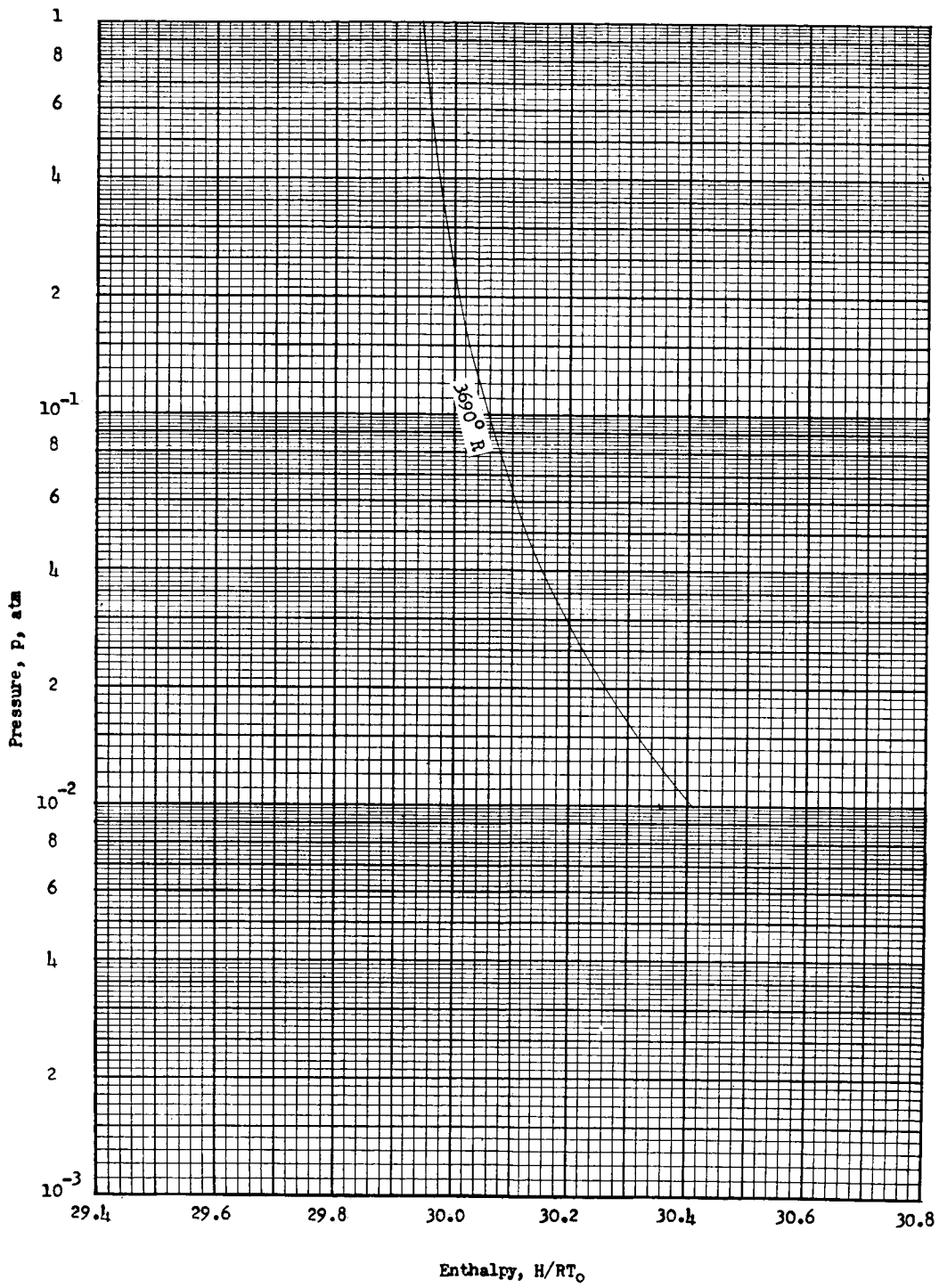

Enthalpy chart 35

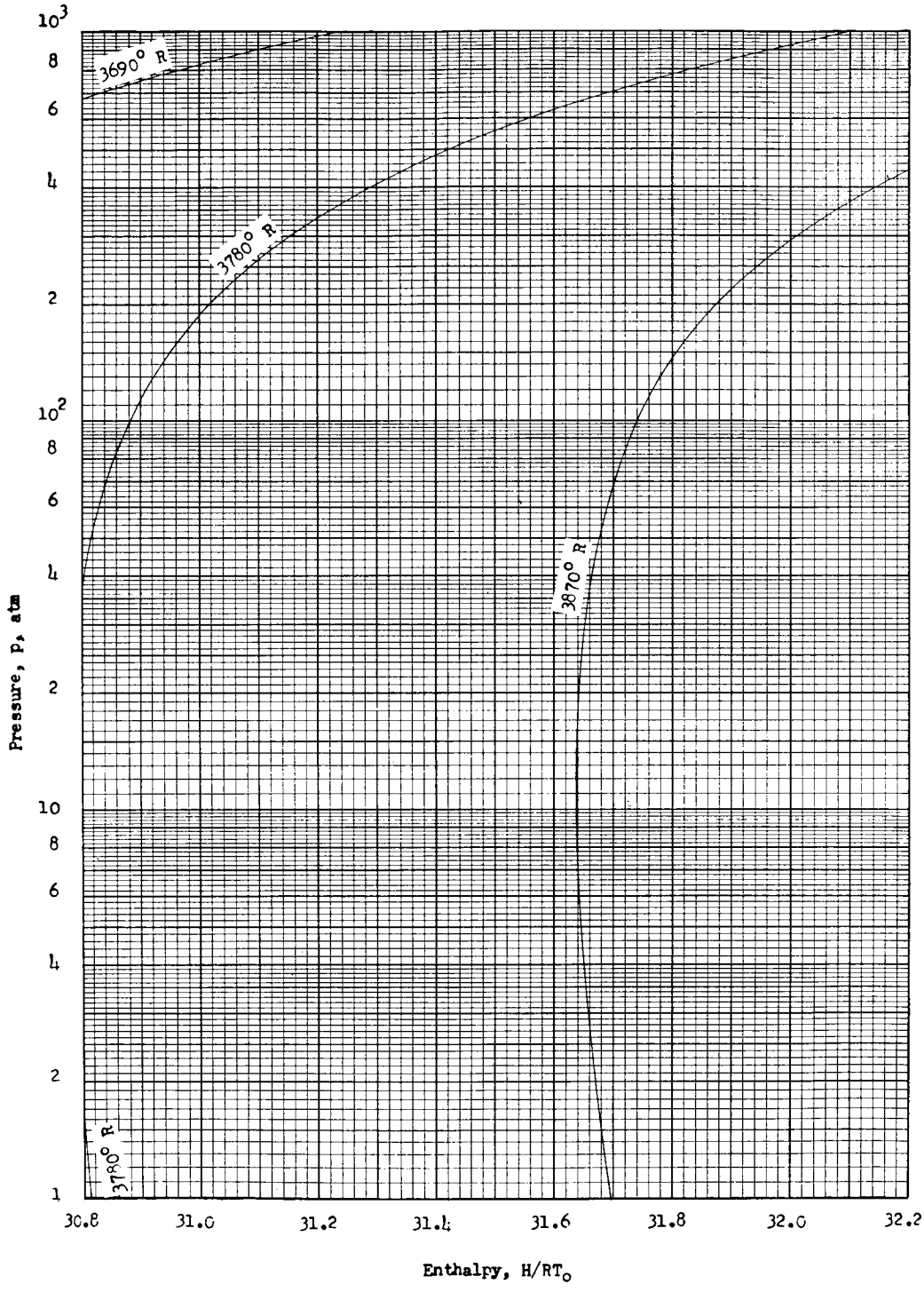

Enthalpy chart 36

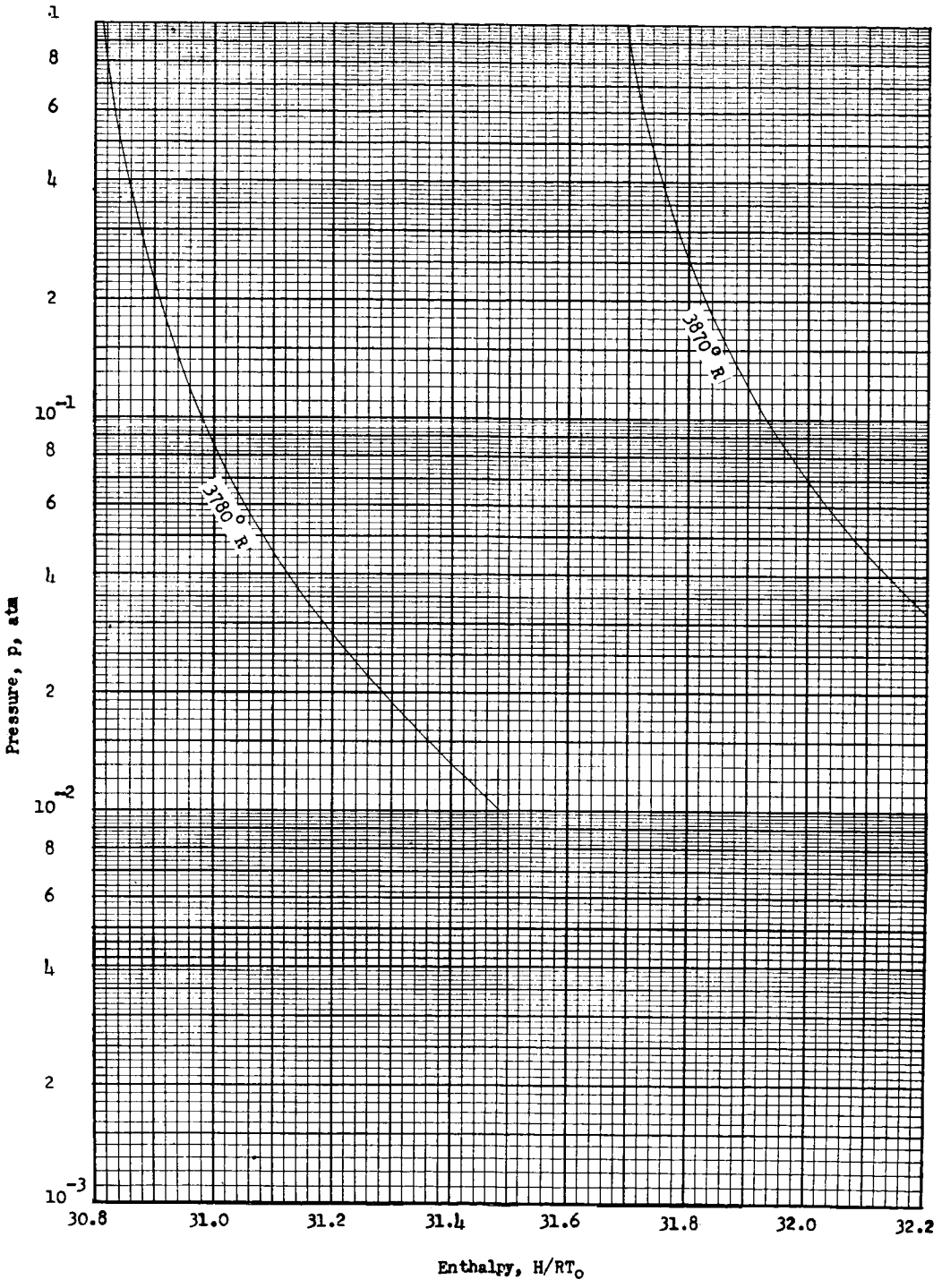

Enthalpy chart 37

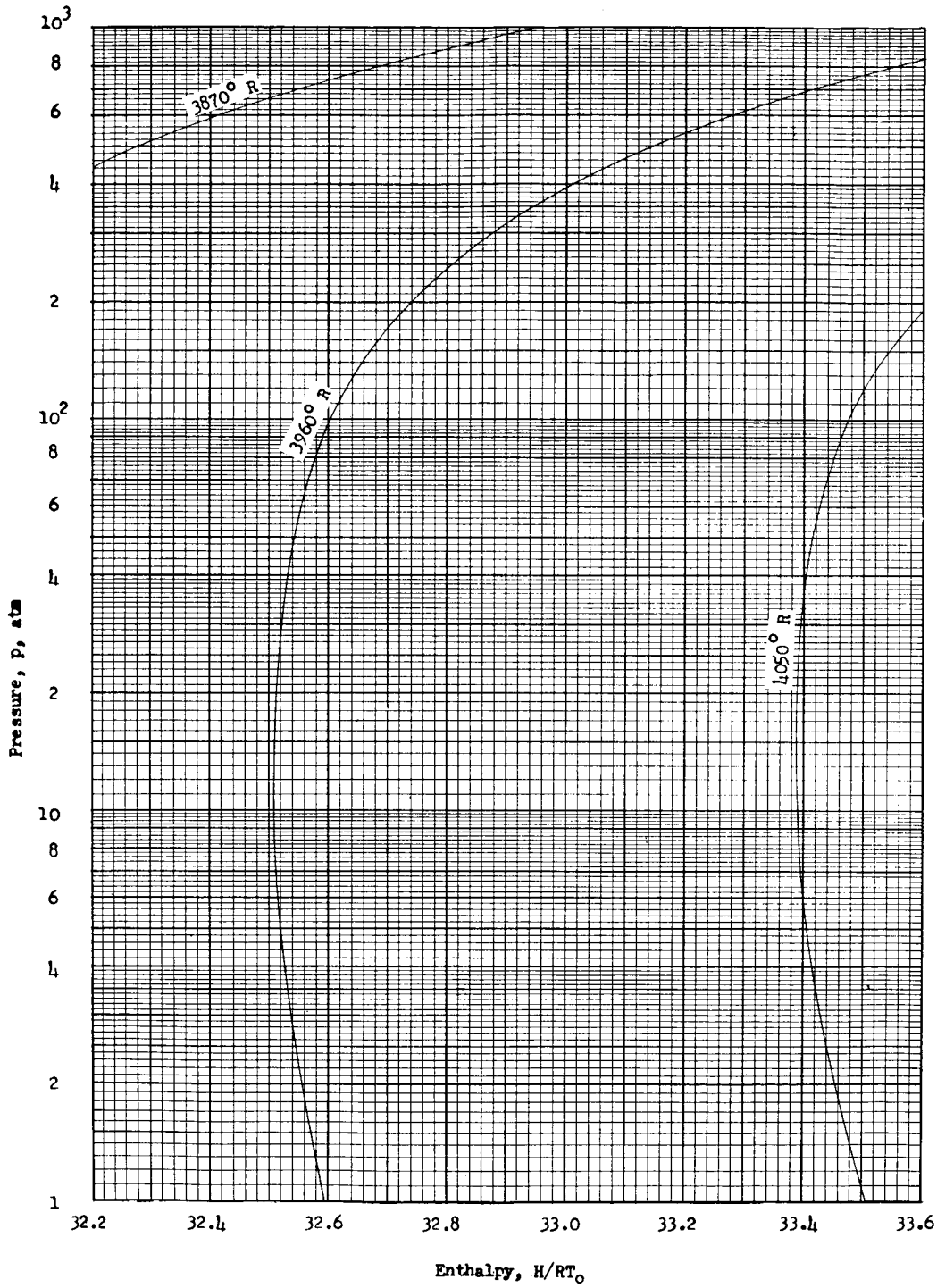

Enthalpy chart 38

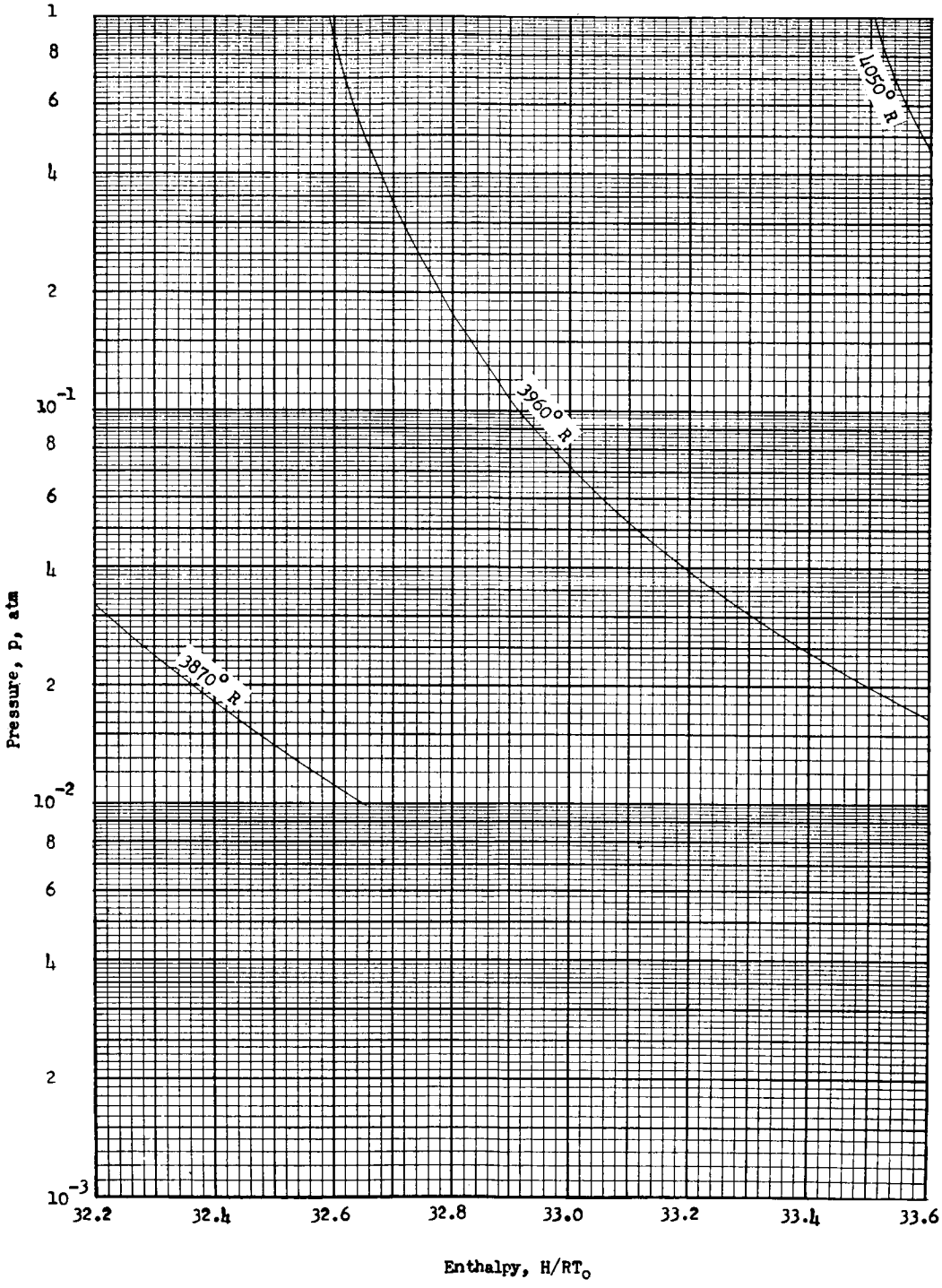

Enthalpy chart 39

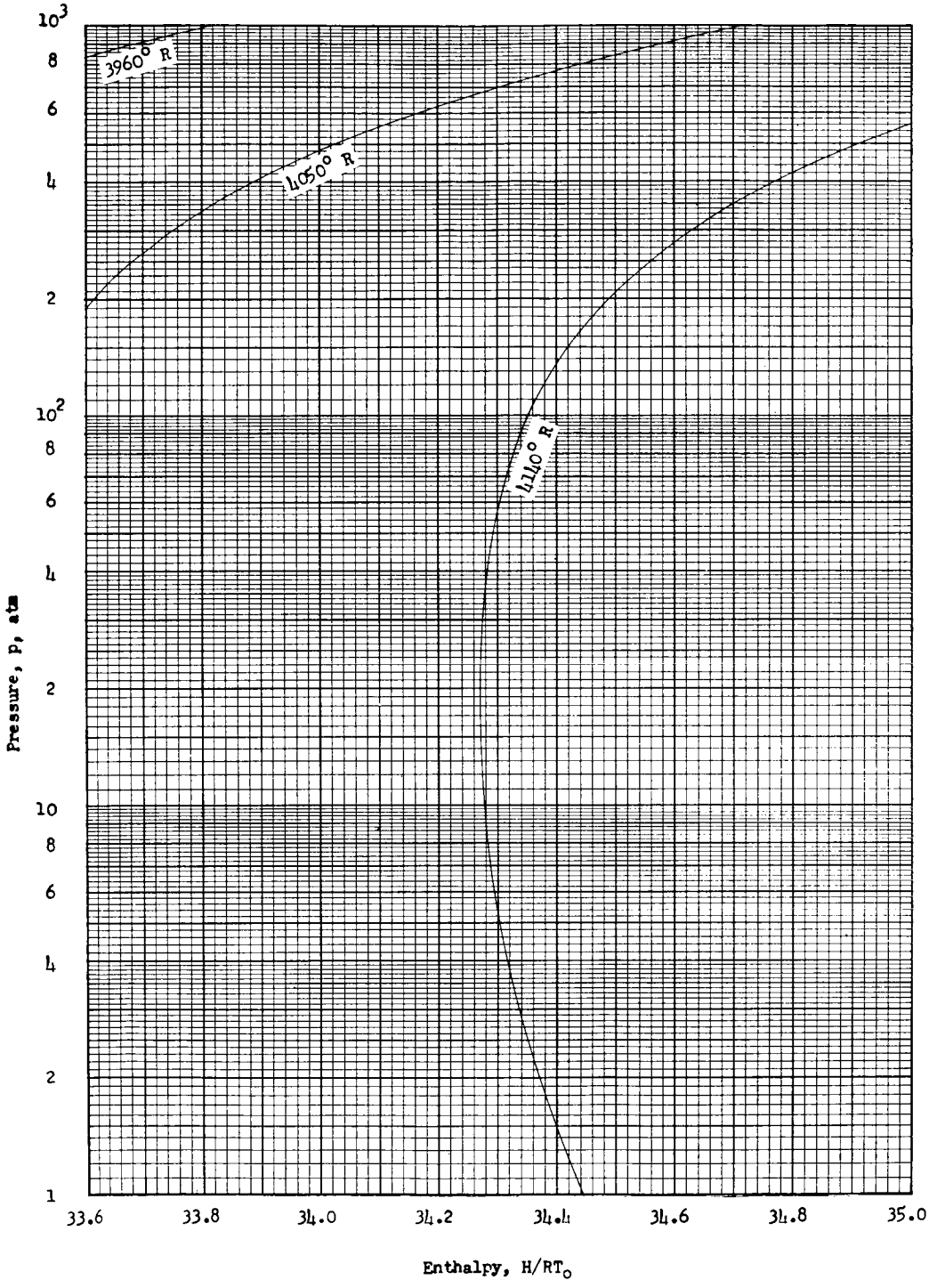

Enthalpy chart 40

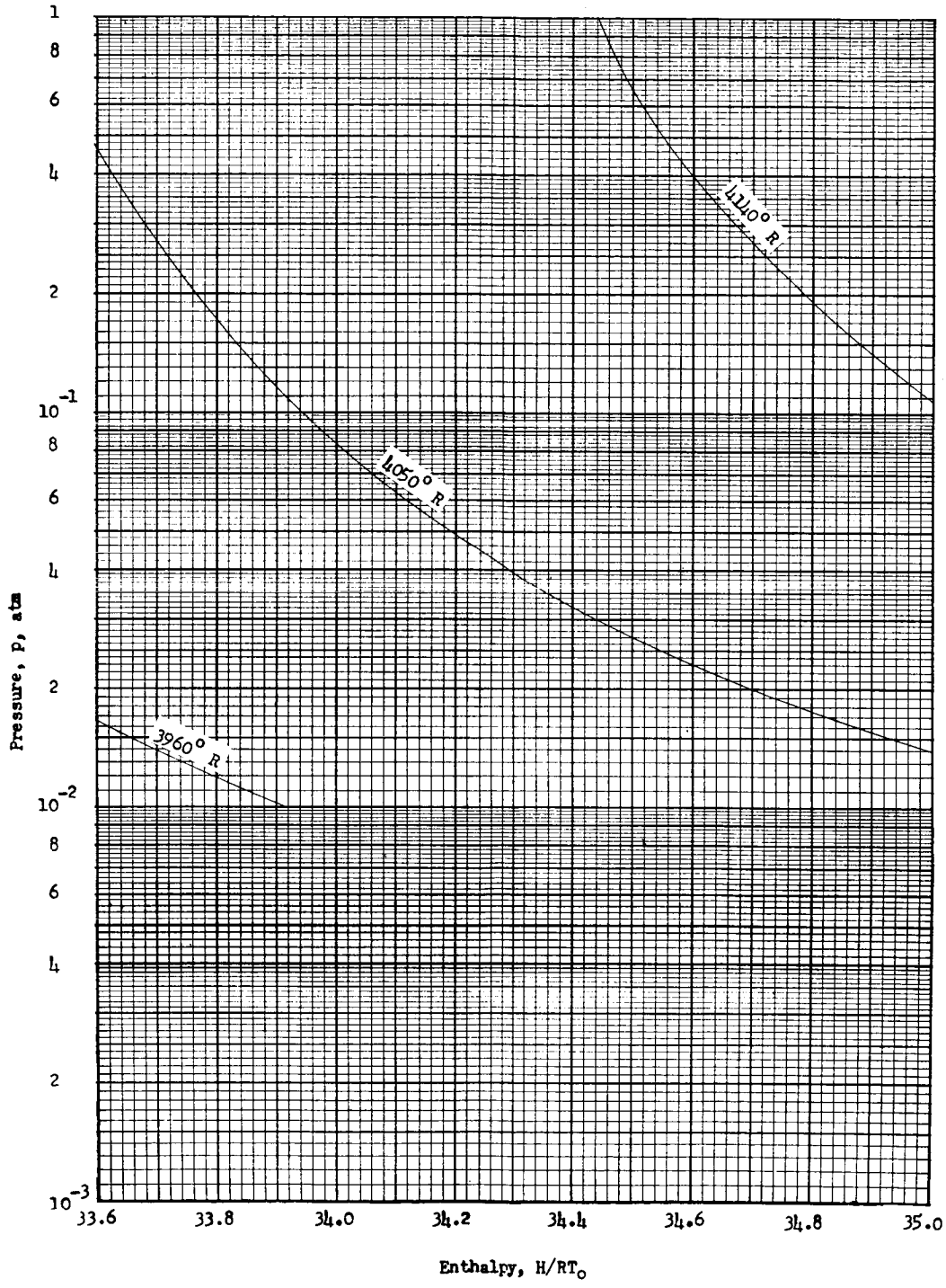

Enthalpy chart 41

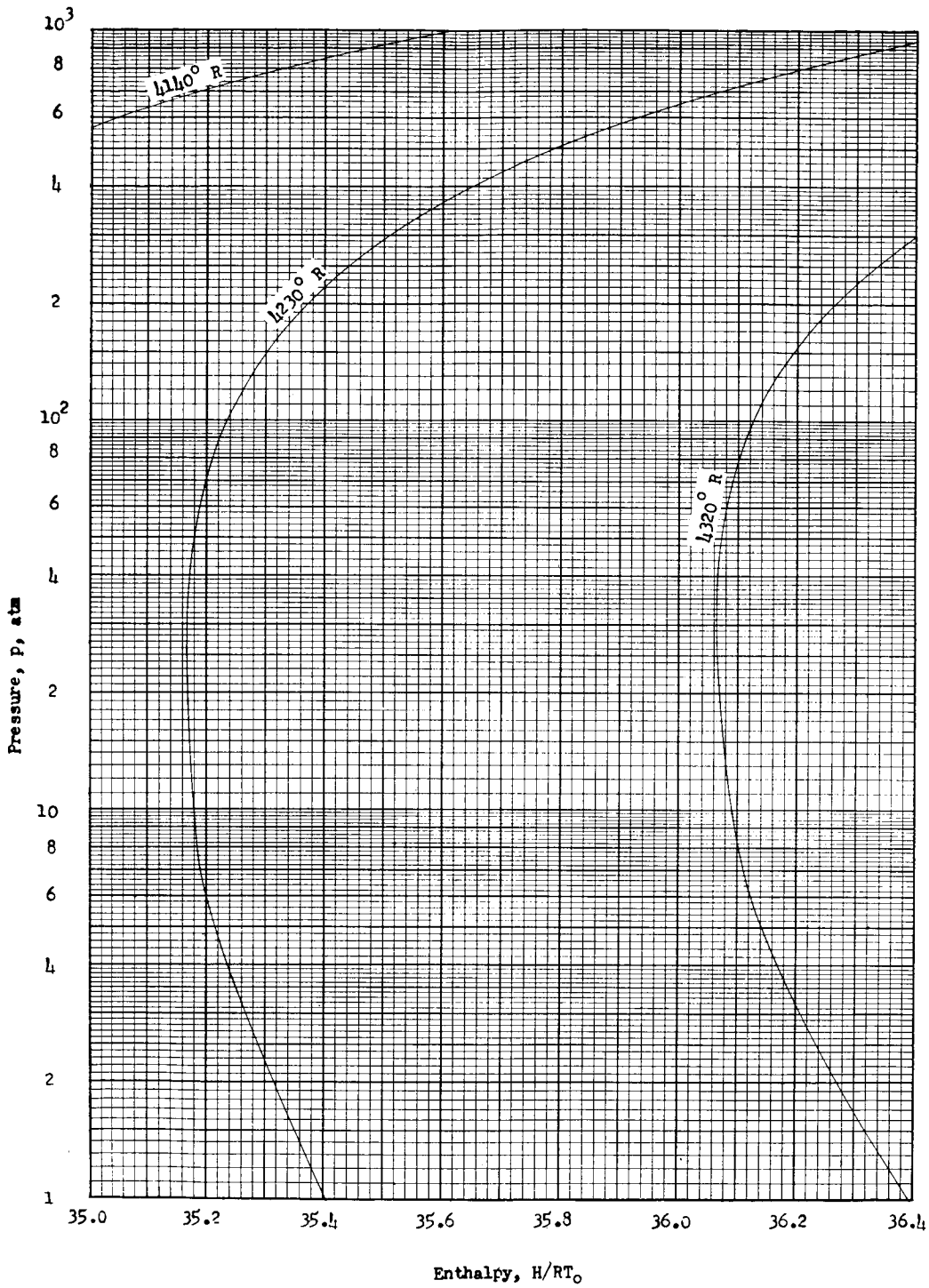

Enthalpy chart 42

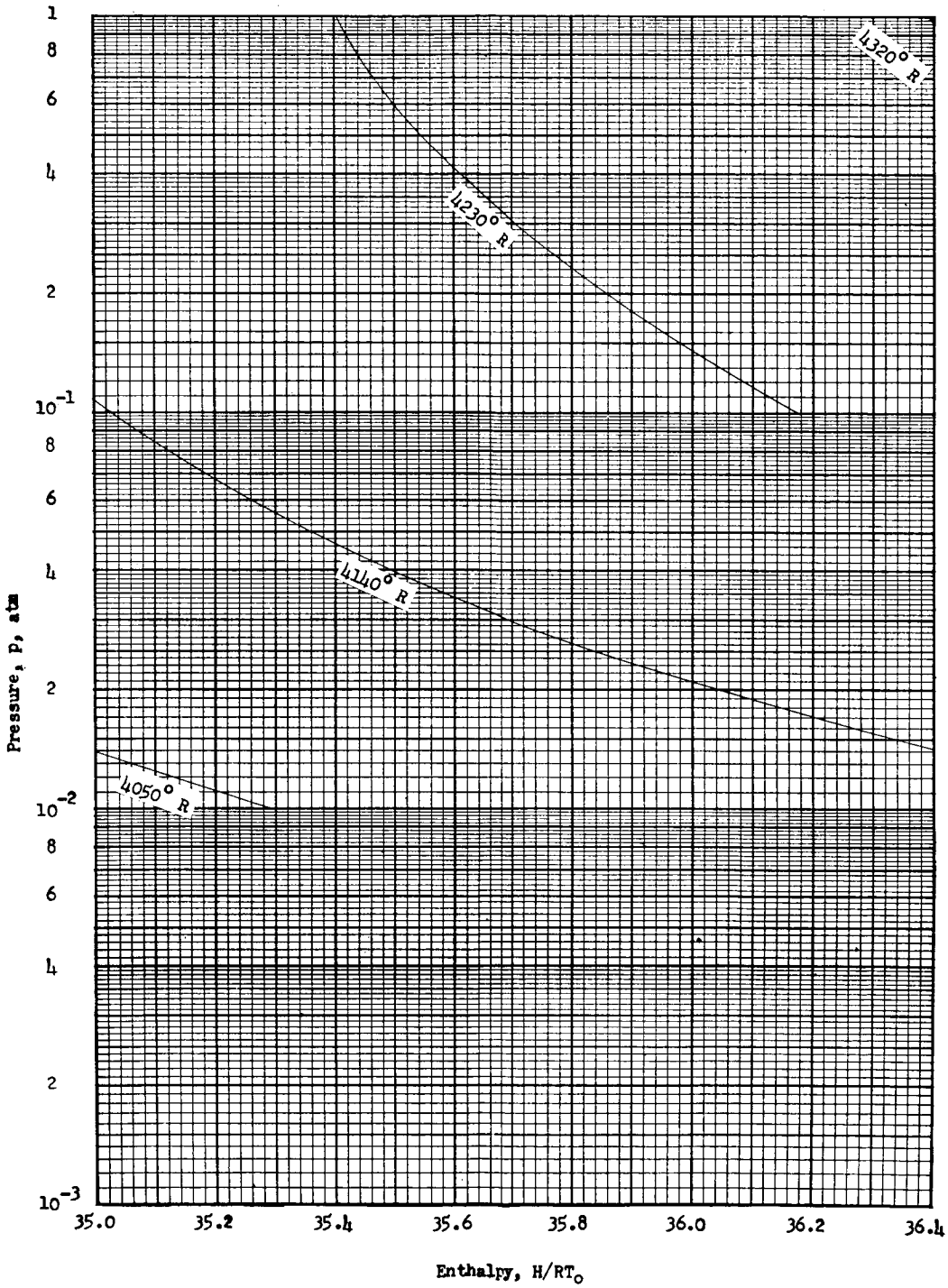

Enthalpy chart 43

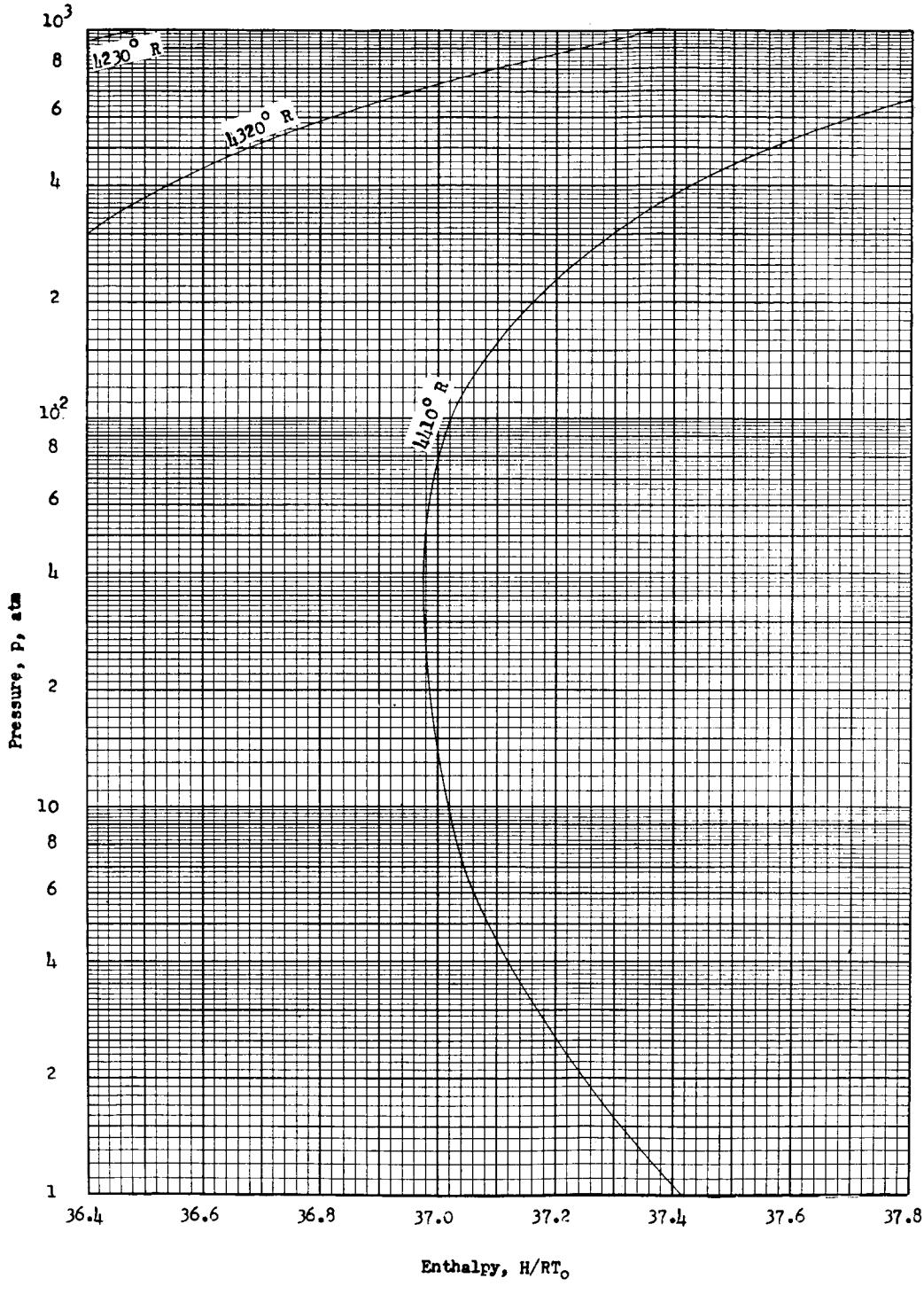

Enthalpy chart 44

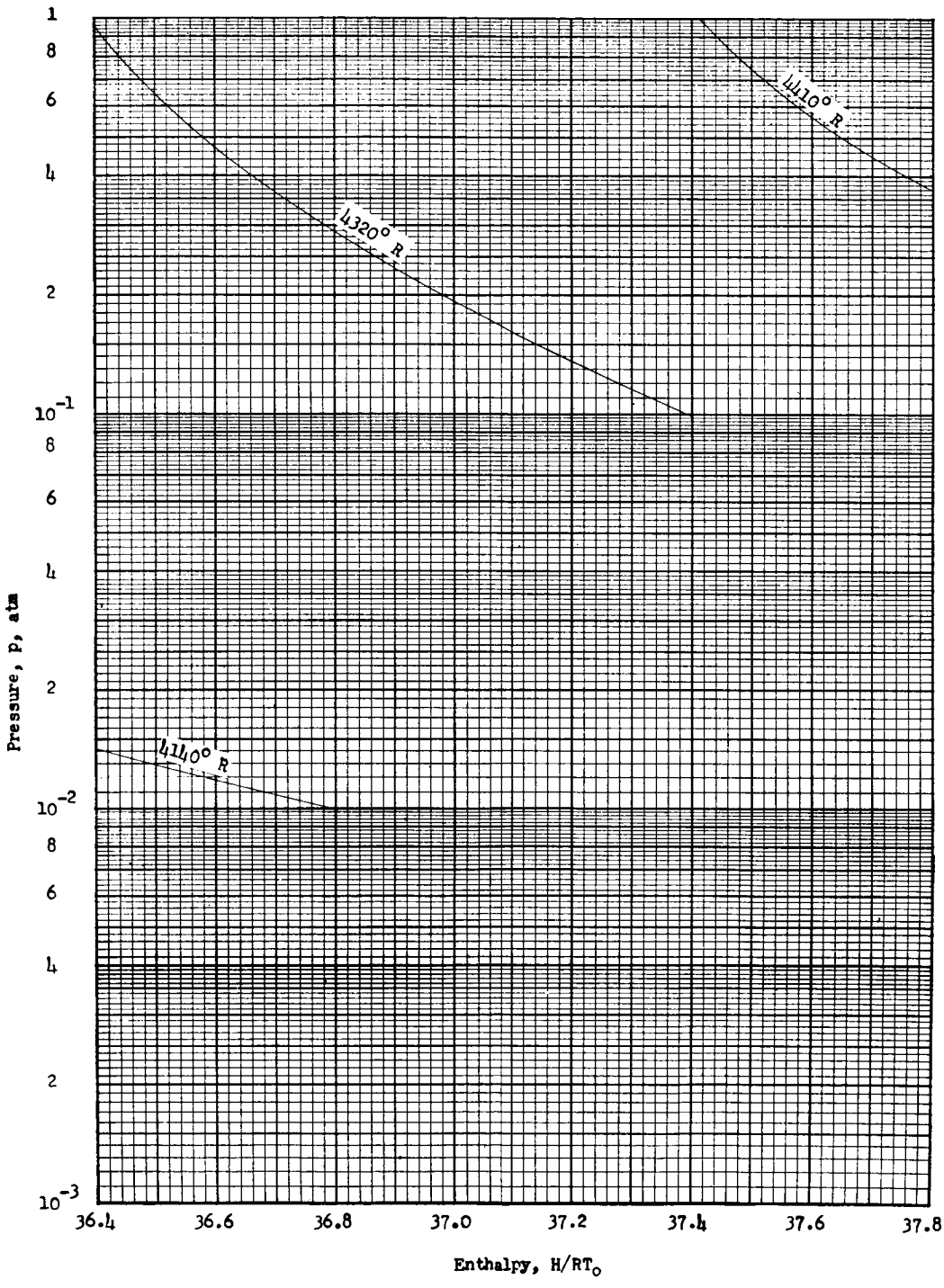

Enthalpy chart 45

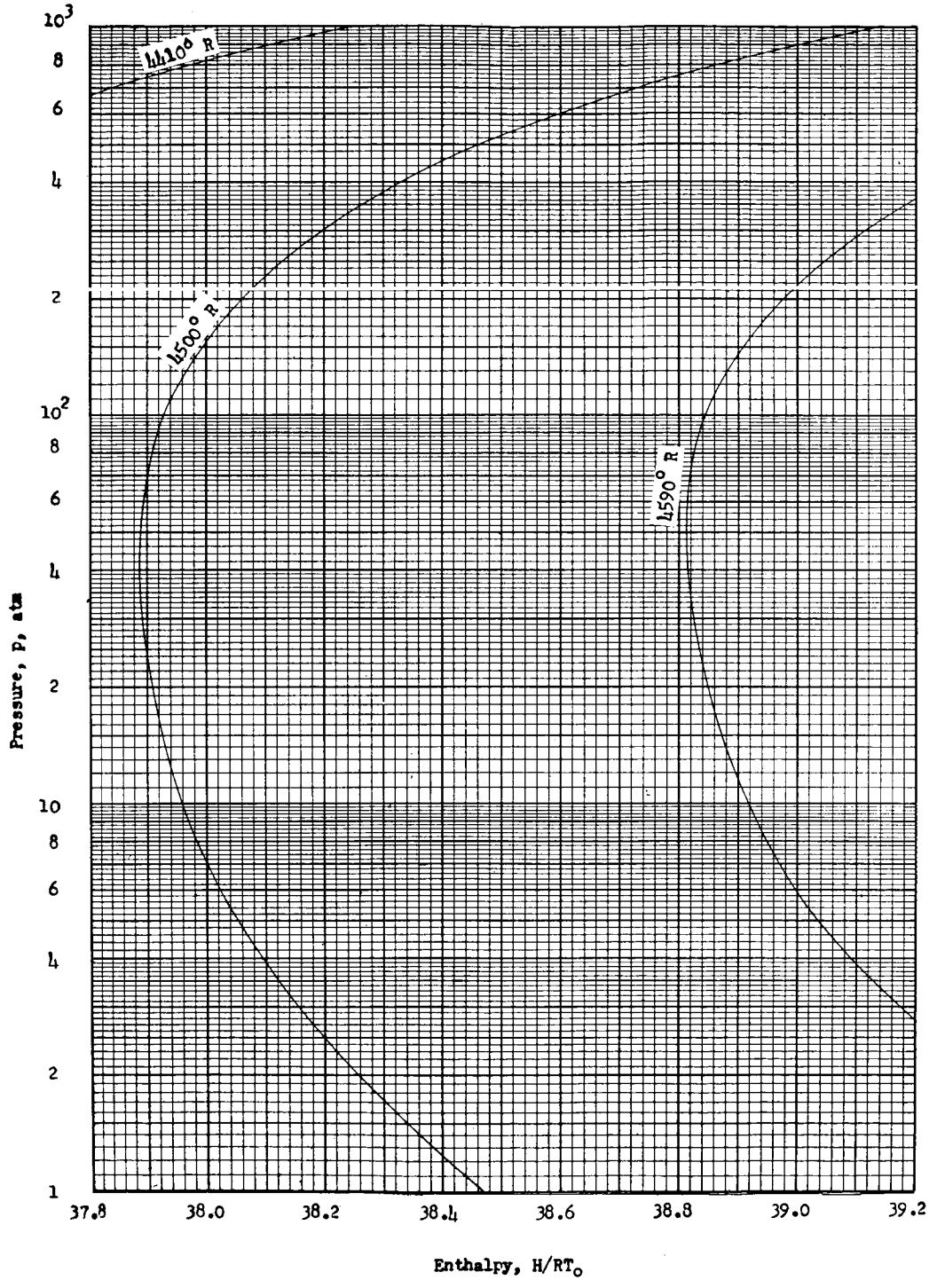

Enthalpy chart 46

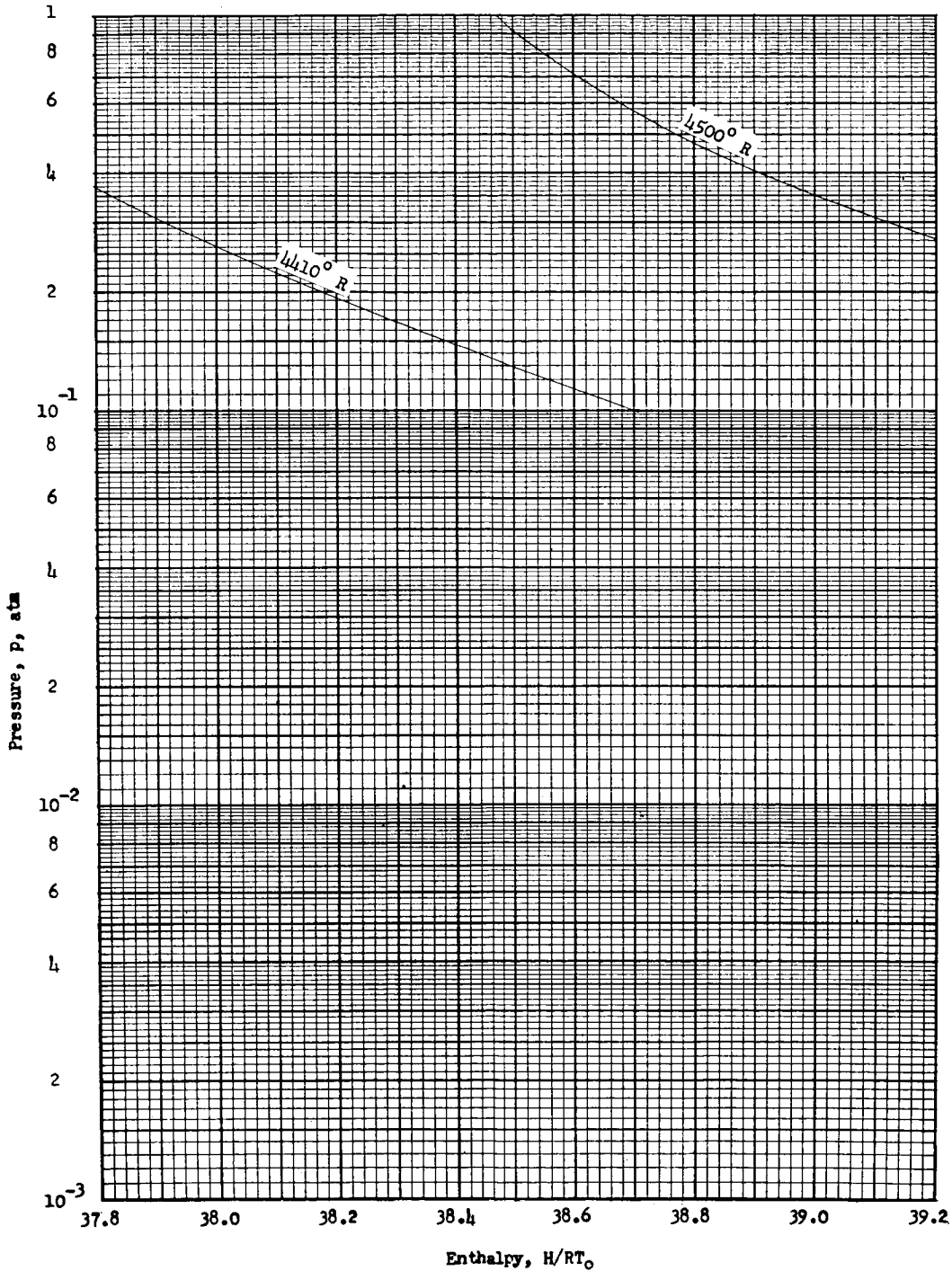

Enthalpy chart 47

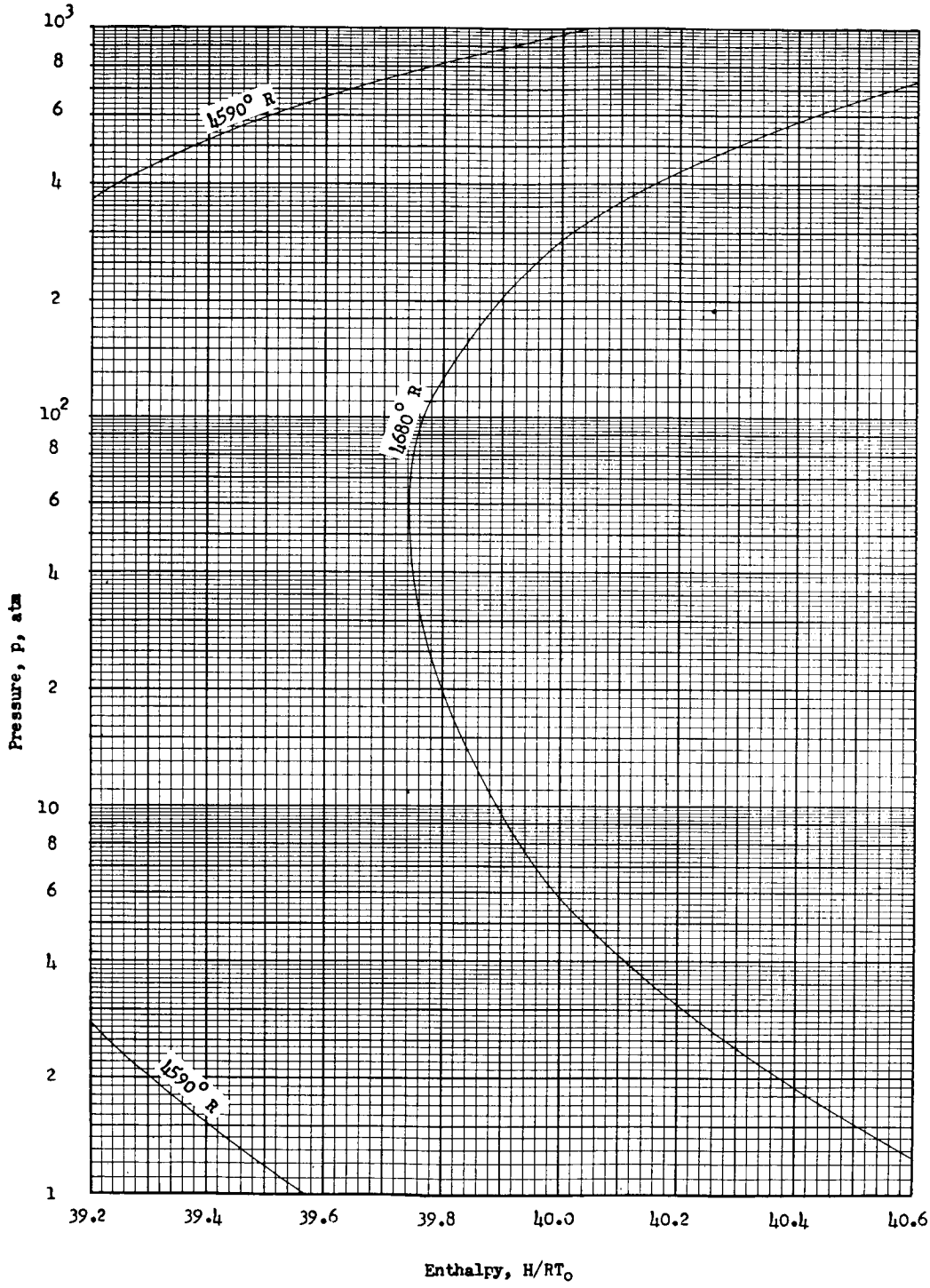

Enthalpy chart 48

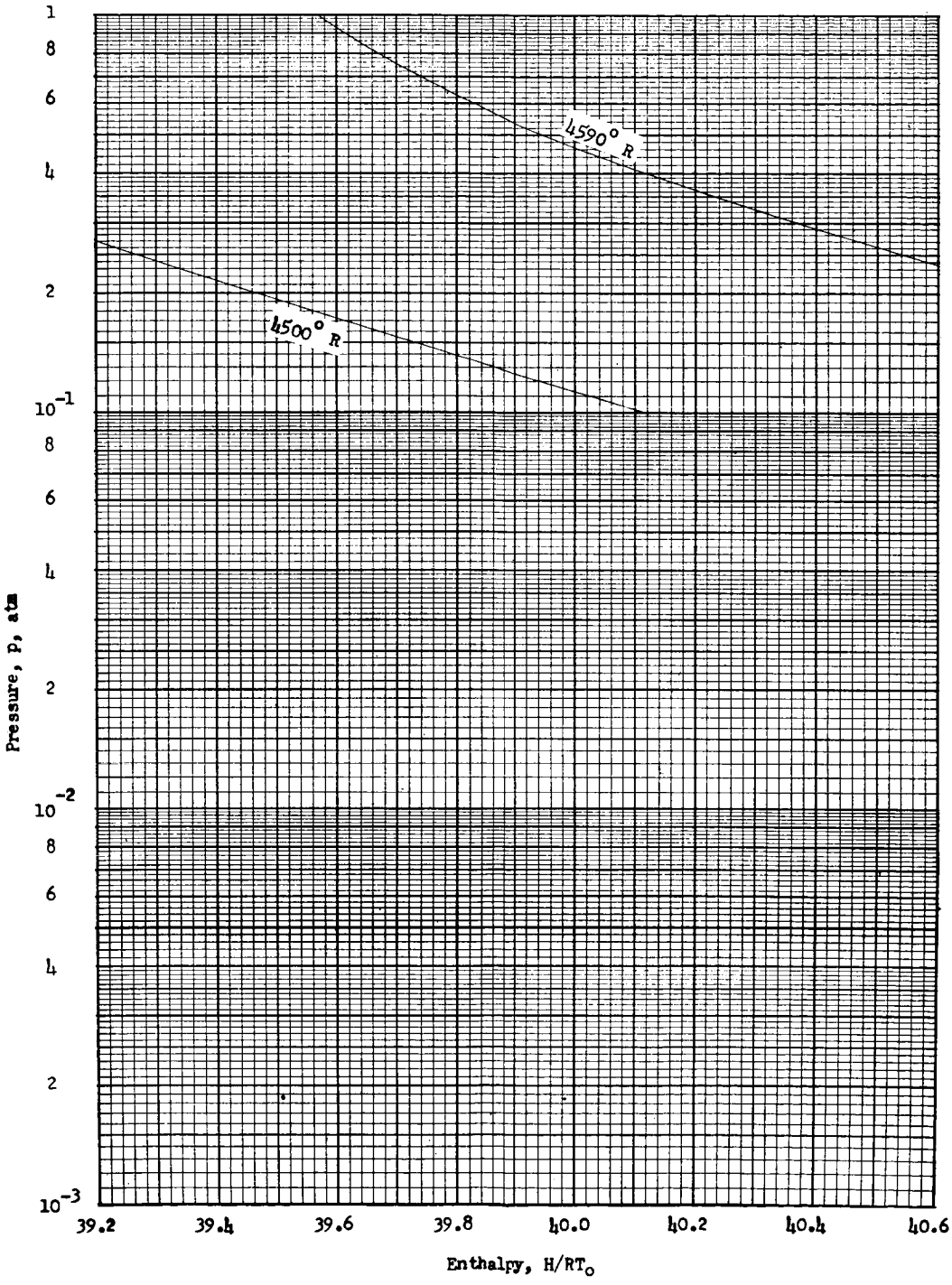

Enthalpy chart 49

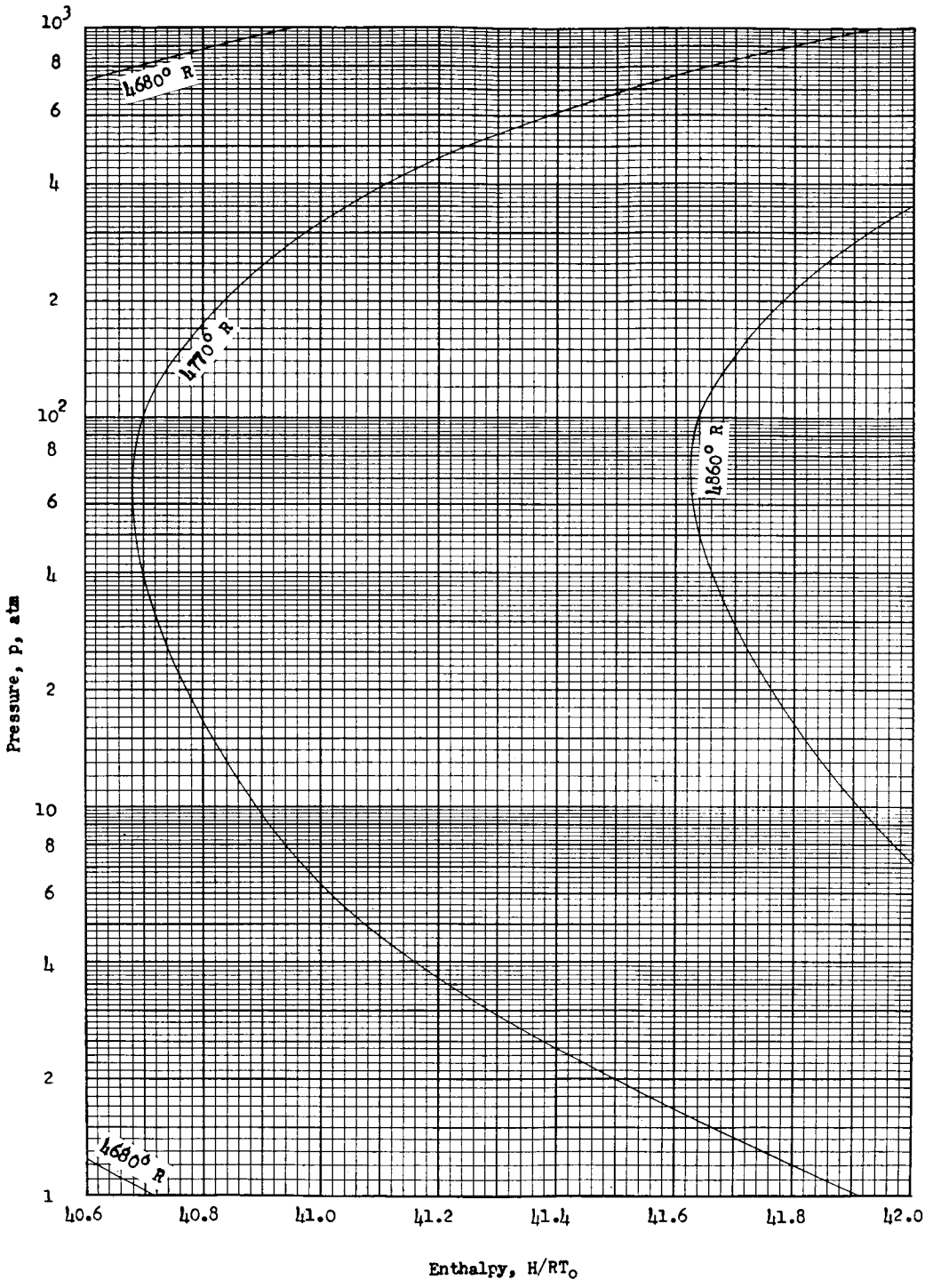

Enthalpy chart 50

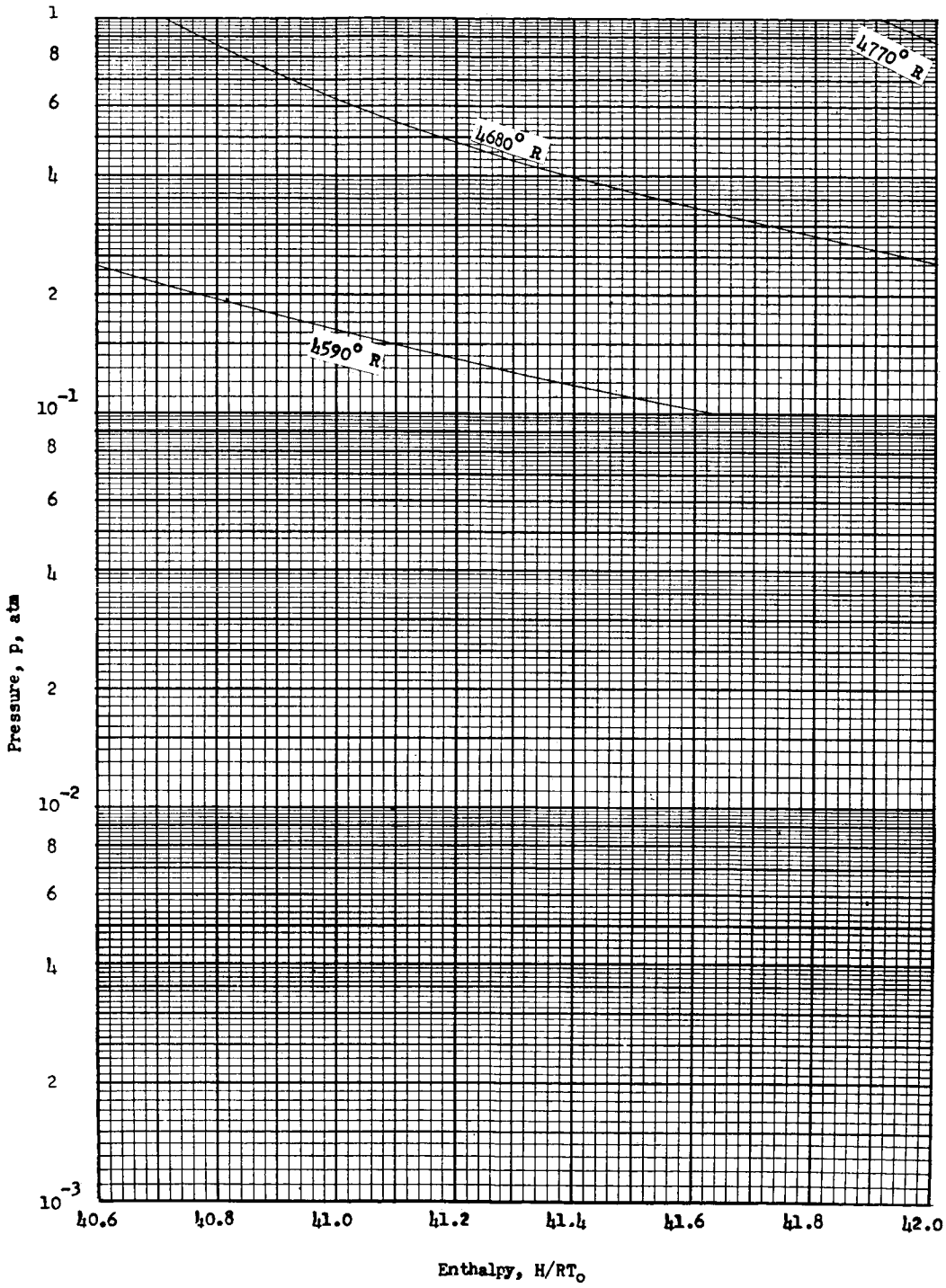

Enthalpy chart 51

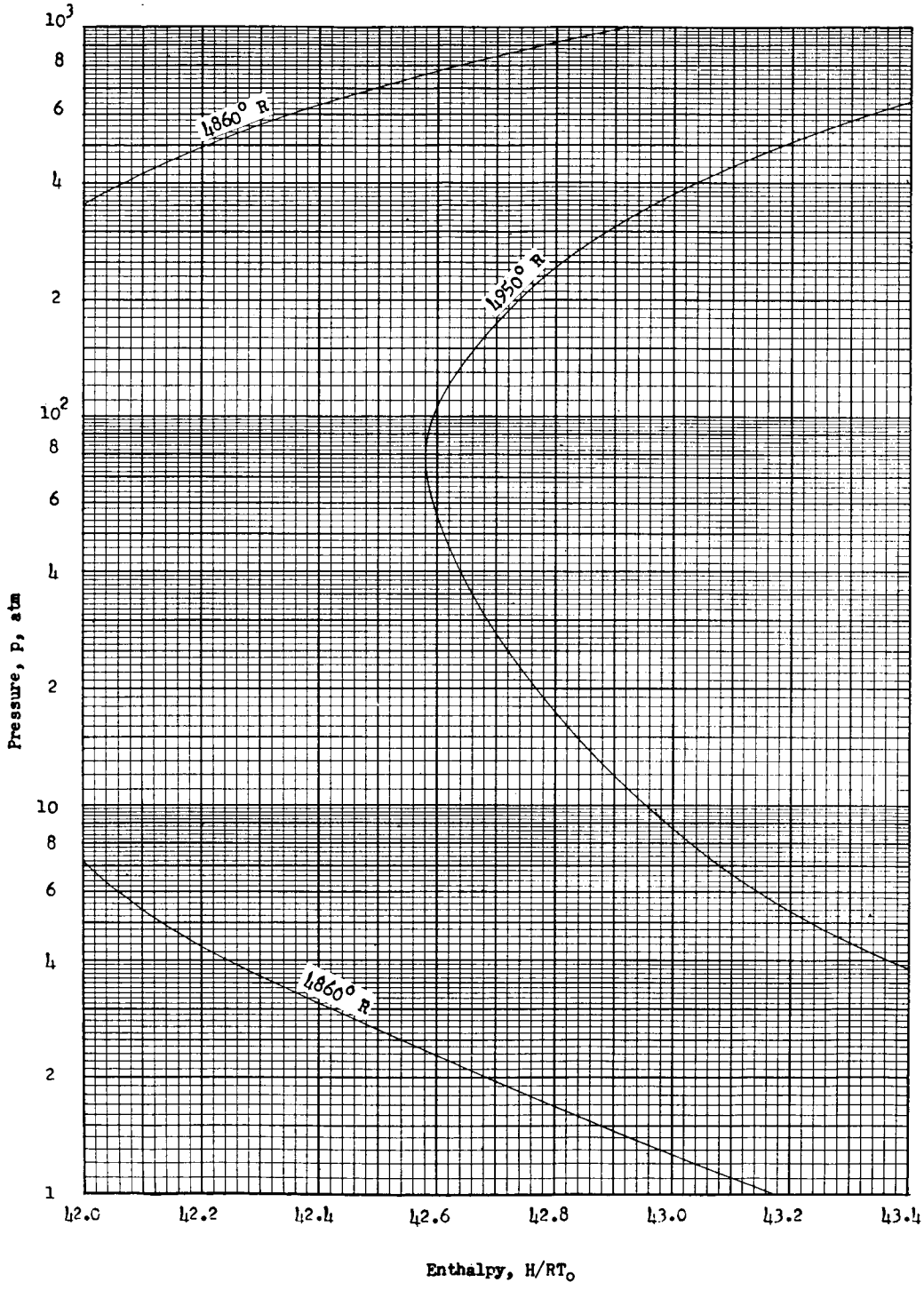

Enthalpy chart 52

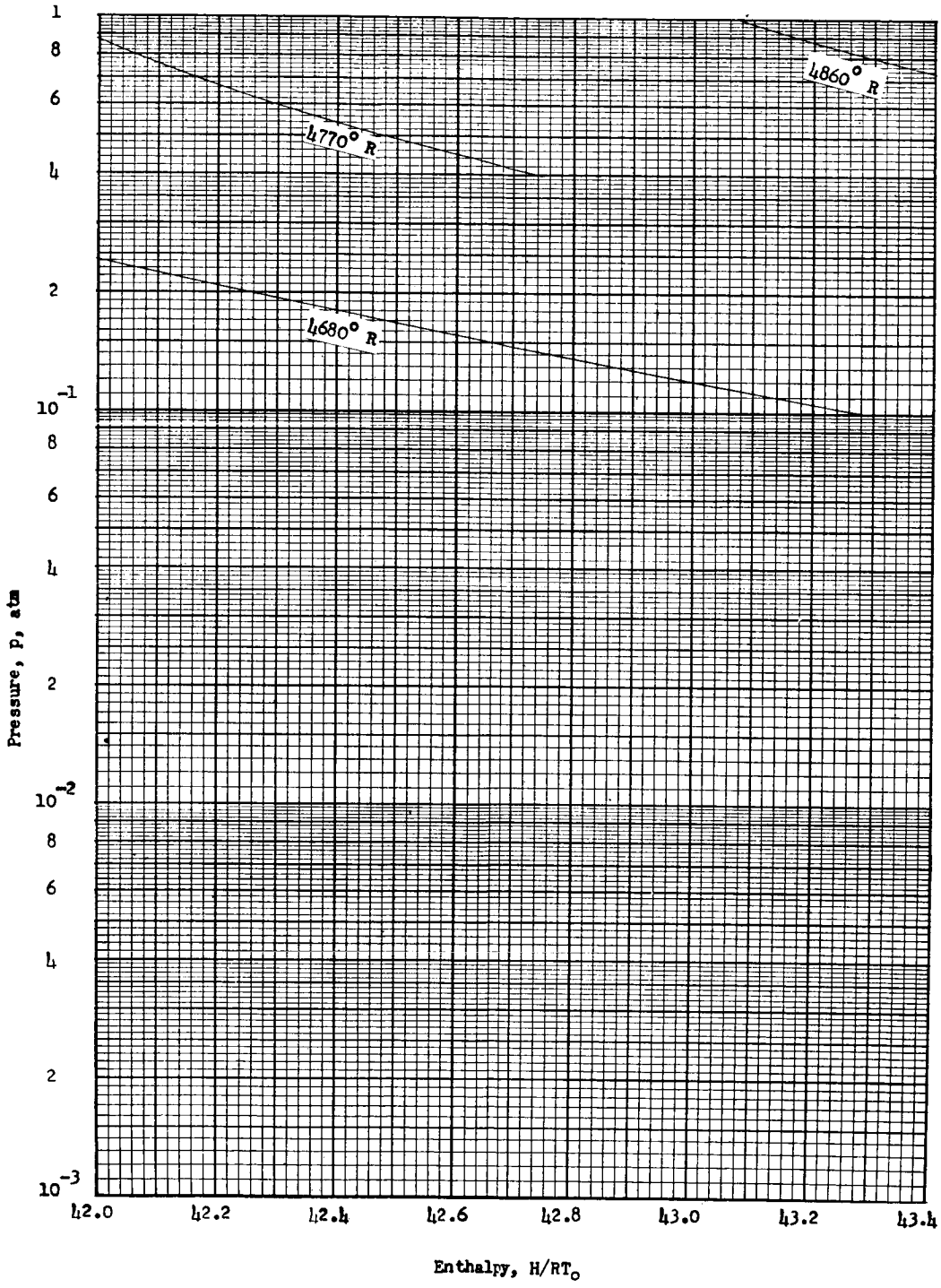

Enthalpy chart 53

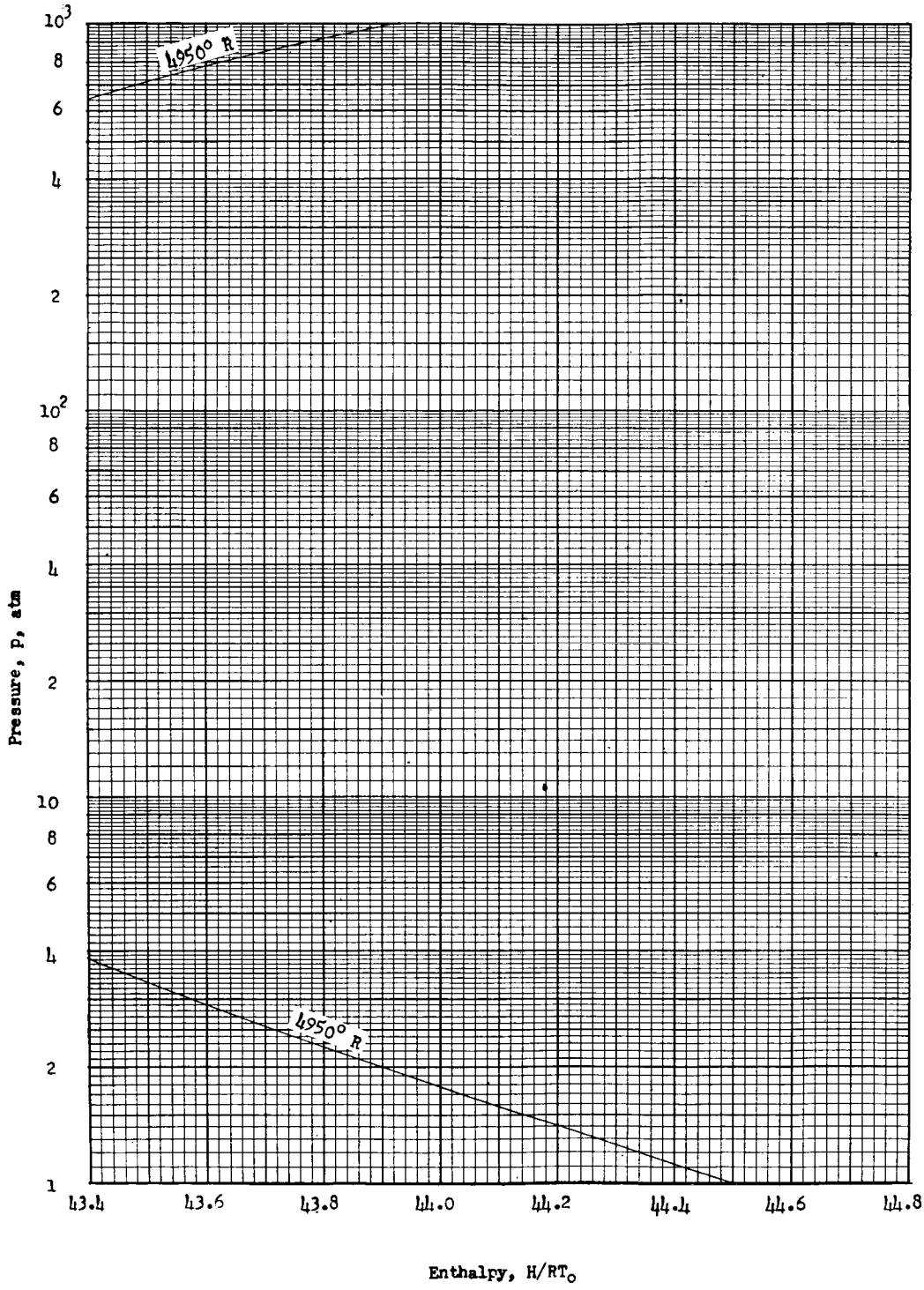

Enthalpy chart 54

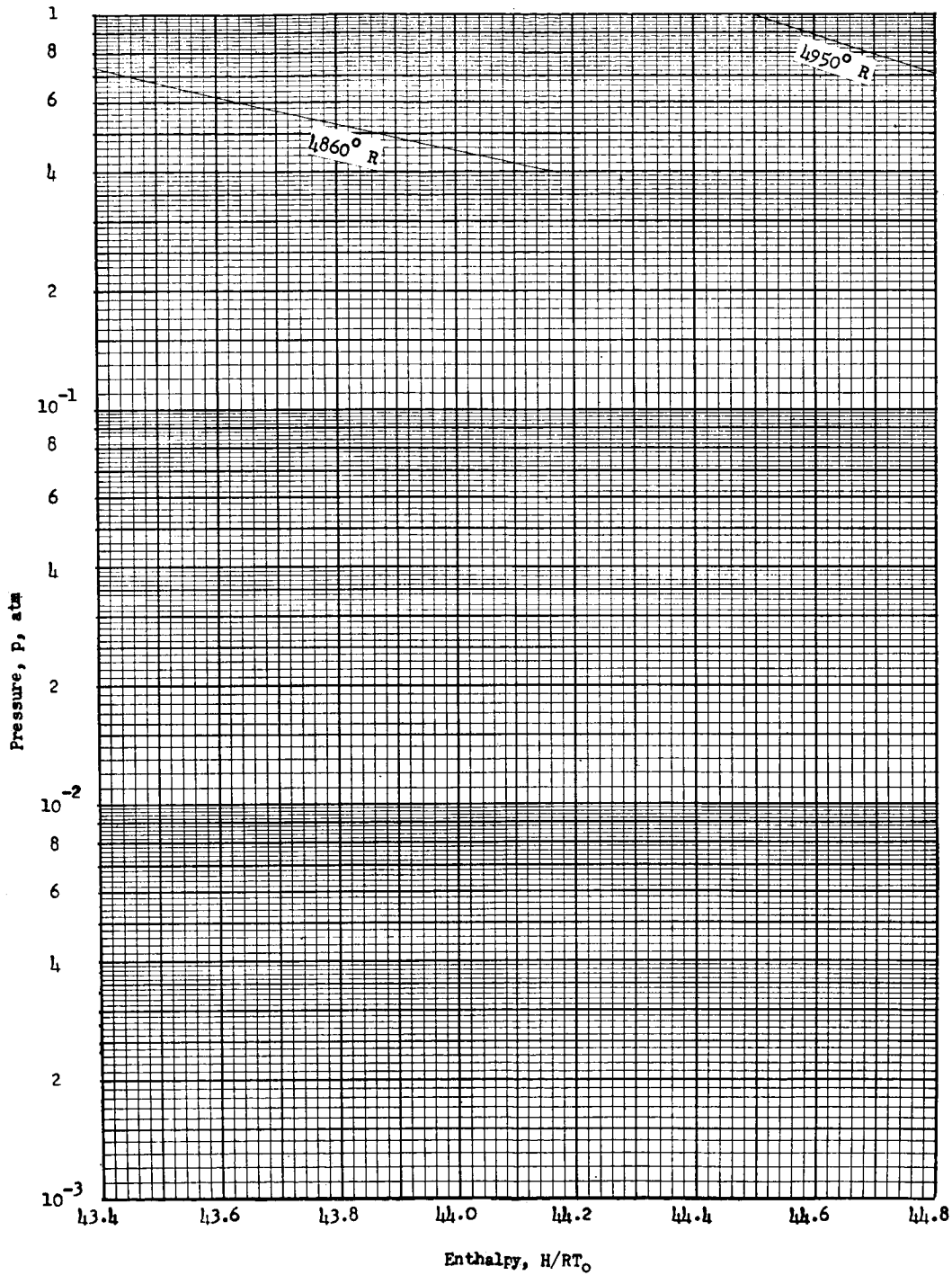

Enthalpy chart 55

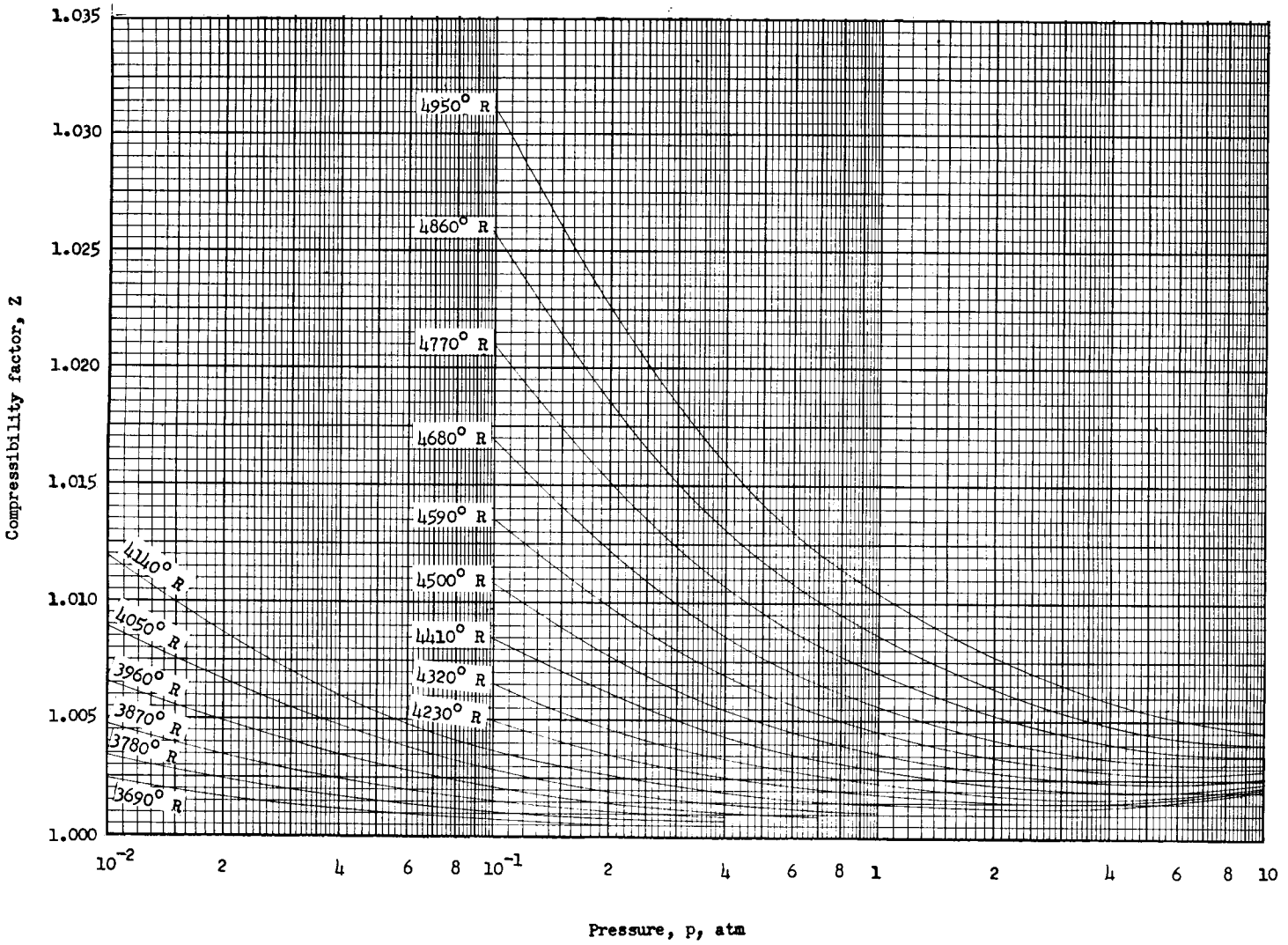

Compressibility-factor chart 1

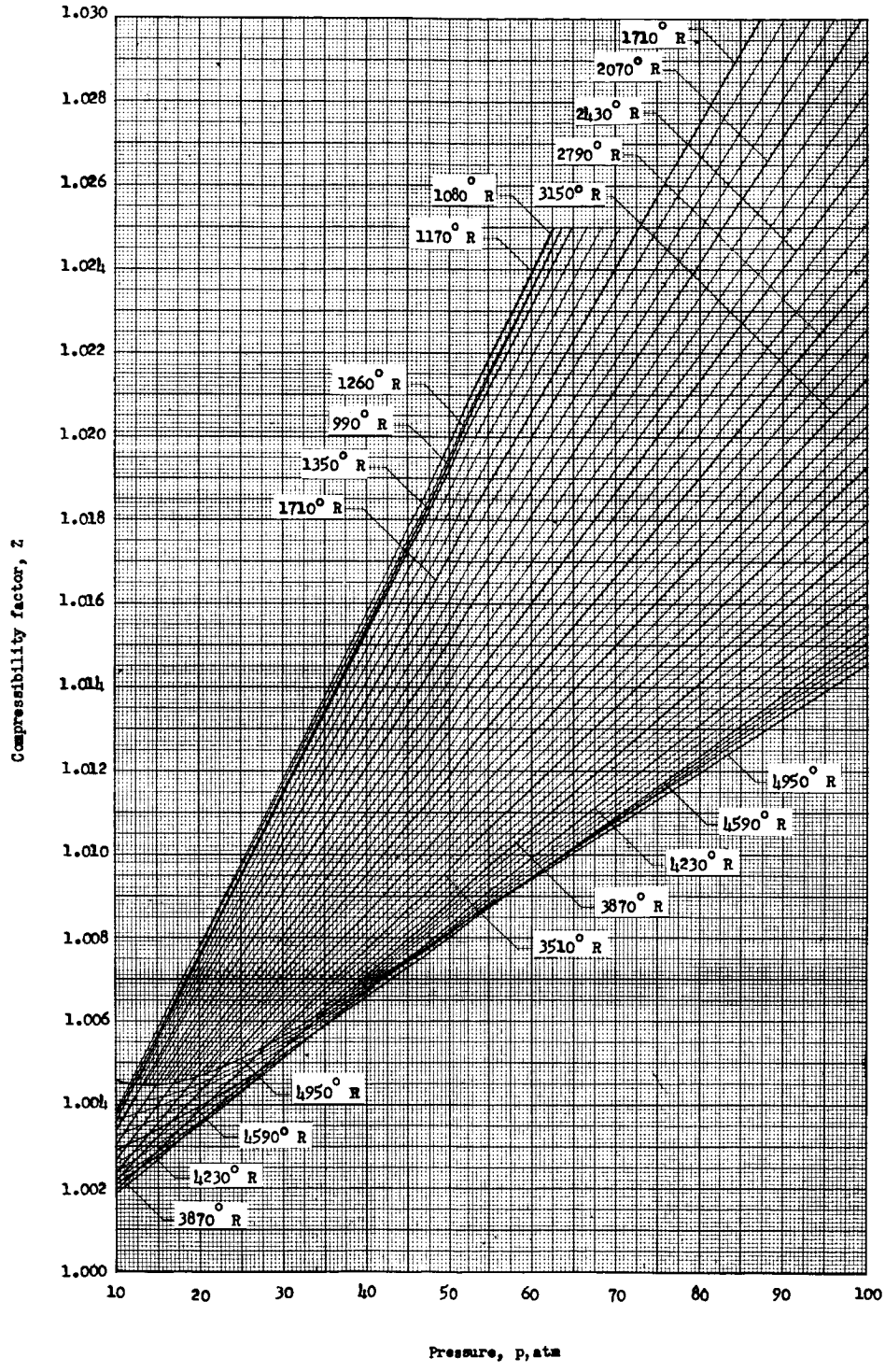

Compressibility-factor chart 2

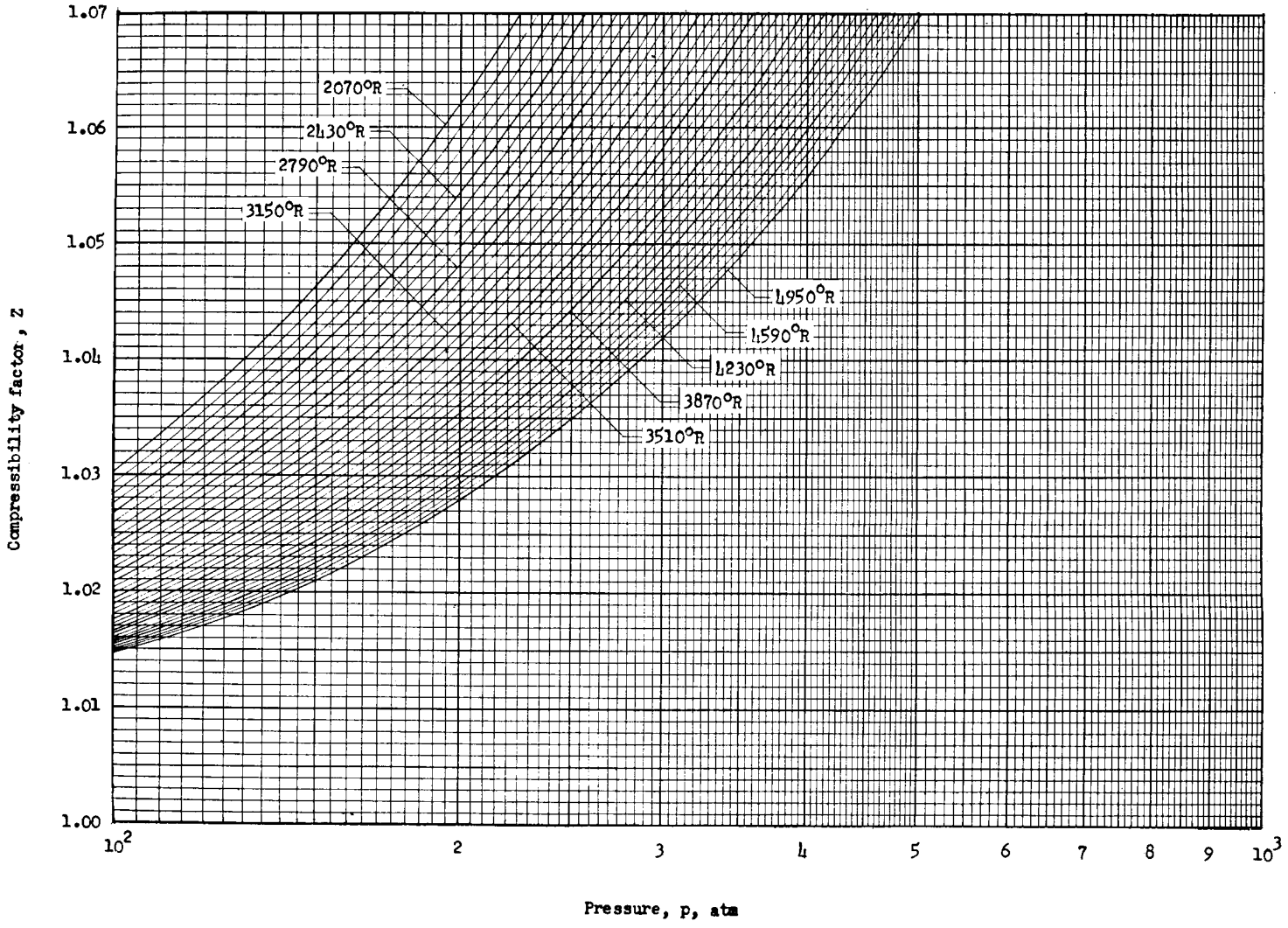

Compressibility-factor chart 3

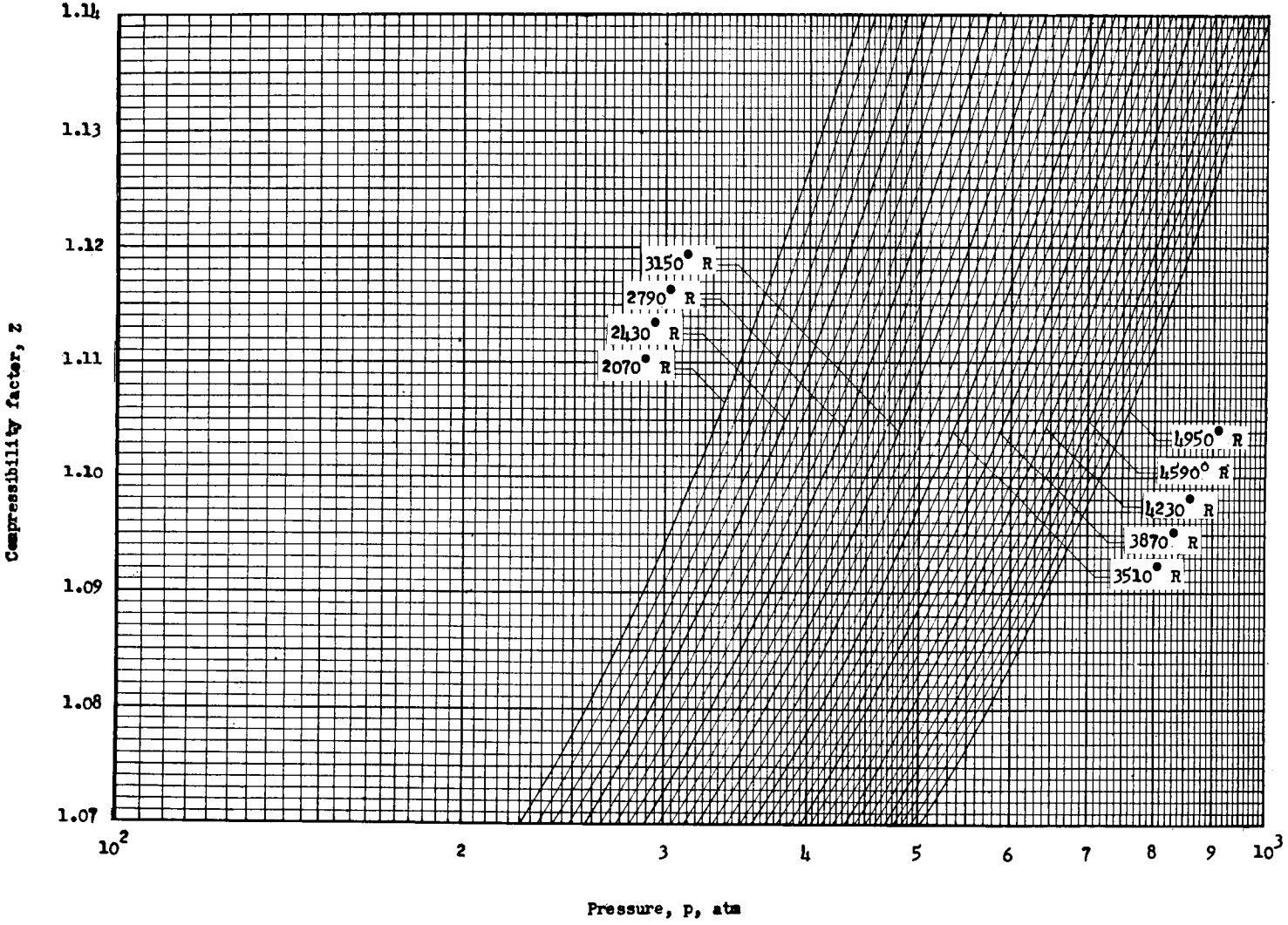

Compressibility-factor chart 4

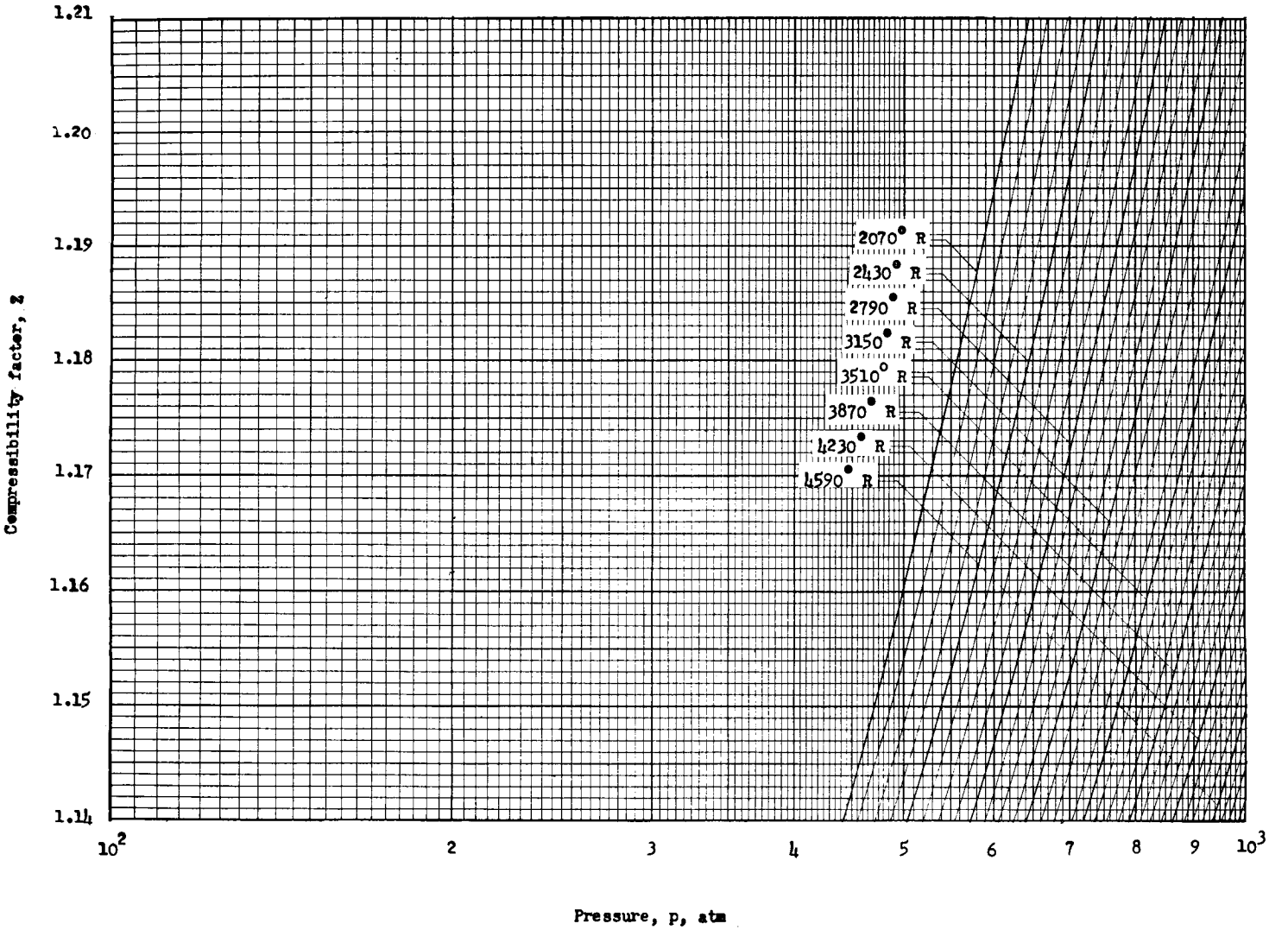

Compressibility-factor chart 5

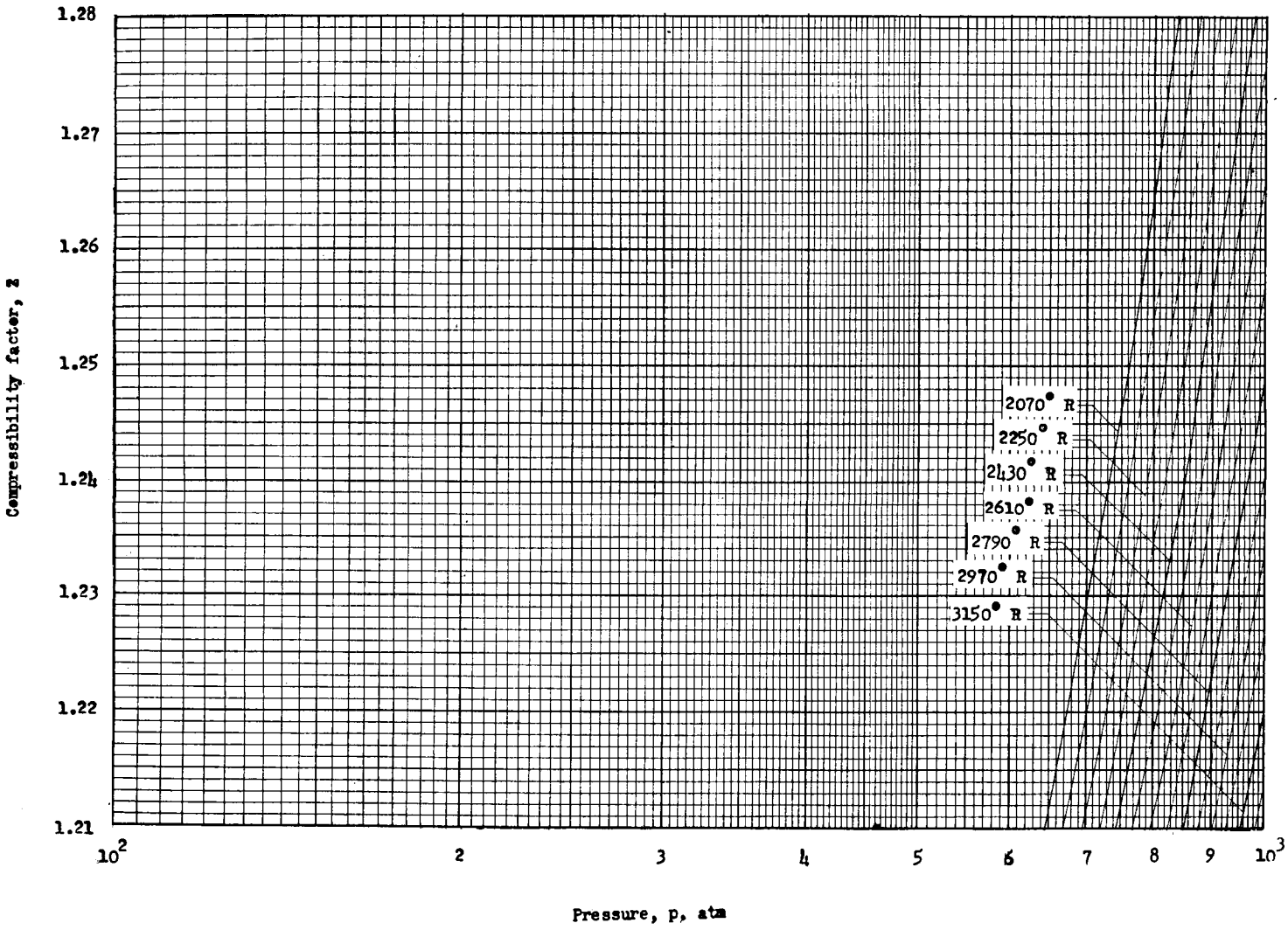

Compressibility-factor chart 6

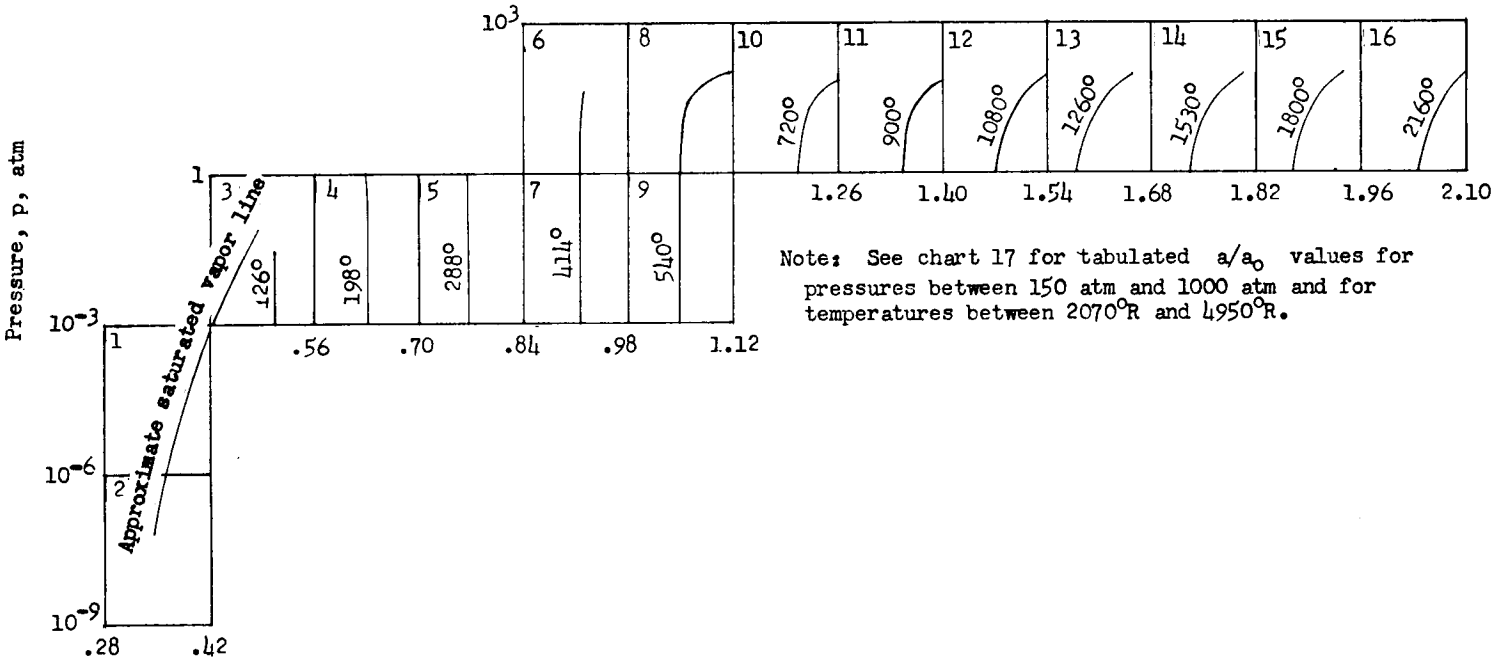

Note: See chart 17 for tabulated a/a_o values for pressures between 150 atm and 1000 atm and for temperatures between 2070°R and 4950°R.

Key to velocity-of-sound charts

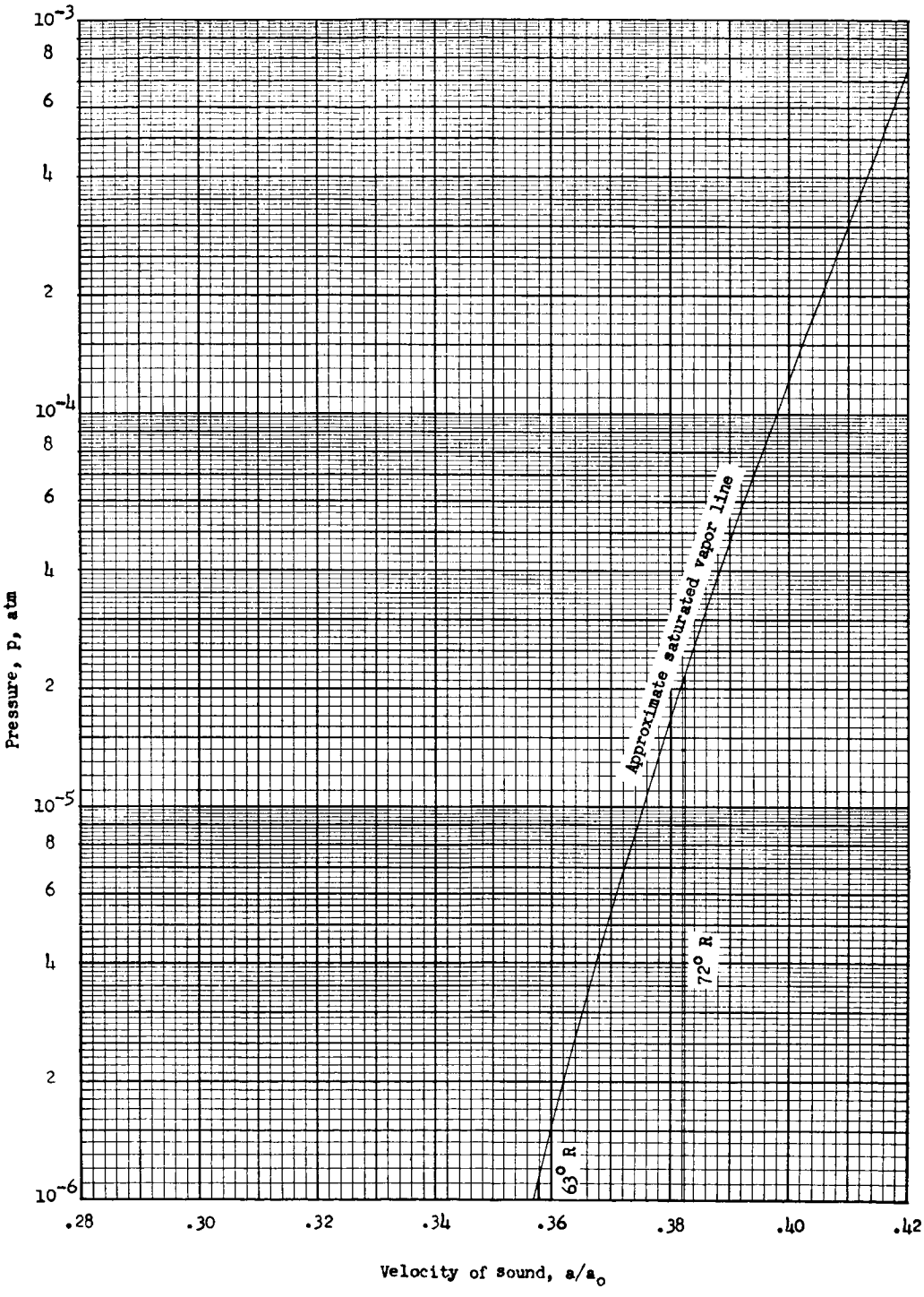

Velocity-of-sound chart 1

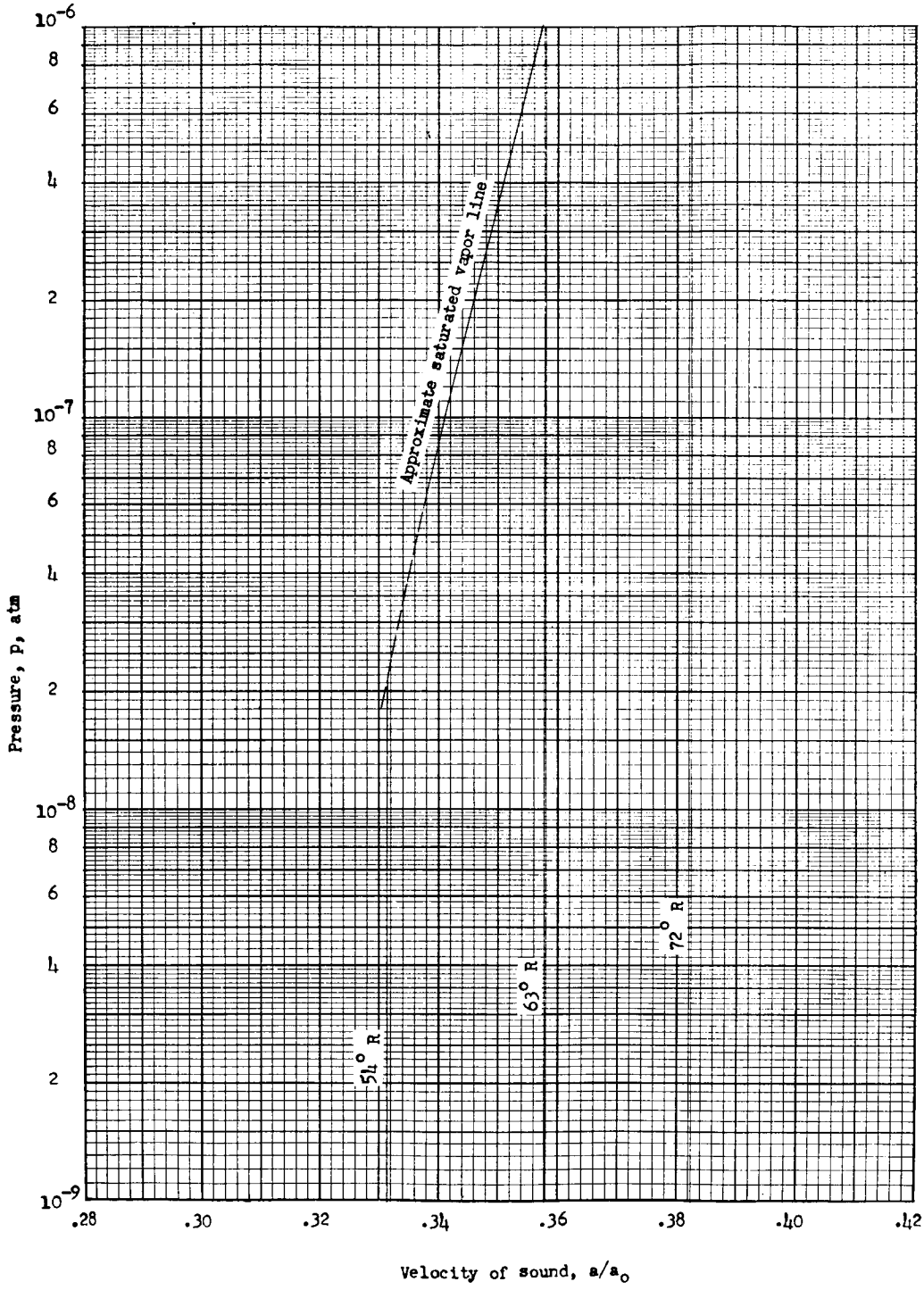

Velocity-of-sound chart 2

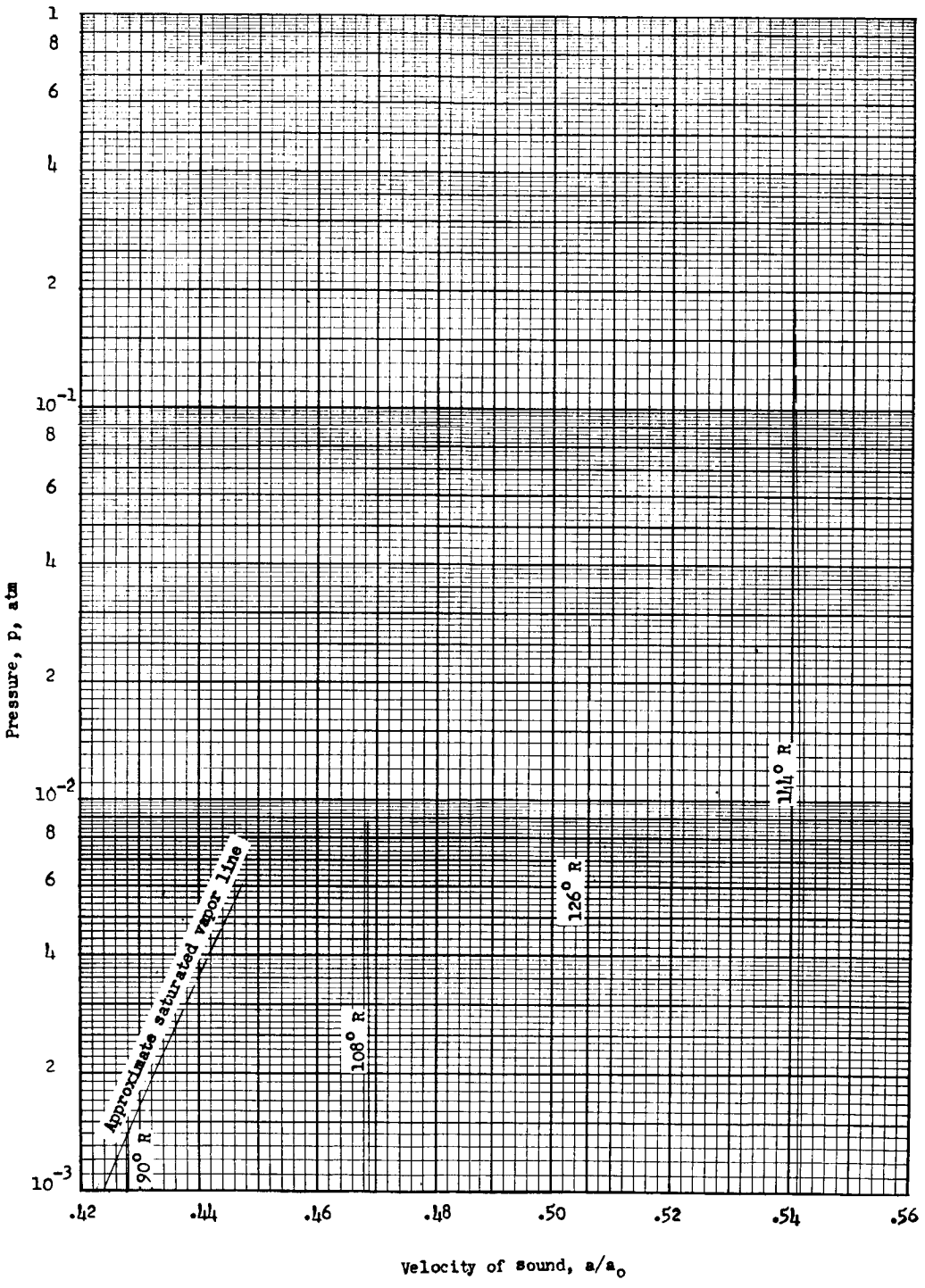

Velocity-of-sound chart 3

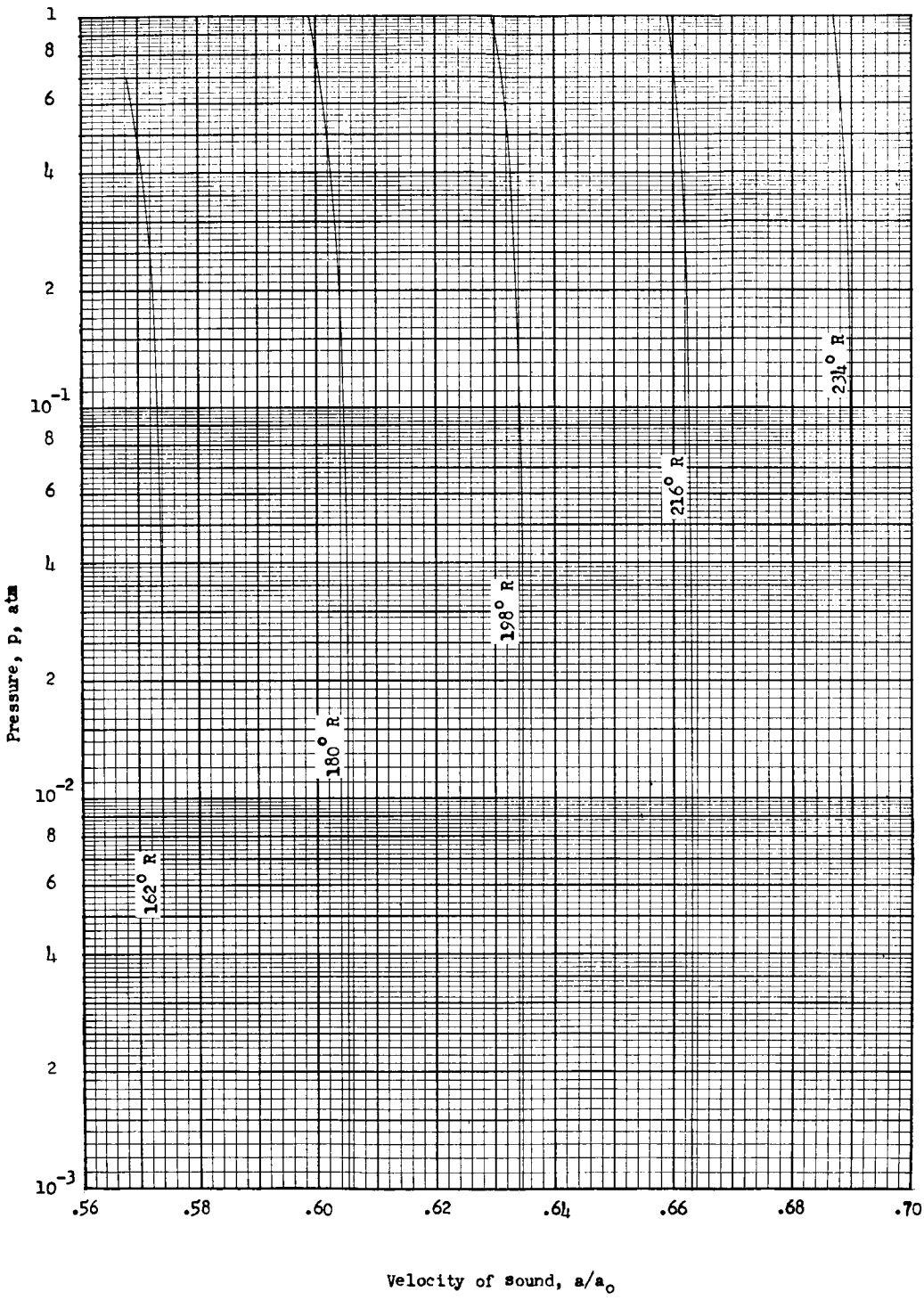

Velocity-of-sound chart 4

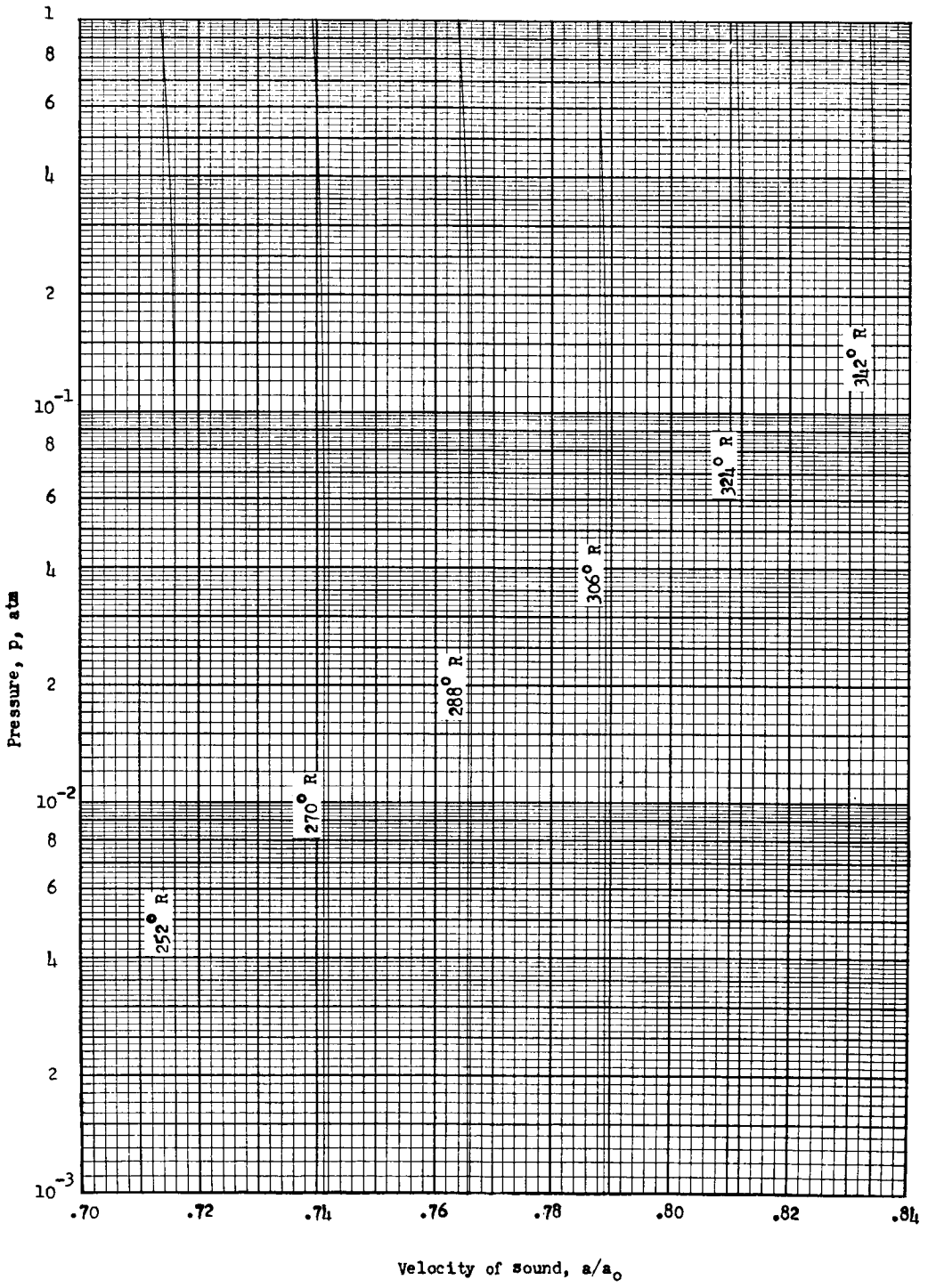

Velocity-of-sound chart 5

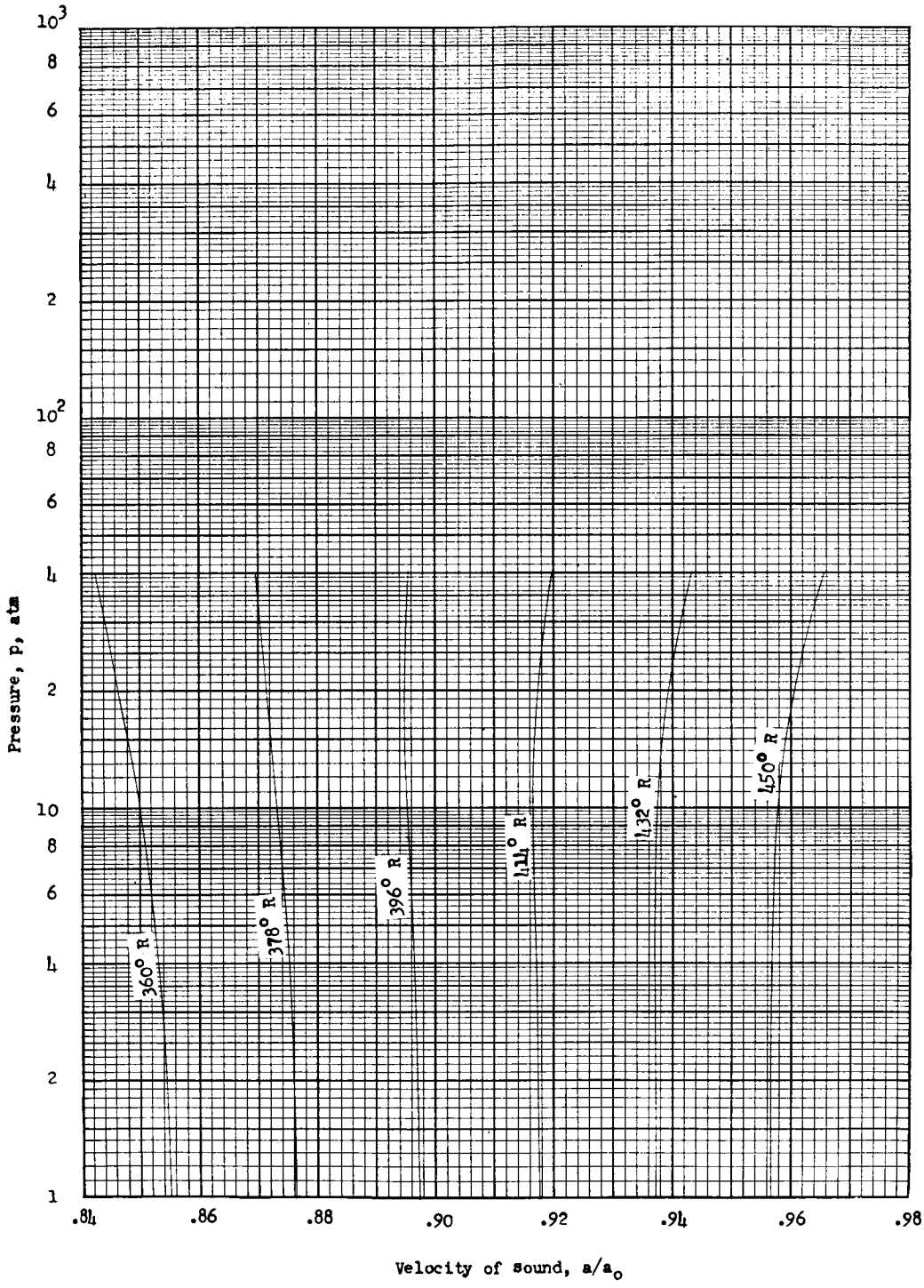

Velocity-of-sound chart 6

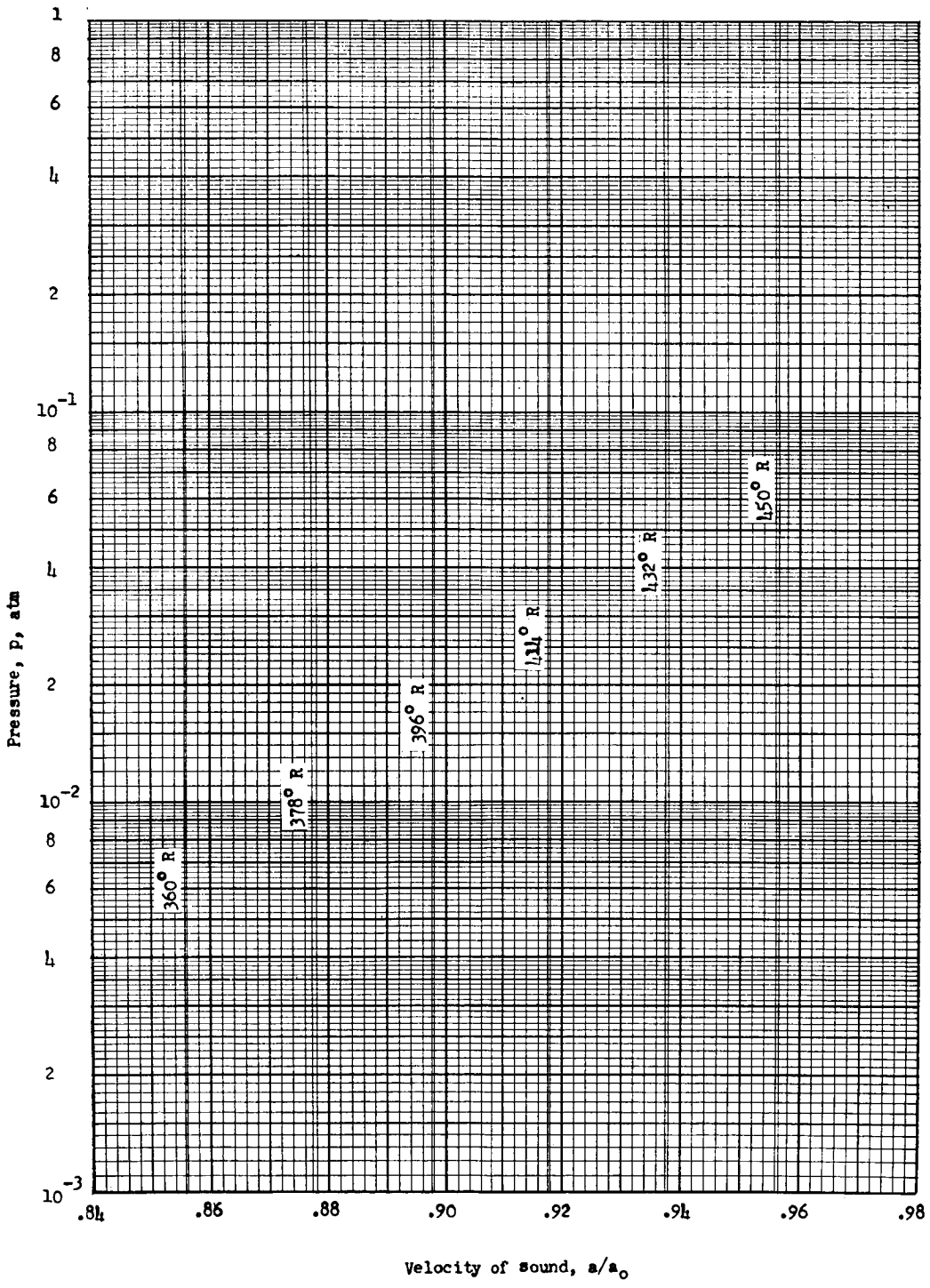

Velocity-of-sound chart 7

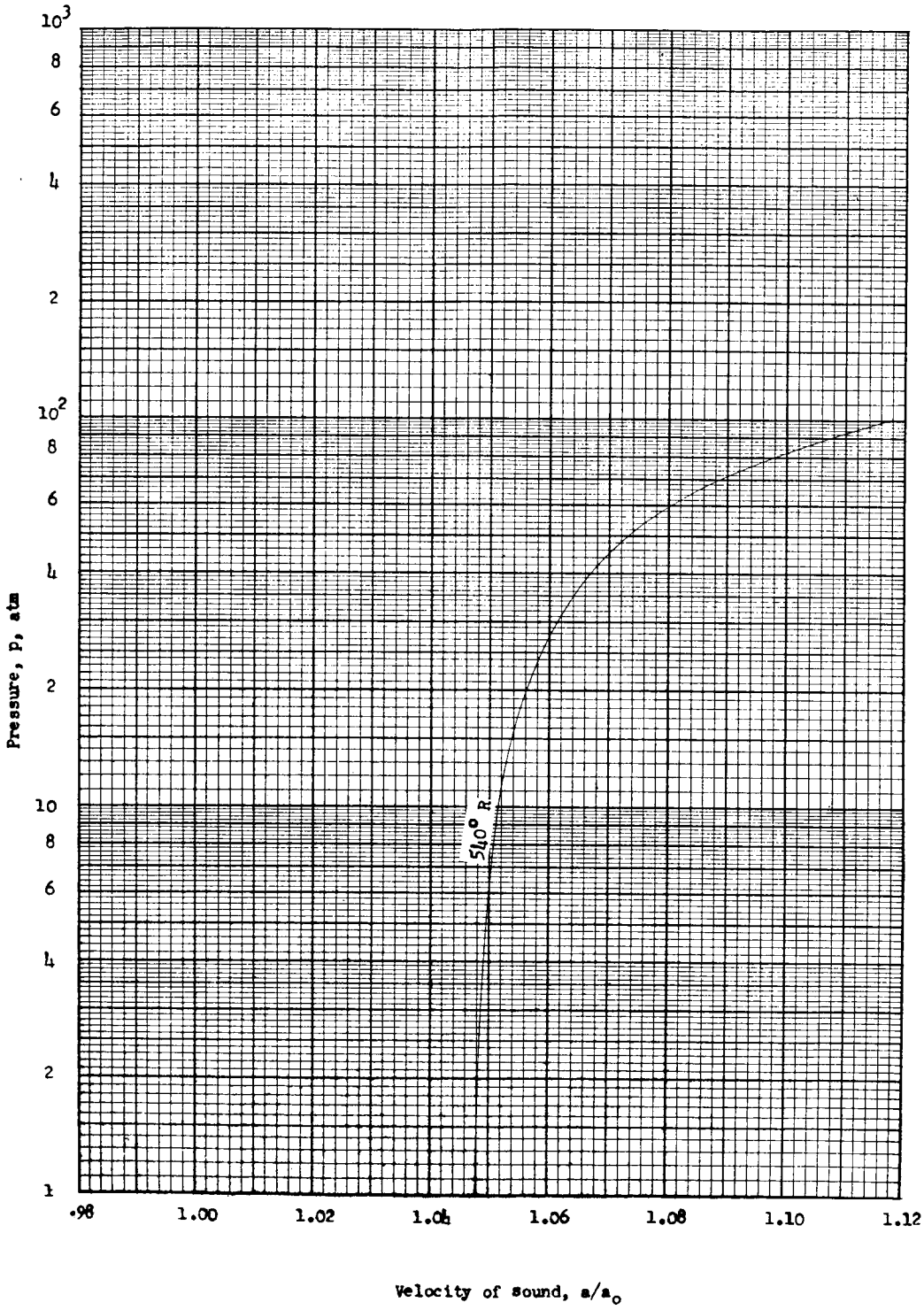

Velocity-of-sound chart 8

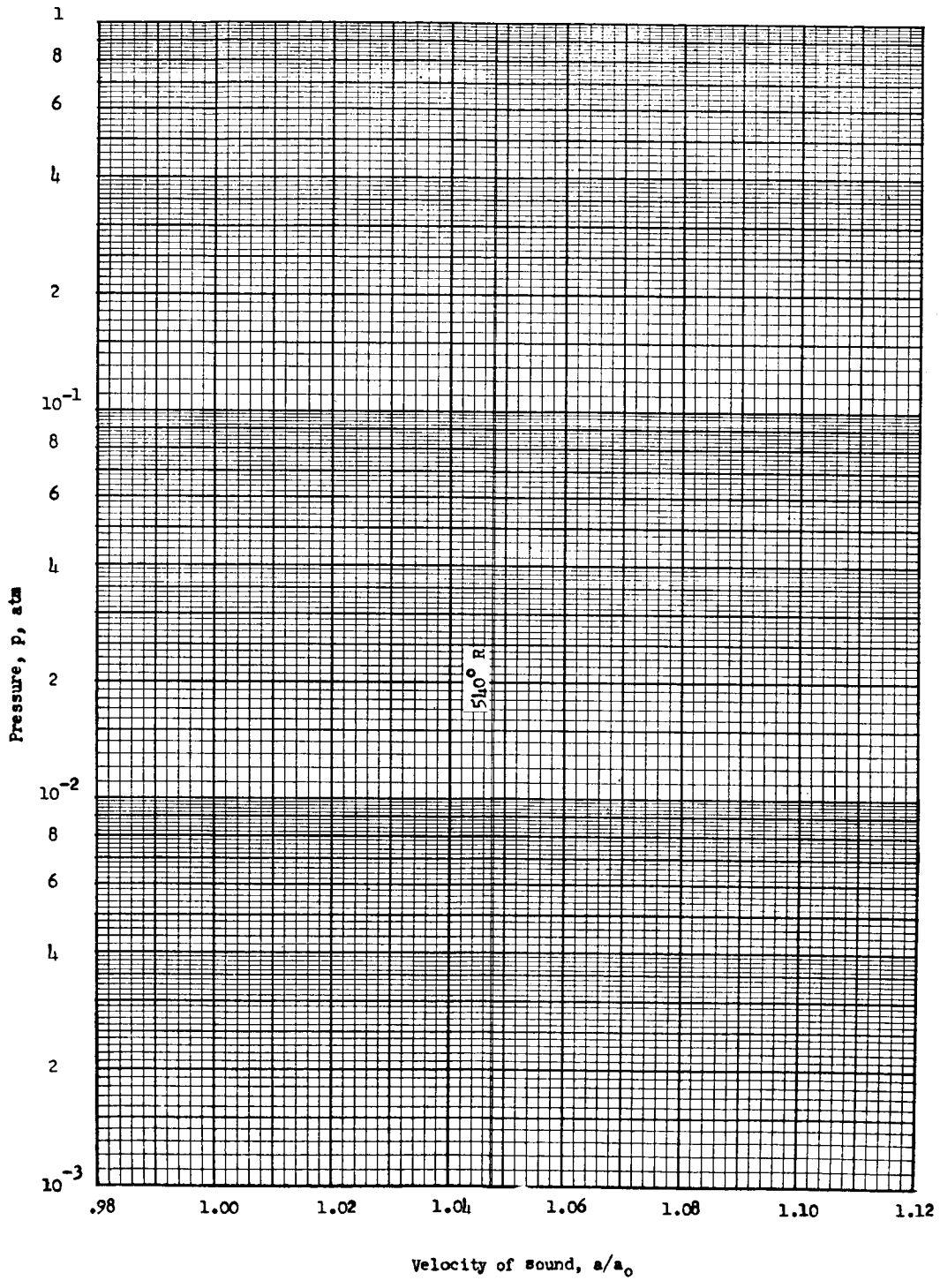

Velocity-of-sound chart 9

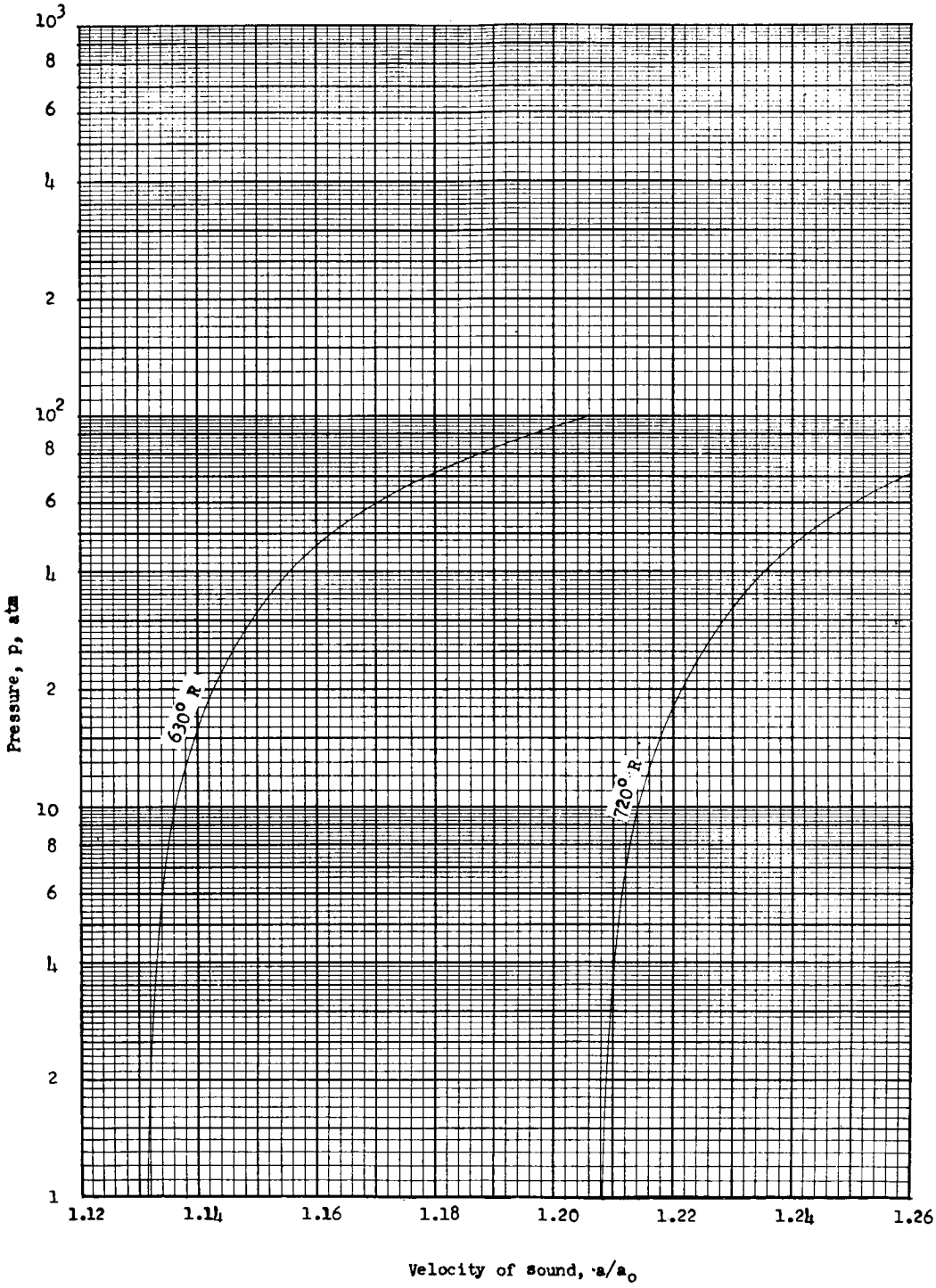

Velocity-of-sound chart 10

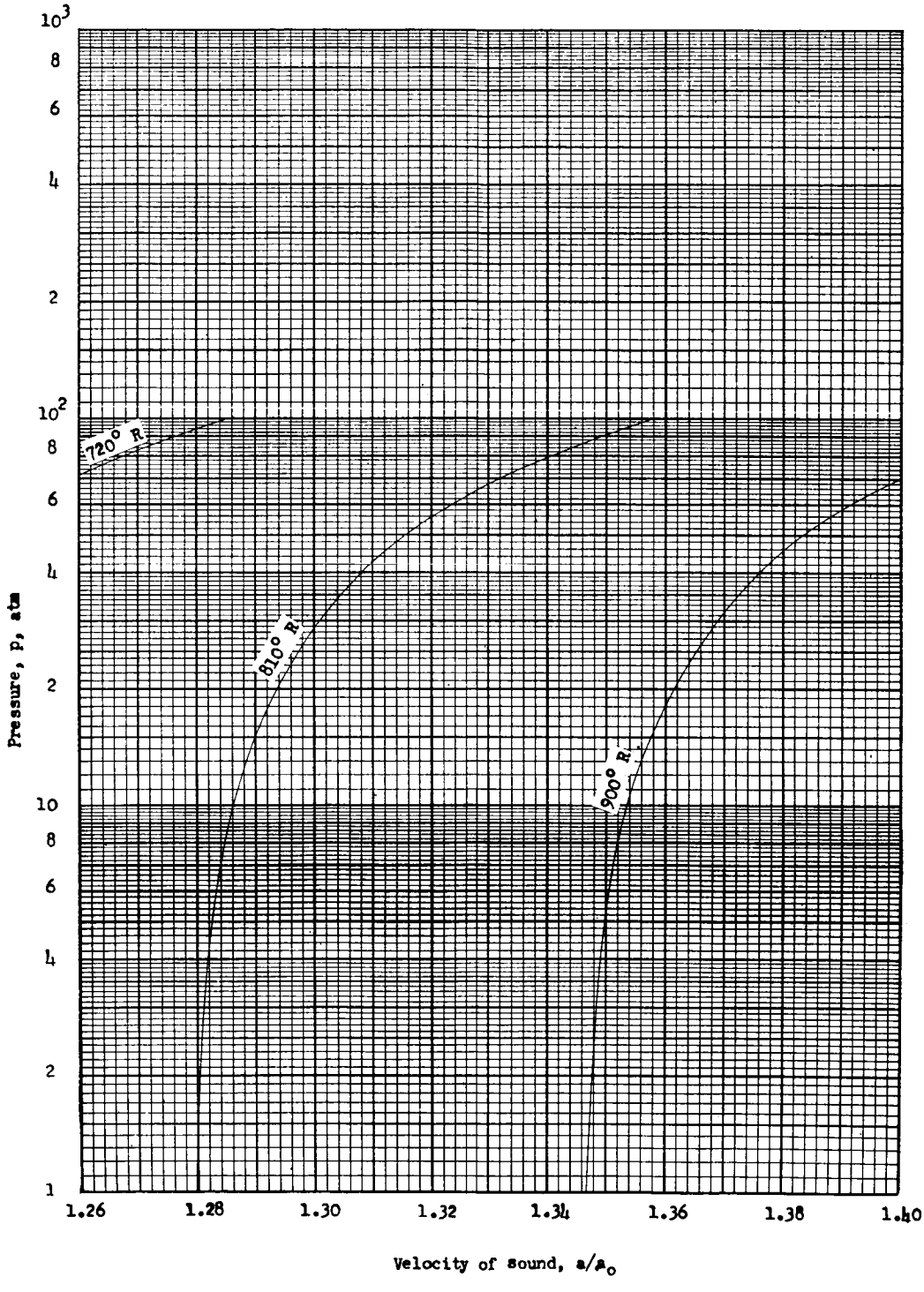

Velocity-of-sound chart 11

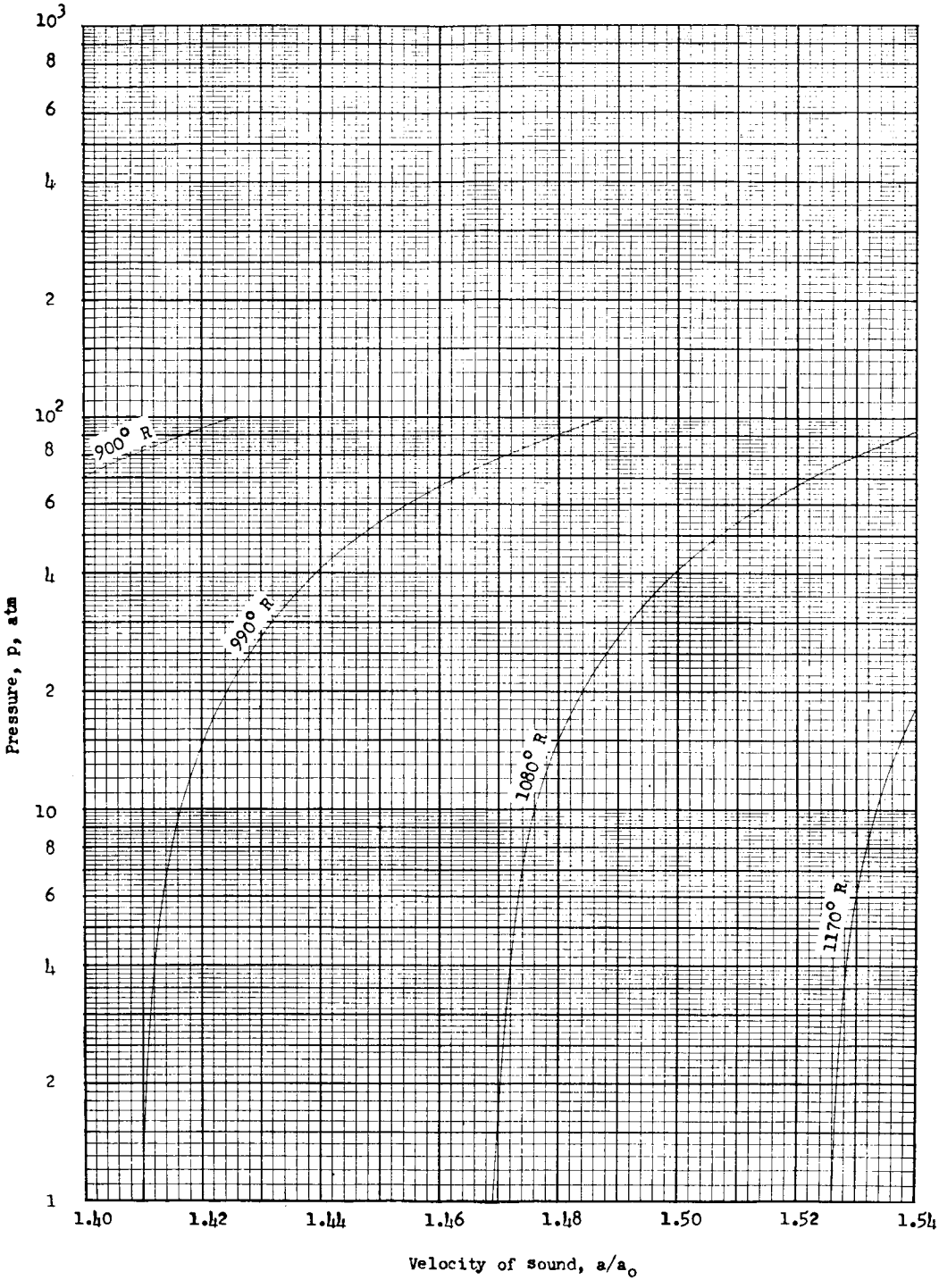

Velocity-of-sound chart 12

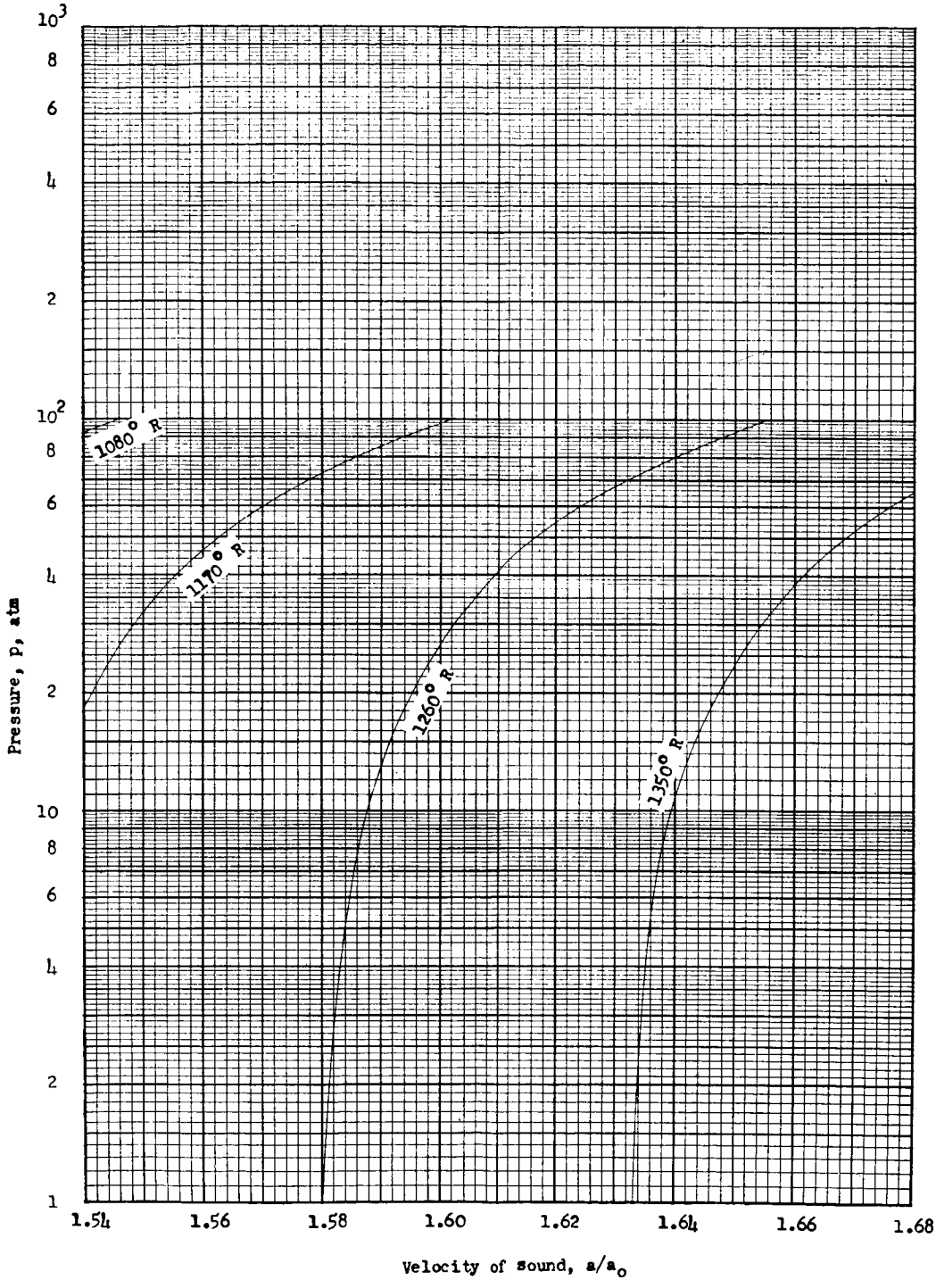

Velocity-of-sound chart 13

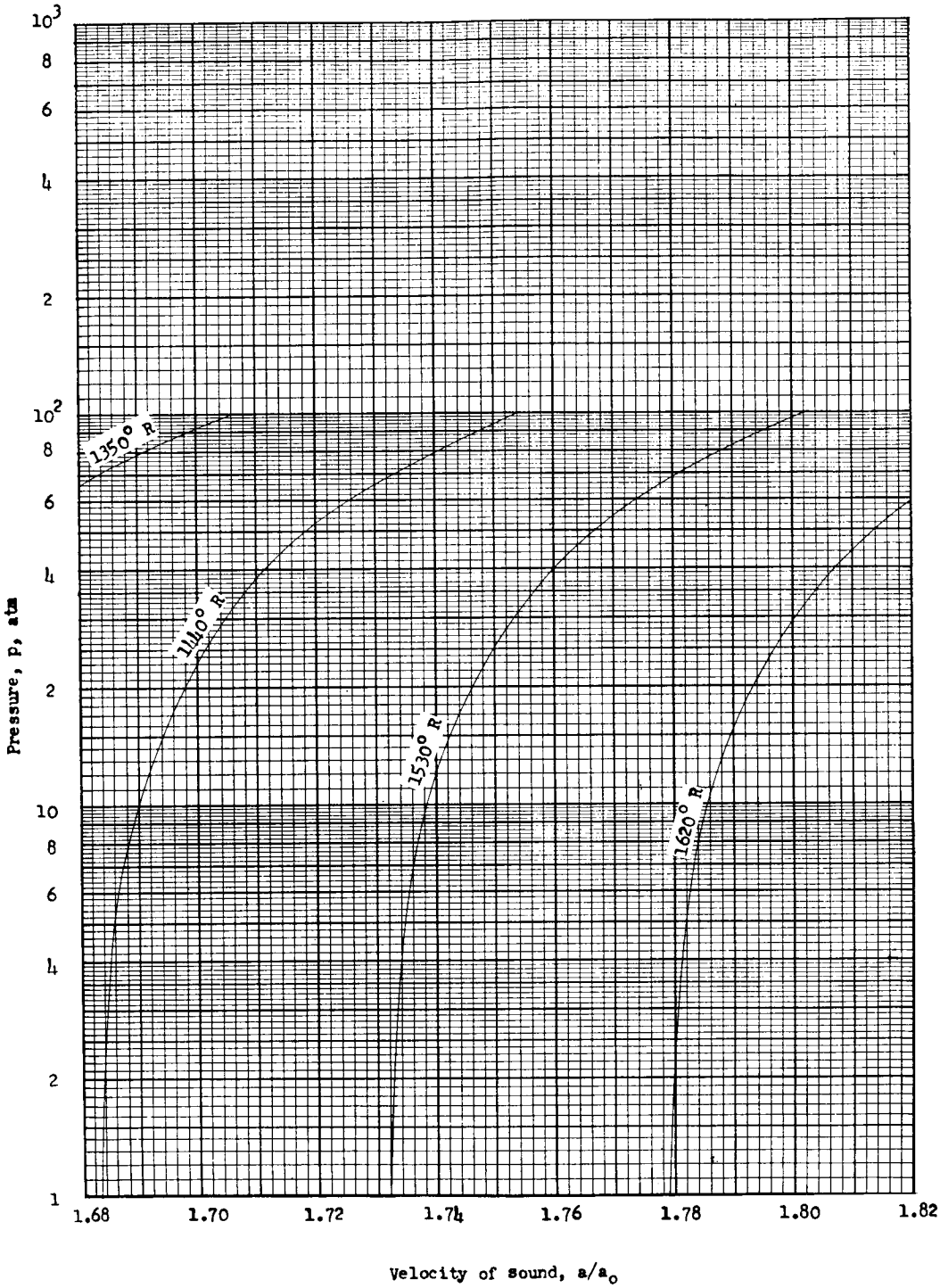

Velocity-of-sound chart 14

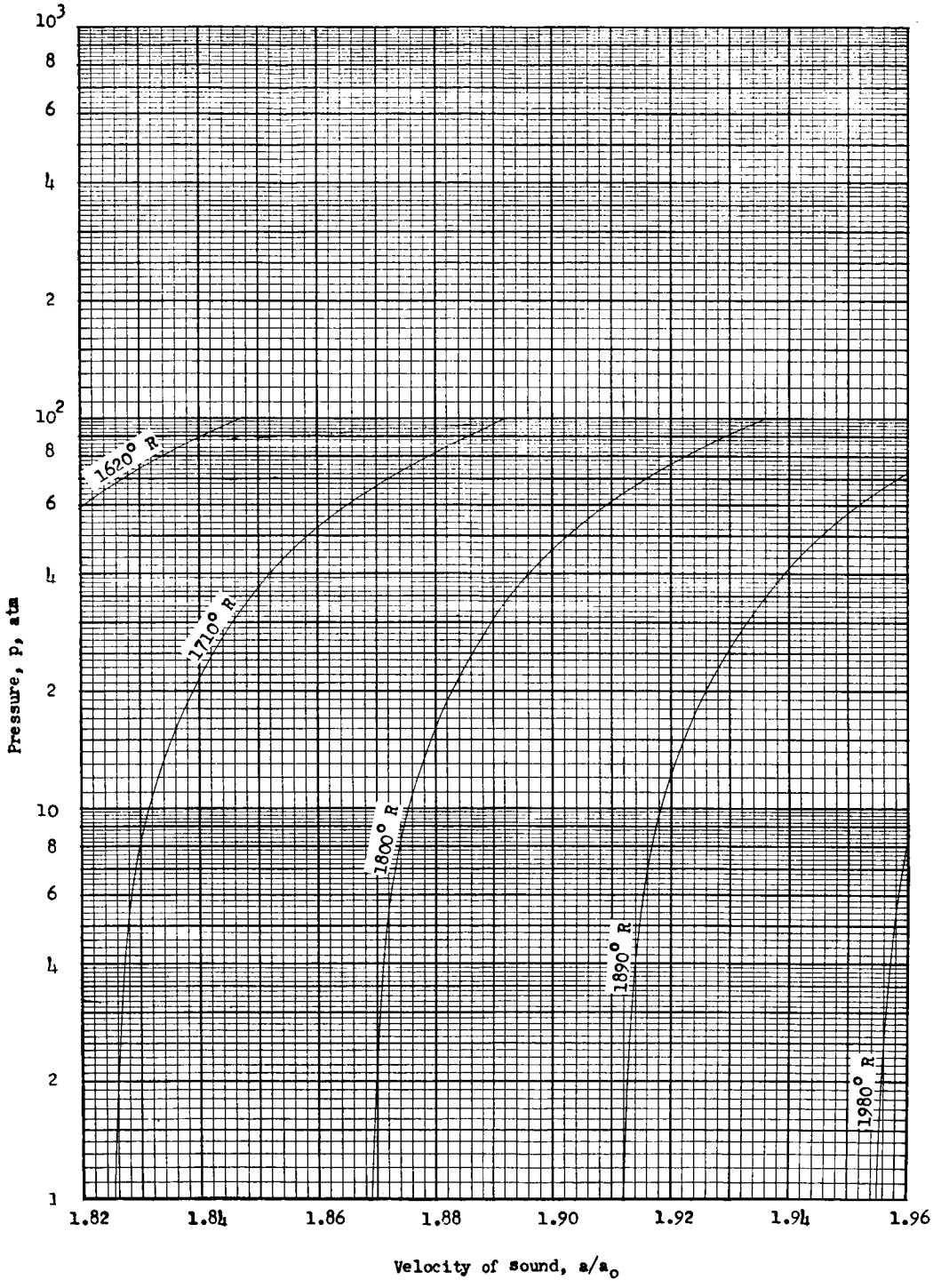

Velocity-of-sound chart 15

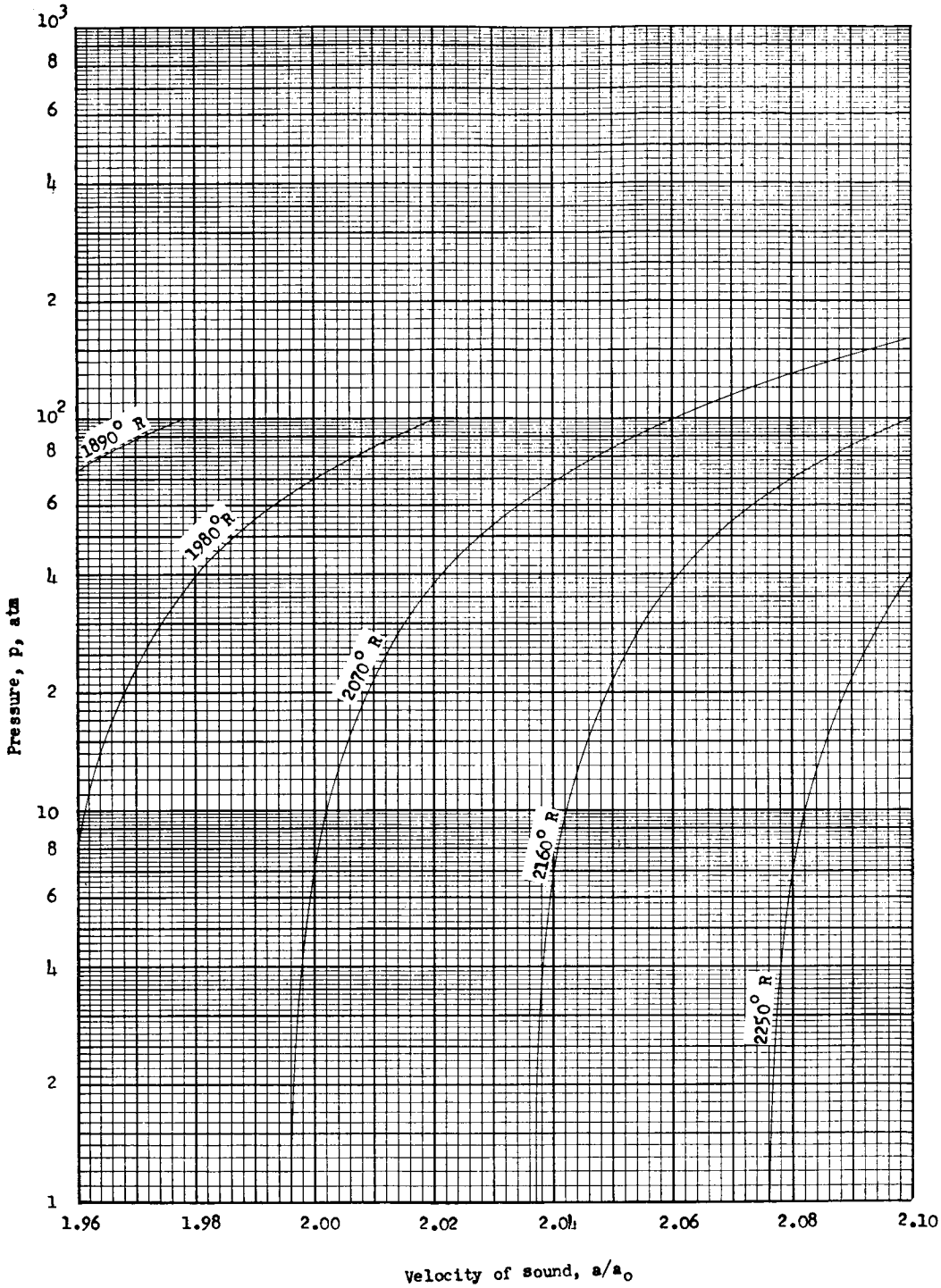

Velocity-of-sound chart 16

Velocity-of-sound, a/a_o, chart 17

Temperature, T, °R	Pressure p, atm, of -									
	150	200	300	400	500	600	700	800	900	1,000
2,070	2.093	2.126	2.194	2.264	2.334	2.407	2.480	2.555	2.631	2.708
2,160	2.132	2.165	2.231	2.299	2.367	2.438	2.509	2.581	2.655	2.729
2,250	2.171	2.203	2.268	2.334	2.401	2.468	2.537	2.608	2.679	2.751
2,340	2.209	2.240	2.302	2.368	2.432	2.497	2.564	2.633	2.702	2.771
2,430	2.243	2.274	2.337	2.399	2.461	2.525	2.591	2.657	2.724	2.791
2,520	2.279	2.310	2.371	2.432	2.493	2.556	2.619	2.683	2.748	2.812
2,610	2.314	2.345	2.403	2.463	2.523	2.585	2.646	2.708	2.771	2.833
2,700	2.350	2.379	2.437	2.495	2.554	2.614	2.674	2.735	2.795	2.855
2,790	2.383	2.412	2.468	2.525	2.583	2.643	2.702	2.760	2.819	2.877
2,880	2.416	2.444	2.500	2.557	2.613	2.671	2.729	2.785	2.842	2.899
2,970	2.448	2.476	2.530	2.586	2.643	2.700	2.756	2.810	2.865	2.922
3,060	2.481	2.509	2.562	2.617	2.672	2.728	2.783	2.836	2.890	2.946
3,150	2.514	2.541	2.593	2.646	2.700	2.756	2.810	2.863	2.916	2.970
3,240	2.545	2.571	2.623	2.675	2.728	2.783	2.836	2.887	2.940	2.992
3,330	2.576	2.602	2.652	2.704	2.756	2.809	2.861	2.912	2.964	3.015
3,420	2.605	2.630	2.680	2.732	2.783	2.835	2.886	2.937	2.988	3.038
3,510	2.634	2.660	2.709	2.760	2.810	2.860	2.911	2.961	3.011	3.061
3,600	2.663	2.688	2.737	2.787	2.837	2.886	2.936	2.985	3.035	3.084
3,690	2.692	2.716	2.765	2.813	2.862	2.910	2.960	3.009	3.058	3.106
3,780	2.720	2.744	2.792	2.840	2.888	2.936	2.985	3.034	3.082	3.129
3,870	2.748	2.772	2.820	2.867	2.914	2.961	3.009	3.057	3.105	3.152
3,960	2.776	2.799	2.846	2.892	2.939	2.986	3.033	3.081	3.128	3.174
4,050	2.804	2.827	2.873	2.919	2.965	3.011	3.058	3.105	3.152	3.197
4,140	2.831	2.854	2.900	2.946	2.991	3.037	3.083	3.129	3.175	3.221
4,230	2.858	2.880	2.925	2.970	3.015	3.061	3.107	3.152	3.198	3.243
4,320	2.883	2.906	2.950	2.995	3.040	3.085	3.130	3.175	3.221	3.266
4,410	2.909	2.931	2.975	3.020	3.065	3.110	3.154	3.198	3.243	3.288
4,500	2.934	2.956	3.000	3.045	3.089	3.134	3.178	3.222	3.266	3.310
4,590	2.959	2.981	3.025	3.069	3.113	3.158	3.202	3.246	3.290	3.333
4,680	2.984	3.006	3.050	3.094	3.137	3.181	3.225	3.269	3.313	3.357
4,770	3.008	3.030	3.074	3.117	3.159	3.203	3.246	3.289	3.332	3.375
4,860	3.034	3.055	3.098	3.140	3.182	3.225	3.267	3.309	3.351	3.394
4,950	3.058	3.079	3.121	3.162	3.203	3.244	3.285	3.326	3.368	3.409